EBM Experimental Biology and Medicine

Volume 249 | Issue 2

Experimental Biology and Medicine

Chief Editor

Steven Richard Goodman
University of Tennessee Health Science Center, Memphis, USA

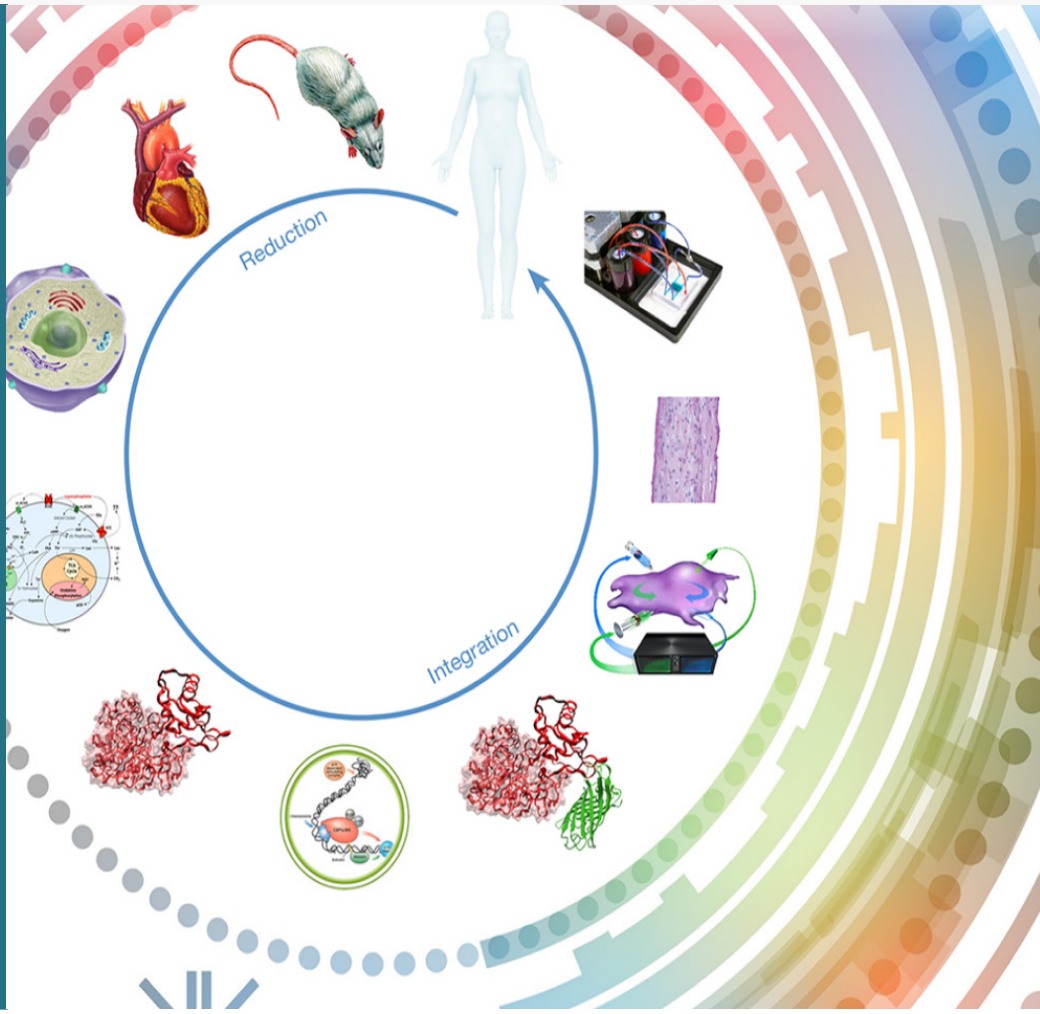

ISBN 978-2-8325-4823-3
DOI 10.3389/978-2-8325-4823-3

frontiers | Publishing Partnerships

SEBM Executive Council

Publication Committee

Society for Experimental Biology and Medicine
3220 N Street NW, #179
Washington DC 20007, USA
Executive Director – ed@sebm.org
Editor-in-Chief – ebm@sebm.org

www.sebm.org

Editorial Board

ISSN 1535-3702
ISBN 978-2-8325-4823-3
DOI 10.3389/978-2-8325-4823-3

EBM Experimental Biology and Medicine

2024 | Volume 249 | Issue 2 | ISSN 1535-3702

Table of contents

Mechanisms of Aging

Highlight

Neuroscience

Highlight

Physiology and Pathophysiology

EBM Experimental Biology and Medicine

TYPE Original Research
PUBLISHED 21 March 2024
DOI 10.3389/ebm.2024.10040

OPEN ACCESS

*CORRESPONDENCE
Hong-Yan Lu,
lhy5154@163.com

RECEIVED 30 October 2023
ACCEPTED 11 March 2024
PUBLISHED 21 March 2024

CITATION
Jiang J-F, Lu H-Y, Wang M-Y, He L-Y, Zhu Y and Qiao Y (2024), Role of regulatory T cells in mouse lung development.
Exp. Biol. Med. 249:10040.
doi: 10.3389/ebm.2024.10040

Role of regulatory T cells in mouse lung development

Jian-Feng Jiang, Hong-Yan Lu*, Ming-Yan Wang, Lang-Yue He, Ying Zhu and Yu Qiao

Department of Pediatrics, Affiliated Hospital of Jiangsu University, Zhenjiang, China

Abstract

Regulatory T cells (Tregs) constitute a specialized subset of T cells with dual immunoregulatory and modulatory functions. Recent studies have reported that Tregs mediate immune responses and regulate the development and repair processes in non-lymphoid tissues, including bone and cardiac muscle. Additionally, Tregs facilitate the repair and regeneration of damaged lung tissues. However, limited studies have examined the role of Tregs in pulmonary development. This study aimed to evaluate the role of Tregs in pulmonary development by investigating the dynamic alterations in Tregs and their hallmark cellular factor Forkhead box P3 (Foxp3) at various stages of murine lung development and establishing a murine model of anti-CD25 antibody-induced Treg depletion. During the early stages of murine lung development, especially the canalicular and saccular stages, the levels of Treg abundance and expression of Foxp3 and transforming growth factor-β (TGF-β) were upregulated. This coincided with the proliferation period of alveolar epithelial cells and vascular endothelial cells, indicating an adaptation to the dynamic lung developmental processes. Furthermore, the depletion of Tregs disrupted lung tissue morphology and downregulated lung development-related factors, such as surfactant protein C (SFTPC), vascular endothelial growth factor A (VEGFA) and platelet endothelial cell adhesion molecule-1 (PECAM1/CD31). These findings suggest that Tregs promote murine lung development.

KEYWORDS

lung development, regulatory T cells, forkhead box P3, surfactant protein C, vascular endothelial growth factor A

Impact statement

Previous studies of regulatory T cells have focused on the role of Tregs in the physiological development of organs (such as the heart) and pathological repair and aberrant cell proliferation in tissues (including the lung). However, limited studies have investigated the role of Tregs during physiological murine lung development. We found that the abundance of Tregs and the expression of Foxp3 were upregulated during the canalicular and early saccular stages of murine lung development, which was aligned with the extensive proliferation of alveolar epithelial cells and vascular endothelial cells. The

depletion of Tregs significantly impaired pulmonary tissue development, which was accompanied by the downregulation of lung development-related factors. This suggests that Tregs contribute to lung development.

Highlights

- In this study, we examined the dynamic changes in Tregs and Foxp3 during various stages of mouse lung development. Subsequently, we established a mouse model with Tregs depletion to observe its impact on mouse lung development.
- We observed that Tregs and Foxp3 themselves undergo dynamic changes during lung development, and these dynamics are correlated with lung morphological changes and the pulmonary development markers SFTPC and VEGFA.
- Following Tregs depletion, we observed significant impediments in mouse lung development, including alterations in lung morphology, as well as reduced levels of SFTPC and VEGFA.
- We further explored potential mechanisms underlying the existence of these phenomena, with the hope of providing a modest theoretical basis for the study of lung development.

Introduction

The lung develops through a series of branching morphogenesis from the endoderm. Lung development involves the gradual generation of various lineages, including airway epithelium and vascular endothelium. Lung development can be broadly categorized into the following five stages: the embryonal period, pseudoglandular stage, canalicular stage, saccular stage, and alveolar period (primarily involving the development of alveolar epithelium and pulmonary vascular endothelium) [1]. Alveolar type II epithelial cells (AEC IIs) serve as the stem cells of the alveolar epithelium. The proliferation and differentiation of AEC IIs have a critical role in alveolar development. Surfactant protein C (SFTPC), a hallmark protein expressed by AEC IIs, is an indirect marker of lung epithelium maturation [2]. Vascular endothelial growth factor A (VEGFA) is a crucial regulatory factor of pulmonary vascular development. The maturity of pulmonary vasculature can be indirectly assessed based on VEGFA expression levels [3].

Recent studies have suggested that Tregs promote cell proliferation and tissue development, Tregs with this functional profile are often characterized by the expression of $CD4^+CD25+Foxp3+$ [4]. Tregs are a distinct subset of $CD4^+$ T cells with immunomodulatory functions. CD25 is predominantly expressed on the surface of immune-related cells, including activated Tregs and effector T cells. CD25 blockade significantly inhibits the proliferation of Tregs, with minimal impact on effector T cells [5]. Forkhead box P3 (Foxp3), a transcriptional factor, serves as a marker of Tregs [6]. Treg depletion is reported to significantly inhibit mouse cardiomyocyte proliferation and differentiation [7]. Additionally, Treg depletion regulates the proliferation and differentiation of injured alveolar epithelial cells and impairs the generation of new blood vessels in damaged lungs [8, 9]. Conversely, Treg overexpression significantly promotes the aberrant proliferation of lung tumor cells [10]. Previous studies have focused on the role of Tregs in the physiological development of organs (such as the heart) and pathological repair and aberrant cell proliferation in tissues (including the lung), and TGF-β plays a role in Tregs regulation between tissue development [11]. However, limited studies have investigated the role of Tregs during physiological murine lung development. This study aimed to provide a theoretical foundation for lung development research by examining the dynamic changes in Tregs and Foxp3 expression at different stages of murine lung development, as well as by establishing a Treg-depleted murine model through the intraperitoneal injection of anti-CD25 antibodies, to explore the potential roles of Tregs in murine lung development.

Materials and methods

Experimental animals

C57BL/6J mice of similar bodyweight (22–25 g) and age (10–12 weeks) were obtained from the Animal Center of Jiangsu University (protocol No. UJS-IACUC-AP-2020030304). Three female mice were housed with one male mouse for mating. The vaginal secretion of the female mice was smeared on the next morning to examine the presence of sperm under a microscope. The day the sperms were detected was considered gestational day 0.5.

Specimen collection and processing

Pregnant mice were anesthetized via intraperitoneal injection of 200 g/L urethane on day 17.5 of gestation. After sacrificing the mice via cervical dislocation, the abdominal cavity was rapidly exposed. The pregnant uterus was separated, and the fetal mouse was removed. The fetal lung on day 17.5 of gestation (E17.5 d, canalicular period) was collected under a microscope. On postnatal days 1 (N1 d, early saccular stage), 4 (N4 d, late saccular stage), 7 (N7 d, early alveolarization stage), 14 (N14 d, mid alveolarization stage), and 21 (N21 d, late alveolarization stage), mice at different stages of lung development were sacrificed. The lungs were harvested at the indicated time points, and the chest cavity was rapidly exposed.

Both lungs were irrigated with phosphate-buffered saline (PBS, pH 7.4) until they exhibited a slightly pale color. The lung tissue was harvested and embedded for histological staining. The remaining tissues were stored at −80°C in the refrigerator for future use.

Analysis of pulmonary tissue morphology and alveolar count

The pulmonary tissue was paraffin-embedded and sectioned into 3-μm-thick sections. The sections were subjected to hematoxylin-eosin (HE) staining. The nuclei exhibited dark blue staining, while the cytoplasm and fibrous tissue exhibited red staining. The pulmonary tissue morphology was observed under a microscope. Next, the radial alveolar count (RAC) was determined. The stained pulmonary tissue sections were placed under an optical microscope and observed at ×200 magnification. A vertical line was drawn from the center of the bronchiole to the nearest fibrotic septum or pleura. The number of alveoli along this line was counted. Five sections from each mouse were selected, and the count was repeated three times for each section to consider average value for the analysis.

Evaluation of Pecam1 content and lung microvascular density

PECAM1 is commonly used to label lung microvascular endothelial cells [12]. The lung tissue sections were routinely dewaxed, hydrated, subjected to antigen retrieval, blocked with bovine serum albumin, and incubated with rabbit anti-Pecam1 primary antibodies (1:50), followed by incubation with goat anti-rabbit IgG secondary antibodies (1:5,000), staining with diaminobenzidine, and counterstaining with hematoxylin. Next, the section was dehydrated, cleared, and sealed. The images of Pecam1 immunohistochemical staining were analyzed using Image J. The presence of brownish-yellow regions in the cells was considered positive staining. The average optical density of the positive cells was recorded as the Pecam1 content in the lung tissue specimen. The lung microvascular density was calculated as follows: lung microvascular density (%) = (area of Pecam1-positive endothelial cells in the lung tissue/total area of lung parenchyma cells) × 100%.

Flow cytometric analysis of the relative number of Tregs

The lung tissues were suspended in PBS and labeled with anti-FVD [detected using allophycocyanin (APC)-A750 channel] and anti-CD45 (detected using BV510 channel) antibodies to isolate living lymphocytes. Next, the cells were incubated with anti-CD4 [detected using phycoerythrin (PE) channel] and anti-CD25 antibodies (detected using APC channel) for 30 min at 4°C in the dark to stain the cell surface antigens. The cells were washed twice with PBS containing 3% calf serum. The cell membrane and nuclear membrane were disrupted using a reagent kit. Next, the cells were incubated with anti-Foxp3 nuclear antibodies [detected using fluorescein isothiocyanate (FITC) channel]. The cells were then centrifuged and washed. The $CD4^{+}CD25+Foxp3+$ cells were considered Tregs. The flow cytometric data were analyzed using FlowJo software.

Quantitative real-time polymerase chain reaction (qRT-PCR) analysis

The lung tissue was weighed (100 mg), transferred to a sterile mortar, and homogenized with 1 mL of Trizol reagent to extract total RNA from the tissue. The isolated RNA was reverse-transcribed into complementary DNA, which served as a template for amplification with primers, using a reverse transcription kit. The PCR conditions were as follows: denaturation at 95°C for 30 s, followed by 40 cycles of 95°C for 5 s and 60°C for 30 s. The Ct value was obtained from the Real-time RT-qPCR instrument. β-actin served as the internal reference. The ΔCt and ΔΔCt values were calculated. The relative expression levels of target mRNAs were calculated using the $2^{-\Delta\Delta CT}$ method.

Western blotting

The lung tissues were cut into small pieces and lysed in lysis buffer containing protease inhibitors. The protein samples (10 μL) were subjected to electrophoresis. The resolved proteins were transferred to a membrane. The membrane was blocked and incubated with rat anti-Foxp3 (1:1,000), rabbit anti-CD4 (1:500), rabbit anti-TGF-β (1:1,000), rabbit anti-SFTPC (1:200), and rabbit anti-VEGFA (1:1,000) antibodies overnight at 4°C. After washing, the membrane was incubated with the secondary antibodies (1: 5,000) at room temperature. Immunoreactive signals were developed using chemiluminescence. The grayscale value of immunoreactive signals was quantified using Image J software.

Establishment of the Treg-depleted mouse model

Previous studies have reported that the intraperitoneal injection of 100 μg of rat anti-mouse CD25 monoclonal antibodies at days 10 and 15 of pregnancy depletes Tregs in pregnant female mice and fetal mice [7]. Mice in the control group were injected with an equal volume of IgG isotype control antibody as a negative control for anti-CD25 antibodies.

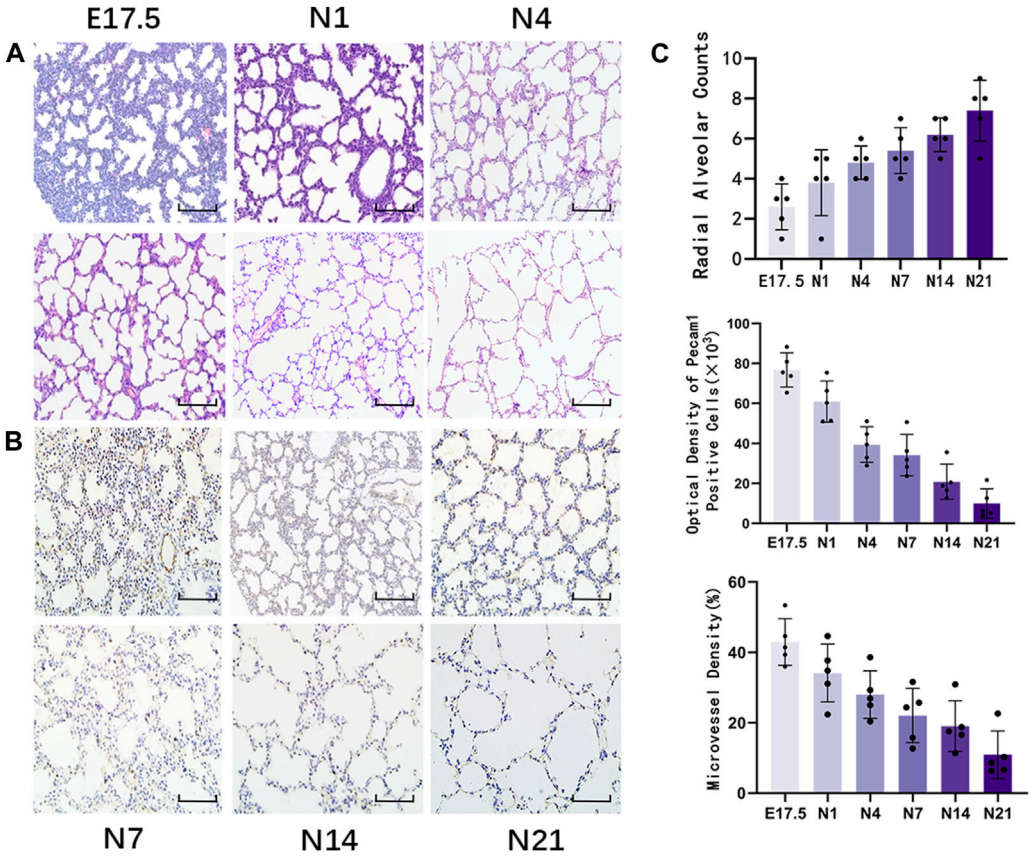

FIGURE 1
Morphological observation of healthy developing mouse lung tissue and pulmonary alveolus and microvessel counting. **(A)** The changes in alveolar structure during different stages of mouse lung development were examined using hematoxylin and eosin (HE) staining (magnification: ×200; scale bar = 50 μm, n = 5); **(B)** The changes in vascular structure during different stages of mouse lung development were analyzed using immunohistochemical staining (magnification: ×200; scale bar = 50 μm, n = 5); **(C)** Radial alveolar counts (RACs) were used to determine alveolar development. Microvascular endothelial cell development was determined based on Pecam1-labeled microvascular endothelial cells. Pulmonary microvascular maturation was determined based on the changes in the proportion of pulmonary microvascular endothelial cells to the pulmonary parenchymal area.

The number of CD25+Foxp3+ cells in the lung tissues was examined using flow cytometry. The expression of CD4 mRNA was detected by RT-qPCR, and the expression of CD4 protein was detected by Western blotting to evaluate the effect of Tregs depletion (Tregs belong to $CD4^+$ T cells). The morphology of the lung tissue, the number of alveoli, the content of Pecam1, the density of microvessels, and the mRNA and protein expression levels of Foxp3, TGF-β, SFTPC, and VEGFA were examined in Treg-depleted mice on day 17.5 of pregnancy, day 1 after birth, and day 4 after birth and compared with those in the control group.

Statistical analysis

Data analysis was performed using GraphPad Prism 9.0 software. Quantitative data with normal distribution are expressed as mean ± standard deviation. Means between the groups were compared using one-way analysis of variance, followed by q-test for pairwise comparisons. Pearson correlation analysis was performed to examine the correlation between two parameters. Differences were considered significant at $p < 0.05$.

Results

Morphological analysis of healthy developing mouse lung tissue

HE staining of lung tissues (Figure 1A) revealed visible alveolar-like structures inside the primitive lung bud at E17.5 d that were arranged in a circular pattern with tall columnar epithelial cells and dense interstitial structures. The lung buds completely separated and became independent with widely increased pulmonary alveolus spaces and comprised mostly single-layer cuboidal epithelial cells

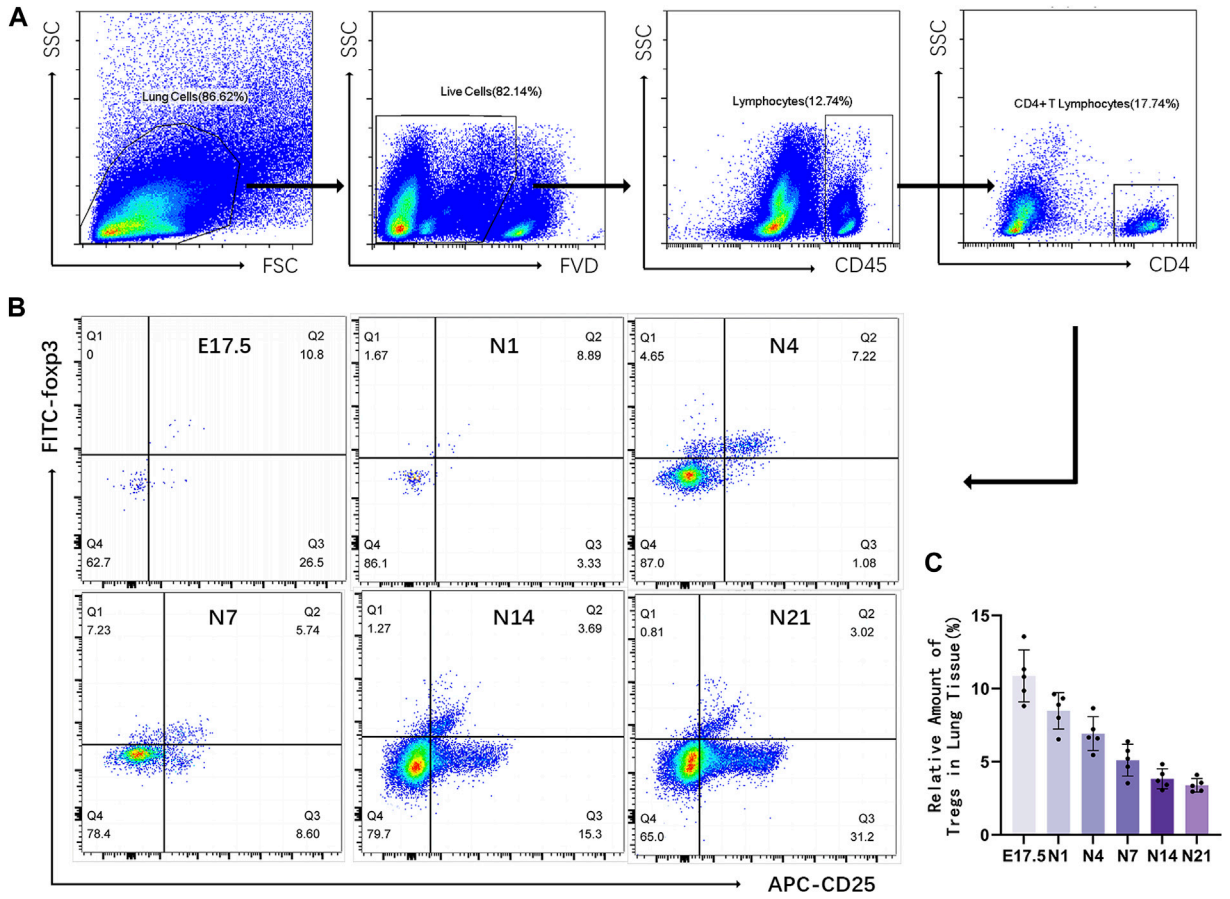

FIGURE 2
Relative number of regulatory T cells (Tregs) in the mouse lung tissue at different stages of development. **(A)** Representative results of flow cytometric analysis of Tregs in the mouse lung tissue (gated on $CD4^+CD25^+Foxp3^+$ Tregs); **(B)** Cluster map of $CD4^+CD25^+Foxp3^+$ Tregs at different stages of lung development; **(C)** Changes in the proportion of $CD25^+Foxp3^+$ Tregs to $CD4^+$ T lymphocytes during different stages of development ($n = 5$).

with enlarged luminal areas at N1 d. At N4 d, primary alveoli appeared with uneven sizes, thin interstitial tissues, and strip-like arrangements. The basic structural unit of the lung tissue at N7 d was primary alveoli with increased partitions and regular structures and ridges protruding into the alveoli. At N14 d, the alveoli matured with thin partitions and exhibited increased numbers. The basic structural unit of the lung tissue at N21 d was mature alveoli with regular structures and thin partitions. Quantification of the RACs at each stage of lung development (Figure 1C) revealed that the RACs gradually increased with mouse age ($p < 0.01$).

Immunohistochemical staining of Pecam1-positive cells in the lung tissue (Figure 1B) revealed that during the canalicular stage of lung development, the number of Pecam1-positive cells significantly increased and that these cells were arranged closely with the epithelium. In the same high-power microscope field, the content of Pecam1-positive cells in the pulmonary microvascular endothelial cells and the density of pulmonary microvessels were the highest. During the saccular stages, the pulmonary vessels continued to develop and the Pecam1 content and pulmonary microvascular density remained at a high level. The pulmonary vessels continued to mature, the pulmonary capillary network continued to expand, and an alveolar capillary layer that was separated from the alveolar septum formed around the mature alveoli during the alveolar period. The content of Pecam1 and the density of pulmonary microvessels continued to decrease and eventually stabilized to form a mature pulmonary microvascular network. The Pecam1 content and microvascular density in the lungs gradually decreased with the mouse age and eventually stabilized at a low level as the lungs matured (Figure 1C).

Flow cytometric analysis of the relative number of Tregs in mouse lung tissues

Flow cytometry was used to detect $CD4^+CD25^+Foxp3^+$ Tregs in the mouse lung tissue (Figure 2). Representative results revealed that the proportion of Tregs varied at different time points as follows: E17.5 d, approximately 10.870% ± 0.795% of

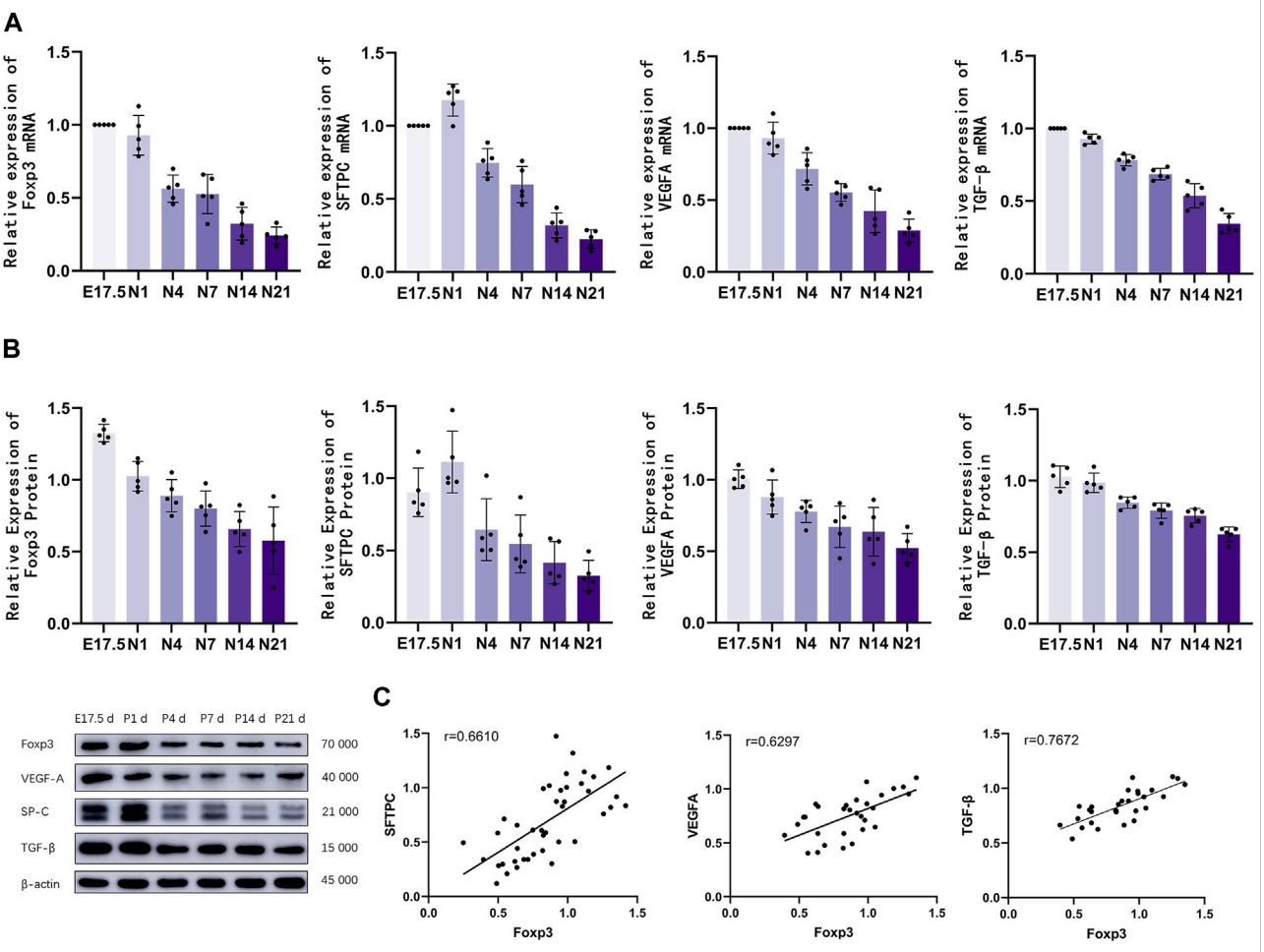

FIGURE 3
The mRNA and protein expression levels of Foxp3, TGF-β, SFTPC, and VEGFA were analyzed. **(A)** Quantitative real-time polymerase chain reaction analysis of pulmonary Foxp3, TGF-β, SFTPC, and VEGFA mRNA levels in different groups (n = 5); **(B)** Western blotting analysis of Foxp3, TGF-β, SFTPC, and VEGFA levels (n = 5); **(C)** Correlation analysis of Foxp3, TGF-β,SFTPC, and VEGFA expression levels during the development of mouse lungs.

$CD4^+$ T cells; N1 d, approximately 8.476% ± 1.246% of $CD4^+$ T cells; N4 d, approximately 6.914% ± 0.519% of $CD4^+$ T cells; N7 d, approximately 5.104% ± 0.486% of $CD4^+$ T cells; N14 d, approximately 3.832% ± 0.307% of $CD4^+$ T cells; N21 d, 3.394% ± 0.205% of $CD4^+$ T cells (Figure 1B). The pooled results revealed that the proportion of Tregs was relatively high during the canalicular stage, slightly decreased during the saccular stage, and gradually decreased with lung development during the alveolar period ($p < 0.01$) (Figure 1C).

Analysis of Foxp3, TGF-β, SFTPC, and VEGFA mRNA and protein levels

The mRNA levels of Foxp3, TGF-β, SFTPC, and VEGFA in the lung tissues of different groups were analyzed using qRT-PCR analysis (Figure 3A). Foxp3 and TGF-β mRNA expression peaked during the canalicular stage at E17.5 d and then gradually decreased. SFTPC mRNA expression peaked on the first day after birth and then gradually decreased until the late alveolar stage. VEGFA mRNA expression peaked at E17.5 d, then gradually decreased, and finally stabilized ($p < 0.01$). The Foxp3, SFTPC, and VEGFA levels were examined using western blotting (Figure 3B). Foxp3, TGF-βwas expressed during the canalicular stages, peaked at the canalicular and saccular stages, and gradually stabilized. VEGFA expression peaked during the canalicular and saccular stages and then gradually decreased. SFTPC expression peaked on the first day after birth, then gradually decreased, and stabilized during the late stage of alveolarization ($p < 0.01$). Correlation analysis (Figure 3C) revealed that Foxp3 expression was positively correlated with SFTPC ($r = 0.6610$), VEGFA ($r = 0.6297$) and TGF-β ($r = 0.7672$).

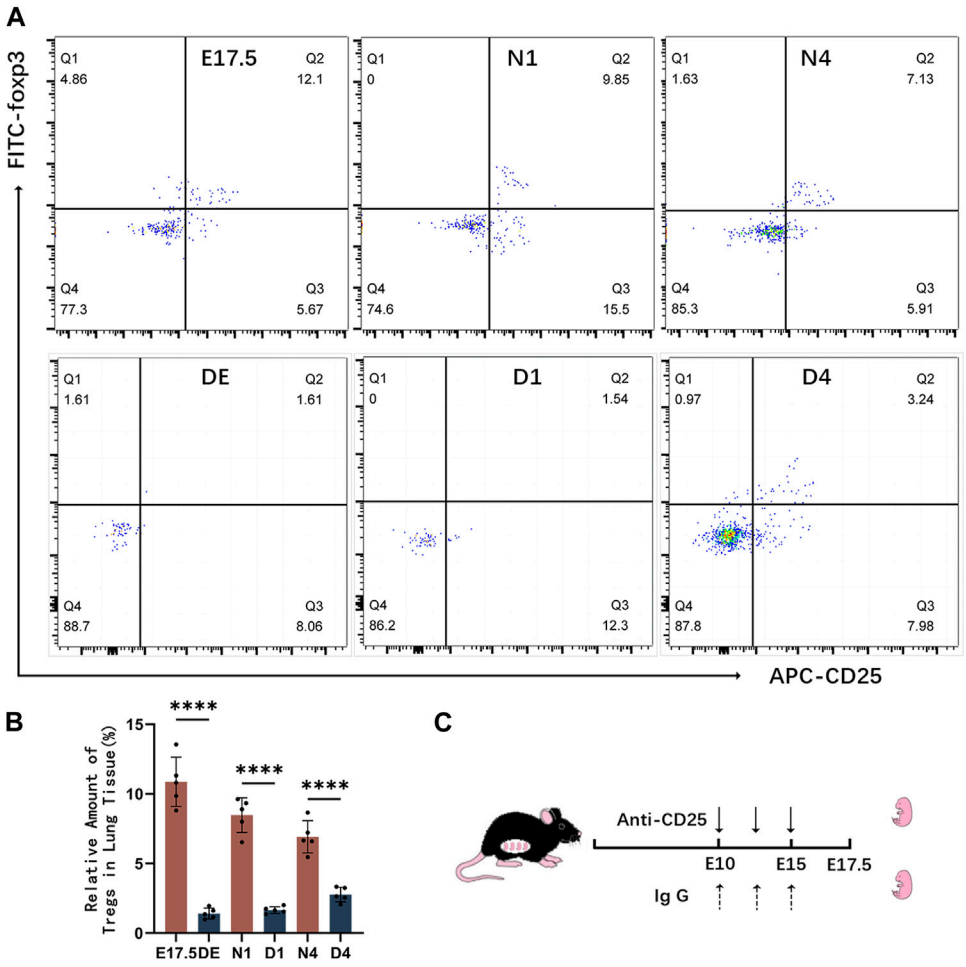

FIGURE 4
Establishment of the regulatory T cell (Treg)-depleted mouse model. **(A)** Representative results of flow cytometric analysis of CD25+Foxp3+ Tregs in the lung tissues of the control and Treg-depleted groups; **(B)** Clustering plot of CD25+Foxp3+ Tregs during prenatal lung development in the control and Treg-depleted groups; **(C)** Summary of the experimental result for Treg depletion in pregnant animals. At embryonic day 10 (E10 d) and embryonic day 15 (E15 d), pregnant mice were intraperitoneally administered with anti-CD25 neutralizing antibodies.

Establishment of the Treg-depleted mouse model

Mice were intraperitoneally injected with anti-CD25 antibodies to deplete Tregs. The effects of Treg depletion were examined using flow cytometry (Figure 4C). The levels of Tregs and pulmonary developmental indicators were upregulated during the canalicular and saccular stages and stabilized during the alveolar period. Hence, mice with Treg depletion were selected on gestational day 17.5 (DE group), postnatal day 1 (D1 group), and postnatal day 4 (D4 group) for comparative analysis with the control group (Figure 4A). During the canalicular and saccular stages with enhanced Treg contents, the DE and D1 groups exhibited enhanced depletion of Tregs with almost no $CD4^+$ CD25+Foxp3+ T cells. Meanwhile, in the D4 group, the number of CD25+Foxp3+ Tregs slightly recovered and accounted for approximately 2.764% ± 0.235% of $CD4^+$ T cells but was significantly lower than that in the N4 control group ($p < 0.01$) (Figure 4B).

Morphological analysis of mouse lungs in the control and Treg-depleted groups

HE staining of mouse lung tissues from the Treg-depleted and control groups (Figure 5A) revealed that compared with those in the control group, the range of airspace-like structures was significantly lower, the interstitial structure was more compact, and the number of alveolar cavities was significantly lower in Treg-depleted mice belonging to the DE group. The number of alveolar cavities was upregulated in the

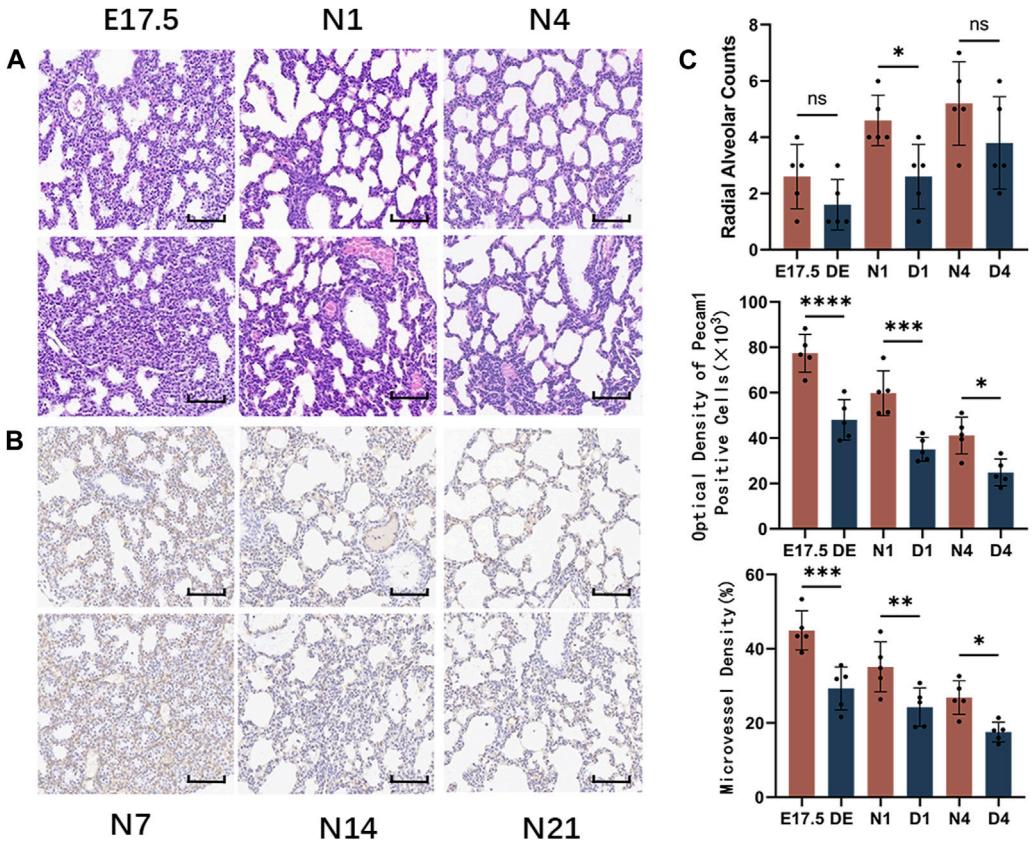

FIGURE 5
Morphological observation of mouse lungs in the control and regulatory T cell (Treg)-depleted groups during the early stage of lung development and the counting of alveolar and microvessels. **(A)** The changes in the alveolar structure during the early stage of mouse lung development in the control and Treg-depleted groups were examined using hematoxylin and eosin (HE) staining (magnification: ×200; scale bar = 50 μm, n = 5); **(B)** The changes in the vascular structure of the mouse lungs in the control and Treg-depleted groups during the early stage of lung development were examined using immunohistochemical staining (magnification: ×200; scale bar = 50 μm, n = 5); **(C)** Comparative analysis of the development of pulmonary alveoli in the control and Treg-depleted groups based on radial alveolar counts (RACs); The development of mouse microvascular endothelial cells in the control and Treg-depleted depletion groups was compared using anti-Pecam1 antibodies to label microvascular endothelial cells. Comparative analysis of the changes in the proportion of lung microvascular endothelial cells to the lung parenchyma area, which indicates the differential maturation of lung microvascular endothelial cells between the control and Treg-depleted groups.

D1 group. However, the alveolar cavity spacing in the D1 group was thicker than that in the N1 group with uneven distribution. Only some epithelial cells were single-layer cuboidal epithelial cells with most being high columnar epithelial cells. Primary alveoli with uneven sizes were observed in the D4 group. Additionally, some alveolar cavities in the D4 group were significantly thicker than those in the N4 group. The RAC in the Treg-depleted group was significantly lower than that in the control group at N1 d. However, the downregulation of RAC at N4 d during pregnancy was not significantly different from that after birth (Figure 5C). The vascular endothelium was labeled with anti-Pecam1 antibodies (Figure 5B). The number of Pecam1-positive cells in the Treg-depleted group was significantly lower than that in the control group (p < 0.05). Additionally, the microvascular density in the Treg-depleted group was lower than that in the control group, especially at E17.5 d and N1 d (Figure 5C).

CD4, Foxp3, TGF-β, SFTPC, and VEGFA mRNA and protein expression levels in the control and Treg-depleted groups

The mRNA and protein levels of CD4, Foxp3, TGF-β, SFTPC, and VEGFA were analyzed using qRT-PCR and western blotting analyses, respectively (Figure 6). The expression of CD4 decreased compared to the control group. The Foxp3 and TGF-β mRNA and protein levels were significantly downregulated in the Treg-depleted group (p < 0.01). The SFTPC mRNA and protein levels, which peaked on day 1 after birth in mice, in the Treg-depleted group were

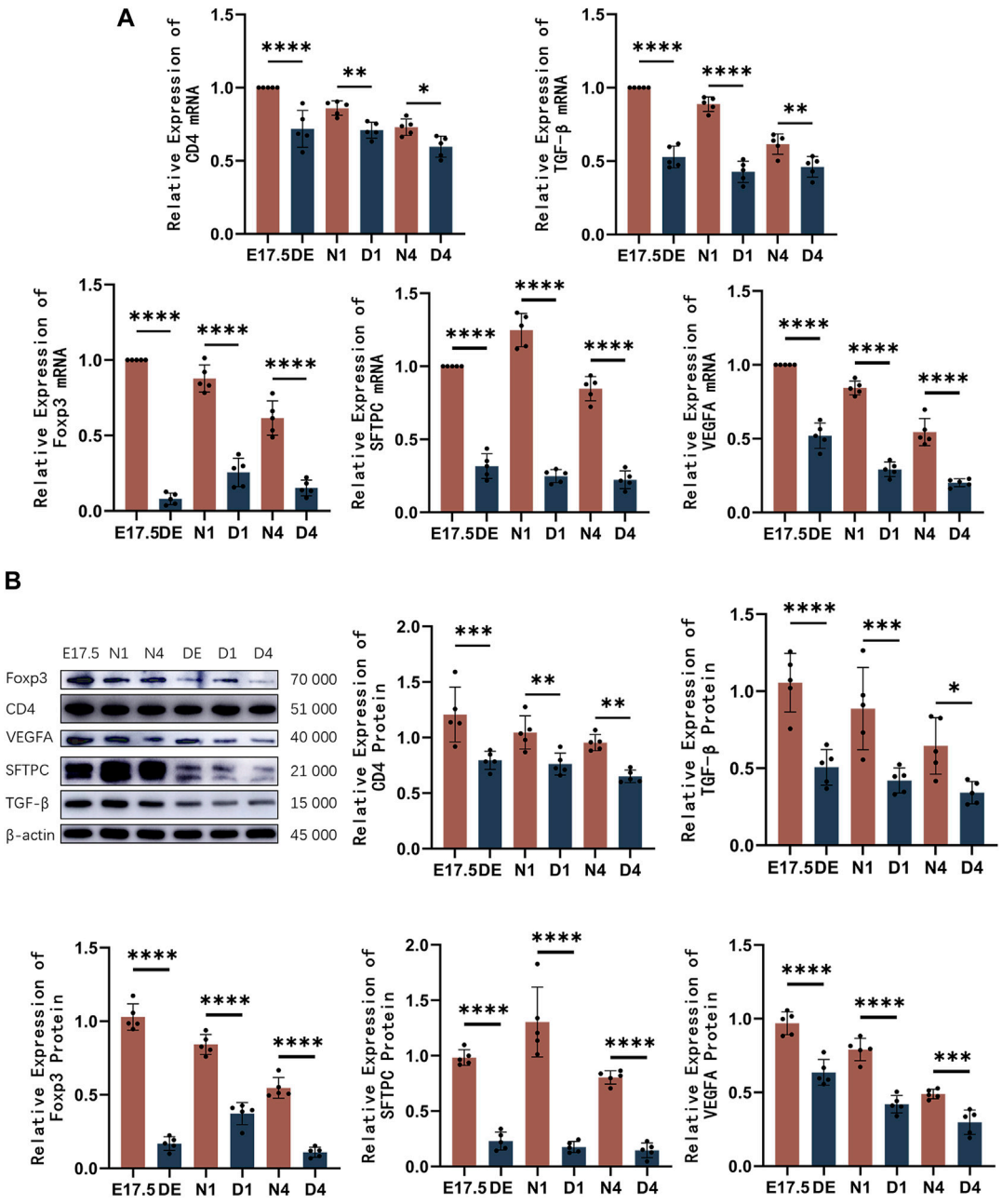

FIGURE 6
The mRNA and protein expression levels of CD4, Foxp3, TGF-β, SFTPC, and VEGFA in mice belonging to the control and regulatory T cell (Treg)-depleted groups. **(A)** Quantitative real-time polymerase chain reaction analysis of CD4, Foxp3, TGF-β, SFTPC, and VEGFA mRNA levels in mice belonging to the control and Treg-depleted groups (n = 5); **(B)** Western blotting analysis of CD4, Foxp3, TGF-β, SFTPC, and VEGFA protein levels in mice belonging to the control and Treg-depleted groups (n = 5).

significantly downregulated when compared with those in the control group, especially in the D1 group ($p < 0.01$). The VEGFA mRNA and protein levels were significantly downregulated in the Treg-depleted group ($p < 0.01$). The levels of these indices were not significantly different between different stages in the Treg-depleted group ($p > 0.05$).

Discussion

In premature infants with a gestational age of less than 36 weeks, lung development is characterized by the canalicular and saccular stages until approximately 36 weeks of gestation when alveolarization begins, continuing until approximately

21 years of age. At the end of the canalicular stage, the lungs may undergo the first gas exchange, enabling the survival of extremely preterm infants [1]. The stages of mouse lung development are similar to those of human lung development. At E17.5 days, the late canalicular stage in mice is similar to that in humans (approximately equivalent to 24 weeks of gestation and alveolarization completion at approximately 36 postnatal days) [13].

The expression of SFTPC serves as an indirect indicator of alveolar epithelial cell development [14]. This study revealed that the SFTPC protein levels were upregulated at the end of the canalicular stage. After entering the mid saccular stage, SFTPC expression peaked, gradually decreased during the late saccular and alveolar stage, and finally stabilized at a low level. During the canalicular stage, the lung undergoes tubularization of the parenchyma, forming primitive alveolar ducts and sacs at the end of this stage. AEC IIs undergo proliferation at this stage, resulting in the accumulation of SFTPC protein. As the development progresses to the early saccular stage, the number of lung sacs remains relatively constant with only a few terminal airways formed during this stage. The number of AEC IIs continues to slightly increase, and SFTPC expression peaks [15]. During the late saccular and alveolar phases, most of the growth in lung volume and surface area occurs within the alveolar sacs. AEC IIs continue to differentiate and AEC Is occupy a growing portion of the area. Additionally, the SFTPC levels steadily decline and stabilize as lung development matures [16].

Vascular endothelial growth factor is one of the critical regulatory factors throughout embryonic, fetal, and postnatal lung vascular development and maintenance. VEGF exerts regulatory effects on the migration, survival, proliferation, and differentiation of pulmonary vascular endothelial cells. VEGFA is the primary structural component [17]. The expression levels of VEGFA are directly associated with the developmental state of pulmonary vasculature. Currently, limited studies have analyzed the dynamic changes in VEGFA levels during lung development. Previous studies have focused on the fetal or alveolar stages. This study revealed the dynamic alterations in VEGFA (lung vascular development-related marker) levels during lung development. During the canalicular and early saccular stages, pulmonary vascular endothelial cells undergo proliferation and differentiation and VEGFA expression is highly active. In the late saccular and alveolar stages, the rates of proliferation and differentiation of microvascular endothelial cells are delayed, which is accompanied by a gradual downregulation of VEGFA. Finally, the expression of VEGFA stabilizes. These findings are consistent with those of this study, which reported that VEGFA expression in the postnatal mouse lung gradually decreases with age [18].

Tregs, a distinct subset of T cells with both immunosuppressive and regulatory functions, are characterized by the expression of the key transcription factor Foxp3 [19]. Recent studies have suggested that Tregs exert regulatory effects on metabolism and tissue repair in non-lymphoid tissues, such as promoting the proliferation and regeneration in bone, myocardium, skin, lung, and the central nervous system [4]. This study revealed dynamic changes in the relative abundance of Tregs and the content of Foxp3 during murine lung development.

During the canalicular and early saccular stages, the contents of Tregs and Foxp3 were upregulated. At the late saccular and alveolar stages, the contents of Tregs and Foxp3 gradually decreased and stabilized during mid-to-late alveolarization. This adaptation corresponds to the extensive proliferation of alveolar epithelial cells and pulmonary vascular endothelial cells during the canalicular and early saccular stages. Correlation analysis revealed that Foxp3 expression is positively correlated with SFTPC, VEGFA and TGF-β expression, suggesting that Tregs may contribute to the development of alveolar epithelium and lung vascular endothelium. To further explore the role of Tregs during the period of extensive lung cell proliferation, a Treg-depleted mouse model was established by intraperitoneally injecting anti-CD25 antibodies. Flow cytometry revealed that the number of Tregs was significantly downregulated in the Treg-depleted group, the expression of CD4 mRNA and CD4 protein also decreased significantly after Treg-depleted, this suggests that CD25 blockade only affects Treg and has less impact on T cells. Compared with that in the control group, pulmonary alveolar development was significantly delayed in the Treg-depleted group at the same developmental stage. This delay was characterized by decreased alveolar count, alveolar septal thickening, and SFTPC downregulation. These findings suggest that Treg depletion impairs physiological pulmonary alveolar development. Limited studies have examined the role of Tregs in lung development, however, in lung injury models, Treg depletion results in the loss of regenerative capacity in damaged alveolar epithelium. Co-culturing Tregs with AEC IIs directly promotes AEC II proliferation [8]. Furthermore, Catherine F. Dial and others have demonstrated that Tregs exhibit keratinocyte growth factor (KGF) expression. Additionally, in the resolution phase of acute lung injury and the *in vivo* models of regenerating lung alveoli, Treg-specific expression of KGF promotes alveolar epithelial cell proliferation [20]. These results suggest that Tregs may directly promote pulmonary alveolar development by enhancing AEC II proliferation.

In this study, compared with those in the control group, the pulmonary levels of Pecam1 and the microvascular density were downregulated in the Treg-depleted group. Additionally, VEGFA production was downregulated, indicating that the absence of Tregs adversely affects physiological pulmonary vascular development. Tregs are involved in angiogenesis. In particular, Tregs can promote vascular formation directly by upregulating VEGFA and/or IL10 levels or indirectly by influencing other immune cells. During early lung injury

repair, the depletion of Foxp3$^+$ Tregs significantly suppresses pulmonary angiogenesis [21]. However, the transfer of healthy splenic cells into Treg-deficient mice promotes the full recovery of vascular generation. This suggests the role of Tregs in promoting the formation of new vessels in the lungs [22]. In this study, similar to their role in angiogenesis, Tregs may have facilitated pulmonary vascular development by directly regulating VEGFA production.

TGF-β not only influences lung development but also plays a role in T cell regulation [11]. TGF-β is required for the induction of Foxp3 in naive T cells and the development of Tregs, accordingly, Tregs also could mediate their regulation via production of TGF-β [23, 24]. Compared with those in the control group, TGF-β mRNA and protein expression levels decreased significantly in the Treg-depleted group, and there is a positive correlation between TGF-β and Foxp3 in murine lung, but the mechanisms that link Treg to TGF-β remain unknown. It is recognized that mammalian target of rapamycin (mTOR) directly links VEGF in the pulmonary branching morphogenesis program [25], threonine kinase mTOR is a critical target of TGF-β signaling in mouse [26], and mTOR signaling is a wellknown positive regulator of Tregs function under homeostasis [27]. However, further investigation is required to elucidate how CD25 blockade impacts the activation of mTOR in Tregs and lung epithelial cells. Moreover, Tregs may potentially facilitate lung development indirectly through interactions with other immune cells. Tregs can modulate development by inhibiting pro-inflammatory macrophage responses, ultimately promoting the proliferation of distal bronchioalveolar stem cells [28]. Additionally, Tregs could be attributed to the effect of macrophages and the cytokines they released in a lung ischemia mouse model. In a lung ischemia mouse model, Tregs promote angiogenesis via macrophages and the cytokines they released [22]. And Tregs may play roles in lung development by activating ILC2s, which in turn regulate homeostatic and repair processes in the lung [29].

In summary, the abundance of Tregs and the expression of Foxp3 were upregulated during the canalicular and early saccular stages of murine lung development, which was aligned with the extensive proliferation of alveolar epithelial cells and vascular endothelial cells. The depletion of Tregs significantly impaired pulmonary tissue development, which was accompanied by the downregulation of lung development-related factors. This suggests that Tregs contribute to lung development. However, the specific mechanisms and the signaling pathways involved in this process need further investigation.

Author contributions

J-FJ conceived and designed the study. J-FJ, M-YW, and L-YH performed the experiments. J-FJ, YQ, and YZ analyzed the data. J-FJ, M-YW, and H-YL prepared the manuscript. M-YW and H-YL reviewed and edited the manuscript. All authors contributed to the article and approved the submitted version.

Data availability statement

The original contributions presented in the study are included in the article/supplementary material, further inquiries can be directed to the corresponding author.

Ethics statement

The animal study was approved by the Ethics Committee of Experimental Animals at Jiangsu University. The study was conducted in accordance with the local legislation and institutional requirements.

Funding

The author(s) declare financial support was received for the research, authorship, and/or publication of this article. The present review was financially supported by the Natural Science Foundation of China (No. 82171702), Zhenjiang Science and Technology Innovation funds-Clinical Medicine Key Laboratory (SS2023012).

Conflict of interest

The authors declare that the research was conducted in the absence of any commercial or financial relationships that could be construed as a potential conflict of interest.

References

1. Schittny JC. Development of the lung. *Cel Tissue Res* (2017) **367**:427–44. doi:10.1007/s00441-016-2545-0

2. Barkauskas CE, Cronce MJ, Rackley CR, Bowie EJ, Keene DR, Stripp BR, et al. Type 2 alveolar cells are stem cells in adult lung. *J Clin Invest* (2013) **123**:3025–36. doi:10.1172/jci68782

3. Chinoy MR, Graybill MM, Miller SA, Lang CM, Kauffman GL. Angiopoietin-1 and VEGF in vascular development and angiogenesis in hypoplastic lungs. *Am J Physiology-Lung Cell Mol Physiol* (2002) **283**(1):L60–L66. doi:10.1152/ajplung.00317.2001

4. Li J, Tan J, Martino MM, Lui KO. Regulatory T-cells: potential regulator of tissue repair and regeneration. *Front Immunol* (2018) **9**:585. doi:10.3389/fimmu.2018.00585

5. Zhang B, Sun J, Yuan Y, Ji D, Sun Y, Liu Y, et al. Proximity-enabled covalent binding of IL-2 to IL-2Rα selectively activates regulatory T cells and suppresses

autoimmunity. *Signal Transduction Targeted Ther* (2023) **8**:28. doi:10.1038/s41392-022-01208-3

6. Georgiev P, Charbonnier LM, Chatila TA. Regulatory T cells: the many faces of Foxp3. *J Clin Immunol* (2019) **39**:623–40. doi:10.1007/s10875-019-00684-7

7. Zacchigna S, Martinelli V, Moimas S, Colliva A, Anzini M, Nordio A, et al. Paracrine effect of regulatory T cells promotes cardiomyocyte proliferation during pregnancy and after myocardial infarction. *Nat Commun* (2018) **9**:2432. doi:10.1038/s41467-018-04908-z

8. Mock JR, Garibaldi BT, Aggarwal NR, Jenkins J, Limjunyawong N, Singer BD, et al. Foxp3+ regulatory T cells promote lung epithelial proliferation. *Mucosal Immunol* (2014) **7**:1440–51. doi:10.1038/mi.2014.33

9. Zhong Q, Jenkins J, Moldobaeva A, D'Alessio F, Wagner EM. Effector T cells and ischemia-induced systemic angiogenesis in the lung. *Am J Respir Cel Mol Biol* (2016) **54**:394–401. doi:10.1165/rcmb.2015-0087oc

10. Yang S, Liu Y, Li MY, Ng CSH, Yang SL, Wang S, et al. FOXP3 promotes tumor growth and metastasis by activating Wnt/β-catenin signaling pathway and EMT in non-small cell lung cancer. *Mol Cancer* (2017) **16**:124. doi:10.1186/s12943-017-0700-1

11. Saito A, Horie M, Nagase T. TGF-B signaling in lung health and disease. *Int J Mol Sci* (2018) **19**:2460. doi:10.3390/ijms19082460

12. De Lisser HM, Christofidou-Solomidou M, Strieter RM, Burdick MD, Robinson CS, Wexler RS, et al. Involvement of endothelial PECAM-1/CD31 in angiogenesis. *Am J Pathol* (1997) **151**(3):671–7.

13. Pan H, Deutsch GH, Wert SE, On behalf of the Ontology Subcommittee, NHLBI Molecular Atlas of Lung Development Program Consortium. Comprehensive anatomic ontologies for lung development: a comparison of alveolar formation and maturation within mouse and human lung. *J Biomed Semantics* (2019) **10**:18. doi:10.1186/s13326-019-0209-1

14. Johansson J, Curstedt T. Synthetic surfactants with SP-B and SP-C analogues to enable worldwide treatment of neonatal respiratory distress syndrome and other lung diseases. *J Intern Med* (2018) **285**:165–86. doi:10.1111/joim.12845

15. Meng X, Cui G, Peng G. Lung development and regeneration: newly defined cell types and progenitor status. *Cell Regen* (2023) **12**:5. doi:10.1186/s13619-022-00149-0

16. Ruaro B, Salton F, Braga L, Wade B, Confalonieri P, Volpe MC, et al. The history and mystery of alveolar epithelial type II cells: focus on their physiologic and pathologic role in lung. *Int J Mol Sci* (2021) **22**:2566. doi:10.3390/ijms22052566

17. Myint MZZ, Jia J, Adlat S, Oo ZM, Htoo H, Hayel F, et al. Effect of low VEGF on lung development and function. *Transgenic Res* (2021) **30**:35–50. doi:10.1007/s11248-020-00223-w

18. Meller S, Bhandari V. VEGF levels in humans and animal models with RDS and BPD: temporal relationships. *Exp Lung Res* (2012) **38**:192–203. doi:10.3109/01902148.2012.663454

19. van der Veeken J, Campbell C, Pritykin Y, Schizas M, Verter J, Hu W, et al. Genetic tracing reveals transcription factor Foxp3-dependent and Foxp3-independent functionality of peripherally induced Treg cells. *Immunity* (2022) **55**:1173–84.e7. doi:10.1016/j.immuni.2022.05.010

20. Dial CF, Tune MK, Doerschuk CM, Mock JR. Foxp3+ regulatory T cell expression of keratinocyte growth factor enhances lung epithelial proliferation. *Am J Respir Cel Mol Biol* (2017) **57**:162–73. doi:10.1165/rcmb.2017-0019oc

21. Lužnik Z, Anchouche S, Dana R, Yin J. Regulatory T cells in angiogenesis. *J Immunol* (2020) **205**:2557–65. doi:10.4049/jimmunol.2000574

22. D'Alessio FR, Zhong Q, Jenkins J, Moldobaeva A, Wagner EM. Lung angiogenesis requires CD4(+) forkhead homeobox protein-3(+) regulatory T cells. *Am J Respir Cel Mol Biol* (2015) **52**:603–10. doi:10.1165/rcmb.2014-0278oc

23. Gutcher I, Donkor M, Ma Q, Rudensky A, Flavell R, Li M. Autocrine transforming growth factor-β1 promotes In Vivo Th17 cell differentiation. *Immunity* (2011) **34**:396–408. doi:10.1016/j.immuni.2011.03.005

24. Moreau JM, Velegraki M, Bolyard C, Rosenblum MD, Li Z. Transforming growth factor–β1 in regulatory T cell biology. *Sci Immunol* (2022) **7**:eabi4613. doi:10.1126/sciimmunol.abi4613

25. Caldeira I, Fernandes-Silva H, Machado-Costa D, Correia-Pinto J, Moura RS. Developmental pathways underlying lung development and congenital lung disorders. *Cells* (2021) **10**:2987. doi:10.3390/cells10112987

26. Viel S, Marçais A, Guimaraes FS-F, Loftus R, Rabilloud J, Grau M, et al. TGF-β inhibits the activation and functions of NK cells by repressing the mTOR pathway. *Sci Signaling* (2016) **9**:ra19. doi:10.1126/scisignal.aad1884

27. Huang H, Long L, Zhou P, Chapman NM, Chi H. mTOR signaling at the crossroads of environmental signals and T-cell fate decisions. *Immunological Rev* (2020) **295**:15–38. doi:10.1111/imr.12845

28. Garibaldi BT, D'Alessio FR, Mock JR, Files DC, Chau E, Eto Y, et al. Regulatory T cells reduce acute lung injury fibroproliferation by decreasing fibrocyte recruitment. *Am J Respir Cel Mol Biol* (2013) **48**:35–43. doi:10.1165/rcmb.2012-0198oc

29. Loering S, Cameron GJM, Starkey MR, Hansbro PM. Lung development and emerging roles for type 2 immunity. *J Pathol* (2019) **247**:686–96. doi:10.1002/path.5211

EBM Experimental Biology and Medicine

TYPE Original Research
PUBLISHED 08 April 2024
DOI 10.3389/ebm.2024.10035

OPEN ACCESS

*CORRESPONDENCE
Haiyan Liu,
haiyan0326@163.com
Lifeng Sun,
lifengsun2008@163.com

‡These authors have contributed equally to this work and share first authorship

RECEIVED 15 October 2023
ACCEPTED 21 March 2024
PUBLISHED 08 April 2024

CITATION
Wang L, Jin Y, Chen Y, Zhao P, Shang X, Liu H and Sun L (2024), Clinical and genetic characteristics of Chinese patients with Shwachman Diamond syndrome: a literature review of Chinese publication.
Exp. Biol. Med. 249:10035.
doi: 10.3389/ebm.2024.10035

Clinical and genetic characteristics of Chinese patients with Shwachman Diamond syndrome: a literature review of Chinese publication

Lijun Wang‡, Youpeng Jin‡, Yuan Chen, Ping Zhao, Xiaohong Shang, Haiyan Liu * and Lifeng Sun*

Department of Pediatrics, Shandong Provincial Hospital Affiliated to Shandong First Medical University, Jinan, China

Abstract

Shwachman Diamond syndrome (SDS) is a rare autosomal recessive genetic disorder and due to its complex and varied clinical manifestations, diagnosis is often delayed. The purpose of this study was to investigate the clinical manifestations and genetic characteristics of SDS in Chinese patients, in order to increase pediatricians' awareness of SDS and to allow early diagnosis. We conducted a search to identify patients presenting SBDS gene pathogenic variant in two Chinese academic databases. We analyzed and summarized the epidemiology, clinical features, gene pathogenic variants, and key points in the diagnosis and treatment of SDS. We reviewed the clinical data of 39 children with SDS from previously published articles. The interval from the onset of the first symptoms to diagnosis was very long for most of our patients. The age of presentation ranged from 1 day to 10 years (median: 3 months). However, the age of diagnosis was significantly delayed, ranging from 1 month to 14 years (median: 14 months). Hematological abnormalities were the most common presentation, 89.7% (35/39) at the beginning and 94.9% (37/39) at diagnosis of SDS. Diarrhea was the second most common clinical abnormality at the time of diagnosis. 59% (23/39) of patients had a typical history of persistent chronic diarrhea. Furthermore, hepatic enlargement or elevation of transaminase occurred in 15 cases (38.5%). 56.4% patients (22/39) had a short stature, and 17.9% (7/39) patients showed developmental delay. Additionally, twenty patients had compound heterozygous pathogenic variants of c.258 + 2T > C and c.183_ 184TA > CT. Children with SDS in China had high incidence rates of chronic diarrhea, cytopenia, short stature, and liver damage. Furthermore, SBDS c.258 + 2T >

C and c.183_ 184TA > CT were the most common pathogenic variants in patients with SDS. The diagnosis of SDS can be delayed if the clinical phenotype is not recognized by the health care provider.

KEYWORDS

child, clinical presentation, diarrhea, gene pathogenic variant, hematological abnormality

Impact statement

Shwachman Diamond syndrome (SDS) is a rare autosomal recessive genetic disorder and due to its complex and varied clinical manifestations, diagnosis is often delayed. This study investigated the clinical manifestations and genetic characteristics of SDS in Chinese patients to increase health care provider's awareness of SDS and to allow early diagnosis.

Introduction

Shwachman Diamond syndrome (SDS) is an autosomal recessive genetic disease. Common clinical features of SDS are exocrine pancreatic dysfunction, bone marrow failure, congenital abnormalities, and susceptibility to myelodysplastic disorders (MDS) and leukemia, especially acute myeloid leukemia (AML). SDS was first described in the 1960 s and its estimated incidence is 1:77,000 to 1:100,000 [1–3]. This condition is rarely identified in adult patients [3, 4].

As this disease is rarely encountered in the clinic, the reported incidence rate in Europe and the United States is only approximately 0.5/100 000–1.5/100 000 [4–6]. The related literature mostly reports individual case or sporadic small samples. The incidence of SDS is low and clinical understanding is insufficient. In addition, some patients show atypical symptoms. Therefore, it is often misdiagnosed or mismanaged, leading to disease progression and/or life-threatening complications. Therefore, to improve the understanding and diagnosis of SDS in Chinese children, it is necessary to comprehensively summarize cases available in the literatures. Herein, we discuss the presentation and characteristic features of SDS over the past 11 years based on data of 39 patients from two Chinese academic databases. We identified a variety of clinical manifestations of SDS in Chinese children, providing clues for the diagnosis of SDS.

Materials and methods

We performed a literature search in two Chinese academic databases, namely Wan Fang Medical Online and the China National Knowledge Infrastructure for articles published from January 2010 to April 2021, using the keywords "Shwachman Diamond syndrome," "SDS," and "SBDS" in Chinese. We downloaded and reviewed these papers. Only patients with *SBDS* pathogenic variants confirmed by genetic testing were included in the study. Thirteen studies met the inclusion criteria, and data from a total of 39 patients were included [7–19].

Neutropenia was defined as an absolute neutrophil count (ANC) $\leq 1.5 \times 10^9$/L, hemoglobin (Hb) below the normal age-related range was used to define anemia (children aged 6 months to 6 years at Hb levels less than 110 g/L, and children aged 6–14 years are considered anemic when Hb levels are less than 120 g/L), and thrombocytopenia was defined by a platelet count $\leq 150 \times 10^9$/L with no other obvious cause of thrombocytopenia [20]. If the patient has any of these conditions, it is cytopenia. While pancytopenia means a patient has all of these conditions. Pancreatic insufficiency was confirmed by measuring serum trypsinogen (patients aged <3 years), serum amylase (patients aged >3 years), fecal elastase, or 72 h fecal fat [4, 20]. Developmental delay is determined with a child does not attain developmental milestones as compared to peers from the same population [21].

We conducted a comprehensive statistical analysis of the above data and summarized the characteristics of clinical manifestations and the results of genetic tests.

Results

In our study, information on 39 SDS patients that was published in articles from two Chinese databases were included. In all cases, genetic testing confirmed the presence of pathogenic variants in *SDS*. There was a slight male predominance, with 22 male (56.4%) and 17 female (43.6%) patients. The male: female ratio was 1.3:1. The age of presentation was 1 day–10 years (median: 3 months). However, the age at diagnosis was significantly delayed, ranging from 1 month to 14 years (median: 14 months). Only 17.9% (7/39) patients showed a classic presentation of diarrhea-associated neutropenia after onset. Most children were misdiagnosed with infectious or allergic diarrhea, periodic granulocytopenia, immune thrombocytopenia (ITP), hemolytic anemia, aplastic anemia, and rheumatoid arthritis at the time of presentation (Table 1).

First clinical manifestations

Among the 39 children with SDS, the most common initial presentation was hematological abnormalities (35 cases, 89.7%). Furthermore, 1 (2.6%), 11 (28.2%) and 14 (35.9%) patients had thrombocytopenia, neutropenia, and anemia,

respectively. Another 5 (12.8%) had neutropenia and anemia simultaneously. One (2.6%) patient had anemia and thrombocytopenia. In addition, three children had pancytopenia. The second-most common initial presentation was fever or infections. Fifteen (38.5%) patients visited the hospital for blood tests and received antibiotics therapy because of fever or infections. They usually had recurrent respiratory and other infections in the early stages of the disease due to cytopenia, especially neutropenia. Some patients were considered to have an immune deficiency disorder. Less than 40% of patients (14 cases, 35.9%) had chronic steatorrhea at the beginning. Transaminase elevation was the first clinical manifestation in 9 (23.1%) patients. Two patients consulted doctors for intellectual disability or growth retardation. Another three patients were admitted to the hospital for dyspnea, hearing impairment, and genu valgum, respectively.

TABLE 1 Initial presentation of SDS patients.

Initial presentation	Number of patients (n = 39)
Sex	
Male	22 (56.4%)
Female	17 (43.6%)
Age of presentation	
Youngest age	1 day
Oldest age	10 years
Median age	3 months
Age at diagnosis	
Youngest age	1 day
Oldest age	14 years
Median age	14 months
Hematological abnormalities (first CBC)	
Neutropenia	11 (28.2%)
Anemia	14 (35.9%)
Thrombocytopenia	1 (2.6%)
Neutropenia and anemia	5 (12.8%)
Anemia and thrombocytopenia	1 (2.6%)
Pancytopenia	3 (7.7%)
Fever or infections	15 (38.5%)
Diarrhea	14 (35.9%)
Transaminase elevation	9 (23.1%)
Intellectual disability or growth retardation	2 (5.13%)
Liver, spleen, and lymph nodes were swollen	1 (2.6%)
Hearing impairment	1 (2.6%)
Genu valgum	1 (2.6%)
Dyspnea	1 (2.6%)

Characteristic clinical manifestations

The interval from the onset of the first symptoms to diagnosis was very long for most of our patients, with a median duration of 12 months. More than 15 children were diagnosed >2 years after the initial presentation. The characteristic clinical manifestations of the children at diagnosis are shown in Table 2 and summarized as follows (Table 2).

Hematologic abnormality at clinical presentation

Hematological abnormalities were the most common clinical abnormality at the time of diagnosis

Briefly, 37 (94.9%) patients had hematologic abnormalities at the time of diagnosis. Neutropenia (ANC $\leq 1.5 \times 10^9$/L) and anemia occurred in 11 (28.2%) and 8 (20.5%) patients, respectively. No patient presented only thrombocytopenia (PLT $\leq 150 \times 10^9$/L). Thirteen patients presented neutropenia together with anemia or thrombocytopenia; five had pancytopenia, four were diagnosed with aplastic anemia (AA), and one patient was diagnosed with AML. A 10-year-old patient initially diagnosed with hypocellular MDS presented neutropenia and mild thrombocytopenia, but there was no history of steatorrhea or failure to thrive or cytopenia.

Diarrhea was the second most common clinical abnormality at the time of diagnosis

Overall, 59% (23/39) of the patients had a typical history of persistent chronic diarrhea. Routine stool examination showed steatorrhea, often with fat droplets, but no red blood cells or pus cells. Most the patients had a history of chronic diarrhea in childhood, which chronic diarrhea resolved and recovered spontaneously in a few years. The results of the serum lipase and/or amylase test were reported in 13 cases, and 11 (28.2%) had a significant reduction in pancreatic enzyme levels, and the remaining two cases had no history of diarrhea. Pancreatic lipomatosis was observed by computerized tomography (CT) or ultrasound in 16 patients (41%).

Liver function tests

Hepatic enlargement (was assessed by ultrasound) or transaminase elevation occurred in 15 cases (38.5%). None of the cases showed positive test results for serotype B or C hepatopathy with diagnostic values. Transaminase levels were restored to normal after treatment by compound glycyrrhizin.

Growth and skeletal abnormalities

Twenty-two (56.4%) patients had short stature, 17 (43.6%) presented with skeletal abnormalities, including metaphyseal

chondrodysplasia, osteoporosis/osteomalacia and thoracic cage defects, and 5 (12.8%) patients presented teeth abnormalities such as tooth loss and enamel dysplasia.

Neurologic disorder

Seven (17.9%) patients exhibited developmental delay, 4 (10.3%) had general weakness/hypotonia, and 2 (5.1%) had underdeveloped myelination. Additionally, one patient had convulsive, one patient had cognitive and attention deficits, one patient had encephalatrophy.

Other anomalies

Some patients showed non-classical presentations. One patient with developmental delay had congenital heart disease (patent ductus arteriosus and patent foramen ovale) and hypospadias. Another patient with developmental delay presented atrial septal defect and patent foramen ovale. Furthermore, one newborn had severe dyspnea after birth. The chest radiograph showed that the rib cage was narrow and that the posterior ribs were obviously bent downward in an arched shape. However, none of the patients had obvious facial features or skin lesions or pigmentation common to other types of inherited bone marrow failure syndrome.

Genetic testing

Genetic testing was carried out in all 39 patients. 23 patients showed *SBDS* heterozygous of c.258 + 2T > C and c.183_184TA>CT, 11 patients had c.258 + 2T > C homozygous pathogenic variants, 3 patients had heterozygous pathogenic variants of c.258 + 2T > C or c.183_ 184TA > CT combined with other pathogenic variants, and one patient had c.8T > C homozygous pathogenic variants. In addition, one patient showed *SRP54* heterozygous pathogenic variants of c.349_351de1 (p.T117de1) (Table 3).

TABLE 2 Characteristic clinical manifestations of SDS at diagnosis.

Clinical manifestations	Number of patients (n = 39)
Hematological abnormalities	
Neutropenia	11 (28.2%)
Anemia	8 (20.5%)
Neutropenia and anemia	10 (25.6%)
Neutropenia and thrombocytopenia	3 (7.7%)
Pancytopenia	5 (12.8%)
Diarrhea	23 (59%)
Pancreatin decrease	11 (28.2%)
Pancreatic fatty infiltration (CT or ultrasound)	16 (41%)
Transaminase elevation	15 (38.5%)
Teeth Anomalies	5 (12.8%)
Skeletal Anomalies	17 (43.6%)
Short stature	22 (56.4%)
Neurological problems	
Developmental delay	7 (17.9%)
Generalized weakness/hypotonia	4 (10.3%)
Myelination is underdeveloped	2 (5.1%)
Convulsive	1 (2.6%)
Cognitive and attention deficits	1(2.6%)
Encephalatrophy	1 (2.6%)
Congenital anomalies	
Atrial septal defect	1 (2.6%)
Patent foramen ovale	2 (5.1%)
Patent ductus arteriosus	1 (2.6%)
Hypospadias	1 (2.6%)
Others	
Arthritis	1 (2.6%)
Transformation	6 (15.4%)
AML	1 (2.6%)
MDS	1 (2.6%)
AA	4 (10.3%)

Discussion

SDS is an autosomal recessive disorder with an incidence of 1:77,000 to 1:100,000 [1]. In 1964, scientists from the United States (Shwachman, Diamond, Oski, and Khaw) and Great Britain (Bodian, Sheldon and Lightwood) reported a series of young patients who developed exocrine pancreatic insufficiency with diarrhea and hematologic abnormalities (especially neutropenia, but also varying degrees of thrombocytopenia and anemia) and subsequently failed to develop normally in infancy [3]. The most prominent symptom in childhood is persistent diarrhea, malnutrition, and growth failure due to fat replacement of pancreatic acinar tissue; however, approximately 50% of patients improve spontaneously with age. In our study, the initial symptom was diarrhea in 14 (35.9%) patients. Only seven (17.9%) patients were >5 years of age at the time of onset. Among the older children, four had no symptoms of diarrhea, but all had anemia or neutropenia. A previous study reported that some patients with SDS only exhibited hematologic abnormalities without any gastrointestinal symptoms [22]. Our study showed that the clinical manifestations of SDS in Chinese children were the same as those in other regions.

Several research groups have studied the hematologic features of patients with SDS [23, 24]. Neutropenia, typically defined as a neutrophil count less than 1.5×10^9/L, is the most common hematologic abnormality and affects 88–100% of

TABLE 3 *SBDS* genetic mutations.

SBDS mutation		Number of patients (n = 39)
c.183_ 184TA>CT, c.258 + 2T>C	compound heterozygous	20 (51.3%)
c.258 + 2T>C	homozygous	11 (28.2%)
c.183_184TA > CT, c.258+2T > C, 292_295delAAAG	compound heterozygous	3 (7.7%)
c.258+2T > C, c.23A > T	compound heterozygous	1 (2.6%)
c.183_184TA > CT, c.201A > G	compound heterozygous	1 (2.6%)
c.8T>C	homozygous	1 (2.6%)
c.258 + 2T>C, c.634_635insAACATACCTGT, c.637_638delGA	compound heterozygous	1 (2.6%)
c.349_351de1 (p. T117del)[a]	heterozygous[a]	1 (2.6%)

[a]This is heterozygous mutation of *SRP54* gene. It is inherited in an autosomal recessive manner.

patients with SDS. MDS and AML are severe life-threatening complications of SDS [24]. In our study, 29 (74.4%) patients had neutropenia. Four (10.3%) patients were diagnosed with AA. An 8-year-old boy developed AML and another 12-year-old patient developed MDS. Previous research showed that the incidence of AML in SDS ranges from 18% to 36% in individuals over 20–30 years, and most patients showing progression to AML are relatively older [25]. Our results were lower than this range. Many pediatricians do not fully understand SDS, and may not do genetic testing and make a proper diagnosis in a timely manner, which may be the main reason.

SDS pancreatic exocrine deficiency typically occurs during the first year of newborn life and is caused by pancreatic acinar cell reduction and fat infiltration. The main manifestations of pancreatic failure are decreased pancreatic elastase content, decreased fat-soluble vitamin content, and increased fecal fat content leading to diarrhea. All these characteristics can often be observed in patients with SDS. Radiographically, magnetic resonance imaging can show pancreatic lipomas. In our study, 23 (62.2%) patients had a typical history of persistent chronic steatorrhea. Two of these patients (cases 11 and 13) were 5 and 6 years old, respectively, and had a history of chronic diarrhea in childhood. Pancreatic lipomatosis was observed in 16 patients.

Other common anomalies, such as hepatomegaly and abnormal liver biochemical tests, are both observed in younger patients. Studies have found that elevated transaminase levels and liver enlargement would gradually return to normal around 5 years of age, which can pose challenges in differential diagnosis. Skeletal abnormalities often occur in late childhood and can occur in 30–50% of patients, including delayed maturation, metaphyseal chondrodysplasia of the long bones, and thoracic abnormalities with thickening of the costal cartilage. Short stature was observed in 22 (56.4%) patients in our study. Some patients had osteoporosis, enamel dysplasia, or cartilage with metaphyseal dysplasia. Some patients were found to have neurological, learning, and/or behavioral disorders [26]. Children with SDS can have significant limitations in academic performance, advanced language skills, intellectual reasoning and perception, including reasoning and visual motor skills [27]. Developmental delay; generalized weakness/hypotonia; underdeveloped myelination; convulsive, cognitive, and attention deficits; and encephalatrophy were found in our study. In addition, some congenital anomalies were presented in our study. One patient had patent foramen ovale, patent arteriosus ductus, and hypospadias. Another patient had atrial septal defect and patent foramen ovale. A wide variety of congenital abnormalities involving the heart, gastrointestinal tract, kidneys, nerves, urinary system, and other organ systems have previously been reported. However, no studies have yet demonstrated that these congenital abnormalities are specific manifestations of SDS.

Chromosome 7q11 plays an important role in bone marrow cell proliferation, mitosis, and the matrix microenvironment, and more than 90% of patients with SDS carry biallelic pathogenic variants in the *SBDS* gene on chromosome 7q11 [1]. We searched for gene pathogenic variants reported in both cases and literature of *SBDS* in the Human Gene Mutation Database (HGMD®). A total of 97 pathogenic variants in the *SBDS* gene were reported and included 59% missense/nonsense pathogenic variants, 11% splicing events, 10% small deletions, 1% small insertion, 6% small indel, and 4% gross deletions, 1% gross insertions, and 8% complex rearrangements (Figure 1). The most common genetic pathogenic variants were c.258 + 2T > C and c.183_184TA > CT [28, 29]. Similarly, in our study, 20 patients had heterozygous pathogenic variants of c.258 + 2T > C and c.183_184TA > CT. Eleven patients harbored c.258 + 2T > C homozygous pathogenic variants, while 7 patients presented heterozygous pathogenic variants of c.258 + 2T > C or c.183_184TA > CT combined with other pathogenic variants. Though the identification of *SBDS* in 2003, *DNAJC21*, *EFL1,* and *SRP54* genes also have been reported causal SDS. In our patients, there was one patient showed *SRP54* heterozygous pathogenic variants. Approximately 90% of patients with typical presentation have

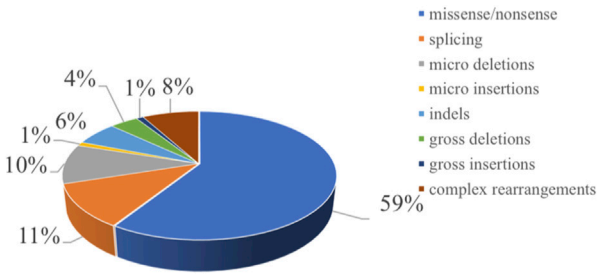

FIGURE 1
Distribution of the mutation spectrum in SBDS reported in HGMD. A total of 97 mutations in SBDS gene including 59% missense/nonsense mutations, II% splicing, 10% micro deletions, 1% micro insertion, 6% mmicro indels, and 4% gross deletions, 1% gross insertions, and 8% complex rearrangements. The mutations in our patients were all documented by HGMD. Missense mutation/nonsense mutation means the codon encoding an amino acid is replaced by a codon of another amino acid by a base, resulting in a change in the amino acid type and sequence of the polypeptide chain. Splicing is a type of mutation that changes the splicing mode of RNA precursors due to mutations in the splicing donor or acceptor sites or conserved sequences on their sides, so that the resulting mature RNA contains introns or missing exon sequences. Micro deletion/insertion refers to the deletion or insertion of a certain point base of the DNA molecule, causing a change in the reading framework, resulting in a series of downstream code changes, so that the original gene encoding a peptide chain into another completely different peptide chain sequence. Insertion—deletion mutations (indels) refer to insertion and/or deletion of nucleotides into genomic DNA and include events less than I kb in length. Gross deletion/insertion means single exon or multiple exons missing/inserted. Complex rearrangements refers to repetitive replication, inversion, translocation, and inter-chromosome trans-location occur in a region within the chromosome. Usually refers to the deletion, insertion, duplication, inversion, translocation, and change in copy number variants (CNVs) of DNA fragments larger than 1 kb in the genome.

pathogenic variants in the *SBDS* gene, but 10% of patients with clinically diagnosed SDS may not have any known pathogenic variant. However, it remains unclear whether these *SBDS* pathogenic variant-negative patients represent different genetic variations in SDS. Therefore, the limitation of this study is that only *SBDS* pathogenic variant-positive SDS were included. Additional clinical and molecular studies are needed to further characterize *SBDS* pathogenic variant-negative patients.

All the clinical features of SDS can occur during childhood and adolescence. Therefore, the clinical diagnosis is usually established in children and only sometimes in adults. *SDBS* genotyping should always be performed for confirmation. The early diagnosis of SDS is challenging, especially in the neonatal period. Through a multidisciplinary approach to the prevention and treatment of symptoms, the early diagnosis of SDS may improve the overall healthcare of patients. The early diagnosis of SDS is crucial to monitor the risk and clinical symptoms of hematologic malignancies. To avoid delayed treatment and to ensure timely detection of the risk of developing MDS or AML, children with recurrent liver dysfunction with unknown etiology and failure to thrive are recommended early genetic testing of SDS [30].

To date, no specific treatment for SDS has been established. Therefore, a multidisciplinary approach to SDS management may be useful. For gastrointestinal manifestations, the primary treatment is pancreatic enzyme therapy, medium chain triglycerides, and fat-soluble vitamin supplements, along with a normal to high-fat diet. Although most SDS-positive individuals present some hematological manifestations of their disease, most do not require transplantation. In SDS, the estimated risk of the development of myelodysplastic syndrome and AML is 19% at 20 years and 36% at 30 years [24]. Recent studies have indicated that for patients with SDS who develop BMF or convert to myeloid malignancy, hematopoietic stem cell transplantation is the only curative approach for the disease. However, transplantation does not prolong the survival of those children. Therefore, further research is needed to improve patient outcomes.

Conclusion

Our study reveals a wide range of clinical presentations for SDS. Analysis of Chinese patients showed that children with SDS in China had high incidence rates of chronic diarrhea, cytopenia, short stature, and liver damage. Furthermore, the most common genetic pathogenic variants in patients with SDS were *SBDS* c.258 + 2T > C and c.183_ 184TA > CT. The diagnosis of SDS can be delayed if the clinical phenotype is not recognized by the health care provider.

Author contributions

All authors listed have made a substantial, direct, and intellectual contribution to the work and approved it for publication.

Data availability statement

The original contributions presented in the study are included in the article/Supplementary material, further inquiries can be directed to the corresponding authors.

Ethics statement

Ethical approval was not required for the study involving humans in accordance with the local legislation and institutional requirements. Written informed consent to participate in this study was not required from the participants or the participants' legal guardians/next of kin in accordance with the national legislation and the institutional requirements.

Funding

The author(s) declare financial support was received for the research, authorship, and/or publication of this article. This study was supported by a grant from Natural Science Foundation of Shandong Province, China (ZR2020MH144).

Conflict of interest

The authors declare that the research was conducted in the absence of any commercial or financial relationships that could be construed as a potential conflict of interest.

References

1. Myers KC, Furutani E, Weller E, Siegele B, Galvin A, Arsenault V, et al. Clinical features and outcomes of patients with Shwachman-Diamond syndrome and myelodysplastic syndrome or acute myeloid leukaemia: a multicentre, retrospective, cohort study. *Lancet Haematol* (2020) **7**(3):e238–e246. doi:10.1016/s2352-3026(19)30206-6

2. Higashi O, Hayashi T, Ohara K, Honda Y, Konno T, Sato Y, et al. Pancreatic insufficiency with bone marrow dysfunction (Shwachman-Diamond-Oski-Khaw's syndrome). Report of a case. *Tohoku J Exp Med* (1967) **92**(1):1–12. doi:10.1620/tjem.92.1

3. Shwachman H, Diamond LK, Oski FA, Khaw KT. The syndrome of pancreatic insufficiency and bone marrow dysfunction. *J Pediatr* (1964) **65**:645–63. doi:10.1016/s0022-3476(64)80150-5

4. Dror Y, Donadieu J, Koglmeier J, Dodge J, Toiviainen-Salo S, Makitie O, et al. Draft consensus guidelines for diagnosis and treatment of Shwachman-Diamond syndrome. *Ann N Y Acad Sci* (2011) **1242**:40–55. doi:10.1111/j.1749-6632.2011.06349.x

5. Mercuri A, Cannata E, Perbellini O, Cugno C, Balter R, Zaccaron A, et al. Immunophenotypic analysis of hematopoiesis in patients suffering from Shwachman-Bodian-Diamond Syndrome. *Eur J Haematol* (2015) **95**(4):308–15. doi:10.1111/ejh.12490

6. Minelli A, Nicolis E, Cannioto Z, Longoni D, Perobelli S, Pasquali F, et al. Incidence of shwachman-diamond syndrome. *Pediatr Blood Cancer* (2012) **59**(7):1334–5. doi:10.1002/pbc.24260

7. Xianhao W, Jianwen X, Jie Y, Ying X, Xxianmin G, Yuxia G. Five cases of Shwachman-Diamond Syndrome in children and literature review. *Chin J Curr Pediatr* (2013) **15**(11):970–4.

8. Rong L, Xiaodong S, Ziqin L, Minye L, Lei Z, Jing C, et al. Case report: clinical and genetic analysis of Shwachman-Diamond syndrome. *Chin J Hematol* (2010) **31**(8):560–2.

9. Mingshu Y, Li W, Ying G, Yingyan S, Zhongwei Q. Cases report: two children of Shwachman-Diamond syndrome. *Radiol Pract* (2013) **28**(10):1087–8.

10. Chao D, Runhui W, Rui Z, Li Z, Wen Z, Hongyun L, et al. One case of non-diarrhea-onset Shwachman-Diamond syndrome. *Chin J Clin Pediatr* (2016) **31**(8):624–5.

11. Tao J, Wenxian O, Yanfang T, Shuangjie L. Liver pathology and gene analysis in children with Shwachman-Diamond syndrome. *J Clin Pediatr* (2017) **35**(7):540–2.

12. Yan L, Lijun Q, Zhe X, Jie C, Tianping C, Chengjun W, et al. Clinical and genetic analysis of Shwachman-Diamond syndrome in children. *Anhui Med* (2017) **38**(4):430–3.

13. Youjia L, Jie C, Lijun Q, Yan L, Jian W. Clinical analysis of shwachman-Diamond syndrome in two cases. *Fam Med* (2017)(10) 4–5.

14. Jing Z, Shu G, Guoli W, Feihong Y, Tianlu M, Huiqing S, et al. Clinical characteristics and gene analysis of 4 children with Shwachman-Diamond syndrome. *Chin J Pract Pediatr* (2019) **34**(1):50–2.

15. Lu W, Hui Y, Xia W. Shwachman-diamond syndrome: a case report and literature review. *J Clin Pediatr* (2020) **38**(4):294–7.

16. Wenbin A, Chao L, Yang W, Lixian C, Xiaoyan C, Xiaofan Z. Clinical characteristics and gene mutation analysis of children with Shwachman-Diamond syndrome and myeloid malignant transformation. *Chin J Curr Pediatr* (2020) **22**(5):460–5.

17. Pingping W, Lianhua J, Yan L, Guohua W. A case of Shwachman-Diamond syndrome. *Chin Pediatr Emerg Med* (2020) **27**(3):239–40.

18. Mi Y, Bijun S, Jia H, Wenjie W, Wenjing Y, Xiaoying H, et al. Shwachman-diamond syndrome: a report of 8 cases. *Chin J Evid Based Pediatr* (2021) **16**(2):146–51.

19. Xiao L, Juan L, Jian M. A case of neonatal Shwachman-Diamond syndrome and literature review. *Chin Pediatr Emerg Med* (2020) **27**(11):868–70.

20. Rothbaum R, Perrault J, Vlachos A, Cipolli M, Alter BP, Burroughs S, et al. Shwachman-Diamond syndrome: report from an international conference. *J Pediatr* (2002) **141**(2):266–70. doi:10.1067/mpd.2002.125850

21. Choo YY, Agarwal P, How CH, Yeleswarapu SP. Developmental delay: identification and management at primary care level. *Singapore Med J* (2019) **60**(3):119–23. doi:10.11622/smedj.2019025

22. Andolina JR, Morrison CB, Thompson AA, Chaudhury S, Mack AK, Proytcheva M, et al. Shwachman-Diamond syndrome: diarrhea, no longer required? *J Pediatr Hematology/Oncology* (2013) **35**(6):486–9. doi:10.1097/mph.0b013e3182667c13

23. Woods WG, Roloff JS, Lukens JN, Krivit W. The occurrence of leukemia in patients with the Shwachman syndrome. *J Pediatr* (1981) **99**(3):425–8. doi:10.1016/s0022-3476(81)80336-8

24. Donadieu J, Fenneteau O, Beaupain B, Beaufils S, Bellanger F, Mahlaoui N, et al. Classification of and risk factors for hematologic complications in a French national cohort of 102 patients with Shwachman-Diamond syndrome. *Haematologica* (2012) **97**(9):1312–9. doi:10.3324/haematol.2011.057489

25. Myers KC, Davies SM, Shimamura A. Clinical and molecular pathophysiology of Shwachman-Diamond syndrome: an update. *Hematology/Oncology Clin North America* (2013) **27**(1):117–28. doi:10.1016/j.hoc.2012.10.003

26. Özçay F, Olcay L, Ceylaner S, Sezer T, Barış Z. A case of shwachman-diamond syndrome who presented with hypotonia. *J Pediatr Genet* (2018) **07**(3):117–21. doi:10.1055/s-0038-1636997

27. Kerr EN, Ellis L, Dupuis A, Rommens JM, Durie PR. The behavioral phenotype of school-age children with shwachman diamond syndrome indicates neurocognitive dysfunction with loss of Shwachman-Bodian-Diamond syndrome gene function. *J Pediatr* (2010) **156**(3):433–8.e1. doi:10.1016/j.jpeds.2009.09.026

28. Menne TF, Goyenechea B, Sanchez-Puig N, Wong CC, Tonkin LM, Ancliff PJ, et al. The Shwachman-Bodian-Diamond syndrome protein mediates translational activation of ribosomes in yeast. *Nat Genet* (2007) **39**(4):486–95. doi:10.1038/ng1994

29. Ganapathi KA, Austin KM, Lee CS, Dias A, Malsch MM, Reed R, et al. The human Shwachman-Diamond syndrome protein, SBDS, associates with ribosomal RNA. *Blood* (2007) **110**(5):1458–65. doi:10.1182/blood-2007-02-075184

30. Thompson AS, Giri N, Gianferante DM, Jones K, Savage SA, Alter BP, et al. Shwachman Diamond syndrome: narrow genotypic spectrum and variable clinical features. *Pediatr Res* (2022) **92**(6):1671–80. doi:10.1038/s41390-022-02009-8

EBM Experimental Biology and Medicine

TYPE Original Research
PUBLISHED 18 March 2024
DOI 10.3389/ebm.2024.10057

OPEN ACCESS

*CORRESPONDENCE
Fangyuan Wang,
fangyuanwang05@163.com
Shiming Yang,
shm_yang@163.com

†These authors have contributed equally to this work

RECEIVED 22 November 2023
ACCEPTED 20 February 2024
PUBLISHED 18 March 2024

CITATION
Liu P, Xue X, Zhang C, Zhou H, Ding Z, Wang L, Jiang Y, Shen W-D, Yang S and Wang F (2024), Transcriptional-profile changes in the medial geniculate body after noise-induced tinnitus.
Exp. Biol. Med. 249:10057.
doi: 10.3389/ebm.2024.10057

Transcriptional-profile changes in the medial geniculate body after noise-induced tinnitus

Peng Liu[1,2,3†], Xinmiao Xue[1,2,3†], Chi Zhang[2,3], Hanwen Zhou[1,2,3], Zhiwei Ding[1,2,3], Li Wang[1,2,3], Yuke Jiang[1,2,3], Wei-Dong Shen[2,3], Shiming Yang[1,2*] and Fangyuan Wang[3*]

[1]Medical School of Chinese PLA, Beijing, China, [2]Department of Otolaryngology, Head and Neck Surgery, Institute of Otolaryngology, Chinese PLA General Hospital, Beijing, China, [3]National Clinical Research Center for Otolaryngologic Diseases, Beijing, China

Abstract

Tinnitus is a disturbing condition defined as the occurrence of acoustic hallucinations with no actual sound. Although the mechanisms underlying tinnitus have been explored extensively, the pathophysiology of the disease is not completely understood. Moreover, genes and potential treatment targets related to auditory hallucinations remain unknown. In this study, we examined transcriptional-profile changes in the medial geniculate body after noise-induced tinnitus in rats by performing RNA sequencing and validated differentially expressed genes via quantitative polymerase chain reaction analysis. The rat model of tinnitus was established by analyzing startle behavior based on gap-pre-pulse inhibition of acoustic startles. We identified 87 differently expressed genes, of which 40 were upregulated and 47 were downregulated. Pathway-enrichment analysis revealed that the differentially enriched genes in the tinnitus group were associated with pathway terms, such as coronavirus disease COVID-19, neuroactive ligand-receptor interaction. Protein–protein-interaction networks were established, and two hub genes (Rpl7a and AC136661.1) were identified among the selected genes. Further studies focusing on targeting and modulating these genes are required for developing potential treatments for noise-induced tinnitus in patients.

KEYWORDS

tinnitus, transcriptional profile, RNA-sequencing, medial geniculate body, gene

Introduction

Tinnitus, a condition in which people with or without hearing loss perceive phantom sounds, has become a major problem affecting millions of people worldwide. Research related to the epidemiology of tinnitus has demonstrated that nearly 25% of all Americans experience abnormal auditory sensations at least once in their lifetime [1]. When tinnitus becomes chronic (>6 months), various co-morbidities including insomnia, and

psychological disorders, such as anxiety, depression, cognitive dysfunction, and stress, influence the quality of patients' lives and even lead to suicide [2]. Although frequently caused by hearing loss and aging, tinnitus is hearing loss- and age-independent, suggesting that an extremely intricate mechanism mediates the onset of this disease [3]. Current therapeutic strategies for treating tinnitus (including drugs, acoustic stimulation, psychological therapy, and repetitive transcranial magnetic stimulation) have generated conflicting evidence regarding beneficial outcomes and alleviation of the disease [4].

Since tinnitus can persist after the destruction of the auditory nerve, recent studies have attributed the generation of tinnitus to the central auditory pathway, which involves the auditory cortex, medial geniculate body (MGB), inferior colliculus, and cochlear nucleus, instead of the peripheral otologic components [5]. The MGB, an obligate auditory brain center, plays an essential role in transmitting acoustic information from the inferior colliculus to the auditory cortex [6]. Not only is the MGB the principle conduit between the thalamic circuits and the cortex, but that there is evidence for altered firing patterns along this ascending input in animal models of tinnitus [7]. Based on its anatomical features, the MGB is a suitable candidate region for studies related to tinnitus [8]. Previous research indicated that the firing of neurons in the MGB changes from the tonic to burst form, which was found to be a significant indicator of hyperactivity after tinnitus [9]. Inhibition of the abnormal response can equally alleviate oscillations induced by tinnitus between the MGB and auditory cortex [10]. Altered biological function of the MGB can lead to abnormal signal transmissions in the auditory pathways, which can subsequently mediate the development of tinnitus.

In the context of biological traits, genes are important hereditary units that modulate numerous life processes, including birth, illness, and death. Recent advancements in genomics have provided insights into relationships between genes associated with different human diseases and genetic heredity in tinnitus [11]. Animal transcriptomics studies have revealed several genes that are expressed differently after tinnitus, such as NR2B, VGLUT1, BDNF, and Gabrb3 [12–15]. In addition, the results of some studies on patients with tinnitus showed that the expression levels of genes related to cardiovascular function, neurotrophic factors, GABAB receptor subunits, and serotonin transporter function were significantly increased [16–19]. Meanwhile, human genetic studies on tinnitus that have been replicated in an independent cohort also revealed that genes, such as *AF131215.5, BLK, C8orf12, COL11A1, GRK6, MSRA, MFHAS1, XKR6, ANK2, AKAP9,* and *TSC2*, could act as major predictors of the development of tinnitus [11, 20, 21]. Although abundant data have been generated regarding the genetic underpinnings of tinnitus, differentially expressed genes (DEGs) in the MGB remain unclear for this clinical enigma, which limits the development of effective treatments. Exploring potential genes in brain regions that underlie tinnitus vulnerability would lay a foundation for understanding tinnitus pathogenesis and exploring effective intervention strategies.

In this study, we performed RNA-sequencing (RNA-seq) to identify DEGs in the MGB that correlated with noise-induced tinnitus and elucidated related signaling pathways. Two hub genes (*Rpl7a* and *AC136661.1*) in the MGB showed potential as effective therapeutic drug targets.

Materials and methods

Animals

Two-month-old male Sprague–Dawley rats were housed in standard cages (12 h day/night cycle) with a normal humidity (50–60%) and an appropriate temperature (22°C) with food and water *ad libitum*. All procedures were performed in accordance with the requirements of the Care and Use of Laboratory Animals of the Chinese PLA General Hospital. All protocols used in this study were approved by the Animal Ethics Committee of the Chinese PLA General Hospital (Code: 2021-X17-85).

Auditory brainstem responses (ABRs)

The animals included in this study were verified by performing ABR tests, which can be used to study noise exposure. Briefly, the rats were administered sodium pentobarbital intraperitoneally (i.p.) and subsequently placed in a soundproof chamber. Tone and click stimuli (0.5 ms rise or fall) were applied using a TDT loudspeaker (Tucker Davis Technologies, Miami, FL, United States). A tube linked to a TDT RZ6 instrument was placed in the external auditory canal. Before ABR testing, the animals were administered reference, active, and ground needle electrodes (Rochester Elektro-Medical, Lutz, FL, United States). The reference needle was placed on the tested mastoid, whereas the ground needle was set contralaterally, and the active needle inserted into the vertex of the skin. The original sound-pressure level (SPL) was set at 90 dB and then it was decreased in 10 dB steps for both the click and tone stimuli (4, 8, 16, and 32 kHz). The recorded amplified responses were filtered through a passband from 100 Hz to 3 kHz and averaged 512 times. To detect the ABR threshold, repeatable wave-III patterns were monitored at every frequency until they disappeared with decreasing SPLs, and the lowest dB SPL at each frequency was recorded.

Gap detection

The establishment of tinnitus in animals after noise exposure was verified by assessing gap-induced pre-pulse inhibition (PPI)

of the acoustic startle responses, as described previously [22]. Briefly, a cage connected to a piezoelectric transducer was used to detect pressure changes caused by acoustic startles and instantaneously transform them into voltage values that were utilized to evaluate the amplitudes of the acoustic startle response (ASR). The "no-gap" pattern was set using background noise (60 dB SPL) centered at 6, 12, or 16 kHz, inserted with a 115 dB SPL startle stimulus lasting for 20 ms. The "gap" pattern was set using a silent cap (50 ms) delivered 100 ms ahead of the startle stimulus onset, and the results were compared with those obtained using the no-gap pattern. A speaker (controlled using startle software, Xeye, Beijing, China) was installed 20 cm above the platform and linked to the piezoelectric transducer to generate auditory stimuli. Ten paired "gap" and "no-gap" trials were conducted in random order for all tests. The ability of animals to detect gap was estimated by gap: PPI (%) ratio, which was calculated as amplitude of the 1-gap ASR divided by the amplitude of the no-gap ASR. The criteria for tinnitus was as follows: At least the startle ratio of single test frequency before exposure was more than 30% before noise exposure and the startle ratio after exposure is required to be below 30%. In addition, decrease in startle ratio for a single frequency should be more than 30% [23]. Otherwise, the animals are considered as non-tinnitus ones.

Noise exposure

Rats wearing foam earplugs (OHRFRIEDEN, Wehrheim, Germany) unilaterally in the right ear were used in this study. The rats were exposed to loud noise at a frequency from 8–16 kHz (126 dB SPL) for 2 h after being deeply anesthetized with an i.p. injection of sodium pentobarbital [24]. Unilateral noise exposure allowed animals to maintain normal hearing, which was essential for gap detection. The sound-delivery system comprised an RA 300 amplifier (Alesis, Cumberland, RI, United States) and a TW67 speaker (Pyramid Car Audio, Brooklyn, NY, United States). Briefly, the speaker was arranged 10 cm away from the ears of each rat, and the RA 300 amplifier and TDT processor were arranged to generate and amplify the tones. Calibration of the SPL was achieved using a sound-level meter connected to a condenser microphone.

RNA-seq analysis

RNA-seq was performed as described elsewhere [25]. Regions (5.2–6.36 mm posterior to bregma; 3.2–4.2 mm, lateral to the midline; 5.2–6.8 mm ventral to the dorsal surface of the skull) were selected as the target area according to brain atlas of rats. Briefly, MGB tissue samples (n = 3) acquired from the non-tinnitus and tinnitus groups were washed immediately, and processed for RNA isolation using TRIzol reagent (Thermo Fisher Scientific, Wilmington, DE, United States). The RNA concentration and purity of each sample were measured using a NanoDrop 2000 spectrophotometer (Thermo Fisher Scientific). The RNA Nano 6000 Assay Kit was used to assess RNA integrity. Sequencing libraries were generated using the NEBNext UltraTM RNA Library Prep Kit for Illumina (New England Biolabs, United States) according to the manufacturer's recommendations, and index codes were added to attribute the sequences to each sample. Raw data (raw reads) in fastq format were first processed using in-house Perl scripts. To obtain clean data (clean reads), reads containing poly-N sequences, adapters, and low-quality reads were removed from the raw data. Then, the Q20, Q30, GC content, and sequence-duplication levels of the clean data were calculated. After cleaning the data, high-quality data were acquired and downstream analyses were performed.

Bioinformatics analysis

Edge R and DEseq2 packages were used to analyze differential gene expression in tissue samples. A p-value of <0.05 and a fold-change of ≥1.5 were used as criteria for identifying genes that are significantly modulated levels [26]. The GOseq R package and KOBAS software were used to analyze enriched processes and pathways identified using the Gene Ontology (GO) and Kyoto Encyclopedia of Genes and Genomes (KEGG) databases, respectively. The DEGs were uploaded to the STRING database,[1] and protein–protein-interaction analysis was performed. Cytoscape software was used to visualize and select hub genes.

Quantitative polymerase chain reaction (qPCR) analysis

All experimental procedures for RNA extraction used in this study were in accordance with those employed in previous studies [27]. Total RNA (n = 5) was extracted using RNA Extraction Reagent (Servicebio, Wuhan, China) and converted to complementary DNA (cDNA) using the Servicebio RT First Strand cDNA Synthesis Kit (Servicebio). qPCR analysis was performed using 2× SYBR Green qPCR Master Mix (Servicebio). The mRNA-expression levels of the target genes were normalized to glyceraldehyde-3-phosphate dehydrogenase (GAPDH) mRNA-expression levels and fold-changes in expression differences were calculated using the $2^{-\Delta\Delta CT}$ method [28]. The sequences of the oligonucleotide primers (Servicebio) used in this study are shown in Table 1.

1 http://stringdb.org/

TABLE 1 Sequences of primers used for qPCR analysis.

Gene	Forward primer (5′–3′)	Reverse primer (5′–3′)
Fau	GACGGTCGCCCAGATCAAA	GGTTGTACTGCATTCGCCTCTT
Rpl7a	GACAAGGGTGCTCTGGCTAAG	GCAATGCGAGCCACAGACTTA
Rps19	AACCAGCAGGAGTTCGTCAGA	ACCACCACGGAGGTACAGGT
LOC100360491	TTCTCCTCTTCCGTGATGGCT	ATCCACAAGAAAATGGCACGC
LOC685085	AAAGAAGAAGTGGTCCAAAGGCA	CTGTGCTTTGAAACCAGCTTGAT
AC136661.1	TACCTGTTCTCCCTGCCCATT	GTAGTCCCCAATAGCGACAAA
Fos	TCCAAGCGGAGACAGATCAACT	TCAAGTCCAGGGAGGTCACAGA
Ebna1bp2	AAGAAGGCGGTGAATGACGA	GCAAAATAATCAGTGGGCCTCTT
Egr1	CCAAACTGGAGGAGATGATGCT	GACTCTGTGGTCAGGTGCTCGTA
LOC689899	AACAAGCACCAGATCAAACAGG	TGGCAACATCTAGAGCATCATAATC
Gapdh	CTGGAGAAACCTGCCAAGTATG	GGTGGAAGAATGGGAGTTGCT

Statistical analysis

GraphPad Prism software (version 9.0.1; San Diego, CA, United States) was used to analyze the behavioral data generated in this study. The ABR thresholds and changes in GAP-PPI ASR were assessed using two-way ANOVA. Changes in the mRNA level determined using qPCR were examined using non-paired Student's t-test. Data are presented as the mean ± standard error of the mean. $p < 0.05$ was applied as the threshold for statistical significance.

Results

Validation of tinnitus established by noise in rats

Figure 1A shows the experimental design of our study. Figure 1B (left panel) shows that the acoustic threshold of the left ear following a significant increase in the noise level. As depicted in Figure 1B (right panel), the acoustic threshold of the left ear (following the noise increase [post]) was significantly higher than before (pre) the noise when the click stimulus was introduced (pre vs. post, 21.67 ± 1.67 vs. 65.00 ± 8.47, $p < 0.01$). Similar findings were observed with different tone stimuli, including 4 kHz (pre vs. post, 20.00 ± 3.65 vs. 71.67 ± 5.43, $p < 0.01$), 8 kHz (pre vs. post, 21.67 ± 3.07 vs. 67.50 ± 4.79, $p < 0.01$), 16 kHz (pre vs. post, 20.00 ± 2.58 vs. 73.33 ± 7.15, $p < 0.001$), and 32 kHz (pre vs. post, 30.00 ± 5.16 vs. 77.5 ± 6.02, $p < 0.01$). The hearing threshold of the right ear was not significantly different after initiating click stimuli (pre vs. post, 28.33 ± 3.07 vs. 31.67 ± 6.54, $p = 0.66$) or tone stimuli, i.e., 4 kHz (pre vs. post, 25.00 ± 3.42 vs. 31.67 ± 3.07, $p = 0.17$), 8 kHz (pre vs. post, 30.00 ± 4.47 vs. 23.33 ± 4.22, $p = 0.33$), 16 kHz (pre vs. post, 26.67 ± 3.33 vs. 30.00 ± 2.58, $p = 0.58$), and 32 kHz (pre vs. post, 30.00 ± 2.58 vs. 45.33 ± 4.28, $p = 0.06$). Unilateral normal hearing enables animals to detect gaps in background sounds. The experimental design used to assess the ability of the animals to detect gaps is shown in Figure 1C. Animals in the control group exhibited comparable Gap-PPI changes at 6 kHz (pre vs. post, 57.82 ± 6.55 vs. 52.79 ± 7.41%, $p = 0.63$), 12 kHz (pre vs. post, 52.96 ± 5.15 vs. 51.74 ± 3.53%, $p = 0.88$), and 16 kHz (pre vs. post, 47.31 ± 3.56 vs. 49.47 ± 3.24%, $p = 0.68$), as shown in Figure 1D. These findings were equally applicable to the non-tinnitus group, which displayed no significant change at 6 kHz (pre vs. post, 48.74 ± 5.29 vs. 61.24 ± 4.08, $p = 0.11$), 12 kHz (pre vs. post, 50.53 ± 5.58 vs. 39.11 ± 4.18, $p = 0.21$), and 16 kHz (pre vs. post, 55.50 ± 2.89 vs. 44.30 ± 4.47, $p = 0.12$) in terms of gap-PPI detection (Figure 1E). In the tinnitus group, the inhibitory effect of the gap on acoustic startling was attenuated at 6 kHz (pre vs. post, 60.99 ± 7.07 vs. 27.63 ± 5.31, $p < 0.01$, Figure 1F). At 12 kHz, the tendency of decreasing inhibition was also observed, where the gap-PPI decreased from 47.67 ± 4.45% to 13.57 ± 4.03% ($p < 0.01$, Figure 1F). This type of change was equally applicable to a 16 kHz background sound, where the gap-PPI of the tinnitus group decreased from 45.38 ± 3.69% to 15.20 ± 4.79% ($p < 0.01$, Figure 1F). In order to exclude the potential loss of hearing in the plugged ear via damage to binaural ascending afferents [29], the ABR threshold of non-tinnitus and tinnitus group was tested which were shown in Supplementary Figures S1A, S1B. There was a similar ABR threshold change in the non-tinnitus and tinnitus group.

Identification of DEGs

To illuminate transcriptional-profile changes associated with noise-induced tinnitus, we performed RNA-seq analysis of brain

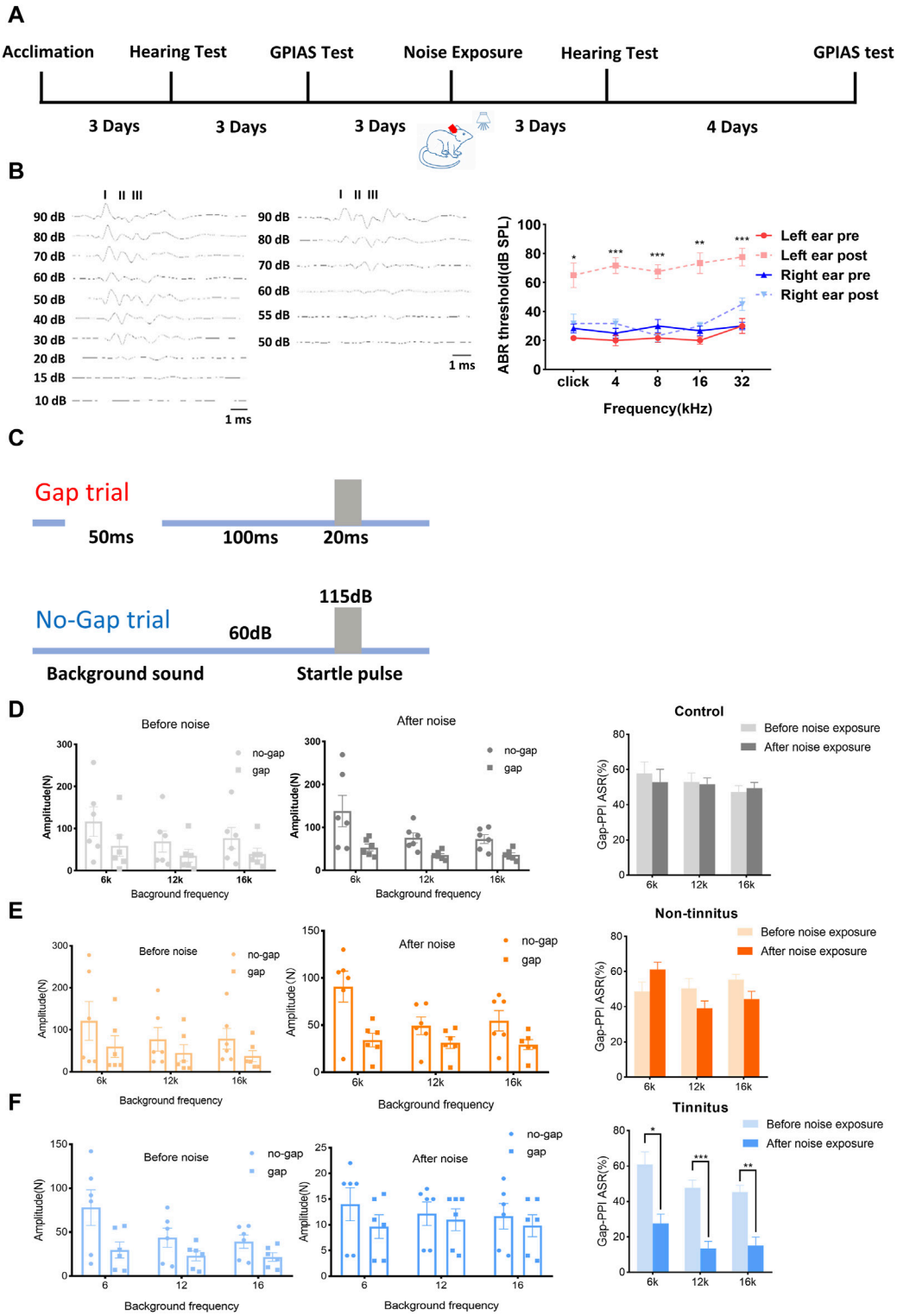

FIGURE 1
Establishment of a rat model of tinnitus induced by loud noise. **(A)** Schematic illustration depicting the experimental timeline. **(B)** Typical image of the ABR threshold upon click stimulation of left ear before (left) and after noise (middle) exposure. The ABR threshold of the left ear after noise exposure was significantly increased after click stimulation or exposure to a tone with a frequency of 4, 8, 16, or 32 kHz (right). **(C)** The experimental paradigm for detecting tinnitus. **(D–F)** Gap-PPI values of **(D)** the control, **(E)** non-tinnitus and **(F)** tinnitus groups at 6, 12, or 16 kHz. $n = 6$ animals. $^{*}p < 0.05$, $^{**}p < 0.01$, $^{***}p < 0.001$.

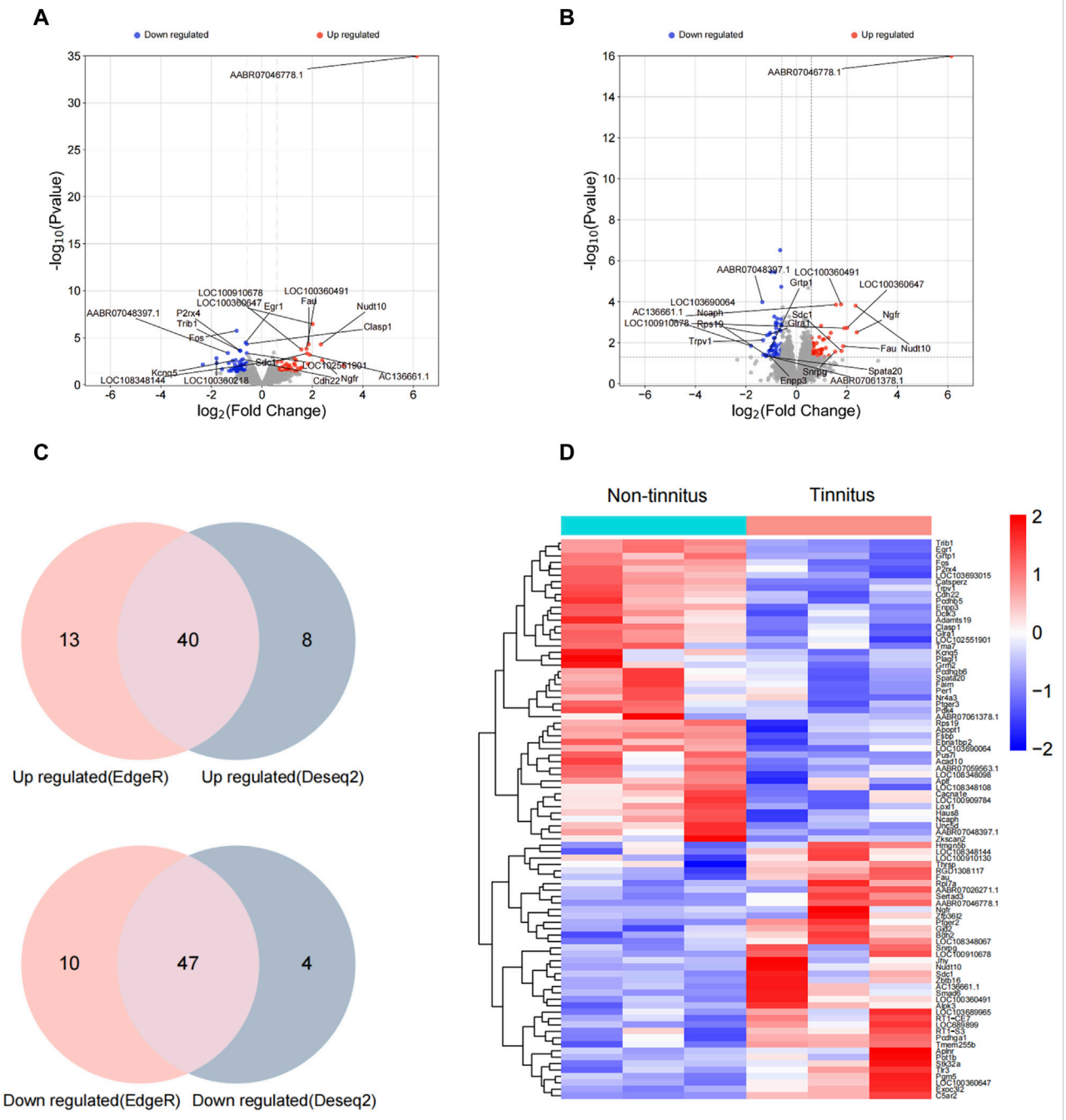

FIGURE 2
Confirmation of differential gene expression between the non-tinnitus and tinnitus groups at the transcriptional level. **(A,B)** Differently expressed genes as screened out by Edger and Deseq2. **(C)** Venn plots of differently expressed genes screened by Edge R and DESeq2. **(D)** Heatmap showing DEGs in the non-tinnitus (left) and tinnitus (right) groups. Blue and red colors indicate downregulated and upregulated DEGs, respectively. *n* = 3 animals.

samples from the non-tinnitus and tinnitus groups. The results of numerous studies related to tinnitus have shown that the MGB plays an important role in the development of this disease [30]; therefore, the MGB was chosen as the target area. Genes exhibited expression differences of >1.5-fold between the non-tinnitus and tinnitus groups were designated as potential DEGs. 110 DEGs and 99 DEGs were identified by EdgeR and DEseq2, respectively (Figures 2A, B). DEGs selected by EdgeR contained

TABLE 2 The top ten upregulated and downregulated DEGs.

Up regulated genes	log2FoldChange	False-discovery rate	*p*-value	Down regulated genes	log2FoldChange	False-discovery rate	*p*-value
AABR07046778.1	6.136147593	1.72E-31	1.03E-16	*LOC103690064*	−1.802058571	1	0.014442155
Ngfr	2.387695704	0.967933878	0.003147254	*AABR07048397.1*	−1.353588127	0.299396874	0.000105157
Nudt10	2.345152966	0.061686258	0.000159045	*Trpv1*	−1.321438256	1	0.007588696
LOC100360647	2.004777335	0.001272584	0.001899531	*AABR07061378.1*	−1.310732471	1	0.039494665
AC136661.1	1.900711856	0.37144022	0.001977346	*Ncaph*	−1.220065263	1	0.039471337
Fau	1.847325179	0.061686258	0.015040405	*Spata20*	−1.206301061	1	0.045839587
Sdc1	1.783174086	0.299396874	0.025586079	*Rps19*	−1.166814696	1	0.004378735
LOC100360491	1.764732106	0.146915516	0.000136002	*Enpp3*	−1.104953628	1	0.03958059
LOC100910678	1.562883998	0.164957053	0.000141141	*Grtp1*	−1.088605849	1	0.026009829
Snrpg	1.533385569	1	0.027685201	*Glra1*	−1.076531654	1	0.004025429

TABLE 3 The hub genes selected by cytohubba.

Hub genes	log2FoldChange	False-discovery rate	*p*-value
LOC689899	6.136147593	1	1.03E-16
Rpl7a	0.606298027	1	0.003766165
LOC100360491	1.764732106	0.146915516	0.000136002
Rps19	−1.166814696	1	0.004378735
LOC685085	−1.306683174	1	0.032988997
Fau	1.848475885	0.061686258	5.05E-05
AC136661.1	1.783174086	0.37144022	0.025586079
Ebna1bp2	−0.817818978	0.967933878	0.002607751
Egr1	−0.64586611	0.056699571	3.26E-05
Fos	−1.006387096	0.004093582	1.83E-06

53 upregulated and 57 downregulated. DEGs selected by DEseq2 contained 48 upregulated and 51 downregulated. By integrating the results from EdgeR and DEseq2, we identified 87 differently expressed genes which include 40 upregulated DEGs and 47 downregulated DEGs (Figure 2C). The selected DEGs are shown in a heat map (Figure 2D). Top ten upregulated and downregulated DEGs selected by Edger and Deseq2 were shown in Table 2.

DEG-enrichment analysis

GO-based enrichment analysis was performed to assess the relevant biological functions of the DEGs in the non-tinnitus and tinnitus groups. Figures 3A–C depicts the enrichment terms in the biological process (BP), cellular component (CC), and molecular function (MF) categories. Three top most BP terms were positive regulation of miRNA transcription, positive regulation of miRNA metabolic process and regulation of miRNA transcription. The most enriched CC term was cytosolic ribosome, followed by side of membrane and external side of plasma membrane with the latter two terms were not significantly enriched. The top three most enriched MF terms were excitatory extracellular ligand-gated monoatomic ion channel activity, structural constituent of ribosome and ubiquitin protein ligase binding with the latter two terms showing no statistical significance. KEGG analysis was performed to elucidate the underlying pathways associated with the DEGs between the tinnitus and non-tinnitus groups. The most significantly enriched pathways identified were coronavirus disease COVID-19 and neuroactive ligand-receptor interaction (Figure 3D).

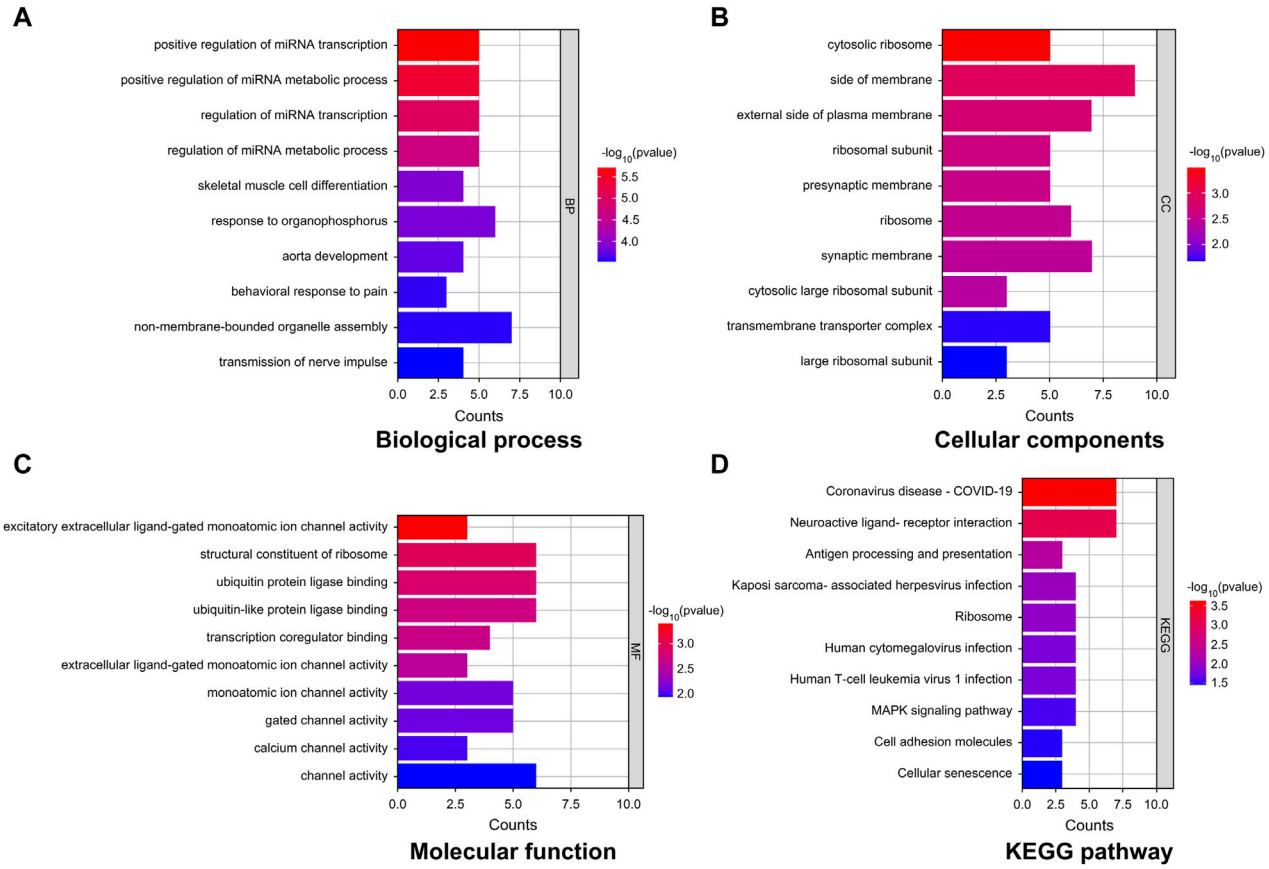

FIGURE 3
GO and KEGG enrichment analyses of key mRNAs. **(A–C)** Representative GO analysis of DEGs enriched for **(A)** Biological Process, **(B)** Cellular Components, and **(C)** Molecular Function. **(D)** The most highly enriched pathways associated with DEGs.

Construction of a protein–protein-interaction network and selection of hub genes

We employed the STRING database to generate a network of protein–protein interactions, according to previous studies [31]. The cut-off criterion for inclusion in the network was that the median confidence level of the interaction score was 0.400. Figure 4A shows all 85 nodes and 50 edges in the protein–protein-interaction network, where the average node degree was 1.18. The Cytohubba plug-in of Cytoscape was used to select the potential hub genes. The following 10 genes had the highest net degree ranking: *LOC689899, Fau, Rpl7a, LOC100360491, Rps19, LOC685085, AC136661.1, Fos, Ebna1bp2, Egr1* (Figure 4B and Table 3).

Verification of the hub genes

We performed qPCR to verify the expression levels of *LOC689899, Fau, Rpl7a, LOC100360491, Rps19, LOC685085, AC136661.1, Fos, Ebna1bp2, and Egr1*. Although LOC689899 had the highest betweenness centrality value, it did not show a significant difference in expression between the two groups ($p = 0.69$, Figure 5A). *Fau* ($p = 0.23$, Figure 5B), *LOC100360491* ($p = 0.50$, Figure 5D), *Rps19* ($p = 0.80$, Figure 5E), *LOC685085* ($p = 0.43$, Figure 5F), *Fos* ($p = 0.36$, Figure 5H), *Ebna1bp2* ($p = 0.53$, Figure 5I) and *Egr1* ($p = 0.78$, Figure 5J) also showed no significant differences. However, *Rpl7a* was expressed at significantly higher levels in the tinnitus group than in the non-tinnitus group ($p < 0.001$, Figure 5C) which was also true for the *AC136661.1* ($p < 0.05$, Figure 5G).

Discussion

Tinnitus is an intractable condition that impairs quality of life and imposes a heavy burden on society when it progresses to a chronic state. Research to identify the best method to treat tinnitus is still ongoing because of its elusive pathogenic mechanisms. In this study, we first established a rat model of tinnitus by exposing the animals to loud noise, which was

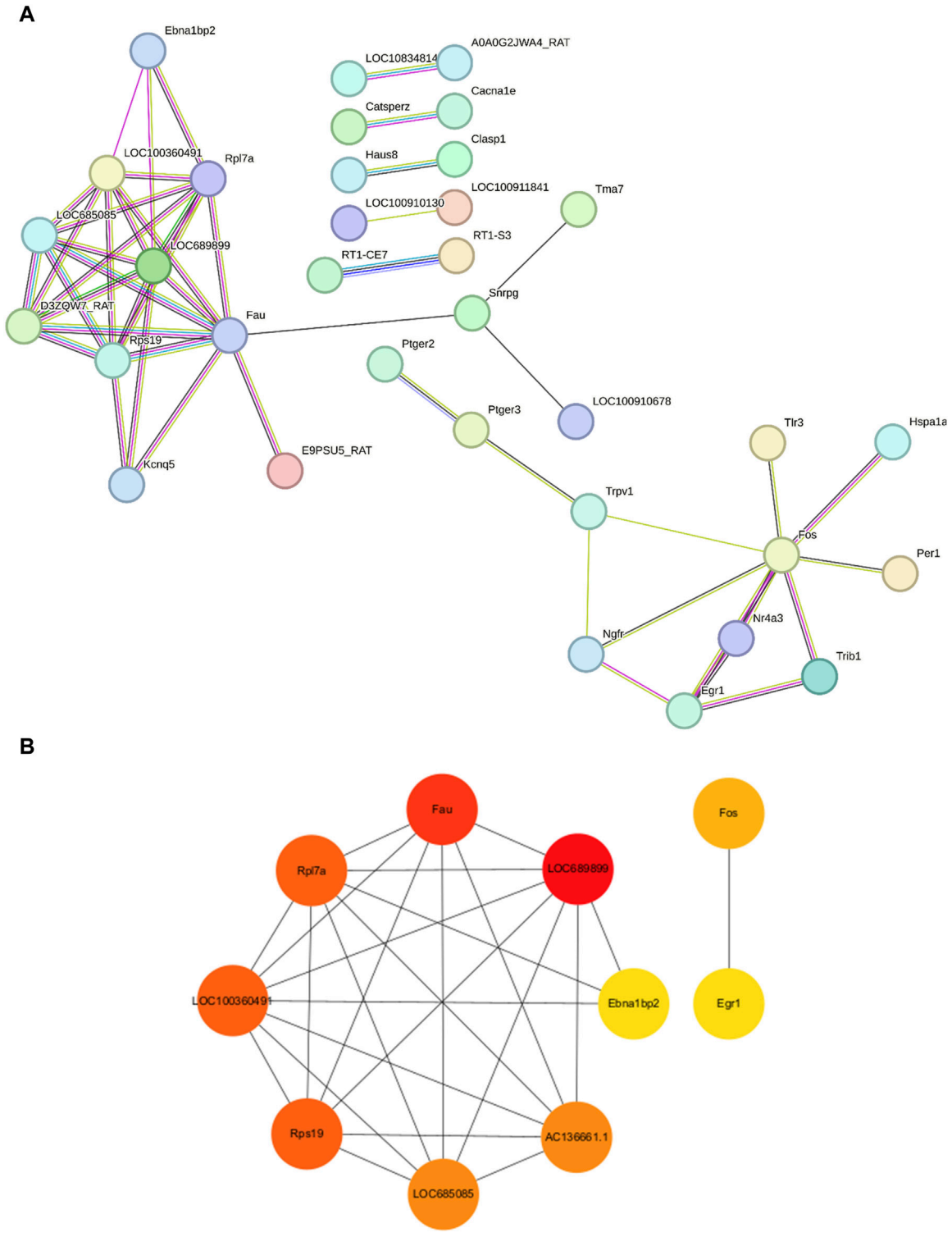

FIGURE 4
Protein–protein-interaction network in the experimental model of tinnitus **(A)** The protein–protein-interaction network established using the STRING database and the hub genes identified in this study. **(B)** Key genes are arranged based on their degree values. The top ten genes were selected as potential hub genes.

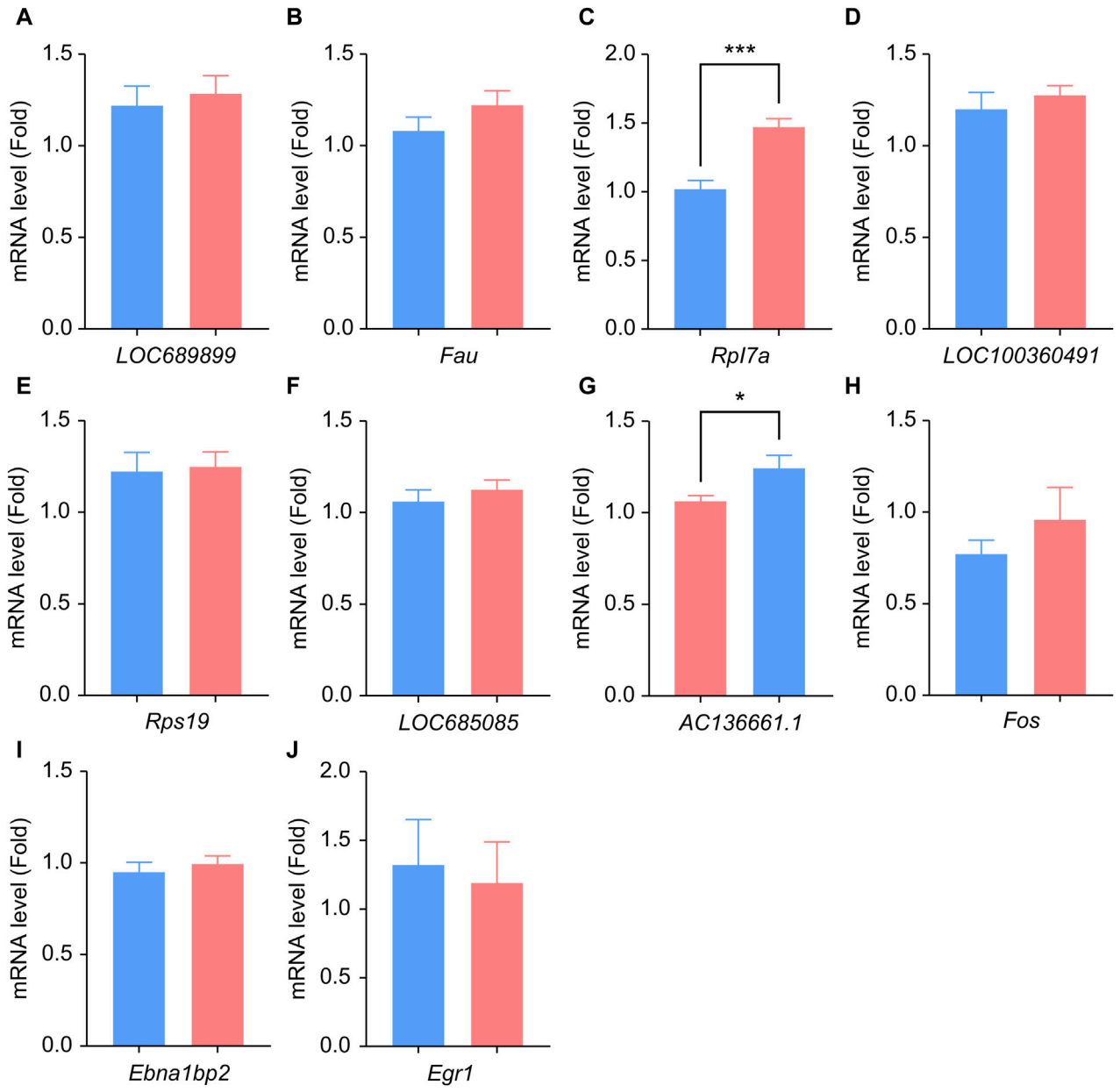

FIGURE 5
Results of qPCR analysis of the selected hub genes. **(A–J)** Differences in the mRNA-expression levels of ten key genes between the non-tinnitus and tinnitus groups are shown, including *LOC689899* **(A)**, *Fau* **(B)**, *Rpl7a* **(C)**, *LOC100360491* **(D)**, *Rps19* **(E)**, *LOC685085* **(F)**, *AC136661.1* **(G)**, *Fos* **(H)**, *Ebna1bp2* **(I)** and *Egr1* **(J)**. $n = 5$ animals, $^*p < 0.05$.

subsequently validated by applying gap-induced, PPI of acoustic startle response (GPIAS) methods. Subsequently, genetic changes in the MGB between the non-tinnitus and tinnitus groups were analyzed using RNA-seq. We identified 87 differentially expressed genes (DEGs; 40 upregulated and 47 downregulated genes) that were highly related to tinnitus. GO analysis of the DEGs was performed to identify their potential functions and KEGG analysis was performed to clarify the signaling pathways involved. Ten hub genes were finally identified based on the protein–protein-interaction network analysis and were tested further at the transcriptional level.

In this study, animals showed tinnitus-related behavior after tonal stimulation at 6, 12, and 16 kHz, which was close to the frequencies of the loud noises used in this study. These results were consistent with those of previous research, which showed that the tinnitus frequency was similar to the noise frequency [32]. The most

upregulated genes *AABR07046778.1, Ngfr, Nudt10, LOC100360647, AC136661.1, Fau, Sdc1, LOC100360491,LOC100910678, and Snrpg.* The glutamate excitotoxicity associated with mitochondrial dysfunction can cause tinnitus [33]. *AABR07046778.1* may modulate tinnitus by participating the same process. The most downregulated genes in the tinnitus (when compared to the non-tinnitus group) were *LOC103690064, AABR07048397.1, Trpv1, AABR07061378.1, Ncaph, Spata20, Rps19, Enpp3, Grtp1, and Glra1*. *LOC103690064* is functionally similar to m7GpppN-mRNA hydrolase, which control the degradation, decay and turnover of mRNA by removing the 5′ cap structure from the mRNA [34–36]. The finding that *LOC103690064* was downregulated the pathological retention of RNAs or the protective compensation of RNAs in the MGB [37].

One of the most enriched pathway terms identified in this study was coronavirus disease COVID-19 pathway. This pathway mainly correlates with the immunologic derangement as well as the dysfunction of blood-brain barrier (BBB) induced by coronavirus in the central nervous system [38, 39]. Previous results have shown that patients with COVID-19 also display increased severity and incidence rate of tinnitus [40, 41]. It is reasonable to speculate that in tinnitus, increased pathological immune proteins or BBB permeability occur in the MGB. The coronavirus disease COVID-19 is also commonly enriched in neurodegenerative diseases, which is often associated with tinnitus, a tentative sign of neurodegeneration [42]. KEGG pathway terms associated with neuroactive ligand-receptor interaction were highly enriched, which further verifies that tinnitus is one type of neurodegenerative disorder that is highly correlated with the damage of synaptic transmission [43]. Genes involved in neuroactive ligand–receptor interactions, such as *Npy2r, Htr2c, and Rxfp1*, were significantly dysregulated during cognitive dysfunction or memory impairment which was tightly related with tinnitus [44, 45].

Identifying the genes encoding key proteins responsible for noise-induced tinnitus could help elucidate the mechanism responsible for the condition. *Rpl7a* which encodes the ribosomal protein large subunit was found to be upregulated in the tinnitus group compared with the non-tinnitus group. Previous research showed that the levels and activity of ribosomal proteins can change during neurodegeneration as well as brain aging [46–48]. *Rpl7a* were found to promote the growth and regeneration of neural axons after optic nerve crush injury suggesting that the elevated level of *Rpl7a* can facilitate the communication between adjacent neurons and increase the output of MGB to auditory cortex [49]. *AC136661.1* was another up-regulated hub gene in tinnitus group, selected by the protein–protein-interaction network. This gene codes the 40S ribosomal protein S2 (RPS2) in rats, a protein responsible for aminoacyl-tRNA binding. This protein is similar to yeast S4 and *Escherichia coli* S5 ribosomal proteins [50]. Upregulation of *AC136661.1* may permit the fidelity of the translation of mRNA ribosomes in mitochondria which guarantee the supply of energy in MGB neurons [51]. This is a reasonable finding because the main cell subtypes (accounting for >99% of cells in the MGB in rodents) are glutamatergic [52]. The increased activity of excitatory neurons led to an increased output from the MGB to the auditory cortex in a model of central gain, which showed increased excitability of neurons in the auditory cortex [53, 54].

Previous research revealed the presence of genes related with axonal branching (*ANK2, AKAP9, and TSC2*) in tinnitus patients [20]. These also support our hypothesis that enhanced excitability of neurons occurred in tinnitus as increased branches promote connections among neurons and even brain regions. Other genes, such as *COL11A1, GRK6, MFHAS1, MSRA, XKR6, C8orf12, AF131215.5, and BLK*, which were reported to be correlated with tinnitus-related disorders were not observed in our study [55]. This may be due to the fact that our study mainly focused on acute tinnitus that is scarcely associated with psychological problems. Meanwhile, other studies have shown that genes such as CACNA1E that influence the firing of neurons are also associated with tinnitus, which is applicable to our study, suggesting the altered excitability of neurons in the brain [56]. Xie *et al.* identified that genes related with the formation of cilia and infiltration of inflammatory cells also participate in the development of tinnitus [57]. Our study did not find such genetic changes as we only focused on the central nervous system instead of the peripheral nervous system. Further investigations need to be done to clarify the regional effect on the candidate genes related to tinnitus. We did not find the similar genes reported in the human studies by Amanat et al. [20]. However, we found gene (NGFR) shares similar functions with ANK2 which is high imperial for the growth and extension of neurons [58]. In addition, we also did not detect the genes reported in the work by Xie et al such as WNT11 and TNFRSF1A [57]. However, we cannot exclude the possibility that genes in different signaling pathway may interact with each other which indirectly influence the tinnitus. For example, WNT family member could activate NGFR transcription in a ZEB1-dependent manner [59]. Additional work also should be done to verify the hypothesis.

This study has certain limitations that should be acknowledged. First, we only utilized male rats as the target to reduce the effects of sex on hearing levels; however, female rats displayed comparable variability in hearing levels to male rats during the reproductive cycle [60]. Additional studies should be performed with female rats before the results are translated to a clinical study. Second, we predominantly focused on the occurrence (rather than the sustainment) of tinnitus (i.e., the chronic phenotype) [61]. Tinnitus lasted longer in our model (established by exposing rats to loud noises) than drug-induced tinnitus lasts. When considering simulating patients disturbed by tinnitus, these results should be cautiously interpreted because in clinical practice, numerous patients experience tinnitus without explicit pathogenesis but with normal bilateral hearing. Third, although similar genetic variability occurs between rodents and humans, the hub genes selected in our study should be translated

cautiously into humans because some human diseases do not occur naturally in rodents [62]. Fourth, the genes encoding proteins related to tinnitus were only confirmed at the transcriptional level. Further studies are required to determine whether these proteins can be translated clinically into effective targets for treating tinnitus.

I In conclusion, we identified 88 DEGs in tinnitus (43 upregulated genes and 45 downregulated genes). Most DEGs enriched were associated with COVID-19 and neuroactive ligand-receptor interaction-related pathways. We selected the genes (*Rpl7a and AC136661.1*), which are highly related to the normal function of ribosome, for further analysis. These findings will contribute significantly to the development of an effective therapeutic approach for tinnitus, resulting in an exciting breakthrough for this debilitating disease.

Author contributions

SY, FW, and PL: conceptualization. PL and XX: investigation. CZ, HZ, and ZD: formal analysis. YJ, LW, and WS writing–original draft. SY, FW, and PL: writing–review and editing. All authors contributed to the article and approved the submitted version.

Data availability statement

The original contributions presented in the study are included in the article/Supplementary material, further inquiries can be directed to the corresponding author/s.

Ethics statement

The animal study was approved by the Animal Ethics Committee of the Chinese PLA General Hospital. The study was conducted in accordance with the local legislation and institutional requirements.

Funding

This work was supported by the National Key Research and Development Program (grant numbers 2020YFC2005203, 2022YFC2402704, and 2022YFC2402701) and the National Natural Science Foundation of China (grant numbers 81820108009 and 81970890) and Beijing Science and Technology New star Program (grant number Z201100006820133).

Conflict of interest

The authors declare that the research was conducted in the absence of any commercial or financial relationships that could be construed as a potential conflict of interest.

Supplementary material

The Supplementary Material for this article can be found online at: https://www.ebm-journal.org/articles/10.3389/ebm.2024.10057/full#supplementary-material

References

1. Shargorodsky J, Curhan GC, Farwell WR. Prevalence and characteristics of tinnitus among US adults. *Am J Med* (2010) **123**:711–8. doi:10.1016/j.amjmed.2010.02.015

2. Langguth B. A review of tinnitus symptoms beyond 'ringing in the ears': a call to action. *Curr Med Res Opin* (2011) **27**:1635–43. doi:10.1185/03007995.2011.595781

3. Langguth B, Kreuzer PM, Kleinjung T, De Ridder D. Tinnitus: causes and clinical management. *Lancet Neurol* (2013) **12**:920–30. doi:10.1016/s1474-4422(13)70160-1

4. Bauer CA. Tinnitus. *New Engl J Med* (2018) **378**:1224–31. doi:10.1056/nejmcp1506631

5. House JW, Brackmann DE. Tinnitus: surgical treatment. *Ciba Found Symp* (1981) **85**:204–16. doi:10.1002/9780470720677.ch12

6. Bartlett EL. The organization and physiology of the auditory thalamus and its role in processing acoustic features important for speech perception. *Brain Lang* (2013) **126**:29–48. doi:10.1016/j.bandl.2013.03.003

7. Henton A, Tzounopoulos T. What's the buzz? The neuroscience and the treatment of tinnitus. *Physiol Rev* (2021) **101**:1609–32. doi:10.1152/physrev.00029.2020

8. Brinkmann P, Kotz SA, Smit JV, Janssen MLF, Schwartze M. Auditory thalamus dysfunction and pathophysiology in tinnitus: a predictive network hypothesis. *Brain Struct Funct* (2021) **226**:1659–76. doi:10.1007/s00429-021-02284-x

9. Kalappa BI, Brozoski TJ, Turner JG, Caspary DM. Single unit hyperactivity and bursting in the auditory thalamus of awake rats directly correlates with behavioural evidence of tinnitus. *J Physiol* (2014) **592**:5065–78. doi:10.1113/jphysiol.2014.278572

10. Richardson BD, Brozoski TJ, Ling LL, Caspary DM. Targeting inhibitory neurotransmission in tinnitus. *Brain Res* (2012) **1485**:77–87. doi:10.1016/j.brainres.2012.02.014

11. Maas IL, Brüggemann P, Requena T, Bulla J, Edvall NK, Hjelmborg JVB, et al. Genetic susceptibility to bilateral tinnitus in a Swedish twin cohort. *Genet Med* (2017) **19**:1007–12. doi:10.1038/gim.2017.4

12. Chan YC, Wang MF, Hwang JH. Effects of spirulina on GABA receptor gene expression in salicylate-induced tinnitus. *Int Tinnitus J* (2018) **22**:84–8. doi:10.5935/0946-5448.20180014

13. Han KH, Mun SK, Sohn S, Piao XY, Park I, Chang M. Axonal sprouting in the dorsal cochlear nucleus affects gap-prepulse inhibition following noise exposure. *Int J Mol Med* (2019) **44**:1473–83. doi:10.3892/ijmm.2019.4316

14. Jang CH, Lee S, Park IY, Song A, Moon C, Cho GW. Memantine attenuates salicylate-induced tinnitus possibly by reducing NR2B expression in auditory cortex of rat. *Exp Neurobiol* (2019) **28**:495–503. doi:10.5607/en.2019.28.4.495

15. Yi B, Wu C, Shi R, Han K, Sheng H, Li B, et al. Long-term administration of salicylate-induced changes in BDNF expression and CREB phosphorylation in the auditory cortex of rats. *Otology & neurotology* (2018) **39**:e173–e180. doi:10.1097/mao.0000000000001717

16. Pg S, Langguth B, Schecklmann M, Kleinjung T. GDNF and BDNF gene interplay in chronic tinnitus. *Int J Mol Epidemiol Genet* (2012) **3**:245–51. doi:10.5167/uzh-69708

17. Sand PG, Langguth B, Itzhacki J, Bauer A, Geis S, Cárdenas-Conejo ZE, et al. Resequencing of the auxiliary GABA(B) receptor subunit gene KCTD12 in chronic tinnitus. *Front Syst Neurosci* (2012) **6**:41. doi:10.3389/fnsys.2012.00041

18. Tyler RS, Coelho C, Noble W. Tinnitus: standard of care, personality differences, genetic factors. *ORL; J oto-rhino-laryngology its Relat specialties* (2006) **68**:14–9. discussion 20-12. doi:10.1159/000090486

19. Yuce S, Sancakdar E, Bağcı G, Koc S, Kucuk Kurtulgan H, Bağcı B, et al. Angiotensin-converting enzyme (ACE) I/D and alpha-adducin (ADD1) G460W gene polymorphisms in Turkish patients with severe chronic tinnitus. *The J Int Adv otology* (2016) **12**:77–81. doi:10.5152/iao.2016.1732

20. Amanat S, Gallego-Martinez A, Sollini J, Perez-Carpena P, Espinosa-Sanchez JM, Aran I, et al. Burden of rare variants in synaptic genes in patients with severe tinnitus: an exome based extreme phenotype study. *EBioMedicine* (2021) **66**:103309. doi:10.1016/j.ebiom.2021.103309

21. Cederroth CR, PirouziFard M, Trpchevska N, Idrizbegovic E, Canlon B, Sundquist J, et al. Association of genetic vs environmental factors in Swedish adoptees with clinically significant tinnitus. *JAMA otolaryngology– head neck Surg* (2019) **145**:222–9. doi:10.1001/jamaoto.2018.3852

22. Yang G, Lobarinas E, Zhang L, Turner J, Stolzberg D, Salvi R, et al. Salicylate induced tinnitus: behavioral measures and neural activity in auditory cortex of awake rats. *Hearing Res* (2007) **226**:244–53. doi:10.1016/j.heares.2006.06.013

23. Longenecker RJ, Chonko KT, Maricich SM, Galazyuk AV. Age effects on tinnitus and hearing loss in CBA/CaJ mice following sound exposure. *SpringerPlus* (2014) **3**:542. doi:10.1186/2193-1801-3-542

24. Kraus KS, Ding D, Jiang H, Lobarinas E, Sun W, Salvi RJ. Relationship between noise-induced hearing-loss, persistent tinnitus and growth-associated protein-43 expression in the rat cochlear nucleus: does synaptic plasticity in ventral cochlear nucleus suppress tinnitus? *Neuroscience* (2011) **194**:309–25. doi:10.1016/j.neuroscience.2011.07.056

25. Fang J, Yuan Q, Du Z, Fei M, Zhang Q, Yang L, et al. Ferroptosis in brain microvascular endothelial cells mediates blood-brain barrier disruption after traumatic brain injury. *Biochem biophysical Res Commun* (2022) **619**:34–41. doi:10.1016/j.bbrc.2022.06.040

26. Yang H, Xu F, Chen Y, Tian Z. Structural N-glycoproteomics characterization of cell-surface N-glycosylation of MCF-7/ADR cancer stem cells. *J Chromatogr B* (2023) **1219**:123647. doi:10.1016/j.jchromb.2023.123647

27. Fang J, Wang H, Zhou J, Dai W, Zhu Y, Zhou Y, et al. Baicalin provides neuroprotection in traumatic brain injury mice model through Akt/Nrf2 pathway. *Drug Des Dev Ther* (2018) **12**:2497–508. doi:10.2147/dddt.s163951

28. Livak KJ, Schmittgen TD. Analysis of relative gene expression data using real-time quantitative PCR and the 2−ΔΔCT method. *Methods (San Diego, Calif.)* (2001) **25**:402–8. doi:10.1006/meth.2001.1262

29. Galazyuk A, Hébert S. Gap-Prepulse inhibition of the acoustic startle reflex (GPIAS) for tinnitus assessment: current status and future directions. *Front Neurol* (2015) **6**:88. doi:10.3389/fneur.2015.00088

30. Caspary DM, Llano DA. Auditory thalamic circuits and GABA(A) receptor function: putative mechanisms in tinnitus pathology. *Hearing Res* (2017) **349**:197–207. doi:10.1016/j.heares.2016.08.009

31. Chen Q, Bei S, Zhang Z, Wang X, Zhu Y. Identification of diagnostic biomarks and immune cell infiltration in ulcerative colitis. *Scientific Rep* (2023) **13**:6081. doi:10.1038/s41598-023-33388-5

32. Brozoski T, Wisner K, Randall M, Caspary D. Chronic sound-induced tinnitus and auditory attention in animals. *Neuroscience* (2019) **407**:200–12. doi:10.1016/j.neuroscience.2018.10.013

33. Song A, Cho GW, Vijayakumar KA, Moon C, Ang MJ, Kim J, et al. Neuroprotective effect of valproic acid on salicylate-induced tinnitus. *Int J Mol Sci* (2021) **23**:23. doi:10.3390/ijms23010023

34. Łabno A, Tomecki R, Dziembowski A. Cytoplasmic RNA decay pathways - enzymes and mechanisms. *Biochim Biophys Acta (Bba) - Mol Cel Res* (2016) **1863**:3125–47. doi:10.1016/j.bbamcr.2016.09.023

35. Steingart KR, Henry M, Ng V, Hopewell PC, Ramsay A, Cunningham J, et al. Fluorescence versus conventional sputum smear microscopy for tuberculosis: a systematic review. *Lancet Infect Dis* (2006) **6**:570–81. doi:10.1016/s1473-3099(06)70578-3

36. Steingart KR, Ramsay A, Pai M. Optimizing sputum smear microscopy for the diagnosis of pulmonary tuberculosis. *Expert Rev anti-infective Ther* (2007) **5**:327–31. doi:10.1586/14787210.5.3.327

37. Canet-Pons J, Sen NE, Arsović A, Almaguer-Mederos LE, Halbach MV, Key J, et al. Atxn2-CAG100-KnockIn mouse spinal cord shows progressive TDP43 pathology associated with cholesterol biosynthesis suppression. *Neurobiol Dis* (2021) **152**:105289. doi:10.1016/j.nbd.2021.105289

38. Chen Y, Yang W, Chen F, Cui L. COVID-19 and cognitive impairment: neuroinvasive and blood–brain barrier dysfunction. *J neuroinflammation* (2022) **19**:222. doi:10.1186/s12974-022-02579-8

39. Li Q, Wang Y, Sun Q, Knopf J, Herrmann M, Lin L, et al. Immune response in COVID-19: what is next? *Cel Death Differ* (2022) **29**:1107–22. doi:10.1038/s41418-022-01015-x

40. Anzivino R, Sciancalepore PI, Petrone P, D'Elia A, Petrone D, Quaranta N. Tinnitus revival during COVID-19 lockdown: how to deal with it? *Eur Arch oto-rhino-laryngology* (2021) **278**:295–6. doi:10.1007/s00405-020-06147-9

41. Savtale S, Hippargekar P, Bhise S, Kothule S. Prevalence of otorhinolaryngological symptoms in covid 19 patients. *Indian J Otolaryngol Head Neck Surg* (2022) **74**:3378–84. doi:10.1007/s12070-021-02410-5

42. Fu YW, Xu HS, Liu SJ. COVID-19 and neurodegenerative diseases. *Eur Rev Med Pharmacol Sci* (2022) **26**:4535–44. doi:10.26355/eurrev_202206_29093

43. Kong Y, Liang X, Liu L, Zhang D, Wan C, Gan Z, et al. High throughput sequencing identifies MicroRNAs mediating α-synuclein toxicity by targeting neuroactive-ligand receptor interaction pathway in early stage of Drosophila Parkinson's disease model. *PloS one* (2015) **10**:e0137432. doi:10.1371/journal.pone.0137432

44. Lee SE, Park S, Jang GY, Lee J, Moon M, Ji YJ, et al. Extract of aster koraiensis nakai leaf ameliorates memory dysfunction via anti-inflammatory action. *Int J Mol Sci* (2023) **24**:5765. doi:10.3390/ijms24065765

45. Lopez-Escamez JA, Perez-Carpena P. Technological advances in the diagnosis and management of tinnitus. *J Clin Med* (2022) **11**:4597. doi:10.3390/jcm11154597

46. Amirbeigiarab S, Kiani P, Velazquez Sanchez A, Krisp C, Kazantsev A, Fester L, et al. Invariable stoichiometry of ribosomal proteins in mouse brain tissues with aging. *Proc Natl Acad Sci* (2019) **116**:22567–72. doi:10.1073/pnas.1912060116

47. Evans HT, Benetatos J, van Roijen M, Bodea LG, Götz J. Decreased synthesis of ribosomal proteins in tauopathy revealed by non-canonical amino acid labelling. *EMBO J* (2019) **38**:e101174. doi:10.15252/embj.2018101174

48. Koren SA, Hamm MJ, Meier SE, Weiss BE, Nation GK, Chishti EA, et al. Tau drives translational selectivity by interacting with ribosomal proteins. *Acta neuropathologica* (2019) **137**:571–83. doi:10.1007/s00401-019-01970-9

49. Xing J, Theune WC, Lukomska A, Frost MP, Damania A, Trakhtenberg EF. Experimental upregulation of developmentally downregulated ribosomal protein large subunits 7 and 7A promotes axon regeneration after injury *in vivo*. *Exp Neurol* (2023) **368**:114510. doi:10.1016/j.expneurol.2023.114510

50. Suzuki K, Olvera J, Wool IG. Primary structure of rat ribosomal protein S2. A ribosomal protein with arginine-glycine tandem repeats and RGGF motifs that are associated with nucleolar localization and binding to ribonucleic acids. *J Biol Chem* (1991) **266**:20007–10. doi:10.1016/s0021-9258(18)54884-5

51. Aseev LV, Chugunov AO, Efremov RG, Boni IV. A single missense mutation in a coiled-coil domain of *Escherichia coli* ribosomal protein S2 confers a thermosensitive phenotype that can be suppressed by ribosomal protein S1. *J Bacteriol* (2013) **195**:95–104. doi:10.1128/jb.01305-12

52. Winer JA, Larue DT. Evolution of GABAergic circuitry in the mammalian medial geniculate body. *Proc Natl Acad Sci* (1996) **93**:3083–7. doi:10.1073/pnas.93.7.3083

53. Schaette R, McAlpine D. Tinnitus with a normal audiogram: physiological evidence for hidden hearing loss and computational model. *J Neurosci* (2011) **31**:13452–7. doi:10.1523/jneurosci.2156-11.2011

54. Zeng FG. An active loudness model suggesting tinnitus as increased central noise and hyperacusis as increased nonlinear gain. *Hearing Res* (2013) **295**:172–9. doi:10.1016/j.heares.2012.05.009

55. Clifford RE, Maihofer AX, Stein MB, Ryan AF, Nievergelt CM. Novel risk loci in tinnitus and causal inference with neuropsychiatric disorders among adults of European ancestry. *JAMA otolaryngology– head neck Surg* (2020) **146**:1015–25. doi:10.1001/jamaoto.2020.2920

56. Gallego-Martinez A, Escalera-Balsera A, Trpchevska N, Robles-Bolivar P, Roman-Naranjo P, Frejo L, et al. Using coding and non-coding rare variants to target candidate genes in patients with severe tinnitus. *NPJ Genomic Med* (2022) **7**: 70. doi:10.1038/s41525-022-00341-w

57. Xie C, Niu Y, Ping J, Wang Y, Yang C, Li Y, et al. Genome-wide association study identifies new loci associated with noise-induced tinnitus in Chinese populations. *BMC genomic data* (2021) **22**:31. doi:10.1186/s12863-021-00987-y

58. Eibl JK, Strasser BC, Ross GM. Structural, biological, and pharmacological strategies for the inhibition of nerve growth factor. *Neurochem Int* (2012) **61**: 1266–75. doi:10.1016/j.neuint.2012.10.008

59. Wu R, Li K, Yuan M, Luo KQ. Nerve growth factor receptor increases the tumor growth and metastatic potential of triple-negative breast cancer cells. *Oncogene* (2021) **40**:2165–81. doi:10.1038/s41388-021-01691-y

60. Lauer AM, Schrode KM. Sex bias in basic and preclinical noise-induced hearing loss research. *Noise & health* (2017) **19**:207–12. doi:10.4103/nah.nah_12_17

61. Thielman EJ, Reavis KM, Theodoroff SM, Grush LD, Thapa S, Smith BD, et al. Tinnitus screener: short-term test–retest reliability. *Am J Audiol* (2023) **32**:232–42. doi:10.1044/2022_aja-22-00140

62. Sjöstedt E, Zhong W, Fagerberg L, Karlsson M, Mitsios N, Adori C, et al. An atlas of the protein-coding genes in the human, pig, and mouse brain. *Science* (2020) **367**:eaay5947. doi:10.1126/science.aay5947

EBM Experimental Biology and Medicine

TYPE Original Research
PUBLISHED 29 February 2024
DOI 10.3389/ebm.2024.10126

OPEN ACCESS

*CORRESPONDENCE
Rodolfo Paredes,
rparedes@unab.cl

RECEIVED 10 July 2023
ACCEPTED 22 November 2023
PUBLISHED 29 February 2024

CITATION
Pereira I, Paludo GP, Hidalgo C, Stoore C, Baquedano MS, Cabezas C, Cancela M, Ferreira HB, Bastías M, Riveros A, Meneses C, Sáenz L and Paredes R (2024), Weighted gene co-expression network analysis reveals immune evasion related genes in *Echinococcus granulosus* sensu stricto. *Exp. Biol. Med.* 249:10126. doi: 10.3389/ebm.2024.10126

Weighted gene co-expression network analysis reveals immune evasion related genes in *Echinococcus granulosus* sensu stricto

Ismael Pereira[1,2], Gabriela Prado Paludo[3], Christian Hidalgo[4], Caroll Stoore[1], María Soledad Baquedano[1], Carolina Cabezas[1], Martín Cancela[3], Henrique Bunselmeyer Ferreira[3], Macarena Bastías[5], Aníbal Riveros[5], Claudio Meneses[5], Leonardo Sáenz[6] and Rodolfo Paredes[1]*

[1]Laboratorio de Medicina Veterinaria, Escuela de Medicina Veterinaria, Facultad de Ciencias de la Vida, Universidad Andres Bello, Santiago, Chile, [2]Programa de Doctorado en Ciencias Silvoagropecuarias y Veterinarias, Universidad de Chile, Santiago, Chile, [3]Laboratório de Genômica Estrutural e Funcional, Centro de Biotecnologia, Universidade Federal do Rio Grande do Sul (UFRGS), Porto Alegre, RS, Brazi, [4]Núcleo de Investigaciones Aplicadas en Ciencias Veterinarias y Agronómicas, Facultad de Medicina Veterinaria y Agronomía, Universidad de Las Américas, Sede Santiago Centro, Santiago, Chile, [5]Centro de Biotecnología Vegetal, Facultad de Ciencias de la Vida, Universidad Andrés Bello, Santiago, Chile, [6]Laboratorio de Vacunas Veterinarias, Facultad de Ciencias Veterinarias y Pecuarias, Universidad de Chile, Santiago, Chile

Abstract

Cystic echinococcosis (CE) is a zoonotic disease caused by the tapeworm *Echinococcus granulosus* sensu lato (s.l). In the intermediate host, this disease is characterized by the growth of cysts in viscera such as liver and lungs, inside of which the parasite develops to the next infective stage known as protoscoleces. There are records that the infected viscera affect the development and morphology of *E. granulosus* s.l. protoscolex in hosts such as buffalo or humans. However, the molecular mechanisms that drive these differences remains unknown. Weighted gene co-expression network analysis (WGCNA) using a set of RNAseq data obtained from *E. granulosus* sensu stricto (s.s.) protoscoleces found in liver and lung cysts reveals 34 modules in protoscoleces of liver origin, of which 12 have differential co-expression from protoscoleces of lung origin. Three of these twelve modules contain hub genes related to immune evasion: tegument antigen, tegumental protein, ubiquitin hydrolase isozyme L3, COP9 signalosome complex subunit 3, tetraspanin CD9 antigen, and the methyl-CpG-binding protein Mbd2. Also, two of the twelve modules contain only hypothetical proteins with unknown orthology, which means that there are a group of unknown function proteins co-expressed inside the protoscolex of liver CE cyst origin. This is the first evidence of gene expression differences in protoscoleces from CE cysts found in different viscera, with co-expression networks that are exclusive to protoscoleces

from liver CE cyst samples. This should be considered in the control strategies of CE, as intermediate hosts can harbor CE cysts in liver, lungs, or both organs simultaneously.

KEYWORDS

cystic echinococcosis, *Echinococcus granulosus*, RNAseq, WGCNA, co-expression network

Impact statement

This is the first report of a Weighted gene co-expression network analysis in *Echinococcus granulosus* sensu stricto protoscolex stage. These networks are useful in understanding parasite basic biology and provide the baseline for further research. Immune evasion is a relevant topic in the host-parasite interaction, and the identified networks could provide new molecular targets in the medical treatment of this disease, such as the COP9 signalosome subunit.

Introduction

Cystic Echinococcosis (CE) is a zoonotic larval disease, caused by the infection of the tapeworm *Echinococcus granulosus* sensu lato (s.l.), and affects both animals and humans globally. According to the World Health Organization (WHO), the global burden of trying to stop this zoonosis exceeds three billion US dollars every year [1]. CE is characterized by the development of cysts (formerly called hydatid cysts) in the viscera (mainly, liver and lungs) of intermediate hosts such as cattle and sheep, among other herbivores, whereas humans act as dead-end hosts [2]. CE cysts are comprised of three layers: the germinal and laminated layer of parasite origin, and an adventitial layer, which is the result of the host immune response against the parasite [3]. The germinal layer produces protoscoleces, the infective stage for the definitive host (dogs and other canids), who become infected when consuming viable protoscoleces [4]. *E. granulosus* s.l. is a cluster that groups different species of *Echinococcus* such as *E. equinus*, *E. ortleppi*, *E. canadensis*, *E. felidis* and *E. granulosus* sensu stricto (s.s.) [5]. The latter, which corresponds to the sheep-dog cycle, is the main *E. granulosus* s.l. species that infects humans [6], and it is found in Asia, Europe, Oceania and the Americas [7]. For causes that remain to be fully understood, some *E. granulosus* s.l. CE cysts are unable to produce viable protoscoleces and are termed non-fertile CE cysts [3]. Since cattle and sheep host can harbor simultaneously fertile and non-fertile CE cysts in the same viscera, from the same *E. granulosus* s.s. species [2], there must be microenvironment factors that affect parasite development and shape the host immune response.

Differences in morphology and fertility of CE cysts regarding infected organ have been previously described. In *E. granulosus* s.l. cysts from buffalo, the maturation rate of protoscoleces of liver origin was found to be different as compared to those of lung origin [8]. Also, a morphological study showed that larger protoscoleces were found in lungs CE cysts compared to those found in liver CE cysts, and presented size variability depending on the organ localization, among other variables [9]. So far, the identification of the molecular mechanisms that drive these differences remain unknown.

In a "classic approach" of gene expression profiles, the analyses focus on the individual genes, ignoring completely the interactions and expression minor variation among them, leaving a gap of information as genes play roles not by isolation but by interaction with each other. The gene-to-gene co-expression analysis emerged as an approach to solve the gene interaction problems [10]. Weighted gene co-expression network analysis (WGCNA) has been applied to many studies since late 2008, when the R package WGCNA was released [11], and then growing exponentially, being the 2012 the first year to reach 10 articles per year with this methodology and in the 2021 reaching more than 600 articles per year already published. Focusing on high complexity and multifactorial biological problems, WGCNA can be used as a data exploratory tool or as a gene screening method; having applications in gene expression and protein interaction data, among others [12]. Comparing gene expression networks (not only an individual gene) between set samples may identify modules of co-expressed genes and expression profiles of intramodular hub genes inside an interesting module, showing the Connectivity (the relative importance of a gene in a network). This approach may be performed to identifying this hub genes as possible therapeutic targets based on the constructed network [13, 14].

WGCNA has been already proposed to explore the parasite—host interaction. In human patients with chronic Chagas disease (*Trypanosoma cruzi*), hub genes were found associated with immune cell signaling pathways, T cell activation and B cell cellular immunity, although gene expression analysis of the parasite were not done [15]. In another instance, transcriptomic analyses of the freshwater snail *Oncomelania hupensis*, were performed after 3 different times of invasion with the parasite *Schistosoma japonicum*, finding a module related to ribosomes, translation, mRNA processing, among others, associated with *Schistosoma* infection [16]. Another work explored the presence of non-conserved modules and its hub genes between complicated

and uncomplicated disease generated by protozoan *Plasmodium falciparum*, finding differences among those groups and identifying key genes for the development of the parasite [17]. Similar experiences have been performed in *Trypanosoma brucei* species, being those findings key in the potential identification of molecular targets to control the disease [18]. These findings show that WGCNA is a useful tool in the analysis of transcriptomic data in samples from parasite diseases, although most of them are focused on the host instead of the parasite.

Thus, it would not be unexpected that more complex statistical methods, such as the generation of co-expression networks, could help to elucidate subtle differences associated with parasite survival in different host organs. Therefore, to understand the differences in gene expression between *E. granulosus* s.s. protoscoleces found in liver and lung CE cysts, a WGCNA was performed. We found several modules with hub genes coding for hypothetical protein products and immune evasion related modules, revealing gene co-expression networks. Furthermore, we discuss possible molecular mechanisms performed by *Echinococcus granulosus* s.s. in response to adverse environments found in different organs that they can parasitize.

Materials and methods

Sample collection and protoscolex viability

Fresh CE cysts were obtained from sheep liver and lung in a slaughterhouse. All CE cysts were visually inspected and each one was considered an individual sample. The protoscoleces obtained were washed with PBS pH 7.2. The viability of protoscoleces was assessed with the trypan blue exclusion test. All samples showing less than 90% of viability were discarded. Suitable protoscolex samples (>90% viability) were conserved in RNAlater® solution and frozen at −80°C.

DNA isolation and genotype identification

To corroborate the genetic identity and molecular diversity of the protoscolex samples, DNA was extracted and the full length of the mitochondrial cox1 was amplified and sequenced, as previously described [2]. Briefly, DNA isolation was performed with WIZARD Plus SV Genomic Purification Systems kit (PROMEGA). The *E. granulosus* s.s. mithocondrial haplotypes were identified using the full length of the cytochrome C oxidase subunit gene (cox1, 1609bp). The PCR was performed with 30–100 ng of DNA, using 0.5 U DNA Taq Pol, 1X Buffer Taq DNA Pol (20 mM Tris-HCl, pH 8.4, 50 mM KCl), 0.04 mM mix dNTP, 1.5 mM $MgCl_2$ and 20 pmol of each primer (5′-TTA CTG CTA ATA ATT TTG TGT CAT-3′ forward and 5′-GCA TGA TGC AAA AGG CAA ATA AAC-3′ reverse) in a final volume of 25 µL. After the amplification, the amplicons were purified and sequenced. Only *E. granulosus* s.s. samples were used in further experiments.

RNA isolation and cDNA library preparation

Total RNA was extracted from CE cyst protoscolex with Rneasy® mini kit, then it was measured by fluorometry (Qubit 2.0, Invitrogen). The inclusion criteria were: high purity (A260/A280 > 1.8), 1ug of total RNA, and an electropherogram similar to the reported from [19]. Libraries were made with Illumina TruSeq® Stranded mRNA Library Prep Kit, following the manufacturer's protocol. These libraries were sequenced in paired-end on Illumina HiSeq4000 platform.

WCGNA analysis

Twelve protoscolex samples were obtained; six samples from sheep liver CE cysts and six samples from sheep lung CE cysts. Six of these samples, three liver and three lung CE cyst samples, where obtained from the same sheep. RAW files were adapter trimmed with TrimmGalore to remove low quality sequences, primers and adapters and trimmed to a set length cutoff of 50 bp. Quality control was performed with FastQC, the alignment was made with STAR and the reference genome was GCA_000524195.1 ASM52419v1. Data normalization and gene count estimation were performed by DESeq2 as described elsewhere [20]. The Gene co-expression calculation was performed with WCGNA R package with bi-weight mid-correlation method [11, 21]. We used a soft-thresholding power for the network construction to obtain the closest scale-free topology. In that regard, we used the β power value of 30 with SFT.R.sq = 0.835000.

Gene clusters were identified by hierarchical method and the expression values were summarized into module eigengenes (ME). Calculation of Intramodular Hub Genes (kME) was performed correlating the expression of each gene and its ME. To choose the hub genes, we picked the 10% of the top genes from the module that also showed kME values higher than 0.95. The set of genes associated with each cluster were categorized and functionally enriched based gene ontology (GO) annotations from the genome (available in WormBase ParaSite: PRJNA182977) using the Blast2GO software. WGCNA co-expression network and only connections with a value > 0.1 were selected to generate the Gen-Gen Interaction network using Cytoscape. The homology search was performed through the web version of BLAST [22].

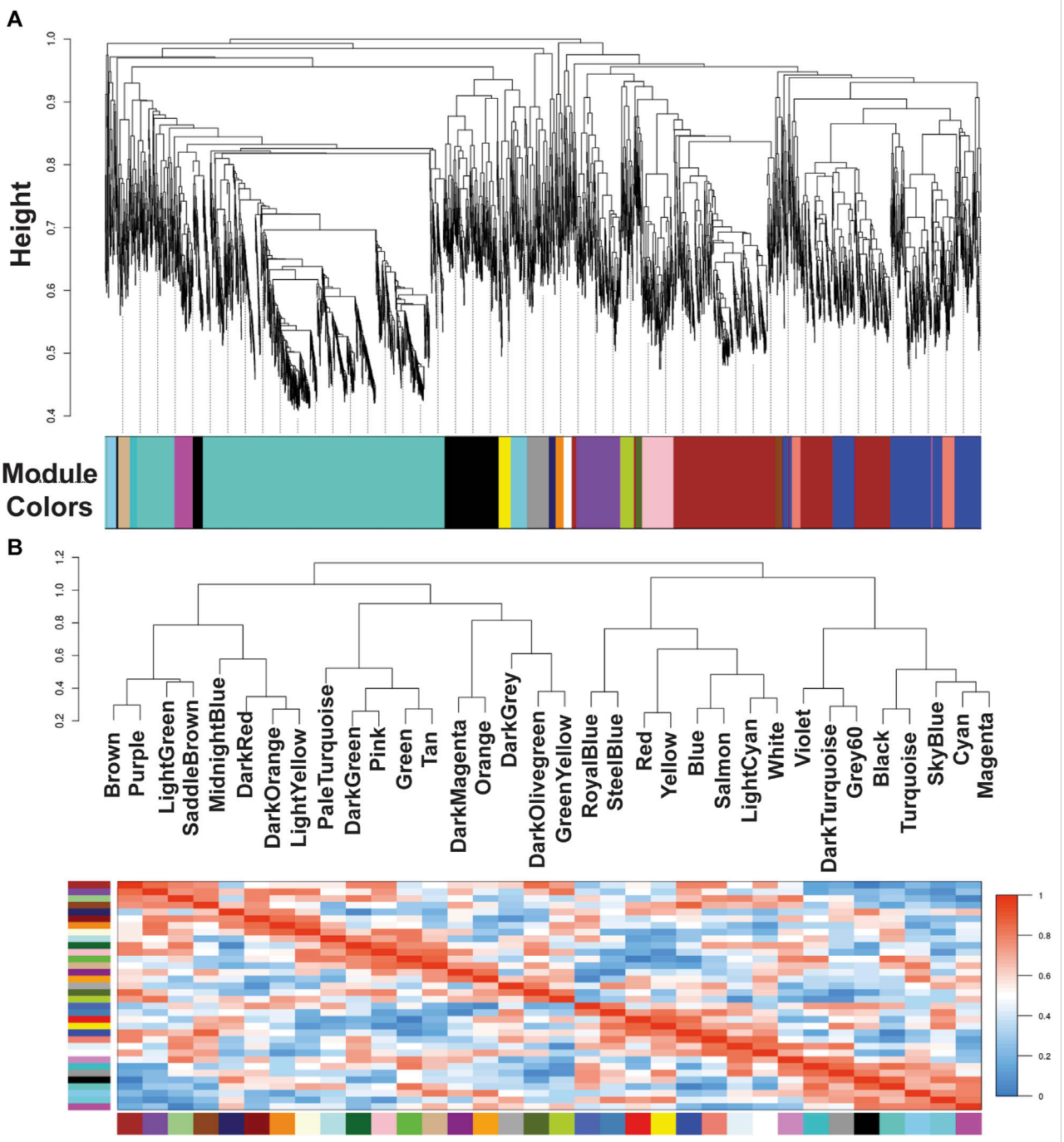

FIGURE 1
Module colors identification and Cluster dendrogram. **(A)** Identification of gene co-expression modules in *Echinococcus granulosus* sensu stricto protoscoleces from sheep liver CE cyst samples. The y-axis (Height) denotes the co-expression distance, and the x-axis corresponds to genes. Each color in the horizontal bar, but grey, represents a module. **(B)** Clustering dendrograms of consensus module eigengenes for identifying meta-modules and Heatmap of eigengene adjacencies in the consensus eigengene network. Each row and column correspond to one eigengene (labeled by consensus module color). Within the heatmap, red indicates high adjacency (positive correlation) and green low adjacency (negative correlation) as shown by the color legend. CE, cystic echinococcosis.

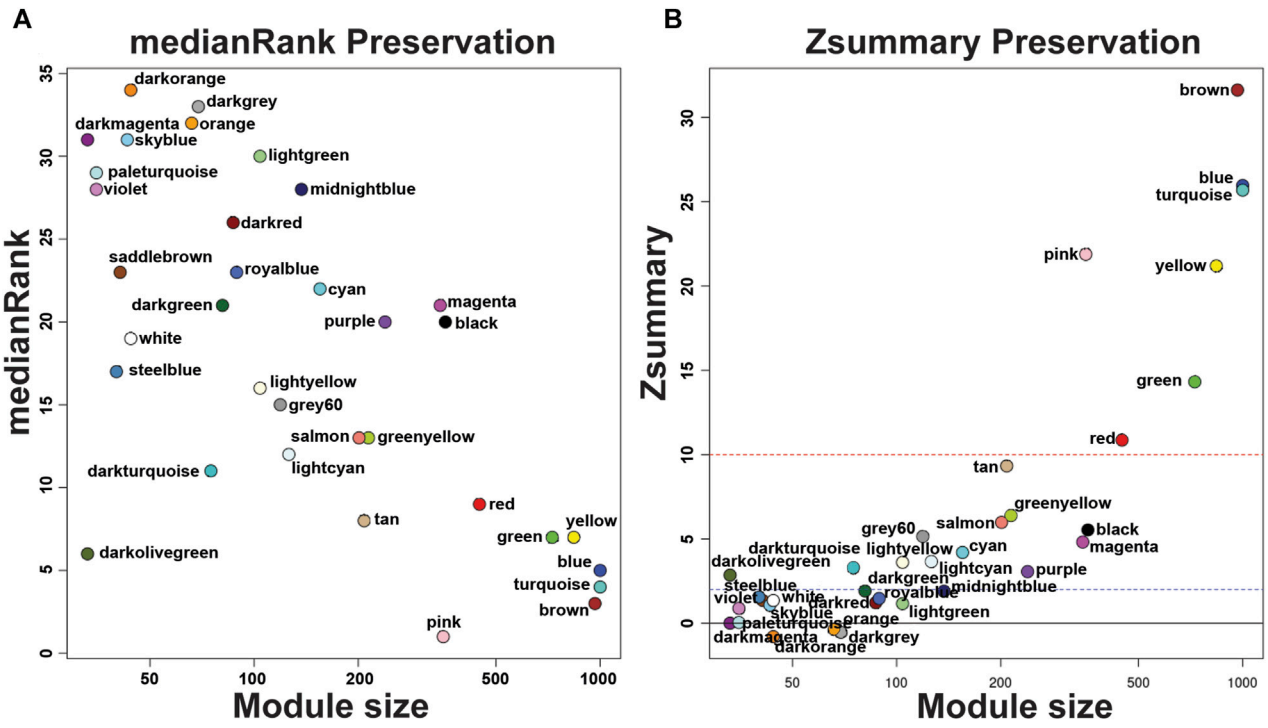

FIGURE 2
medianRank Preservation graph and Preservation Zsummary graph of *Echinococcus granulosus* sensu stricto protoscoleces genes from sheep liver CE cysts. **(A)** medianRank Preservation graph. Modules close to zero indicates a high degree of module preservation. **(B)** Preservation Zsummary graph. The dashed blue line indicates threshold Z = 2 and the red dashed line indicates threshold Z = 10. Each dot and its color belong to a module. Modules over the red line (high threshold) show strong evidence of conservation. Modules under the blue line (low threshold) show non-conservated modules. CE, cystic echinococcosis.

Results

Functional analysis of co-expressed genes from liver

Our group previously described that the transcriptome analysis of protoscoleces shows a difference in immune modulation gene expression from cattle compared with sheep CE cysts. Besides, RNA-seq data were used to generate specific gene co-expression networks for each organ, lung and liver and determine the differentially immune genes expressed [23]. Using the information of the transcriptome analysis indicated above, through the WGCNA package pipeline, we identified that none of the transcriptome samples were identified as outlier and all 12 (6 for each organ-related network) samples were used in the following analyses. The soft thresholding measurement method was used, and for protoscoleces obtained from lung CE cysts the R^2 was 0.58000, which could lead to a loss of information since the WGCNA analyzes are optimized for this type of network. In the case of the liver-related network, it approached the free scale with a R^2 0.8350. We found 34 modules in the liver-related network, of which 12 have differential co-expression evidence in lung-related data (Figures 1, 2), namely: DarkGreen, DarkMagenta, DarkRed, LightGreen, MidnightBlue, PaleTurquoise, RoyalBlue, SaddleBrown, SkyBlue, SteelBlue, Violet, and White. These poorly conserved modules between the organ-related networks bring evidence of possible differentially regulated functions in each organ and were used for the following analyses.

In each module we determined the hub genes, based on the top 10% genes of each module and high modular membership values (kME > 0.95). Based on this criteria, the DarkGreen module contains 81 genes with 8 hub genes, being all of them known protein products (EGR_02690, EGR_01846, EGR_05826, EGR_02913, EGR_07704, EGR_01998, EGR_10154, EGR_09352), the DarkMagenta module contains 33 genes with 3 hub genes, two of them being known protein products (EGR_02218, EGR_04252) and one hypothetical protein (EGR_06698), the DarkRed module containing 87 genes with 9 hub genes, 6 of them being known protein products (EGR_00876, EGR_07433, EGR_04831, EGR_09718, EGR_00075, EGR_08644) and 3 hypothetical protein (EGR_11274, EGR_04917, EGR_08751), the LightGreen module contains 104 genes with 10 hub genes, being 7 genes with known protein products (EGR_10065, EGR_05327, EGR_00014, EGR_00729, EGR_08745, EGR_01426, EGR_02708) and

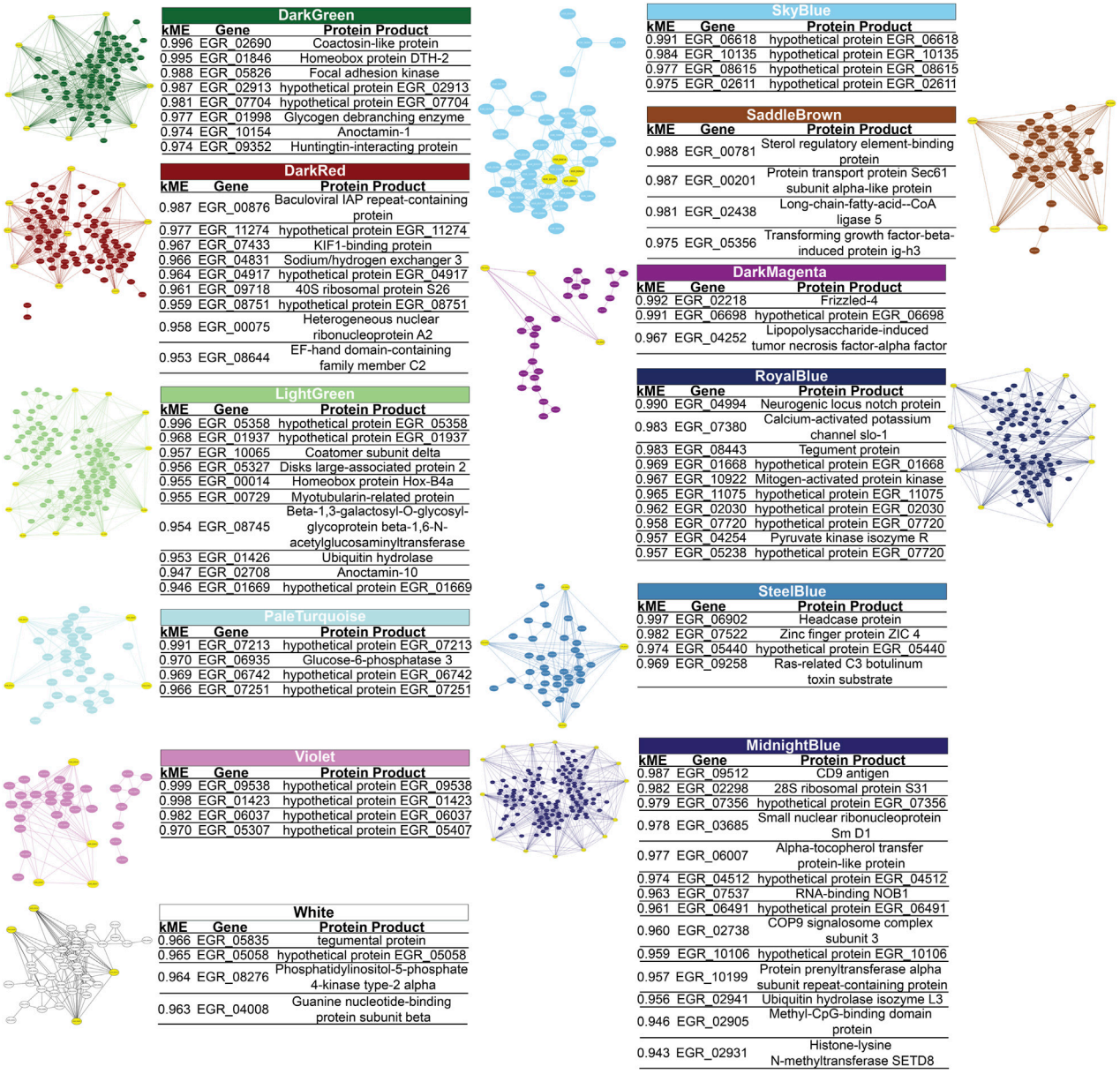

FIGURE 3
Gene-Gene interaction network of *Echinococcus granulosus* sensu stricto protoscoleces genes from sheep liver CE cysts inside each module. Yellow genes indicate hub genes based on the top 10% genes of each module and high modular membership (kME) values > 0.95. CE, cystic echinococcosis. Three modules contain hub genes related to immune evasion: inside the RoyalBlue module there is the gene that codes for tegument antigen (EGR_08443) and inside the White there is the gene that codes for tegumental protein (EGR_05835), being both genes specific from *E. granulosus* s.l., and inside the MidnightBlue module we found genes for ubiquitin hydrolase isozyme L3 (EGR_02941), COP9 signalosome complex subunit 3 (EGR_02738), tetraspanin CD9 antigen (EGR_09512), and the methyl-CpG-binding protein Mbd2 (EGR_02905).

3 hypothetical proteins (EGR_05358, EGR_01937, EGR_01669). The MidnightBlue module contains 137 genes with 14 hub genes, 10 of known protein products (EGR_09512, EGR_02298, EGR_03685, EGR_06007, EGR_07537, EGR_02738, EGR_10199, EGR_02941, EGR_02905, EGR_02931) and 4 hypothetical protein products (EGR_07356, EGR_04512, EGR_06491, EGR_10106). The PaleTurquoise module contains 35 genes, with 4 hub genes, being only one (EGR_06935) a known protein product and the rest of them (EGR_07213, EGR_06742, EGR_07251) being hypothetical proteins. The RoyalBlue module contains 89 genes, being 10 of them hub genes, 5 with known protein products (EGR_04994, EGR_07380,

EGR_08443, EGR_10922, EGR_04254) and 5 with hypothetical protein products (EGR_01668, EGR_11075, EGR_02030, EGR_07720, EGR_05238). The SaddleBrown module contains 41 genes and 4 hub genes (EGR_00781, EGR_00201, EGR_02438, EGR_05356), no one of these genes were hypothetical proteins. The SkyBlue module shows 43 genes, being 4 of them hub genes (EGR_06618, EGR_10135, EGR_08615, EGR_02611) corresponding all to hypothetical proteins. The SteelBlue module contains 40 genes, with 4 hub genes, all of them corresponding to known protein products (EGR_06902, EGR_07522, EGR_05440, EGR_09258). In the Violet module we found 35 genes, with 4 hub genes being all hypothetical proteins (EGR_09538, EGR_01423, EGR_06037, EGR_05307). Finally, in the White module we found 44 genes, 4 of them are hub genes, 3 of them with known protein products (EGR_05835, EGR_08276, EGR_04008), and only 1 as a hypothetical protein (EGR_05058). These results are summarized in Figure 3.

Hypothetical protein similar sequences

Analyzing the percentage of hypothetical proteins involved as Hub Genes in each module, two modules (SkyBlue and Violet) contain 100% of these kinds of proteins. PaleTurquoise module shows 75% of Hypothetical proteins as Hub Genes. In the Royal blue, 50% of hub genes belongs to hypothetical proteins. The Midnightblue, DarkMagenta, DarkRed and LightGreen modules presents 36%, 33%, 33% 30% of Hypothetical Proteins as Hub Genes, respectively. Finally, DarkGreen, SteelBlue and White Modules has Hypothetical Proteins as Hub genes in a 25% of the total hub genes. The SaddleBrown module did not show any Hypothetical Protein as Hub gene inside the module.

Since there are many hypothetical proteins as hub genes in the modules, we also performed a sequence similarity search with the Basic Local Alignment Search Toll (BLAST) in each hypothetical protein from each module. In the DarkGreen module EGR_02913 has a 90,91% of identity with *Hymenolepis microstoma* genome assembly, chromosome: 4 (*H. microstoma*) and EGR_07704 has 82,3% of identity with *H. microstoma* genome assembly, chromosome: 1 (*H. microstoma*), both with a Query cover less than 2%. Inside the RoyalBlue module, the EGR_01668 gene has a 79.62% of identity with *Taenia asiatic*a clone TaHC4-G1 mRNA sequence (*T. asiatica*) and a Query cover of 63%, and EGR_11075 has an identity of 81.75% with *E. granulosus* s.l. SH2 domain-containing protein 4A (EGR_05675), partial mRNA (*E. granulosus* s.l.) with a Query cover of 28%. In the SkyBlue module, the EGR_06618 gene has 100% of identity with *Echinococcus multilocularis* DNA, microsatellite EMms2 (*E. multilocularis*) and the EGR_10135 gene have 95,54% of identity with *E. granulosus* s.l. hypothetical protein (EGR_10285), partial mRNA (*E. granulosus* s.l.), both with a Query cover less than 2%. Finally, inside the Violet module the EGR_09538 presents 78,69% of identity with *E. granulosus* s.l. hypothetical protein (EGR_05124), partial mRNA (*E. granulosus* s.l.) with a Query cover of 100% and the EGR_05307 gene has 26 matches with identity percentage between 80.28% and 100% but a Query cover of less than 18% with other genes from *E. granulosus* s.l. No matches were found inside other modules. A detailed view of the gene orthology may be seen in Table 1.

Discussion

Despite morphological and pathophysiological differences in *E. granulosus* s.l. protoscoleces from lung and liver that have been previously documented [8, 24, 25], molecular processes associated with this issue has never been addressed based on next-generation sequence data. WGCNA is a method for the analysis of the gene expression patterns of multiple samples, clustering genes and form modules by similar gene expression patterns, creating co-expression networks and identifying intramodular hub genes (highly connected genes inside each module). The main differences among classical differential expression analysis and functional enrichment analysis, is that they cannot reveal connections and interactions among genes that are crucial in biological processes [26, 27]. A recent work involving 10 parasitic platyhelminths (strobilated and non-strobilated) species, identified a set of 34 evolutionary conserved cestode proteins, as possible components of developmental pathways required for strobilation, including *E. granulosus* s.l. inside the group of strobilated platyhelminths [28], This work is the only one to explore in this way some aspects of the *E. granulosus* s.s. development, but did not assess differences among parasites collected from different viscera. A previous transcriptome work did not identify differential gene expression among viscera in protoscoleces from sheep liver CE cyst and sheep lung CE cyst [23].

From the identified modules of this work, there are two interesting approaches for the discussion. The first one is to look for immune related hub genes in the modules, that can add information about the host-parasite relationship and/or immunoregulation mechanisms. The second one is the hypothetical proteins found as hub genes, as interesting targets for the study of specific and unknown mechanisms of parasitism in each organ.

On the first approach we may highlight the RoyalBlue, White and specially the MidnightBlue modules, in first two modules there is an immune related hub gene specific to *E. granulosus s.l.*, which is composed of tegument protein and tegumentary antigen. The tegumentary antigen is an immunomodulatory molecule associated with chronic infection, as it inhibits chemotaxis, induces IL-4-positive T lymphocytes and non-complement fixing antibodies (IgG4) [29]. As a specific protein from *E. granulosus s.l.*, this data suggest that suppression of a co-expressed gene may consequently also suppress the tegumentary antigen, but it has been demonstrated in our work that it will occur in liver CE cysts and could not happen in lung CE cysts.

TABLE 1 Hypothetical protein gene orthology found in the twelve modules[a] of protoscoleces from liver CE cysts.

Gene ID	Species	Description	Total score	Query cover	E value	Identity (%)	Accession N°.
DarkGreen Module							
EGR_02913	*Hymenolepis microstoma*	*Hymenolepis microstoma* genome assembly, chromosome: 4	87.9	0%	1.00 E−11	90.91	LR215995.1
EGR_07704	*Hymenolepis microstoma*	*Hymenolepis microstoma* genome assembly, chromosome: 1	99	2%	3.00 E−15	82.3	LR215989.1
DarkMagenta Module							
EGR_06698	No results						
DarkRed Module							
EGR_11274	No results						
EGR_04917							
EGR_08751							
LightGreen Module							
EGR_05358	No results						
EGR_01937							
EGR_01669							
PaleTurquoise Module							
EGR_07213	No results						
EGR_06742							
EGR_07251							
RoyalBlue Module							
EGR_01668	*Taenia asiatica*	*Taenia asiatica* clone TaHC4-G1 mRNA sequence	503	63%	1.00 E−137	79.62	EF420605.1
EGR_11075	*Echinococcus granulosus*	*Echinococcus granulosus* SH2 domain-containing protein 4A (EGR_05675), partial mRNA	209	28%	2.00 E−49	81.75	XM_024494924.1
EGR_02030	No results						
EGR_07720							
EGR_05238							
SkyBlue Module							
EGR_06618	*Echinococcus multilocularis*	*Echinococcus multilocularis* DNA, microsatellite EMms2	1759	7%	1.00 E−82	100	XM_024495867.1
EGR_10135	No results						
EGR_08615							
EGR_02611							
SteelBlue Module							
EGR_05440	No results						
Violet Module							
EGR_09538	No results						

(Continued on following page)

TABLE 1 (*Continued*) Hypothetical protein gene orthology found in the twelve modules[a] of protoscoleces from liver CE cysts.

Gene ID	Species	Description	Total score	Query cover	E value	Identity (%)	Accession N°.
EGR_05307	*Echinococcus granulosus*	*Echinococcus granulosus* clone Eg-fos-43 sequence, complete sequence	337	6	3.00 E−87	97.47	KC585049.1
		Echinococcus granulosus clone Eg-fos-02 sequence, complete sequence	593	6	9.00 E−78	94.95	KC585045.1
		E. granulosus EgBRep repetitive DNA element	305	6	9.00 E−78	94.47	X67152.1
		E. granulosus EgDRep repetitive DNA element	303	6	3.00 E−77	94.47	X67153.1
		Echinococcus granulosus clone Eg-fos-22 sequence, complete sequence	547	7	5.00 E−75	91.63	KC585042.1
		Echinococcus granulosus clone Eg-fos-45 sequence, complete sequence	276	6	7.00 E−69	92.35	KC585050.1
		Echinococcus granulosus Peripheral plasma membrane protein CASK (EGR_01323), partial	226	6	7.00 E−54	87.82	XM_024490572.1
		Echinococcus granulosus Calmodulin (EGR_01226), partial mRNA	185	4	1.00 E−41	93.60	XM_024490475.1
		Echinococcus granulosus Nucleoside diphosphate kinase A 2 (EGR_05582), partial mRNA	183	4	4.00 E−41	93.55	XM_024494831.1
		Echinococcus granulosus Neurogenic locus notch protein (EGR_04994), partial mRNA	176	4	7.00 E−39	92.62	XM_024494243.1
		Echinococcus granulosus GST (GST) gene, promoter and 5′ untranslated region	147	3	6.00 E−30	90.83	AY174162.1
		Echinococcus granulosus DNA-binding protein HEXBP (EGR_00594), partial mRNA	58.4	1	0.003	97.06	XM_024489843.1
		Echinococcus granulosus Ecdysone-induced protein 78C (EGR_04406), partial mRNA	56.5	1	0.01	100	XM_024493655.1
		Echinococcus granulosus prokaryotic DNA topoisomerase (EGR_03189), partial mRNA	56.5	1	0.01	100	XM_024492438.1
EGR_01423	No results						
EGR_06037							
White Module							
EGR_05058	No results						

[a]MidnightBlue and SaddleBrown modules had no hypothetical proteins.

In the MidnightBlue module, there are two genes related to protein degradation pathway, first, the ubiquitin hydrolase isozyme L3 (EGR_02941) has been reported before, highlighting that this protein can hydrolyze UBB(+1), (a form of ubiquitin associated with neurogenerative disorders) which is not effectively degraded by the proteasome [30]. On the other hand, we also found the COP9 signalosome complex subunit 3 (EGR_02738), an essential component of COP9 signalosome. This COP9 signalosome is a conserved molecule found in various disease-causing protozoans such as *Leishmania* spp., *Trypanosoma* spp., *Toxoplasma* spp., *and Entamoeba histolytica*. Moreover, in the latter, it was found to be essential for the normal functioning and a druggable parasite target, since disruption of the COP9 from the parasite, leads to a disrregulation of the ubiquitin proteasome pathway, impairing degradation of the proteins and leading to cell death [31]. Also, the COP9 complex

has been involved in the immune response, regulating the NF-kB function by protecting the IκBα (an inhibitor of NF-kB) from degradation, leading to reduction of the NF-kB under TNF stimulation [32]. With those two Hub genes inside this module, we speculate that this non-conserved module represents an important part of the protein degradation pathway and could be useful for the parasite to suppress the immune response from the host. Interestingly, NF-κB signaling pathway has particular relevance to several liver diseases and hepatoprotective agents, which could explain why the MidnightBlue module would be specific to this organ [33].

In the same context of the immune response, inside the MidnightBlue module, it is important to note that the tetraspanin CD9 antigen (EGR_09512) acts also as a hub gene in this module. It is known that mononuclear phagocytes fuse to form multinucleated giant cells, a hallmark of the immune response in the adventitial layer of non-fertile CE cysts [34]., When these cells cannot eliminate pathogens, cell-mediated immunity is activated and mononuclear phagocytes coalesce to form Langhans giant cells [35]. A study investigated the role of this tetraspanin associated with CD81 tetraspanin, finding that CD9 and CD81 coordinately prevent the fusion of mononuclear phagocytes [36]. These results suggest a potential role of tetraspanins associations in the immune evasion of the host.

The methyl-CpG-binding protein Mbd2 (EGR_02905) is another important hub gene found in the MidnightBlue, in a study performed in bone marrow-derived dendritic cells (DC) from wild-type (WT) and $Mbd2^{-/-}$ mice, the DC from $Mbd2^{-/-}$ mice presented different mRNA expression, with 70 genes downregulated and 49 genes upregulated (compared with WT). Among these downregulated genes, many of them were related to immunological processes like antigen presentation, showing that this gene is able to induce control over other genes and also suggesting that the inhibition of Mbd2 may impair the optimal DC function and the initiation of a Th2 immune response (which is the main response against helminths [37]). It is curious that a parasite expresses a gene which is responsible of maintaining an adequate immune response against helminthes. We hypothesize that the parasite molecule can mimics host molecule and then evading the immune response, although more studies are needed to confirm this.

With these findings we may think that the MidnightBlue module is important in the immune evasion response and may represent possible therapeutic targets, as all hub genes inside the module are highly connected. This approach opens a window to new therapeutic strategies, as we found specific gene interaction occurring only in protoscoleces from liver but not in lung CE cysts. These differences should be taken into account as the generation of the cyst in the liver may involve different pathways than the occurring in the lung, so it is not misguided to think, as it seems to be a different process of cyst development, as different strategies to control the liver and lung echinococcosis.

Another interesting approach is that SkyBlue and Violet hub genes are exclusively Hypothetical proteins. It means that there are a group of unknown function proteins performing key roles in the parasitism of protoscolex in liver CE cysts, that are not co-expressed in lung CE cysts protoscoleces. This finding also suggests that the microenvironment promoted by the host induces changes in parasite gene expression, which could not be identified by more conventional transcriptomic analyses [23]. As no significative results of homology analysis, we may think that there are many genes of the unknown function that should be explored.

An important limitation of our work that is important to know, is that this approach needs mainly RNA-seq data that considers large number of replicates with low variation among them [28]. Despite this difficulties, choosing a topology close to a scale free-network seems to be a good model to work on, as despite universality of scale-free networks remains controversial, biological networks appear strongly scale free [38]. Conversely, while it is true that would be better to work with more samples, our data will be available for future exploration complemented with more samples obtained from other researchers.

A second approach is to find non-conserved modules in the protoscoleces from lung CE cysts compared to protoscoleces from liver CE cysts. Attempts to perform were unsuccessful, as it was not possible to get a scale-free network in protoscoleces from lung CE cysts, which could lead to a loss of information since the WGCNA analyzes are optimized for this type of network. However, the impossibility of obtaining the scale-free network only prevented an analysis of the conservation of the data of protoscoleces from liver CE cysts data for the identified modules in protoscoleces from lung CE cysts. Thus, data regarding the possible existence of new protoscoleces from lung CE cyst modules, which are not identified in protoscoleces from liver CE cysts, were not included in this work.

Nonetheless, the investigation into hub genes presents a promising avenue for translational research, potentially informing the development of novel therapeutic or control strategies against *E. granulosus*. A pertinent example is the work of Cancela et al. [39], who identified a novel subfamily of nuclear receptors with two DNA-binding domains (2DBDs)—a feature not yet reported in vertebrates. Their elucidation of the full-length 3D structure of the, Eg2DBDα.1 nuclear receptor in *E. granulosus* offers valuable insights into the receptor and structure-function relationship, highlighting its potential as a target for novel anthelmintic drugs.

This research contributes to the understanding of differential gene expression regulation in *E. granulosus*, underscoring the potential role of the organ-specific environment in exerting selective pressure on the parasite. Such environmental influences may have been pivotal in the evolution of certain *E. granulosus* s.l. lineages, enhancing their infective efficacy under specific conditions.

Conclusion

This work shows that there are differences in gene expression in protoscoleces from Cystic Echinococcosis cysts found in the

liver and lungs. We found 34 modules in protoscoleces from liver CE cysts, 12 of which showed differential co-expression compared to protoscoleces from lung CE cysts. Several of these differentially co-expressed modules contain genes related to immune evasion as well as hypothetical proteins of unknown function that are co-expressed exclusively in protoscoleces from liver CE cysts. This suggests there are molecular differences in protoscoleces based on the organ environment of the CE cyst, which has implications for understanding and controlling CE infection.

Author contributions

IP, GPP, MB, and AR conducted the experiments, CM supplied critical reagents (Bioanalyzer), IP, GPP, and CH drafted the manuscript. All authors contributed to the article and approved the submitted version.

Data availability statement

The original contributions presented in the study are included in the article/supplementary material, further inquiries can be directed to the corresponding author.

Ethics statement

This study was approved by the Universidad Andres Bello bioethics committee, Protocol Number 012/2019.

Funding

The authors disclosed receipt of the following financial support for the research, authorship, and/or publication of this article: This work was supported by the Agencia Nacional de Investigación y Desarrollo (ANID) (FONDECYT grant number 1231620).

Conflict of interest

The authors declare that the research was conducted in the absence of any commercial or financial relationships that could be construed as a potential conflict of interest.

Publisher's note

Please note that the review of this paper was conducted at the previous publisher, SAGE.

References

1. Almulhim AM, John S. *Echinococcus granulosus*. Treasure Island: StatPearls Publishing (2022).

2. Hidalgo C, Stoore C, Pereira I, Paredes R, Alvarez Rojas CA. Multiple haplotypes of Echinococcus granulosus sensu stricto in single naturally infected intermediate hosts. *Parasitol Res* (2020) **119**:763–70. doi:10.1007/s00436-019-06578-2

3. Hidalgo C, Stoore C, Baquedano MS, Pereira I, Franco C, Hernandez M, et al. Response patterns in adventitial layer of Echinococcus granulosus sensu stricto cysts from naturally infected cattle and sheep. *Vet Res* (2021) **52**:66. doi:10.1186/s13567-021-00936-8

4. Hidalgo C, Garcia MP, Stoore C, Ramirez JP, Monteiro KM, Hellman U, et al. Proteomics analysis of Echinococcus granulosus protoscolex stage. *Vet Parasitol* (2016) **218**:43–5. doi:10.1016/j.vetpar.2015.12.026

5. Wang X, Zhu A, Cai H, Liu B, Xie G, Jiang R, et al. The pathology, phylogeny, and epidemiology of Echinococcus ortleppi (G5 genotype): a new case report of echinococcosis in China. *Infect Dis Poverty* (2021) **10**:130. doi:10.1186/s40249-021-00907-3

6. Alvarez Rojas CA, Romig T, Lightowlers MW. Echinococcus granulosus sensu lato genotypes infecting humans--review of current knowledge. *Int J Parasitol* (2014) **44**:9–18. doi:10.1016/j.ijpara.2013.08.008

7. Yanagida T, Mohammadzadeh T, Kamhawi S, Nakao M, Sadjjadi SM, Hijjawi N, et al. Genetic polymorphisms of Echinococcus granulosus sensu stricto in the Middle East. *Parasitol Int* (2012) **61**:599–603. doi:10.1016/j.parint.2012.05.014

8. Irshadullah M, Nizami W. Development of protoscoleces of Echinococcus granulosus from buffalo liver and lung cysts in dogs. *Parasitologica Hungarica* (1992) **25**:15–22.

9. Almeida FB, Rodrigues-Silva R, Neves RH, Romani EL, Machado-Silva JR. Intraspecific variation of Echinococcus granulosus in livestock from Peru. *Vet Parasitol* (2007) **143**:50–8. doi:10.1016/j.vetpar.2006.07.028

10. Liu BH. Differential coexpression network analysis for gene expression data. *Methods Mol Biol* (2018) **1754**:155–65. doi:10.1007/978-1-4939-7717-8_9

11. Langfelder P, Horvath S. WGCNA: an R package for weighted correlation network analysis. *BMC Bioinformatics* (2008) **9**:559. doi:10.1186/1471-2105-9-559

12. Dai Y, Sun X, Wang C, Li F, Zhang S, Zhang H, et al. Gene co-expression network analysis reveals key pathways and hub genes in Chinese cabbage (Brassica rapa L.) during vernalization. *BMC Genomics* (2021) **22**:236. doi:10.1186/s12864-021-07510-8

13. Zhao W, Langfelder P, Fuller T, Dong J, Li A, Hovarth S. Weighted gene coexpression network analysis: state of the art. *J Biopharm Stat* (2010) **20**:281–300. doi:10.1080/10543400903572753

14. Liu X, Hu AX, Zhao JL, Chen FL. Identification of key gene modules in human osteosarcoma by co-expression analysis weighted gene co-expression network analysis (WGCNA). *J Cell Biochem* (2017) **118**:3953–9. doi:10.1002/jcb.26050

15. Zhou L, Li Z, Li J, Yang S, Gong H. Detecting imperative genes and infiltrating immune cells in chronic Chagas cardiomyopathy by bioinformatics analysis. *Infect Genet Evol* (2021) **95**:105079. doi:10.1016/j.meegid.2021.105079

16. Feng X, Zhu L, Qin Z, Mo X, Hao Y, Jiang Y, et al. Temporal transcriptome change of Oncomelania hupensis revealed by Schistosoma japonicum invasion. *Cel Biosci* (2020) **10**:58. doi:10.1186/s13578-020-00420-4

17. Subudhi AK, Boopathi PA, Pandey I, Kaur R, Middha S, Acharya J, et al. Disease specific modules and hub genes for intervention strategies: a co-expression network based approach for Plasmodium falciparum clinical isolates. *Infect Genet Evol* (2015) **35**:96–108. doi:10.1016/j.meegid.2015.08.007

18. Mwangi KW, Macharia RW, Bargul JL. Gene co-expression network analysis of Trypanosoma brucei in tsetse fly vector. *Parasites and Vectors* (2021) **14**:74. doi:10.1186/s13071-021-04597-6

19. Bai Y, Zhang Z, Jin L, Kang H, Zhu Y, Zhang L, et al. Genome-wide sequencing of small RNAs reveals a tissue-specific loss of conserved microRNA families in Echinococcus granulosus. *BMC genomics* (2014) **15**:736–13. doi:10.1186/1471-2164-15-736

20. Love MI, Huber W, Anders S. Moderated estimation of fold change and dispersion for RNA-seq data with DESeq2. *Genome Biol* (2014) **15**:550. doi:10.1186/s13059-014-0550-8

21. Song L, Langfelder P, Horvath S. Comparison of co-expression measures: mutual information, correlation, and model based indices. *BMC Bioinformatics* (2012) **13**:328. doi:10.1186/1471-2105-13-328

22. Liu Y, Gu H-Y, Zhu J, Niu Y-M, Zhang C, Guo G-L. Identification of hub genes and key pathways associated with bipolar disorder based on weighted gene co-expression network analysis. *Front Physiol* (2019) **10**:1081. doi:10.3389/fphys.2019.01081

23. Pereira I, Hidalgo C, Stoore C, Baquedano MS, Cabezas C, Bastias M, et al. Transcriptome analysis of Echinococcus granulosus sensu stricto protoscoleces reveals differences in immune modulation gene expression between cysts found in cattle and sheep. *Vet Res* (2022) **53**:8. doi:10.1186/s13567-022-01022-3

24. Torgerson PR, Ziadinov I, Aknazarov D, Nurgaziev R, Deplazes P. Modelling the age variation of larval protoscoleces of Echinococcus granulosus in sheep. *Int J Parasitol* (2009) **39**:1031–5. doi:10.1016/j.ijpara.2009.01.004

25. Zhang X, Gong W, Cao S, Yin J, Zhang J, Cao J, et al. Comprehensive analysis of non-coding RNA profiles of exosome-like vesicles from the protoscoleces and hydatid cyst fluid of Echinococcus granulosus. *Front Cel Infect Microbiol* (2020) **10**: 316. doi:10.3389/fcimb.2020.00316

26. Tian Z, He W, Tang J, Liao X, Yang Q, Wu Y, et al. Identification of important modules and biomarkers in breast cancer based on WGCNA. *OncoTargets Ther* (2020) **13**:6805–17. doi:10.2147/ott.s258439

27. Chen S, Yang D, Lei C, Li Y, Sun X, Chen M, et al. Identification of crucial genes in abdominal aortic aneurysm by WGCNA. *PeerJ* (2019) **7**:e7873. doi:10.7717/peerj.7873

28. Paludo GP, Thompson CE, Miyamoto KN, Guedes RLM, Zaha A, de Vasconcelos ATR, et al. Cestode strobilation: prediction of developmental genes and pathways. *BMC Genomics* (2020) **21**:487. doi:10.1186/s12864-020-06878-3

29. Ortona E, Margutti P, Delunardo F, Nobili V, Profumo E, Riganò R, et al. Screening of an Echinococcus granulosus cDNA library with IgG4 from patients with cystic echinococcosis identifies a new tegumental protein involved in the immune escape. *Clin Exp Immunol* (2005) **142**:528–38. doi:10.1111/j.1365-2249.2005.02939.x

30. Dennissen FJ, Kholod N, Hermes DJ, Kemmerling N, Steinbusch HW, Dantuma NP, et al. Mutant ubiquitin (UBB+1) associated with neurodegenerative disorders is hydrolyzed by ubiquitin C-terminal hydrolase L3 (UCH-L3). *FEBS Lett* (2011) **585**: 2568–74. doi:10.1016/j.febslet.2011.06.037

31. Ghosh S, Farr L, Singh A, Leaton LA, Padalia J, Shirley DA, et al. COP9 signalosome is an essential and druggable parasite target that regulates protein degradation. *Plos Pathog* (2020) **16**:e1008952. doi:10.1371/journal.ppat.1008952

32. Asare Y, Shagdarsuren E, Schmid JA, Tilstam PV, Grommes J, El Bounkari O, et al. Endothelial CSN5 impairs NF-κB activation and monocyte adhesion to endothelial cells and is highly expressed in human atherosclerotic lesions. *Thromb Haemost* (2013) **110**:141–52. doi:10.1160/th13-02-0155

33. Sun B, Karin M. NF-κB signaling, liver disease and hepatoprotective agents. *Oncogene* (2008) **27**:6228–44. doi:10.1038/onc.2008.300

34. Hidalgo C, Stoore C, Strull K, Franco C, Correa F, Jimenez M, et al. New insights of the local immune response against both fertile and infertile hydatid cysts. *PLoS One* (2019) **14**:e0211542. doi:10.1371/journal.pone.0211542

35. Steinberg TH, Hiken JF. P2 receptors in macrophage fusion and osteoclast formation. *Purinergic Signal* (2007) **3**:53–7. doi:10.1007/s11302-006-9036-9

36. Takeda Y, Tachibana I, Miyado K, Kobayashi M, Miyazaki T, Funakoshi T, et al. Tetraspanins CD9 and CD81 function to prevent the fusion of mononuclear phagocytes. *J Cel Biol* (2003) **161**:945–56. doi:10.1083/jcb.200212031

37. Cook PC, Owen H, Deaton AM, Borger JG, Brown SL, Clouaire T, et al. A dominant role for the methyl-CpG-binding protein Mbd2 in controlling Th2 induction by dendritic cells. *Nat Commun* (2015) **6**:6920. doi:10.1038/ncomms7920

38. Broido AD, Clauset A. Scale-free networks are rare. *Nat Commun* (2019) **10**: 1017. doi:10.1038/s41467-019-08746-5

39. Cancela S, Esteves A, Alvite G, Paulino M. Modeling, molecular dynamics and docking studies of a full-length Echinococcus granulosus 2DBD nuclear receptor. *J Biomol Struct Dyn* (2023) **41**:1414–23. doi:10.1080/07391102.2021.2023641

EBM Experimental Biology and Medicine

TYPE Original Research
PUBLISHED 02 April 2024
DOI 10.3389/ebm.2024.10059

OPEN ACCESS

*CORRESPONDENCE
Osbourne Quaye,
oquaye@ug.edu.gh

RECEIVED 23 November 2023
ACCEPTED 22 February 2024
PUBLISHED 02 April 2024

CITATION
Amegashie EA, Asamoah P, Ativi LEA, Adusei-Poku M, Bonney EY, Tagoe EA, Paintsil E, Torpey K and Quaye O (2024), Clinical outcomes and immunological response to SARS-CoV-2 infection among people living with HIV.
Exp. Biol. Med. 249:10059.
doi: 10.3389/ebm.2024.10059

Clinical outcomes and immunological response to SARS-CoV-2 infection among people living with HIV

Esimebia Adjovi Amegashie[1], Prince Asamoah[1], Lawrencia Emefa Ami Ativi[2], Mildred Adusei-Poku[2], Evelyn Yayra Bonney[3], Emmanuel Ayitey Tagoe[4], Elijah Paintsil[5], Kwasi Torpey[6] and Osbourne Quaye[1]*

[1]Department of Biochemistry, Cell and Molecular Biology, West African Centre for Cell Biology of Infectious Pathogens (WACCBIP), University of Ghana, Accra, Ghana, [2]Department of Medical Microbiology, University of Ghana Medical School, College of Health Sciences, University of Ghana, Accra, Ghana, [3]Department of Virology, Noguchi Memorial Institute for Medical Research, University of Ghana, Accra, Ghana, [4]Department of Medical Laboratory Sciences, School of Biomedical and Allied Health Sciences, University of Ghana, Accra, Ghana, [5]Department of Paediatrics, Yale School of Medicine, Yale University, New Haven, CT, United States, [6]Department of Population, Family and Reproductive Health, School of Public Health, University of Ghana, Accra, Ghana

Abstract

People living with HIV (PLWH) usually suffer from co-infections and co-morbidities including respiratory tract infections. SARS-CoV-2 has been reported to cause respiratory infections. There are uncertainties in the disease severity and immunological response among PLWH who are co-infected with COVID-19. This review outlines the current knowledge on the clinical outcomes and immunological response to SARS-CoV-2 among PLWH. Literature was searched in Google scholar, Scopus, PubMed, and Science Direct conforming with the Preferred Reporting Items for Systematic reviews and Meta-analyses (PRISMA) guidelines from studies published from January 2020 to June 2023. A total of 81 studies from 25 countries were identified, and RT-PCR was used in confirming COVID-19 in 80 of the studies. Fifty-seven studies assessed risk factors and clinical outcomes in HIV patients co-infected with COVID-19. Thirty-nine of the studies indicated the following factors being associated with severe outcomes in HIV/SARS-CoV-2: older age, the male sex, African American race, smoking, obesity, cardiovascular diseases, low $CD4^+$ count, high viral load, tuberculosis, high levels of inflammatory markers, chronic kidney disease, hypertension, diabetes, interruption, and delayed initiation of ART. The severe outcomes are patients' hospitalization, admission at intensive care unit, mechanical ventilation, and death. Twenty (20) studies, however, reported no difference in clinical presentation among co-infected compared to mono-infected individuals. Immune response to SARS-CoV-2 infection was investigated in 25 studies, with some of the studies reporting high levels of inflammatory markers, T cell exhaustion and lower positive conversion rate of IgG in PLWH. There is scanty information on the cytokines that predisposes to

severity among HIV/SARS-CoV-2 co-infected individuals on combined ART. More research work should be carried out to validate co-infection-related cytokines and/or immune markers to SARS-CoV-2 among PLWH.

KEYWORDS

people living with HIV, immunological response, clinical outcomes, COVID-19, HIV/SARS-CoV-2 coinfection

Impact statement

People living with HIV often experience co-infections and co-morbidities, including respiratory tract infections. SARS-CoV-2 which is known to cause severe respiratory tract infections, has been reported among PLWH. There are, however, conflicting reports on HIV patients co-infected with SARS-CoV-2 with scanty information on other human coronaviruses. Studies that reported on clinical outcomes and immunological responses were reviewed through search engines and PRISMA selection criteria, with most studies indicating similar risk factors that predisposes to disease severity. High levels of inflammatory markers, T cell exhaustion and lower positive conversion rate of IgG were identified in individuals co-infected with HIV/SARS-CoV-2. Research on cytokines and immune markers in HIV/SARS-CoV-2 co-infected individuals on combined ART is limited and therefore, necessitating further validation.

Introduction

People living with HIV (PLWH) usually suffer from co-infections and co-morbidities including respiratory tract infections, renal impairment, hypertension, diabetes, obesity, hyperlipidemia, chronic viral hepatitis, and non-AIDS-defining malignancies among others [1, 2]. These co-infections and co-morbidities tend to limit the efficacy of the antiretroviral therapy [3]. Respiratory tract infections are of a major concern due to the compromised immune state of PLWH that makes them vulnerable to severe diseases [4].

In 2019, the novel SARS-CoV-2, a new coronavirus broke out in China, also known as (COVID-19). As of September 2023, WHO reported 770,875,433 confirmed cases of COVID-19, and 6,959,316 deaths [5] spreading throughout the globe. SARS-CoV-2 has been reported to also cause more severe RTIs in HIV patients [6, 7]. Co-infections in humans have become a topic among researchers with wide interest to know their clinical importance [8, 9].

PLWH infected with COVID-19, are thought to have more complicated clinical presentations due to immunodeficiency and immune imbalance [6]. Research has reported COVID-19 in PLWH to be severe [10]. Other studies however, indicated similarity in prevalence and deleterious outcomes among both the co-infected and mono-infected [11, 12]. Bhaskaran and others reported an increased COVID-19 mortality and morbidity risk among PLWH [13], but other researchers were not convinced about this assertion and cautioned its authenticity [14].

T cell immune activation and some cytokines play a role in HIV progression [15]. COVID-19 infection has also been investigated to be associated with some immune profiles [16]. This usually leads to a cytokine storm where cytokines are then released to control inflammation causing more white blood cells to accumulate, creating a cycle of inflammation thereby damaging the lung cells. This indicates that co-infections of these HIV/SARS-CoV-2 conditions among humans may lead to harmful immunological response and a poor prognosis of disease.

This review paper sought to outline the current knowledge of clinical outcomes and immunological response to SARS-CoV-2 infection among PLWH. It also sought to identify gaps in relation to this coinfection study.

Materials and methods

Selection criteria

All studies reporting on clinical outcomes and immune response among PLWH co-infected with SARS-CoV-2 were included. All immunological studies with observational studies, cohort studies, case reports, randomized controlled trials, and case series were also included. All studies meeting the above stated criteria, published from January 2020 to June 2023 and in the English language were included. Studies that do not address clinical outcomes and immunological response among PLWH co-infected with COVID-19 were excluded from this review. Letters to editors, editorials, commentaries, and brief reports that did not report on any clinical data were excluded. Literature reviews, systematic review and meta-analysis data were excluded.

Data sources and search strategy

We searched in PubMed, Google scholar, Scopus, and Science Direct using relevant terms such as “SARS-CoV-2” or “COVID-19” and ‘HIV or “Human Immunodeficiency Syndrome” or AIDS or “Acquired Immunodeficiency Disease” or PLWH or “People

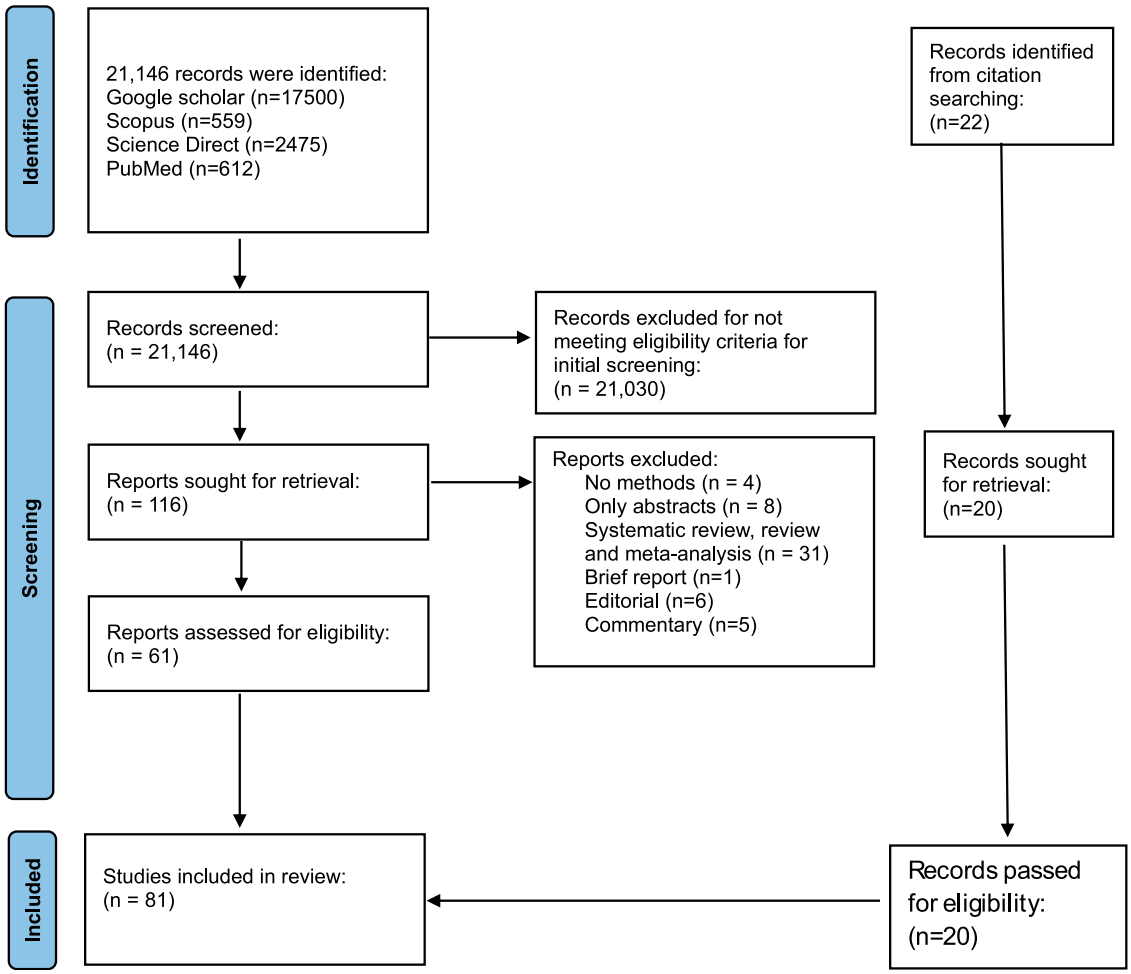

FIGURE 1
PRISMA flow diagram showing the selection criteria of studies.

Living With HIV." We then applied extra filters to access articles on "Immunological Response" or "Immune Characterization" or "Immunological Profiles" or "T-Cell Activation and Cytokines Profiles" and "Outcomes." Also, eligible studies were identified by scanning references by manual search.

Study selection

Titles were imported into Endnotes for every search, and duplicates were eliminated. Titles and abstracts were used by two researchers to independently check records for eligibility. The complete texts of any publications that were thought to be possibly eligible were then retrieved, evaluated, and unanimously chosen to be included in the study. Conflicts were arbitrated by a third investigator or resolved by consensus.

Data extraction and synthesis

Extracted data were imputed into a table. All data were in English language. Studies were curated by sampling date, study design, study place, study participants, assay type, additional tests, author, and year of publication.

Results

Studies selection was done using PRISMA guidelines (Figure 1). Databases searches (Google scholar: 17,500, Scopus: 559, ScienceDirect: 2,475, PubMed: 612) identified a total of 21,146. Eighty-three (81) studies met the eligibility criteria after the selection process (Figure 1). Endnote Software was used to remove duplicates. Also, studies that did

not meet the eligibility criteria in the initial screening were 21,031. Fifty-five (55) studies were excluded due to the following reasons: No methods (4), only abstract (8), systematic review, literature review, meta-analysis (3), Brief report (1), editorial (6) and commentary (5). A manual scanning of references resulted in 22 additional reports. Eighty-one studies were included in this analysis.

Characteristics of included studies

Studies were identified in 25 countries in this review with United State of America contributing 17 of the included studies. Other countries where studies were carried out included South Africa (12), Italy (10), China (9), Spain (7), United Kingdom (5), France (3), Russia (2) and Brazil (2). Only one study was identified in the following countries (Korea, UAE, Iran, Germany, Japan, Guinea Bissau, Netherlands, Taiwan, Sweden, Israel, Belgium, Zambia, and Indonesia). Study participants included HIV patients, HIV naïve groups, COVID-19 patients. All studies were conducted among HIV patients. RT-PCR was used in confirming human coronaviruses in 99% of the studies. ELISA techniques were also used in 14 of the studies, followed by flow cytometry (n = 9), neutralization assay (n = 5), ELISpot (n = 4).

Fifty-seven studies have assessed clinical outcomes in HIV patients that were co-infected with SARS-CoV-2 (Table 1). Immune response to COVID-19 infection was investigated by 25 studies (Table 2). 18 studies were made up of brief reports, case reports and editorials with clinical and laboratory data. All the studies were carried out from 2020 to 2023.

Thirty (38) studies reported the following risk factors as associated with severity of diseases (Table 1). This includes older age, higher BMI, male sex, deprivation, ethnicity, obesity, smoking, Tuberculosis, chronic kidney disease, higher inflammatory markers, diabetes, cardiovascular disease, lung cancer, African American, high viral load, low $CD4^+$ count, high neutrophil-lymphocyte ratio, discontinued ART usage and some ART regimen. Twenty studies however indicated that clinical presentations among the co-infected were the same as the general population therefore there was low risk of disease severity (Table 1).

Twenty-five studies looked at immunological responses (Table 2), out of which four suggested that high inflammatory markers and immune dysregulation are linked to severity of disease and death among people who are coinfected with HIV/SARS-CoV-2 and are on ART, even though the ART is supposed to help with HIV viral suppression and immune reconstitution [17–22]. HIV/SARS-CoV-2 individuals with higher pro-inflammatory markers such as C-reactive protein (CRP), IL-8, IL-6 presented with disease severity and higher mortality than those who recovered [17]. Three other studies on co-infections linked reduction of T cell numbers to increased IL-6, IL-8, and CRP levels, causing a cytokine storm [23–25]. Among the co-infected individuals, unsuppressed HIV hampers T cell cross-recognition and responses to SARS-CoV-2 infection, and thereby leading to severe outcomes [26, 27]. The pre-symptom and post recovery $CD4^+$, and $CD8^+$ counts showed no significant difference between PLWH and HIV negative individuals who are infected with SARS-CoV-2 [28]. PLWH saw a brief decline in $CD4^+$, and $CD8^+$ counts during the acute phase of COVID-19 with the CD4+/CD8+ ratio remaining unchanged [11, 28].

Most of the studies were either retrospective or prospective with one time point sample collection, therefore, no subsequent $CD4^+$ counts and viral loads to determine relationship with clinical outcomes. Two of the studies were longitudinal with one study investigating two waves of SARS-CoV-2 infection [26] and the other following up for a period of 3 months on HIV/SARS-CoV-2 patients [12]. Snyman *et al.,* indicated in their study that anti-SARS-CoV-2 IgM, IgG, and IgA levels in non-HIV individuals and PLWH on full HIV suppression on ART have similar seroconversion rates [12]. The conversion rate of anti-SARS-CoV-2 IgG was lower and quickly lost in PLWH as compared to HIV negative persons who are SARS-CoV-2 positive [29–31]. Three of the studies indicated that slower generation of anti SARS CoV2 antibodies were attributed to increased COVID-19 severity among PLWH [32–34].

Discussion

We conducted a scoping review to assess specific COVID-19 clinical outcomes and immune response in patients with human immunodeficiency virus (PLWH) and identify gaps. Hospitalisation risk, intensive care unit admission, mechanical ventilation and mortality were the four categories identified as clinical outcomes. Our review showed varied reports on risk of hospitalisation, ICU admission, mechanical ventilation and mortality in cohort studies, case series, and case reports. PLWH who died exhibited higher levels of soluble immune activation and inflammation markers, which are linked to disease severity in COVID-19 [22]. Individuals with non-suppressed HIV viremia have reported lower levels of antibodies against SARS-CoV-2 in their humoral response [35]. Some studies however, associated low risk of hospitalization and death to Tenofovir usage as compared to those on other regimen [35–37].

Immune response to SARS-CoV-2 infection among PLWH on ART

ART does not eradicate HIV completely but significantly reduces morbidity and mortality associated with the virus

[38]. ART may also reduce the severity of COVID-19 through immunological reconstitution, although these effects have not yet been confirmed [10, 36, 39]. PLWH with mild COVID-19 presentation, in the presence of high proinflammatory markers, suggested that certain antiretroviral drugs were protective against severity of COVID-19 disease [20]. A study in Russia among 376 HIV/COVID-19 patients (171 without ART and 205 with ART) suggested that elevated anti-inflammatory markers such as IL-10 and TGFβ, reduced CD4+/CD8+ cell ratios led to an increase in exhausted T cells in ART naïve patients. This led to Adverse Respiratory Distress Syndrome among the ART naïve group [32]. Sharov also reiterated that in the presence of uninterrupted ART, HIV patients do not progress to severe SARS-CoV-2 infection [32]. Other studies hypothesized that specific ART (NRTIs, NNRTIs and PI) predisposes to severe COVID-19 but no conclusive findings have been made because of studies involving smaller sample size and inconsistent cases and reports [40, 41].

Signaling pathway of HIV/SARS-CoV-2 coinfection

Viral infections interact mainly with the activated Signal Transducer and Activators of Transcription 1, 2, and 3 (STAT1, STAT2 and STAT3) to release pro-inflammatory cytokines to eliminate viruses [42]. The IL-6-JAK-STAT3 axis is significantly linked to the onset of severe COVID-19 [43, 44]. The dimerized epidermal growth factor receptor (EGFR) can tyrosine-phosphorylate STAT3, which is elevated in cases of acute lung injury [45] and in cases where STAT1 is lacking [46, 47]. As a result, in COVID-19, EGFR signalling may develop into a different pathway that stimulates STAT3 when lung damage occurs, and SARS-CoV-2 infection significantly reduces IFN-I production [48]. This aberrant transcriptional rewiring towards STAT3 may lead to the symptoms most typically reported in hospitalised COVID-19 patients: fast coagulopathy/thrombosis, proinflammatory conditions, profibrotic state, and T cell lymphopenia [49].

Some HIV proteins have been reported to inhibit effective IFNα signalling by degrading certain components of the JAK/STAT signalling pathway like STAT1 and STAT3 [50]. The impaired JAK/STAT signalling pathway is however restored in the presence of uninterrupted combined Antiretroviral therapy (cART) for more than 6 months [51]. Per our search, we found one study available on HIV/COVID-19 signalling pathway that investigated STAT3 but did not look at other STAT pathways [52], and therefore creates a gap that needs to be researched. Understanding the viral co-infection, immune response, and signalling pathway dynamics will help identify particulate markers that predisposes to severity of disease.

Oxidative stress responses among HIV/SARS-CoV-2 coinfection

Hyperactivation of STAT3 affect various biological and physiological functions, leading to oxidative stress (OxS) and poor prognosis of disease [22]. Oxidative stress (OxS) comes about by accumulating reactive oxygen and nitrogen species, which are free radicals that causes injury to organs. Under physiological conditions, these OxS are wiped out by antioxidants especially glutathione (GSH) [53]. Glutathione are endogenous intracellular antioxidants that neutralizes free radical released due to oxidative stress [54]. Deficiency in GSH however, leads to high levels of OxS due to compromised antioxidant defences [55]. Oxidative stress has been studied in HIV or SARS-CoV 2 alone with higher levels reported in each disease [55–58]. There is however scanty information on oxidative stress among HIV/COVID-19 patients, hence the need to investigate if the presence of ART usage affects oxidative stress response.

Limitations

There is lack of information on cellular immunity in other hCoVs apart from COVID-19 co-infection. Cytokine have been studied extensively in HIV or COVID-19 alone but not as a co-infection. The oxidative stress levels among HIV/SARS-CoV-2 co-infection are yet to be studied although research has been done for other co-morbidities or co-infections.

Conclusion

This study highlights the paucity of clinical and immunological data on HIV/SARS-CoV-2 co-infection in sub-Saharan Africa, even though this region has the highest HIV prevalence. Review shows conflicting reports on severity of the co-infection. HIV/SARS-CoV-2 severity and outcomes appear to be worse, when coexisting age-related comorbidities and CD4 + T-cell depletion is present. Discontinued or no evidence of ART usage have also been shown to increase disease severity, which needs to be studied further to ascertain its authenticity.

$CD4^+$ T cell lymphopenia in both diseases is influenced by various mechanisms including direct attacks, immune activation, and redistribution of $CD4^+$ T cells. Cytokines investigation will help identify markers that are implicated in disease severity among HIV/SARS-CoV-2 patients. Further investigation is needed to confirm co-infection-associated

10.3389/ebm.2024.10059

TABLE 1 Summary of clinical outcomes on HIV and SARS-CoV-2 co-infection studies and their spatial distribution.

Sample date	Study design	Study place	Study participants/ Sample size	Assay type	Additional tests	Key findings/ Outcomes	Limitations	References
2nd March-15th April 2020	brief report	United States	72 HIV patients	RT-PCR	Viral load, $CD4^+$ count, IL6, CRP, IL8, fibrinogen, D-dimer, TNF, IL-1B	High inflammatory markers and immune dysregulation linked to death in PLWH.	Study was a retrospective record limited to 1 hospital system. Complete HIV history was not available on all patients, and laboratory markers were obtained at the discretion of treating physicians	[17]
21st February-15th April 2020	Case report	Italy	383 COVID-19 patients 2 HIV co-infected	RT-PCR	Viral load, $CD4^+$ count, FBC, LFT, CRP, procalcitonin, Chest Radiograph	Not Reported	Small sample size	[59]
1st March-7th June 2020	cohort study	United States	2988 HIV participants	RT-PCR	Viral load	PLWH were more prone to hospitalization or death as compared to non-PLWH.	Analyses were limited to demographic and laboratory data available in registry and COVID-19 database, with inadequate information on co-morbidities and underlying medical conditions	[60]
1st April-1st July 2020	Non random sampling	United States	286 HIV participants	RT-PCR	Viral load, $CD4^+$ count	Older age, chronic lung disease, low $CD4^+$ count, and hypertension were associated with mortality	COVID-19 testing, treatment, and hospitalization were all done at the discretion of individual healthcare providers. There may be selection bias due to error in entries of data	[61]
1st February-15th April 2020	Observational cohort study	Spain	77,590 HIV+ patients 236 confirmed positive for COVID-19, 151 hospitalized	RT-PCR		PLWH on TDF/FTC treatment have lower risk of diagnosis and hospitalization compared to those on other ART regimen	Confounding by individual clinical characteristics cannot completely explain lower risk of COVID-19 diagnosis and hospitalization among HIV-positive individuals receiving TDF/FTC.	[10]
Dec, 2020	Retrospective cohort study	England	17,282,905 adults, 27,480 HIV +, 14,882 COVID-19 death, 25 with HIV+	RT-PCR	Glucose and HbAic measurement, Renal Function test	Deprivation, ethnicity, smoking, and obesity were linked to high risk of COVID-19 death	There were no available routinely collected data on injection drug use, occupation, or contact patterns	[13]

(Continued on following page)

TABLE 1 (*Continued*) Summary of clinical outcomes on HIV and SARS-CoV-2 co-infection studies and their spatial distribution.

Sample date	Study design	Study place	Study participants/ Sample size	Assay type	Additional tests	Key findings/ Outcomes	Limitations	References
March-April 2020	Case Report	Italy	26 HIV PATIENTS	RT-PCR	Viral load, CD4+count, FBC, CRP, Oxygen saturation, LDH	No death among PLWH co-infected with COVID-19	Small sample size	[8]
8th March-23rd April 2020	Observational Cohort study	United States	530 COVID-19, 20 PWLH	RT-PCR	Viral load, $CD4^+$ count, Oxygen saturation, X-ray, CT scan	Co-morbidities among PLWH linked to COVID-19 deaths	Smaller sample size among the co-infected	[7]
21st February-16th April 2020	Retrospective study	Italy	47 HIV patients	RT-PCR	x-ray, CT scan, Oxygen saturation, Viral load, $CD4^+$ count	45 PLWH fully recovered and 2 died	Not all the patients with HIV were confirmed to have COVID-19, and therefore limited the number of co-infected individual	[62]
23rd January-31st March 2020	Case series	China	12 HIV patients	RT-PCR	$CD4^+$ count, Viral load	ART naïve patients presented with severe symptoms, and therefore had longer hospitalization	Study underestimated the proportion of serious cases among PLWH co-infected with COVID-19	[63]
1st January-16th April 2020	Retrospective study	China	6001 PLWH, 35 coinfected with COVID-19	RT-PCR, Magnetic Chemiluminescence Enzyme Immunoassay	Viral load, $CD4^+$ count	15 HIV/SARS-CoV-2 co-infected patients had severe illness with 2 deaths. Older age and discontinued cART were associated with severe illness and death	Results from the small number of HIV/SARS-CoV-2 coinfected cannot be generalized to the population	[35]
3rd March-15th May 2020	Retrospective cohort study	United States	30 HIV patients, 90 control groups without HIV	RT-PCR	Viral load, $CD4^+$ count, Lymphocyte count, LDH, D-dimer, Procalcitonin, CRP	No difference in the need for mechanical ventilation during hospitalization, length of stay or mortality between PLWH and non-PLWH who are co-infected with COVID-19	Small sample size	[64]
March-April 2020	Retrospective study	United Kingdom	18 PLWH, 16 + with COVID-19	RT-PCR	Viral load, $CD4^+$ count	3 out of 18 PLWH died	Small sample size	[65]
April 10, 2020	Case Report	South Africa	2 HIV+/COVID-19+	RT-PCR	Oxygen saturation level, Arterial blood gas, X-ray, CT scan, Viral load, $CD4^+$ scan	PLWH have a good outcome due to their impaired immune response	Small sample size	[66]

(Continued on following page)

10.3389/ebm.2024.10059

10.3389/ebm.2024.10059

TABLE 1 (*Continued*) Summary of clinical outcomes on HIV and SARS-CoV-2 co-infection studies and their spatial distribution.

Sample date	Study design	Study place	Study participants/ Sample size	Assay type	Additional tests	Key findings/ Outcomes	Limitations	References
1st March-30th June 2020	Retrospective study	Italy	31 HIV+/COVID-19+	RT-PCR	Viral load, $CD4^+$ count, Oxygen saturation level	Patients did not require ventilation and recovered 9 days after admission	Small sample size	[67]
Not stated	Case report	United Arab Emirates	1 HIV+/COVID-19+, Kaposi +	RT-PCR	FBC, Viral load, T cell differential count, Renal function test, Blood culture, Respiratory pathogen panel, LDH, D-dimer, Fibrinogen, Ferritin Procalcitonin, CRP	Co-morbidities were associated with death	Small sample size	[68]
12th March-23rd April 2020	Cohort study	United States, New York	4402 COVID-19+, 88 PLWH	RT-PCR	White blood count, creatinine, ALT, ferritin, IL-6, D-dimer, LDH, Procalcitonin, CRP, oxygen saturation level	There was frequent hospitalization among PLWH compared to non-PLWH.	Small sample size of PLWH	[11]
20th March-30th April 2020	Retrospective study	United States	14 PLWH coinfected with COVID-19	RT-PCR	X-ray, Viral load	8 patients were hospitalized and 6 self-quarantined. There was no death	Small sample size	[69]
January-April 2020	Cohort study	France	30 HIV patients, 90 control groups without HIV	RT-PCR	$CD4^+$ count, Viral load	80% recovered from COVID-19 infection, 10% required ventilation, 6.7% died and 13.3% required hospitalization	Not reported	[70]
January-April 2020	Observational prospective study	Spain	51 HIV patients	RT-PCR	Viral load, $CD4^+$ count, Full blood count, Renal function test, ALT, Procalcitonin, CRP, ferritin, IL-6, IL-12, LDH, D-dimer, X-ray, Oxygen saturation level	4% of the HIV/SARS-CoV-2 individuals died	The small number of individuals prevented generalisation of results	[6]
8th February 2020	Case report	China	2 HIV patients	RT-PCR	IL-6, procalcitonin, ferritin, CRP, Albumin, $CD4^+$ count, Viral load, X-ray, Sars CoV2 abs test	Patients recovered.	Results were based on only two patients, and no follow-up was done due to limit resource	[71]
2nd March-23rd April 2020	Retrospective study	United States, New York	21 HIV+, 2617 HIV-COVID-19+	RT-PCR	FBC, procalcitonin, CRP, Troponin, D-dimer, ferritin, LDH, Creatinine, Creatinine phosphokinase, Respiratory rate, $CD4^+$ count, Temperature, Blood pressure	Co-morbidity, higher inflammatory markers were associated with higher admission. All patients with comorbidity died	Lack of clinical data on participants Small sample size	[72]

(Continued on following page)

TABLE 1 (*Continued*) Summary of clinical outcomes on HIV and SARS-CoV-2 co-infection studies and their spatial distribution.

Sample date	Study design	Study place	Study participants/ Sample size	Assay type	Additional tests	Key findings/ Outcomes	Limitations	References
11th March-17th April 2020	Retrospective study	Germany	33 HIV participants	RT-PCR	Respiratory rate, $CD4^+$ count, Viral load, Oxygen saturation	3 of the patients died, 91% recovered and 76% mild cases	Small uncontrolled case series with limited follow up	[73]
January-9th March 2020	Case series	Spain	543 COVID-19 patients 5 HIV patients: 3 MSM, 2 transgenders	RT-PCR	Viral load, $CD4^+$ count, oxygen saturation, CRP, LDH, D-dimer, FBC	4 out of 5 patients were cured by the end of the study	Small sample size	[74]
15th March-15th April 2020	Case report	United States, New York	31 PLWH infected with COVID-19	RT-PCR	Vural load, $CD4^+$ count, CRP, D-dimer, Ferritin, Procalcitonin, radiological findings	8 patients died, and 21 recovered	Smaller sample size There was no comparison with patients without HIV.	[75]
March 2020-September 2021	Case series	Tokyo, Japan	17 HIV-COVID-19 patients	RT-PCR	$CD4^+$ count, lymphocyte, $CD8^+$ count	All patients recovered. No difference in $CD4^+$ and $CD8^+$ counts between onset of symptoms and after recovery	Small sample size	[28]
2nd January–31st October 2020	Observational retrospective monocentric cohort	Paris, France	129 HIV individuals with COVID-19	RT-PCR	Viral load, $CD4^+$ count	Older age, higher BMI, diabetes, chronic kidney disease, transgender women were prone to disease severity with poor outcomes	Not all patients were confirmed to have COVID-19 by PCR.	[76]
January 2020- Not stated	Retrospective cohort study	Italy, Rome	1647 hospitalized patients, 43 PLWH, 1605 non PLWH	RT-PCR	$CD4^+$ count, Full blood count, Viral load, Potassium, CRP, D-dimer, Ferritin, oxygen saturation	There was less death among PLWH as compared to non-PLWH.	Small sample size Analysis done at the study site cannot be generalized to other sites	[77]
29th March 2020	Case Report	Korea	1 HIV positive man	RT-PCR	$CD4^+$ and $CD8^+$ count, Viral load, Chest X-ray, CT scan, ESR and platelet count	Patient recovered	small sample size	[78]
May 2020	Case Report	Brazil	1 HIV positive woman	RT-PCR	$CD4^+$ count, $CD8^+$ count, Viral load, Chest X-ray, Oxygen saturation level	Patient recovered after a week	Small sample size	[79]
1st march–9th June 2020	Cohort study	Cape Town, South Africa	3,460,932 public patients, 3978 HIV patients with COVID-19	RT-PCR	$CD4^+$ count, $CD8^+$ count, Viral load	HIV and tuberculosis were associated with COVID-19 mortality	There was lack of data on co-morbidities and potential risk factors	[80]

(Continued on following page)

TABLE 1 (*Continued*) Summary of clinical outcomes on HIV and SARS-CoV-2 co-infection studies and their spatial distribution.

Sample date	Study design	Study place	Study participants/ Sample size	Assay type	Additional tests	Key findings/ Outcomes	Limitations	References
11th June–28th August 2020	Observational case control study	Cape-Town, South Africa	104 COVID-19 positive patients, 31 HIV/COVID-19 patients	RT-PCR, Neutralization assay, Flow cytometry	Cd4+ count, Viral load, LDH, Ferritin, D-dimer	30 patients died	Analysis was not empowered to reproduce relationships between HIV and severity of COVID-19	[81]
1st June–1st October 2021	Observation study	Guinea Bissau	294 PLWH 55 PLWH positive for SARS-CoV-2	COVID-19 IgM/IgG rapid test kit	-	Six deaths reported	The study population consisted only of patients on follow-up	[82]
1st March–30th April 2020	Observational prospective monocentric study	France	54 PLWH coinfected with COVID-19	RT-PCR	Viral load, $CD4^+$ count, IL-6	Male sex, age, ethnic origin, metabolic disorder was associated with severity of disease. 2 deaths were recorded	Study did not assess the risk linked to immune deficiency	[83]
17th January–18th June 2020	Prospective Observational study	United Kingdom	115 HIV patients 47,424 HIV negative patient	RT-PCR	Full blood count, prothrombin time, Creatinine, CRP	63% increased risk of day 28 mortality among PLWH hospitalized with COVID-19 compared to HIV negative	Risk factors for a COVID-19 related hospitalisation among PLWH, and the role of certain antiretroviral agents in modulating such risks were not addressed	[84]
Not stated	Prospective study	China	1178 HIV patients, 8 co-infected	RT-PCR	$CD4^+$ count, Viral loads, CT scan	Older ages were prone to get infected with COVID-19	Small co-infection size	[85]
Not stated	Retrospective cohort study	Massachusetts, United States	49,673 non PLWH, 404 PLWH	RT-PCR	CRP, LDH, ALT, AST, Bilirubin, Ferritin	PLWH had higher mortality at day 30 and were likely to be hospitalized that non PLWH.	Lack of clinical data	[86]
9th March 2020–8th March 2020	Retrospective study	Burkina Faso	419 PLWH	RT-PCR, ELISA		PLWH on integrase inhibitors were more likely to be infected than PLWH on non-nucleoside inhibitors	Study could not investigate if COVID-19 natural infection may confer comparable antibody immunity among PLWH.	[87]

(Continued on following page)

10.3389/ebm.2024.10059

TABLE 1 (*Continued*) Summary of clinical outcomes on HIV and SARS-CoV-2 co-infection studies and their spatial distribution.

Sample date	Study design	Study place	Study participants/ Sample size	Assay type	Additional tests	Key findings/ Outcomes	Limitations	References
June 2020–May 2021	Prospective Cohort study	South Africa	236 PLWH, 143 non-PLWH	RT-PCR. Flow cytometry	$CD4^+$ and $CD8^+$ count, Viral load, Full blood count	Higher disease severity was associated with low CD4+count and higher Neutrophil to lymphocyte ratio in first wave as compared to second wave	Limited information on HIV related immune perturbations influencing long-term immunity to SARS-CoV-2 infection	[88]
Until March 2022	Cross-sectional study	South Africa	600,00 PLWH	RT-PCR	CD4+count, Viral load	Mortality occurred in 5.7% of PLWH. Mortality was associated with lower recent $CD4^+$ count, no evidence of ART usage, high viral load, and co-morbidities	Study did not assess the impact of prior SARS-CoV-2 infection on COVID-19 outcomes	[89]
Not stated	Case Report	Netherlands	A 38-year-old male HIV patient	RT-PCR	$CD4^+$ count, Viral load, Chest X-ray	Patient was admitted with prolong COVID-19 infection with undiagnosed HIV and severe impaired cellular immunity	Small sample size	[90]
1st March 2020–30th November, 2020	Prospective Cohort study	United States	1785 PLWH, 189,350 non-PLWH	RT-PCR	Viral load, $CD4^+$ count	15% were hospitalized and 5% died. Tenofovir was associated with reduction in clinical events	Results covered the first 9 months of the pandemic and did not include follow up during second wave	[36]
1st June 2020–15th June 2020	Prospective cohort study	Italy	55 COVID-19 positive patients, 69 HIV patients negative for COVID-19	RT-PCR, ELISA	CD4 and $CD8^+$ counts, Viral load, Chest X-ray	4 deaths were recorded Age and number of co-morbidities were associated with death	Small sample size prevents generalization of results	[91]
Not stated	Case report	New York, United States	A 54-year-old man	RT-PCR	$CD4^+$ count, Biochemical test, Coagulation profile, Ferritin, Il-6, Procalcitonin, CK-MB, Chest X-ray	Patient recovered	Small sample size	[92]
February 2020–October 2021	Retrospective study	Sweden	64, 815 COVID-19 patients: 121 HIV positive	RT-PCR	Viral load, $CD4^+$ count	8% of PLWH died. HIV infection was not a risk factor for severe COVID-19	Number of hospitalized PLWH were small therefore limited the power	[93]

(Continued on following page)

10.3389/ebm.2024.10059

TABLE 1 (*Continued*) Summary of clinical outcomes on HIV and SARS-CoV-2 co-infection studies and their spatial distribution.

Sample date	Study design	Study place	Study participants/ Sample size	Assay type	Additional tests	Key findings/ Outcomes	Limitations	References
1st January 2020–31st December, 2020	Retrospective study	Spain	117,694 COVID-19: 234 HIV positive	RT-PCR	Comorbidity assessment	9.4% mortality among PLWH. Advanced liver disease was a predictor of death	Overestimation of hospitalization among PLWH.	[94]
10th March 2020–30th May 2020	Retrospective cohort study	Israel	23 PLWH coinfected with COVID-19	RT-PCR	Full blood count, Viral load, $CD4^+$ count	13% of in-hospital death, 9% mechanical ventilation, and 9% intensive care unit admission were recorded	Small sample size	[95]
15th February–31st May 2020	Retrospective multicentre cohort study	Belgium	16,000 HIV patients: 101 COVID-19 patients	RT-PCR	$CD4^+$ count, Viral load, CT scan	46% of patients were hospitalized, and 9% of patients died. Older age, sub-Saharan patients and those on integrase inhibitor were associated with hospitalization	Small sample size No comparison made with non-HIV patient	[96]
1st March 2020–15th December 2020	Observational prospective cohort study	Spain	13,142 followed up HIV patients: 749 COVID-19 positive	RT-PCR	Viral load, $CD4^+$ and $CD8^+$ count	13 patients died. Chronic co-morbidities were associated with severe outcomes	Not all cohorts were tested for SARS-CoV-2 so incidence rate was not assessed. Data did not include information on smoking and BMI.	[97]
December 2021	Brief report	South Africa	45-year-old man	RT-PCR, Viral sequencing	Viral load, $CD4^+$ count, Chest x-ray, IgG and IgA antibodies	Prolonged infection in HIV individuals may lead to evolution of SARS-CoV-2 lineages	Not reported	[98]
10th March 2020–6th June 2020	Retrospective matched cohort study	New York, United States	853 PLWH and 1621 HIV negative patients	RT-PCR	Viral load, $CD4^+$ count, FBC, Biochemical test, CRP, D-dimer, Ferritin, Procalcitonin, ESR, fibrinogen	Hospitalized PLWH and controls show no difference in-hospital death. Co-morbidities and inflammatory markers differ for each cohort upon hospitalization indicating different mechanisms leading to severe COVID-19	Data from Medical record did not include a history of treatment for co-morbidities, which prevented accounting for severity or progression of these conditions	[99]
March 2020–September 2020 March 2021–December 2021	Observation Retrospective cohort study	Brazil	17,101 COVID-19 patients: 130 PLWH	R- PCR	Viral load, $CD4^+$ count, full blood count, Kidney function test, Liver function test, Arterial pH, pO_2, pCO_2	27.9% mortality in PLWH in 2020. No difference in mortality among PLWH and non-PLWH in 2021	Small sample size	[23]

(Continued on following page)

10.3389/ebm.2024.10059

TABLE 1 (*Continued*) Summary of clinical outcomes on HIV and SARS-CoV-2 co-infection studies and their spatial distribution.

Sample date	Study design	Study place	Study participants/ Sample size	Assay type	Additional tests	Key findings/ Outcomes	Limitations	References
1st January 2020–21st May 2021	Retrospective cohort study	United States	1,446,913 COVID-19 patients: 3660 PLWH	RT-PCR	Viral load, $CD4^+$ count	PLWH with immune dysfunction have greater risk for severe COVID-19 outcomes	There was less representation of admission practices and disease severity in medical records from study site	[100]
1st March 2020–30th November 2020	Retrospective cohort study	United States	487 COVID-19 patients: 88 PLWH	RT-PCR	Viral load, $CD4^+$ count	People living with HIV have a higher risk of COVID-19 diagnosis than those without HIV, but the outcomes are similar in both groups	Study could not implement routine SARS-CoV-2 screening to identify all patients with SARS-CoV-2 infection	[101]
1st January 2020–8th May 2021	Retrospective cohort study	United States	1, 436, 622 COVID-19 patients: 13, 170 HIV patients	RT-PCR	$CD4^+$ count, Viral load	A low $CD4^+$ count was associated with all the adverse COVID-19 outcomes, while viral suppression was only associated with reduced hospitalisation	Though was a large sample size, this did not represent all the COVID-19 infections in the country	[102]
1st March–31st December 2020	Retrospective cohort study	Indonesia	4134 PLWH 342 PLWH with COVID-19	RT-PCR	Viral load, $CD4^+$ count	23 patients developed severe-critical COVID-19, and the mortality rate was 3.2%	The incidence of infection in the study population could not be assessed because not all participants were tested for SARS-CoV-2	[103]
28th January 2020	Editorial	China	61-year-old HIV man	RT-PCR	FBC, oxygen saturation, CT scan, $CD4^+$ count	HIV infection need to be regarded as vulnerable group	Small sample size	[104]

10.3389/ebm.2024.10059

TABLE 2 Summary of immunological response on HIV and SARS-CoV-2 co-infection studies and their spatial distribution.

Sampling date	Study design	Study place	Study participants/ Sample size	Assay type	Additional tests	Clinical outcomes/key findings	Limitations	References
2nd March-15th April 2020	brief report	United States	72 HIV patients	RT-PCR	Viral load, $CD4^+$ count, IL6, CRP, IL8, fibrinogen, D-dimer, TNF, IL-1B	High inflammatory markers and immune dysregulation were linked to death in PLWH.	Study was limited to 1 hospital. Complete HIV history was not available on all patients, and laboratory markers were obtained at the discretion of treating physicians	[17]
June-October 2020	Prospective study	Iran	155 HIV-1 patients	RT-PCR, Enzyme immunoassay	Viral load, $CD4^+$ count, Hepatitis B, C, Tb test,	Higher anti-SARS-CoV-2 were reported in males than females	Screening and identification of HIV-1-infected individuals were limited due to COVID-19 lockdown	[29]
June-November 2020	Longitudinal study	South Africa	72 COVID-19 patients, 42 without HIV, 30 with HIV, 25 on ART	RT-PCR, Enzyme immunoassay (IgA, Igg, IgM), Microneutralization assay, Whole genome sequencing	$CD4^+$ count, $CD8^+$ count, Viral load	Antibody response among PLWH were comparable to those of non-PLWH.	Sample size small. There is a possibility of missing peak IgM response due to time of sampling Only 16 out of 72 full genomes were sequenced	[12]
January-June 2020	retrospective study	Italy, Spain & Germany	175 HIV patients	RT-PCR	Viral load, $CD4^+$ count	Low $CD4^+$ count was associated with high mortality rate in PLWH.	Only data on absolute CD4 T cells were available. Data on other lymphocyte subpopulations such as CD8 T cells were lacking	[105]
December 2020	Case report	Spain	1 HIV patient	RT-PCR, Whole Genome sequencing, Flow cytometry	Viral load, $CD4^+$ count, full blood count, Computed Topography (CT) scan	T cell exhaustion was associated with severity of disease among PLWH.	Small sample size	[18]
Not stated	Case report	Italy	1 HIV patient	RT-qPCR, flow cytometry, RT-PCR	$CD4^+$ and $CD8^+$ count, viral load, FBC, Arterial blood gas, Computed Topography scan	IFNα/β mRNAs and T cell activation were associated with severe pneumonia	Small sample size	[19]
15th January-20th November 2020	Prospective Cohort study	China	18 PLWH, 185Non PLWH	RT-PCR, Immunochromatography assay	Lymphocyte count	Positive conversion rate of IgG was lower and quickly lost in PLWH compared to non-PLWH.	Lack of an antibody detection kit in the early days of the SARS-CoV-2 epidemic prevented early antibody testing	[30]

(Continued on following page)

TABLE 2 (*Continued*) Summary of immunological response on HIV and SARS-CoV-2 co-infection studies and their spatial distribution.

Sampling date	Study design	Study place	Study participants/ Sample size	Assay type	Additional tests	Clinical outcomes/key findings	Limitations	References
20th March-15th June 2020	Cohort study	Russia	376 (171 ART experienced, 205 ART naïve) 382 control groups	RT-PCR, Flow cytometry, ELISA	Respiratory score	HIV ART-naïve was reported as a strong co-morbidity of severe COVID-19	Not reported	[32]
1st March-12th May 2020	Observational study	Italy	604 HIV participants	RT-PCR, Immunofluorescence, Microneutralization test, Flow cytometry, Elispot assay, ELISA	CT scan, Lymphocyte count, LDH, D-dimer, Fibrinogen, Ferritin	Adaptive cellular immune response correlated with disease severity	Small sample size makes it difficult to distinguish real effects from random variations thereby no definitive conclusions can be made	[20]
11th February 2020	Case report	China	1 HIV patient	RT-PCR	CRP, LFT, LDH, FBC, oxygen saturation	Slower generation of antibodies was attributed to severity of disease	Small sample size	[31]
6th March–11th September 2020	Retrospective study	South Africa	676 COVID-19 patients: 108 HIV	RT-PCR, ELISA	$CD4^+$ count, Viral load, FBC, RFT, LFT, CRP, Troponin T, LDH, D-dimer, Troponin T, Ferritin, beta-d-glucan, procalcitonin	No significant difference in mortality between the HIV-positive and HIV-negative groups. HIV-positive patients who died were younger than the HIV-negatives	It was a single centre study, and so the data may not be generalized. some data capturing was retrospective, due to rapidly increasing patient numbers and staff shortages, and as a result some data were missing	[106]
8th February 2020	Case report	China	2 HIV patients	RT-PCR	IL-6, procalcitonin, ferritin, CRP, Albumin, $CD4^+$ count, Viral load, X-ray, Sars CoV2 abs test	Patients recovered	Small sample size	[71]
8th June 2020–25th September, 2020	Cross sectional study	South Africa	126 HIV participants	RT-PCR, Flow cytometry, ELISA	$CD4^+$ and $CD8^+$ counts, Viral load	B cell responses were rapid but gave rise to lower affinity antibodies, less durable long-term memory, and reduced capacity to adapt to new variants	Study could not determine long-term effects of HIV on SARS-CoV-2 immunity, as new variants emerge	[27]

(Continued on following page)

TABLE 2 (*Continued*) Summary of immunological response on HIV and SARS-CoV-2 co-infection studies and their spatial distribution.

Sampling date	Study design	Study place	Study participants/ Sample size	Assay type	Additional tests	Clinical outcomes/key findings	Limitations	References
June–December 2020–1st wave January–June 2021- 2nd wave	Longitudinal observational cohort study	South Africa	25 HIV participants 1st wave 23 HIV participant 2nd wave HIV negative 17	RT-PCR, Flow cytometry	Viral load, $CD4^+$ count	Unsuppressed HIV infection impaired T cell responses to SARS-CoV-2 infection and diminishes T cell cross-recognition	Study did not examine relationship between $CD8^+$ and CD19 subset at antigen-specific level due to sample limitations	[26]
Not stated	Case report	Taiwan	A 38-year-old man	RT-PCR, ELISA, Virus neutralization assay	CRP, Viral load, $CD4^+$ count, ALT, AST, Chest X-ray	Neutralizing antibody reached a plateau from 26th to 47th day onset but decreased on 157th day after symptoms	Small sample size	[107]
4th March 2020	Cross sectional study	China	24 HIV patients: 21 had COVID-19	RT-PCR	Ct scan, Chest X-ray, CRP, Procalcitonin, Viral load, $CD4^+$ count, Full blood count, coagulation profile, Biochemical test	Reduction in T-cell number positively correlates with the serum levels of interleukin 6 (IL-6) and C-reactive protein (CRP)	Small sample size. Lack of detection of TCR zeta-chain expression	[30]
Not stated	Prospective cohort study	Zambia	46 HIV negative patients 39 HIV positive patients	RT-PCR, Immuno-spot assay. Immunofluorescence assay, flow cytometry	$CD4^+$ count, viral load	SARS-CoV-2-specific T cell immune responses may be delayed in individuals who are HIV +, even in those on antiretroviral therapy. There is no difference in SARS-CoV-2-specific humoral immunity between individuals who are HIV- and HIV+	Small sample size limited study's ability to elicit some of the differences that might exist between the sub-groups	[33]
25th January 2020	Brief Report	China	38-year-old HIV man	RT-PCR, Chemiluminescence assay	FBC, CRP	Total Ab level was largely increased, and IgM remained at the peak level 1 week later, suggesting that the antibody responses against SARS-CoV-2 in this HIV-infected case was delayed	Studies did not to address the mechanism underlying the delayed antibody response to SARS-CoV-2 with a history of coinfection of HIV-1 infection	[108]

(Continued on following page)

10.3389/ebm.2024.10059

TABLE 2 (*Continued*) Summary of immunological response on HIV and SARS-CoV-2 co-infection studies and their spatial distribution.

Sampling date	Study design	Study place	Study participants/ Sample size	Assay type	Additional tests	Clinical outcomes/key findings	Limitations	References
June 2020–August 2020	Prospective cohort study	South Africa	133 hospitalized patients: 95 COVID-19 patients (31 positive for HIV) 30 non COVID-19 patients (with 13 positives for HIV)	Flow cytometry, RT-PCR, electro chemiluminescent immunoassay	$CD4^+$ count, Viral load, CRP, D-dimer, LDH, ferritin, WBC	SARS-CoV-2–specific $CD4^+$ T cell attributes were associated with disease severity Severe disease was characterized by poor polyfunctional potential, reduced proliferation capacity, and enhanced HLA-DR expression	Study could not use different approaches (such as the activation-induced markers assay) to confirm the inability of lymphopenia patients to mount a T cell response to SARS-CoV-2	[21]
5th May 2020–22nd February, 2021	Retrospective Cohort study	United States	2464 PLWH: 283 COVID-19 positives	RT-PCR, ELISA, Luminex assay	Viral load, $CD4^+$ count	SARS-CoV-2–specific humoral immune profiles among PLWH with obesity or lower nadir $CD4^+$ T cell count was associated with worse outcomes	The study's cross-sectional nature limits the ability to assess humoral repertoire changes over time in relation to COVID-19. Study was not able to control for statin use, given the ongoing nature of the trial	[109]
May 2020–October 2020	Observational cohort study	United States, Peru	43 PLWH, 330 non PLWH	RT-PCR. ELISA	Viral load, $CD4^+$ count	Decreased SARS-CoV-2–specific antibodies among PLWH compared to non PLWH. PLWH who recovered from COVID-19 had diminished immune responses and lacked an increase in SARS-CoV-2 antibodies	The median duration from diagnosis to enrolment was nearly 2 months, which did not fully represent the convalescent period	[34]
Not stated	Prospective study	Barcelona, Spain	50 patients, 11 PLWH, 39 non PLWH	RT-PCR, EliSpot immune assay, Fluorospot immune assay, ELISA	Oxygen saturation	PLWH developed a comparable short and long-term natural functional cellular and humoral immune response than non PLWH convalescent patients, which are highly influenced by the clinical severity of the COVID-19 infection	Patients with critical COVID-19 (requiring Mechanical ventilation) could not be obtained during the first wave of the pandemic and may be under-represented in this study	[110]

(Continued on following page)

TABLE 2 (*Continued*) Summary of immunological response on HIV and SARS-CoV-2 co-infection studies and their spatial distribution.

Sampling date	Study design	Study place	Study participants/ Sample size	Assay type	Additional tests	Clinical outcomes/key findings	Limitations	References
September–November 2020	Observational cohort study	Italy	HIV with COVID-19: 30 HIV without COVID-19: 52 COVID-19 without HIV: 58	RT-PCR, micro-neutralization assay, ELISpot assay,	Viral load, $CD4^+$ count, oxygen saturation	Significantly higher levels of IL-6, IL-8, and TNF-α in COVID-19 without HIV compared to HIV/ COVID-19 patients were observed	Studies did not evaluate the persistence of these immunity and its ability to expand after exposure	[24]
April-September, 2020	cohort study	Italy	Young HIV patients 85 ART experienced control group 13	RT-qPCR, ELISA, Magnetic bead immunoassay, Geneplex assay, cytokine multiplex assay	$CD4^+$ count, Liver function test, Renal function test, Clotting Profile	IL-10 could play a crucial role in the course of SARS-CoV-2 infection in HIV-positive individuals	Small sample size could lead to higher variability	[52]
March 2020–September 2021	Cohort study	United Kingdom	47 HIV individuals, 24 confirmed COVID-19, 35 HIV negative	RT-PCR	Lymphocyte count, $CD4^+$ count, $CD8^+$ count, Spike IgG, N IgG antibodies, IFN-γ, TNF-α	Inadequate immune reconstitution on ART, could hinder immune response to SARS-CoV-2	Study was not well powered	[25]

Legend: PLWH, people living with HIV; HIV, human immunodeficiency virus; CRP, C-reactive protein; FBC, full blood count; TNF, Tumour Necrotic factor; LFT, liver function test; RFT, renal function test; IL, interleukin; LDH, lactate dehydrogenase; RT PCR, Real time polymerase chain reaction; IgG, Immunoglobulin G; ALT, alanine transferase; AST, Aspartate Transferase; CT, scan, Computed topography scan; ESR, erythrocyte sedimentation rate; WBC, white blood cells; pCO2, Partial pressure of carbon dioxide; pO2, partial pressure of oxygen.

10.3389/ebm.2024.10059

cytokines and/or immunological markers to SARS-CoV-2 in PLWH.

Author contributions

Study conception was performed by EA, EB, ET, EP, KT, and OQ. Original draft preparation was performed by EA, PA, LA, and MA-P. Methodology was performed by EA, PA, LA, and MA-P. EB, ET, EP, KT, and OQ critically reviewed the manuscript. All authors contributed to the article and approved the submitted version.

Data availability statement

The original contributions presented in the study are included in the article/supplementary material, further inquiries can be directed to the corresponding author.

Funding

The author(s) declare financial support was received for the research, authorship, and/or publication of this article. This research was funded in part by the Fogarty International Center of National Institute of Alcohol Abuse and Alcoholism of the National Institutes of Health (NIH) [D43 TW011526], the World Bank African Centres of Excellence grant [WACCBIP+NCDs: Awandare], and the Science for Africa Foundation to Developing Excellence in Leadership, Training and Science in Africa (DELTAS Africa) programme [DEL-22-014] with support from Wellcome and the UK Foreign, Commonwealth and Development Office (FCDO) which is part of the EDCPT2 programme supported by the European Union. The content of the research is solely the responsibility of the authors and does not necessarily represent the official views of the NIH, World Bank, Wellcome Trust, or the FCDO.

Acknowledgments

The authors acknowledge the support of the West African Centre for Cell Biology of Infectious Pathogens (WACCBIP) and the HIVComRT.

Conflict of interest

The authors declare that the research was conducted in the absence of any commercial or financial relationships that could be construed as a potential conflict of interest.

References

1. Schouten J, Wit FW, Stolte IG, Kootstra NA, van der Valk M, Geerlings SE, et al. Cross-sectional comparison of the prevalence of age-associated comorbidities and their risk factors between HIV-infected and uninfected individuals: the AGEhIV cohort study. *Clin Infect Dis* (2014) **59**(12):1787–97. doi:10.1093/cid/ciu701

2. Önen NF, Overton ET, Seyfried W, Stumm ER, Snell M, Mondy K, et al. Aging and HIV infection: a comparison between older HIV-infected persons and the general population. *HIV Clin trials* (2010) **11**(2):100–9. doi:10.1310/hct1102-100

3. Brown TT, Guaraldi G. Multimorbidity and burden of disease. *Interdiscip Top Gerontol Geriatr* (2017) **42**:59–73. doi:10.1159/000448544

4. Kanwugu ON, Adadi P. HIV/SARS-CoV-2 coinfection: a global perspective. *J Med Virol* (2021) **93**(2):726–32. doi:10.1002/jmv.26321

5. WHO. *COVID-19 weekly epidemiological update*. 134 edn (2023).

6. Vizcarra P, Pérez-Elías MJ, Quereda C, Moreno A, Vivancos MJ, Dronda F, et al. Description of COVID-19 in HIV-infected individuals: a single-centre, prospective cohort. *The lancet HIV* (2020) **7**(8):e554–e564. doi:10.1016/s2352-3018(20)30164-8

7. Collins LF, Moran CA, Oliver NT, Moanna A, Lahiri CD, Colasanti JA, et al. Clinical characteristics, comorbidities and outcomes among persons with HIV hospitalized with coronavirus disease 2019 in Atlanta, Georgia. *AIDS (London, England)* (2020) **34**(12):1789–94. doi:10.1097/qad.0000000000002632

8. Calza L, Bon I, Tadolini M, Borderi M, Colangeli V, Badia L, et al. COVID-19 in patients with HIV-1 infection: a single-centre experience in northern Italy. *Infection* (2021) **49**(2):333–7. doi:10.1007/s15010-020-01492-7

9. Hartley DM, Perencevich EN. Public health interventions for COVID-19: emerging evidence and implications for an evolving public health crisis. *Jama* (2020) **323**(19):1908–9. doi:10.1001/jama.2020.5910

10. Del Amo J, Polo R, Moreno S, Díaz A, Martínez E, Arribas JR, et al. Antiretrovirals and risk of COVID-19 diagnosis and hospitalization in HIV-positive persons. *Epidemiology (Cambridge, Mass.)* (2020) **31**(6):e49–e51. doi:10.1097/ede.0000000000001235

11. Sigel K, Swartz T, Golden E, Paranjpe I, Somani S, Richter F, et al. Coronavirus 2019 and people living with human immunodeficiency virus: outcomes for hospitalized patients in New York City. *Clin Infect Dis* (2020) **71**(11):2933–8. doi:10.1093/cid/ciaa880

12. Snyman J, Hwa SH, Krause R, Muema D, Reddy T, Ganga Y, et al. Similar antibody responses against severe acute respiratory syndrome coronavirus 2 in individuals living without and with human immunodeficiency virus on antiretroviral therapy during the first South African infection wave. *Clin Infect Dis* (2022) **75**(1):e249–e256. doi:10.1093/cid/ciab758

13. Bhaskaran K, Rentsch CT, MacKenna B, Schultze A, Mehrkar A, Bates CJ, et al. HIV infection and COVID-19 death: a population-based cohort analysis of UK primary care data and linked national death registrations within the OpenSAFELY platform. *The lancet HIV* (2021) **8**(1):e24–e32. doi:10.1016/s2352-3018(20)30305-2

14. Waters LJ, Pozniak AL. COVID-19 death in people with HIV: interpret cautiously. *The Lancet HIV* (2021) **8**(1):e2–e3. doi:10.1016/s2352-3018(20)30332-5

15. Scagnolari C, Antonelli G. Type I interferon and HIV: subtle balance between antiviral activity, immunopathogenesis and the microbiome. *Cytokine Growth Factor Rev* (2018) **40**:19–31. doi:10.1016/j.cytogfr.2018.03.003

16. Zhou Z, Ren L, Zhang L, Zhong J, Xiao Y, Jia Z, et al. Heightened innate immune responses in the respiratory tract of COVID-19 patients. *Cell host & microbe* (2020) **27**(6):883–90. doi:10.1016/j.chom.2020.04.017

17. Ho H-e., Peluso MJ, Margus C, Matias Lopes JP, He C, Gaisa MM, et al. Clinical outcomes and immunologic characteristics of coronavirus disease 2019 in people with human immunodeficiency virus. *J Infect Dis* (2021) **223**(3):403–8. doi:10.1093/infdis/jiaa380

18. Álvarez H, Ruiz-Mateos E, Juiz-González PM, Vitallé J, Viéitez I, Vázquez-Friol MC, et al. SARS-CoV-2 evolution and spike-specific CD4+ T-cell response in persistent COVID-19 with severe HIV immune suppression. *Microorganisms* (2022) **10**(1):143. doi:10.3390/microorganisms10010143

19. d'Ettorre G, Recchia G, Ridolfi M, Siccardi G, Pinacchio C, Innocenti GP, et al. Analysis of type I IFN response and T cell activation in severe COVID-19/HIV-

1 coinfection: a case report. *Medicine* (2020) **99**(36):e21803. doi:10.1097/md.0000000000021803

20. Mondi A, Cimini E, Colavita F, Cicalini S, Pinnetti C, Matusali G, et al. COVID-19 in people living with HIV: clinical implications of dynamics of the immune response to SARS-CoV-2. *J Med Virol* (2021) **93**(3):1796–804. doi:10.1002/jmv.26556

21. Riou C, du Bruyn E, Stek C, Daroowala R, Goliath RT, Abrahams F, et al. Relationship of SARS-CoV-2-specific CD4 response to COVID-19 severity and impact of HIV-1 and tuberculosis coinfection. *J Clin Invest* (2021) **131**(12):e149125. doi:10.1172/jci149125

22. Ruan Q, Yang K, Wang W, Jiang L, Song J. Clinical predictors of mortality due to COVID-19 based on an analysis of data of 150 patients from Wuhan, China. *Intensive Care Med* (2020) **46**(5):846–8. doi:10.1007/s00134-020-05991-x

23. Sales TLS, Souza-Silva MVR, Delfino-Pereira P, Neves JVB, Sacioto MF, Assis VC, et al. COVID-19 outcomes in people living with HIV: peering through the waves. *Clinics* (2023) **78**:100223. doi:10.1016/j.clinsp.2023.100223

24. Vergori A, Boschini A, Notari S, Lorenzini P, Castilletti C, Colavita F, et al. SARS-CoV-2 specific immune response and inflammatory profile in advanced HIV-infected persons during a COVID-19 outbreak. *Viruses* (2022) **14**(7):1575. doi:10.3390/v14071575

25. Alrubayyi A, Gea-Mallorquí E, Touizer E, Hameiri-Bowen D, Kopycinski J, Charlton B, et al. Characterization of humoral and SARS-CoV-2 specific T cell responses in people living with HIV. *Nat Commun* (2021) **12**(1):5839. doi:10.1038/s41467-021-26137-7

26. Nkosi T, Ndhlovu ZM, Chasara C, Papadopoulos AO, Nguni TL, Karim F, et al. Unsuppressed HIV infection impairs T cell responses to SARS-CoV-2 infection and abrogates T cell cross-recognition. *Elife* (2022) **11**:e78374. doi:10.7554/elife.78374

27. Krause R, Snyman J, Shi-Hsia H, Muema D, Karim F, Ganga Y, et al. HIV skews the SARS-CoV-2 B cell response towards an extrafollicular maturation pathway. *Elife* (2022) **11**:e79924. doi:10.7554/eLife.79924

28. Adachi E, Saito M, Nagai H, Ikeuchi K, Koga M, Tsutsumi T, et al. Transient depletion of T cells during COVID-19 and seasonal influenza in people living with HIV. *J Med Virol* (2022) **94**(5):1789–91. doi:10.1002/jmv.27543

29. Garshasbi S, Bokharaei-Salim F, Khanaliha K, Kiani SJ, Kalantari S, Jamshidi Makiani M, et al. SARS-CoV-2 infection in Iranian people living with human immunodeficiency virus-1 infection. *Jundishapur J Microbiol* (2022) **15**(1). doi:10.5812/jjm.121929

30. Liu Y, Xiao Y, Wu S, Marley G, Ming F, Wang X, et al. People living with HIV easily lose their immune response to SARS-CoV-2: result from a cohort of COVID-19 cases in Wuhan, China. *BMC Infect Dis* (2021) **21**(1):1029–7. doi:10.1186/s12879-021-06723-2

31. Wang M, Luo L, Bu H, Xia H. One case of coronavirus disease 2019 (COVID-19) in a patient co-infected by HIV with a low CD4+ T-cell count. *Int J Infect Dis* (2020) **96**:148–50. doi:10.1016/j.ijid.2020.04.060

32. Sharov KS. HIV/SARS-CoV-2 co-infection: T cell profile, cytokine dynamics and role of exhausted lymphocytes. *Int J Infect Dis* (2021) **102**:163–9. doi:10.1016/j.ijid.2020.10.049

33. Ngalamika O, Lidenge SJ, Mukasine MC, Kawimbe M, Kamanzi P, Ngowi JR, et al. SARS-CoV-2-specific T cell and humoral immunity in individuals with and without HIV in an African population: a prospective cohort study. *Int J Infect Dis* (2023) **127**:106–15. doi:10.1016/j.ijid.2022.12.009

34. Schuster DJ, Karuna S, Brackett C, Wesley M, Li SS, Eisel N, et al. Lower SARS-CoV-2–specific humoral immunity in people living with HIV-1 recovered from nonhospitalized COVID-19. *JCI insight* (2022) **7**(21):e158402. doi:10.1172/jci.insight.158402

35. Huang J, Xie N, Hu X, Yan H, Ding J, Liu P, et al. Epidemiological, virological and serological features of coronavirus disease 2019 (COVID-19) cases in people living with human immunodeficiency virus in Wuhan: a population-based cohort study. *Clin Infect Dis* (2021) **73**(7):e2086–e2094. doi:10.1093/cid/ciaa1186

36. Lea AN, Leyden WA, Sofrygin O, Marafino BJ, Skarbinski J, Napravnik S, et al. Human immunodeficiency virus status, Tenofovir exposure, and the risk of poor coronavirus disease 19 outcomes: real-world analysis from 6 United States cohorts before vaccine rollout. *Clin Infect Dis* (2023) **76**(10):1727–34. doi:10.1093/cid/ciad084

37. Del Amo J, Polo R, Moreno S, Jarrín I, Hernán MA. SARS-CoV-2 infection and coronavirus disease 2019 severity in persons with HIV on antiretroviral treatment. *Aids* (2022) **36**(2):161–8. doi:10.1097/qad.0000000000003132

38. Lohse N, Obel N. Update of survival for persons with HIV infection in Denmark. *Ann Intern Med* (2016) **165**(10):749–50. doi:10.7326/l16-0091

39. Suwanwongse K, Shabarek N. Clinical features and outcome of HIV/SARS-CoV-2 coinfected patients in the Bronx, New York city. *J Med Virol* (2020) **92**(11):2387–9. doi:10.1002/jmv.26077

40. Costenaro P, Minotti C, Barbieri E, Giaquinto C, Donà D. SARS-CoV-2 infection in people living with HIV: a systematic review. *Rev Med Virol* (2021) **31**(1):1–12. doi:10.1002/rmv.2155

41. Mirzaei H, McFarland W, Karamouzian M, Sharifi H. COVID-19 among people living with HIV: a systematic review. *AIDS Behav* (2021) **25**:85–92. doi:10.1007/s10461-020-02983-2

42. Luo Y, Alexander M, Gadina M, O'Shea JJ, Meylan F, Schwartz DM. JAK-STAT signaling in human disease: from genetic syndromes to clinical inhibition. *J Allergy Clin Immunol* (2021) **148**(4):911–25. doi:10.1016/j.jaci.2021.08.004

43. Giamarellos-Bourboulis EJ, Netea MG, Rovina N, Akinosoglou K, Antoniadou A, Antonakos N, et al. Complex immune dysregulation in COVID-19 patients with severe respiratory failure. *Cell host & microbe* (2020) **27**(6):992–1000. doi:10.1016/j.chom.2020.04.009

44. Hirano T, Murakami M. COVID-19: a new virus, but a familiar receptor and cytokine release syndrome. *Immunity* (2020) **52**(5):731–3. doi:10.1016/j.immuni.2020.04.003

45. Finigan JH, Downey GP, Kern JA. Human epidermal growth factor receptor signaling in acute lung injury. *Am J Respir Cel Mol Biol* (2012) **47**(4):395–404. doi:10.1165/rcmb.2012-0100tr

46. Venkataraman T, Coleman CM, Frieman MB. Overactive epidermal growth factor receptor signaling leads to increased fibrosis after severe acute respiratory syndrome coronavirus infection. *J Virol* (2017) **91**(12):e00182-17. doi:10.1128/jvi.00182-17

47. Yang L, Xu J, Guo L, Guo T, Zhang L, Feng L, et al. Porcine epidemic diarrhea virus-induced epidermal growth factor receptor activation impairs the antiviral activity of type I interferon. *J Virol* (2018) **92**(8):e02095-17. doi:10.1128/jvi.02095-17

48. Hadjadj J, Yatim N, Barnabei L, Corneau A, Boussier J, Smith N, et al. Impaired type I interferon activity and inflammatory responses in severe COVID-19 patients. *Science* (2020) **369**(6504):718–24. doi:10.1126/science.abc6027

49. Matsuyama T, Kubli SP, Yoshinaga SK, Pfeffer K, Mak TW. An aberrant STAT pathway is central to COVID-19. *Cel Death Differ* (2020) **27**(12):3209–25. doi:10.1038/s41418-020-00633-7

50. Gargan S, Ahmed S, Mahony R, Bannan C, Napoletano S, O'Farrelly C, et al. HIV-1 promotes the degradation of components of the type 1 IFN JAK/STAT pathway and blocks anti-viral ISG induction. *EBioMedicine* (2018) **30**:203–16. doi:10.1016/j.ebiom.2018.03.006

51. Liu M-Q, Zhao M, Kong WH, Tang L, Wang F, Zhu ZR, et al. Combination antiretroviral therapy (cART) restores HIV-1 infection-mediated impairment of JAK-STAT signaling pathway. *Oncotarget* (2017) **8**(14):22524–33. doi:10.18632/oncotarget.15121

52. Vanetti C, Trabattoni D, Stracuzzi M, Amendola A, Fappani C, Rubinacci V, et al. Immunological characterization of HIV and SARS-CoV-2 coinfected young individuals. *Cells* (2021) **10**(11):3187. doi:10.3390/cells10113187

53. Ballatori N, Krance SM, Notenboom S, Shi S, Tieu K, Hammond CL. Glutathione dysregulation and the etiology and progression of human diseases. *bchm* (2009) **390**:191–214. doi:10.1515/bc.2009.033

54. Yan Y, Yang Y, Wang F, Ren H, Zhang S, Shi X, et al. Clinical characteristics and outcomes of patients with severe covid-19 with diabetes. *BMJ Open Diabetes Res Care* (2020) **8**(1):e001343. doi:10.1136/bmjdrc-2020-001343

55. Kumar P, Osahon O, Vides DB, Hanania N, Minard CG, Sekhar RV. Severe glutathione deficiency, oxidative stress and oxidant damage in adults hospitalized with COVID-19: implications for GlyNAC (glycine and N-acetylcysteine) supplementation. *Antioxidants* (2021) **11**(1):50. doi:10.3390/antiox11010050

56. Pace GW, Leaf CD. The role of oxidative stress in HIV disease. *Free Radic Biol Med* (1995) **19**(4):523–8. doi:10.1016/0891-5849(95)00047-2

57. Repetto M, Reides C, Gomez Carretero ML, Costa M, Griemberg G, Llesuy S. Oxidative stress in blood of HIV infected patients. *Clinica Chim Acta* (1996) **255**(2):107–17. doi:10.1016/0009-8981(96)06394-2

58. Ntyonga-Pono M-P. COVID-19 infection and oxidative stress: an under-explored approach for prevention and treatment? *Pan Afr Med J* (2020) **35**(2):12. doi:10.11604/pamj.2020.35.2.22877

59. Sasset L, Di Meco E, Cavinato S, Cattelan AM. Coinfection of severe acute respiratory syndrome coronavirus 2 and HIV in a teaching hospital: still much to learn. *AIDS* (2020) **34**(11):1694–6. doi:10.1097/qad.0000000000002609

60. Tesoriero JM, Swain CAE, Pierce JL, Zamboni L, Wu M, Holtgrave DR, et al. COVID-19 outcomes among persons living with or without diagnosed HIV infection in New York State. *JAMA Netw open* (2021) **4**(2):e2037069. doi:10.1001/jamanetworkopen.2020.37069

61. Dandachi D, Geiger G, Montgomery MW, Karmen-Tuohy S, Golzy M, Antar AAR, et al. Characteristics, comorbidities, and outcomes in a multicenter registry of

patients with human immunodeficiency virus and coronavirus disease 2019. *Clin Infect Dis* (2021) **73**(7):e1964–e1972. doi:10.1093/cid/ciaa1339

62. Gervasoni C, Meraviglia P, Riva A, Giacomelli A, Oreni L, Minisci D, et al. Clinical features and outcomes of patients with human immunodeficiency virus with COVID-19. *Clin Infect Dis* (2020) **71**(16):2276–8. doi:10.1093/cid/ciaa579

63. Hu Y, Ma J, Huang H, Vermund SH. Coinfection with HIV and SARS-CoV-2 in Wuhan, China: a 12-person case series. *J acquired immune deficiency syndromes* (2020) **85**(1):1–5. doi:10.1097/QAI.0000000000002424

64. Stoeckle K, Johnston CD, Jannat-Khah DP, Williams SC, Ellman TM, Vogler MA, et al. COVID-19 in hospitalized adults with HIV. *Open Forum Infect Dis* (2020) **7**:ofaa327. Oxford University Press US. doi:10.1093/ofid/ofaa327

65. Madge S, Barber TJ, Hunter A, Bhagani S, Lipman M, Burns F. Descriptive account of 18 adults with known HIV infection hospitalised with SARS-CoV-2 infection. *Sex Transm Infections* (2021) **97**(5):392–3. doi:10.1136/sextrans-2020-054660

66. Mitha M, Maharaj A, Nyamande K. People living with HIV and COVID-19: a report on 2 clinical cases from South Africa. *Afr J Thorac Crit Care Med* (2020) **26**(2):59–60. doi:10.7196/ajtccm.2020.v26i2.078

67. Calza L, Bon I, Borderi M, Colangeli V, Borioni A, Re MC, et al. COVID-19 outcomes in patients with uncontrolled HIV-1 infection. *JAIDS J Acquired Immune Deficiency Syndromes* (2021) **86**(1):e15–e17. doi:10.1097/qai.0000000000002537

68. Qasim A, Mansour M, Kousa O, Awad D, Abuhazeem B, Millner P, et al. A case of coronavirus disease 2019 in acquired immunodeficiency syndrome patient: a case report and review of the literature. *Intractable Rare Dis Res* (2020) **9**(4):256–9. doi:10.5582/irdr.2020.03081

69. Gudipati S, Brar I, Murray S, McKinnon JE, Yared N, Markowitz N. Descriptive analysis of patients living with HIV affected by COVID-19. *JAIDS J Acquired Immune Deficiency Syndromes* (2020) **85**(2):123–6. doi:10.1097/qai.0000000000002450

70. Isernia V, Julia Z, Le Gac S, Bachelard A, Landman R, Lariven S, et al. SARS-COV2 infection in 30 HIV-infected patients followed-up in a French University Hospital. *Int J Infect Dis* (2020) **101**:49–51. doi:10.1016/j.ijid.2020.09.1436

71. Zhang J-C, Yu XH, Ding XH, Ma HY, Cai XQ, Kang SC, et al. New HIV diagnoses in patients with COVID-19: two case reports and a brief literature review. *BMC Infect Dis* (2020) **20**(1):771–10. doi:10.1186/s12879-020-05480-y

72. Karmen-Tuohy S, Carlucci PM, Zervou FN, Zacharioudakis IM, Rebick G, Klein E, et al. Outcomes among HIV-positive patients hospitalized with COVID-19. *JAIDS J Acquired Immune Deficiency Syndromes* (2020) **85**:6–10. doi:10.1097/qai.0000000000002423

73. Härter G, Spinner CD, Roider J, Bickel M, Krznaric I, Grunwald S, et al. COVID-19 in people living with human immunodeficiency virus: a case series of 33 patients. *Infection* (2020) **48**:681–6. doi:10.1007/s15010-020-01438-z

74. Blanco JL, Ambrosioni J, Garcia F, Martínez E, Soriano A, Mallolas J, et al. COVID-19 in patients with HIV: clinical case series. *The lancet HIV* (2020) **7**(5):e314–e316. doi:10.1016/s2352-3018(20)30111-9

75. Shalev N, Scherer M, LaSota ED, Antoniou P, Yin MT, Zucker J, et al. Clinical characteristics and outcomes in people living with human immunodeficiency virus hospitalized for coronavirus disease 2019. *Clin Infect Dis* (2020) **71**(16):2294–7. doi:10.1093/cid/ciaa635

76. Bachelard A, Sautereau A, Digumber M, Isernia V, Phung B, Lehur AC, et al. Risk factors associated with severe/critical COVID-19 in people living with HIV-1. *Int J Infect Dis* (2022) **122**:152–4. doi:10.1016/j.ijid.2022.05.055

77. Gagliardini R, Vergori A, Lorenzini P, Cicalini S, Pinnetti C, Mazzotta V, et al. Characteristics and outcomes of COVID-19-related hospitalization among PLWH. *J Clin Med* (2022) **11**(6):1546. doi:10.3390/jcm11061546

78. Kim J-Y, Kim JM, Peck KR. The first case of an HIV patient diagnosed with COVID-19 in Korea. *J Korean Med Sci* (2020) **35**(39):e358. doi:10.3346/jkms.2020.35.e358

79. Cipolat MM, Sprinz E. COVID-19 pneumonia in an HIV-positive woman on antiretroviral therapy and undetectable viral load in Porto Alegre, Brazil. *Braz J Infect Dis* (2020) **24**:455–7. doi:10.1016/j.bjid.2020.07.009

80. Davies M-A. HIV and risk of COVID-19 death: a population cohort study from the Western Cape Province, South Africa. MedRxiv (2020). Available from: https://doi.org/10.1101/2020.07.02.20145185.

81. Du Bruyn E, Stek C, Daroowala R, Said-Hartley Q, Hsiao M, Schafer G, et al. Effects of tuberculosis and/or HIV-1 infection on COVID-19 presentation and immune response in Africa. *Nat Commun* (2023) **14**(1):188. doi:10.1038/s41467-022-35689-1

82. Dutschke A, Wejse C, Nanque J, Medina C, Hønge B, Jespersen S, et al. SARS-CoV-2 seroprevalence among people living with HIV in Guinea–Bissau. *Public Health* (2022) **209**:36–8. doi:10.1016/j.puhe.2022.05.017

83. Etienne N, Karmochkine M, Slama L, Pavie J, Batisse D, Usubillaga R, et al. HIV infection and COVID-19: risk factors for severe disease. *AIDS (London, England)* (2020) **34**(12):1771–4. doi:10.1097/qad.0000000000002651

84. Geretti AM, Stockdale AJ, Kelly SH, Cevik M, Collins S, Waters L, et al. Outcomes of COVID-19 related hospitalisation among people with HIV in the ISARIC WHO Clinical Characterisation Protocol UK Protocol: prospective observational study. MedRxiv (2020). Available from: https://doi.org/10.1101/2020.08.07.20170449.

85. Guo W, Ming F, Dong Y, Zhang Q, Zhang X, Mo P, et al. A survey for COVID-19 among HIV/AIDS patients in two districts of Wuhan, China (2020). Available from: http://dx.doi.org/10.2139/ssrn.3550029.

86. Hadi YB, Naqvi SF, Kupec JT, Sarwari AR. Characteristics and outcomes of COVID-19 in patients with HIV: a multicentre research network study. *AIDS (London, England)* (2020) **34**(13):F3–F8. doi:10.1097/qad.0000000000002666

87. Kaboré OD, Poda A, Ouattara CA, Michodigni FN, Belem AA, Sawadogo Y, et al. Seroprevalence of SARS-CoV-2 IgG and associated factors among people living with HIV over the first 12 months following the outbreak of COVID-19 in Burkina Faso, a sub-Saharan African country. *Plos one* (2023) **18**(6):e0286665. doi:10.1371/journal.pone.0286665

88. Karim F, Gazy I, Cele S, Zungu Y, Krause R, Bernstein M, et al. HIV status alters disease severity and immune cell responses in Beta variant SARS-CoV-2 infection wave. *Elife* (2021) **10**:e67397. doi:10.7554/eLife.67397

89. Kassanjee R, Davies M, Ngwenya O, Osei-Yeboah R, Jacobs T, Morden E, et al. COVID-19 among adults living with HIV: correlates of mortality among public sector healthcare users in Western Cape, South Africa. *J Int AIDS Soc* (2023) **26**(6):e26104. doi:10.1002/jia2.26104

90. Ketels T, Gisolf J, Claassen M, Swanink C, van Lochem E, Moonen L, et al. Short communication: prolonged COVID-19 infection in a patient with newly diagnosed HIV/AIDS. *AIDS Res Hum retroviruses* (2022) **38**(5):399–400. doi:10.1089/aid.2021.0145

91. Maggiolo F, Zoboli F, Arosio M, Valenti D, Guarneri D, Sangiorgio L, et al. SARS-CoV-2 infection in persons living with HIV: a single center prospective cohort. *J Med Virol* (2021) **93**(2):1145–9. doi:10.1002/jmv.26352

92. Mahmood K, Rashed ER, Oliveros E, Chau VQ, Hermle T, Jacobs S, et al. Predisposition or protection? COVID-19 in a patient on LVAD support with HIV/AIDS. *JACC: Case Rep* (2020) **2**(9):1337–41. doi:10.1016/j.jaccas.2020.05.015

93. Möller IK, Gisslén M, Wagner P, Sparén P, Carlander C. COVID-19 hospitalization outcomes in adults by HIV status; a nation-wide register-based study. *HIV Med* (2023) **24**:1045–55. doi:10.1111/hiv.13515

94. Moreno-Torres V, de Mendoza C, Martínez-Urbistondo M, Mills P, Treviño A, de la Fuente S, et al. Predictors of in-hospital mortality in HIV-infected patients with COVID-19. *QJM: Int J Med* (2023) **116**(1):57–62. doi:10.1093/qjmed/hcac215

95. Nagarakanti SR, Okoh AK, Grinberg S, Bishburg E. Clinical outcomes of patients with COVID-19 and HIV coinfection. *J Med Virol* (2021) **93**(3):1687–93. doi:10.1002/jmv.26533

96. Nasreddine R, Florence E, Moutschen M, Yombi J, Goffard J, Derdelinckx I, et al. Clinical characteristics and outcomes of COVID-19 in people living with HIV in Belgium: a multicenter, retrospective cohort. *J Med Virol* (2021) **93**(5):2971–8. doi:10.1002/jmv.26828

97. Nomah DK, Reyes-Urueña J, Díaz Y, Moreno S, Aceiton J, Bruguera A, et al. Sociodemographic, clinical, and immunological factors associated with SARS-CoV-2 diagnosis and severe COVID-19 outcomes in people living with HIV: a retrospective cohort study. *The Lancet HIV* (2021) **8**(11):e701–e710. doi:10.1016/s2352-3018(21)00240-x

98. Peters JL, Fall A, Langerman SD, El Asmar M, Nakazawa M, Mustapha A, et al. Prolonged severe acute respiratory syndrome coronavirus 2 Delta variant shedding in a patient with AIDS: case report and review of the literature. *Open Forum Infect Dis* (2022) **9**:ofac479. Oxford University Press US. doi:10.1093/ofid/ofac479

99. Rosenthal EM, Rosenberg ES, Patterson W, Ferguson WP, Gonzalez C, DeHovitz J, et al. Factors associated with SARS-CoV-2-related hospital outcomes among and between persons living with and without diagnosed HIV infection in New York State. *PLoS One* (2022) **17**(5):e0268978. doi:10.1371/journal.pone.0268978

100. Sun J, Patel RC, Zheng Q, Madhira V, Olex AL, Islam JY, et al. COVID-19 disease severity among people with HIV infection or solid organ transplant in the United States: a nationally-representative, multicenter, observational cohort study. Medrxiv (2021). Avaialble from: https://doi.org/10.1101/2021.07.26.21261028.

101. Tang ME, Gaufin T, Anson R, Zhu W, Mathews W, Cachay ER. People with HIV have a higher risk of COVID-19 diagnosis but similar outcomes to the general population. *HIV Med* (2022) **23**(10):1069–77. doi:10.1111/hiv.13312

102. Yang Y, Iwasaki A. Impact of chronic HIV infection on SARS-CoV-2 infection, COVID-19 disease and vaccines. *Curr HIV/AIDS Rep* (2022) **19**:5–16. doi:10.1007/s11904-021-00590-x

103. Yunihastuti E, Karjadi TH, Widhani A, Mahdi HIS, Sundari S, Hapsari AF, et al. Incidence and severity prediction score of COVID-19 in people living with HIV (SCOVHIV): experience from the first and second waves of the pandemic in Indonesia. *AIDS Res Ther* (2022) **19**(1):47–8. doi:10.1186/s12981-022-00472-1

104. Zhu F, Cao Y, Xu S, Zhou M. Co-infection of SARS-CoV-2 and HIV in a patient in Wuhan city, China. *J Med Virol* (2020) **92**:529–30. doi:10.1002/jmv.25732

105. Hoffmann C, Casado JL, Härter G, Vizcarra P, Moreno A, Cattaneo D, et al. Immune deficiency is a risk factor for severe COVID-19 in people living with HIV. *HIV Med* (2021) **22**(5):372–8. doi:10.1111/hiv.13037

106. Venturas J, Zamparini J, Shaddock E, Stacey S, Murray L, Richards GA, et al. Comparison of outcomes in HIV-positive and HIV-negative patients with COVID-19. *J Infect* (2021) **83**(2):217–27. doi:10.1016/j.jinf.2021.05.020

107. Liu W-D, Hung CC, Wang JT, Tsai MJ, Kuo PH, Chao TL, et al. Evolution of SARS-CoV-2 neutralizing antibody in an HIV-positive patient with COVID-19. *J Formos Med Assoc* (2021) **120**(12):2186–90. doi:10.1016/j.jfma.2021.04.010

108. Zhao J, Liao X, Wang H, Wei L, Xing M, Liu L, et al. Early virus clearance and delayed antibody response in a case of coronavirus disease 2019 (COVID-19) with a history of coinfection with human immunodeficiency virus type 1 and hepatitis C virus. *Clin Infect Dis* (2020) **71**(16):2233–5. doi:10.1093/cid/ciaa408

109. Schnittman SR, Jung W, Fitch KV, Zanni MV, McCallum S, Lee JSL, et al. Effect of host factors and COVID-19 infection on the humoral immune repertoire in treated HIV. *JCI insight* (2023) **8**(5):e166848. doi:10.1172/jci.insight.166848

110. Donadeu L, Tiraboschi JM, Scévola S, Torija A, Meneghini M, Jouve T, et al. Long-lasting adaptive immune memory specific to SARS-CoV-2 in convalescent coronavirus disease 2019 stable people with HIV. *AIDS* (2022) **36**(10):1373–82. doi:10.1097/qad.0000000000003276

EBM Experimental Biology and Medicine

TYPE Original Research
PUBLISHED 25 March 2024
DOI 10.3389/ebm.2024.10117

OPEN ACCESS

*CORRESPONDENCE
Qi Li,
qili_md@126.com
Peng Xie,
xiepeng@cqmu.edu.cn

†PRESENT ADDRESS
Anatol Manaenko,
Clinical Neuroanatomy Section, Department of Neurology, Ulm University, Ulm, Germany

‡These authors have contributed equally to this work

RECEIVED 01 September 2023
ACCEPTED 23 February 2024
PUBLISHED 25 March 2024

CITATION
Li X, Xiao Z, Li P, Yang W, Shen Y, Liu F, Xiong X, Wu Q, Wang P, Dang R, Gui S, Deng L, Manaenko A, Xie P and Li Q (2024), Age-related changes after intracerebral hemorrhage: a comparative proteomics analysis of perihematomal tissue.
Exp. Biol. Med. 249:10117.
doi: 10.3389/ebm.2024.10117

Age-related changes after intracerebral hemorrhage: a comparative proteomics analysis of perihematomal tissue

Xinhui Li[1,2‡], Zhongsong Xiao[1,2‡], Peizheng Li[1,2], Wensong Yang[1,2], Yiqing Shen[1,2], Fangyu Liu[1,2], Xin Xiong[3], Qingyuan Wu[2,4], Peng Wang[1,2], Ruozhi Dang[1,2], Siwen Gui[1,2], Lan Deng[1], Anatol Manaenko[1,2†], Peng Xie[1,2*] and Qi Li[1,2,5*]

[1]Department of Neurology, The First Affiliated Hospital of Chongqing Medical University, Chongqing, China, [2]NHC Key Laboratory of Diagnosis and Treatment on Brain Functional Diseases, The First Affiliated Hospital of Chongqing Medical University, Chongqing, China, [3]Department of Neurology, Chongqing Hospital of Traditional Chinese Medicine, Chongqing, China, [4]Department of Neurology, Chongqing University Three Gorges Hospital, Chongqing, China, [5]Department of Neurology, The Second Affiliated Hospital of Anhui Medical University, Hefei, Anhui, China

Abstract

The risk factors and causes of intracerebral hemorrhage (ICH) and the degree of functional recovery after ICH are distinct between young and elderly patients. The increasing incidence of ICH in young adults has become a concern; however, research on the molecules and pathways involved ICH in subjects of different ages is lacking. In this study, tandem mass tag (TMT)-based proteomics was utilized to examine the protein expression profiles of perihematomal tissue from young and aged mice 24 h after collagenase-induced ICH. Among the 5,129 quantified proteins, ICH induced 108 and 143 differentially expressed proteins (DEPs) in young and aged mice, respectively; specifically, there were 54 common DEPs, 54 unique DEPs in young mice and 89 unique DEPs in aged mice. In contrast, aging altered the expression of 58 proteins in the brain, resulting in 39 upregulated DEPs and 19 downregulated DEPs. Bioinformatics analysis indicated that ICH activated different proteins in complement pathways, coagulation cascades, the acute phase response, and the iron homeostasis signaling pathway in mice of both age groups. Protein–protein interaction (PPI) analysis and ingenuity pathway analysis (IPA) demonstrated that the unique DEPs in the young and aged mice were related to lipid metabolism and carbohydrate metabolism, respectively. Deeper paired-comparison analysis demonstrated that apolipoprotein M exhibited the most significant change in expression as a result of both aging and ICH. These results help illustrate age-related protein expression changes in the acute phase of ICH.

KEYWORDS

proteomics, intracerebral hemorrhage, aging, protein-protein interaction, tandem mass tag

Impact statement

The increasing incidence of intracerebral hemorrhage (ICH) in young adults has become a concern; however, research on susceptible molecules and pathways specifically targeting ICH in subjects of different ages remains lacking. We aimed to investigate the underlying interaction relationship between aging and ICH by proteomics approaches. In this study, we performed tandem mass tag (TMT)-based proteomics on young and aged mice after constructing collagenase-induced ICH models to screen protein expression in brain perihematomal tissue among groups.

Introduction

Intracerebral hemorrhage (ICH) is a devastating stroke subtype that is associated with low treatable rates and high mortality rates [1]. Approximately 50% of patients die within the first 48 h, and most patients suffer from a severe disability after being discharged from the hospital [2]. Previous studies have revealed that young adult and elderly patients with acute ICH exhibit distinct incidence rates, causes and functional recoveries [3]. Recently, the increasing incidence of ICH in young adults has become a major concern, and permanent disability and death caused by ICH in this demographic bring heavy economic burdens to society and public health organizations [4, 5]. To optimize preventive and protective approaches for young adults with ICH, the pathological changes that occur in young subjects after ICH need to be investigated.

Recently, genome-wide studies of ICH populations have been carried out [6–8]. High-throughput sequencing has provided evidence that age-specific changes occur after ICH events. A proteomics analysis detected differentially expressed proteins (DEPs) in plasma among young, middle-aged, and older healthy individuals and confirmed that insulin-like growth factor 1 is a promising novel approach for ameliorating aging-associated acute brain injury after ICH [9]. The other transcriptomic analysis distinguished the expression pattern of oxylipin enzymes between middle-aged and aged rats 3 days after experimental ICH induction and revealed that among the specific differentially expressed genes (DEGs), Cyp1a1 and Cyp2e1 were the most significant DEGs in the two age groups [10]. In addition, in pathological findings of animals with ICH, more severe brain swelling was observed in aged animals than in young animals, and aged animals exhibited different glial responses from young animals, impaired lesion resolution, and neuronal death [11]. Interestingly, a recent study based on another classic stroke model, middle cerebral artery occlusion mice, found that O-GlcNAcylation was a pro-survival pathway that was impaired in the stroke penumbra in aged mice but was activated in young mice, and this study introduced a therapeutic strategy for treating ischemic stroke in an age-specific manner [12]. However, relatively little is known about the different responses to ICH in aged and young subjects. Therefore, understanding the discrepancies in the mechanisms of internal molecular injury in young and aged patients after ICH is highly desirable.

In ICH, primary injury occurs due to the mechanical compression of the brain parenchyma caused by an expanding intracranial hematoma, resulting in brain edema and neuron damage in the perihematomal area [13]. Furthermore, local ischemia and hypoxia in brain tissue, along with the release of blood components from ruptured blood vessels, initiate secondary brain injury, activating microglia and resident macrophages within the brain and recruiting peripheral leukocytes through the compromised blood–brain barrier to the perihematomal area, further exacerbating inflammatory injury [14]. Therefore, the perihematomal region is the most commonly studied region in the field of ICH [15–18]. Experimental analysis of perihematomal tissue can provide an in-depth understanding of the mechanisms of secondary injury, the related role of inflammatory mediators, and the processes of neuroprotection and neuronal repair, yielding valuable evidence for the development of strategies for treating brain injury, inhibiting inflammatory responses, and promoting neuroprotection.

This study aimed to explore the differences in protein expression in perihematomal tissue between young and aged mice using proteomics data. The functions and pathways of common and unique DEPs that were identified by comparative proteomics between young and aged mice were investigated, and possible targets and pathways for follow-up studies across different life periods were identified.

Materials and methods

Animals

Specific-pathogen-free 10-week-old and 22-month-old male C57BL/6 mice were purchased from the Laboratory Animal Center of Chongqing Medical University (CQMU). Animals were maintained in a pathogen-free facility and were fed *ad libitum* in a 12/12-h light-dark environment at 25°C. All experimental protocols were approved by the Ethical

TABLE 1 Label information of 12 samples.

TMT label	126	127N	127C	128N	128C	129N	129C	130N	130C	131N	131C	132N	No.
sample	aged-ICH-1	aged-ICH-2	aged-ICH-3	aged-sham-1	aged-sham-2	aged-sham-3	young-ICH-1	young-ICH-2	young-ICH-3	young-sham-1	young-sham-2	young-sham-3	1

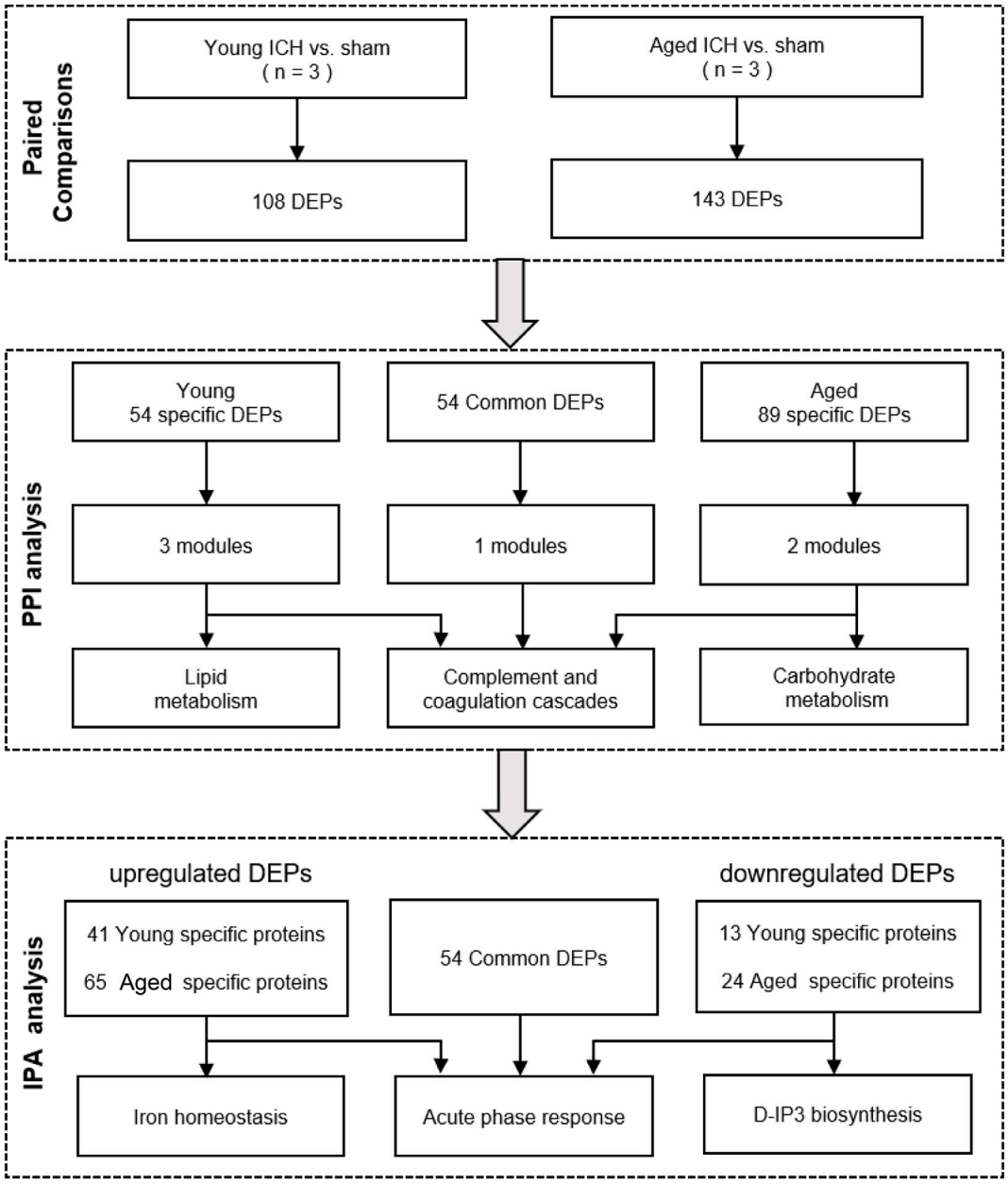

FIGURE 1
Bioinformatics analysis procedure.

Committee of CQMU. All efforts were made to reduce the number of animals and the amount of suffering they endured.

Animal models

The collagenase IV-induced ICH mouse model was established based on a previous study [19]. Anaesthesia was administered to the mice through the inhalation of 4% isoflurane. After remaining under anaesthesia with 1.5% isoflurane, the mice were placed on a stereotaxic apparatus (Rivard, China) in a prone position with a rectal temperature that was maintained at 37.5°C. A 26-gauge microsyringe (Hamilton, the United States) was inserted into the right striatum through an eyehole that was drilled in the skull (the anterior fontanelle was the origin of the coordinate with 0.6 mm anterior and 2.3 mm lateral directions

and a 3.7 mm depth). ICH models or sham controls were induced by 0.075 U collagenase (Sigma, the United States) in 0.4 μL of 0.9% physiological saline or an equivalent dose of saline at a rate of 0.5 μL/min. The mice were placed on a warming pad until consciousness was recovered.

Sampling

Mice were randomly divided into a young sham group, a young ICH group, an aged sham group, and an aged ICH group. Twenty-four hours after ICH, the mice were anaesthetized with pentobarbital sodium. Approximately 2 minutes later, after the mice were successfully anaesthetized, they were perfused transcardially with 30 mL sterile phosphate-buffered saline within 6 min. Immediately after perfusion, the brains of the mice were removed, and 1 mm coronal brain sections of perihematomal tissue from the basal ganglia were prepared according to our previous study [20]. The tissues were shock frozen in liquid nitrogen for 30 min and stored at −80°C until use.

Protein extraction and peptide fractionation

Eight mice in each group were used for the proteomic analysis, and 2 or 3 brain samples were pooled as one biological replicate (n = 3 in each group). The samples were lysed in 4% SDS, 10 mM Tris-HCl, and 1 mM DTT (pH = 7.6). Then, the lysates were transferred to a 2 mL centrifuge tube prefilled with an appropriate amount of quartz sand and a 1/4-inch ceramic bead (MP 6540-424), homogenized twice for 120 s (24 × 2, 6.0 m/s) by a FastPrep-24 instrument (MP Biomedicals, the United States) and ultrasonicated 10 times for 100 s (100 W, sonication for 10 s, rest for 5 s). Next, the samples were boiled in water for 15 min and centrifuged at 14,000 *g* for 30 min, and the supernatant was filtered via 0.22 μm filters. The concentration of the final extracted proteins was quantified using a BCA Protein Assay Kit (Bio-Rad, the United States). Protein digestion and peptide fractionation were performed based on a filter-aided sample preparation (FASP) protocol [21]. In brief, 200 μg of protein sample was incubated with the detergent dithiothreitol to remove residual low-molecular-weight molecules, and then iodoacetamide was added for the alkylation reaction. Peptide concentrations were measured using the ultraviolet spectral density method at 280 nm.

Tandem mass tag (TMT)-based liquid chromatography–mass spectrometry (LC–MS) proteomics analysis

The digested peptides were labelled by the Tandem Mass Tags (TMT) reagent kit (Thermo Scientific, the United States). The label information of 12 samples is shown in Table 1. After TMT labeling, the samples were specifically identified and analyzed using database search software. LC/MS-MS analysis was carried out using Easy nLC Proxeon Biosystems coupled with a Q Exactive mass spectrometer (Thermo Scientific, the United States) for 60/90 min. The digested peptides were loaded onto a nano Viper C18 trap column (100 μm i.d. ×2 cm, Acclaim PepMap100) (Thermo Scientific, the United States) and separated on a capillary C18-reversed-phase analytical column (75 μm i.d. ×10 cm, 3 μm resin, Easy Column) (Thermo Scientific, the United States) with an eluent buffer composed of 0.1% formic acid (FA) and a linear gradient buffer composed of 0.1% FA and 84% acetonitrile at a flow rate of 0.300 μL/min. The 10 most abundant precursor ions were processed during each scan cycle by higher energy collision-induced dissociation (HCD) fragmentation. The automatic gain control (AGC) target value was 3 x e6, and the mass range was 300–1800 m/z. The duration time for the dynamic exclusion was 2/3 min, and the injection time did not exceed 10 ms. The resolutions for the survey scans and HCD spectra were set to 70,000 at m/z 200 and 30,000 at m/z 200, respectively. The underfill rate was 0.1%, the normalized collision energy was adjusted to 30 eV, and the width parameter of isolation was 2 m/z. The mass spectrometer was run in positive mode, and the apparatus was operated in peptide recognition mode.

Protein identification

The raw proteomics data were analyzed by Proteome Discoverer software (v.1.4) using the MASCOT engine (v.2.2) (Matrix Science, Britain). Tandem mass spectra data were matched against the UniProt database[1]. Trypsin was defined as the cleavage enzyme, and the maximum missing cleavage was 2. The peptide ion mass tolerance was ±20 ppm, and the fragment ion mass tolerance was 0.1 Da. The false discovery rate (FDR) for protein and peptide identification was ≤0.01. Protein quantitative analysis was performed according to the median of the exclusive specific peptides in the MS/MS spectra. The carbamidomethylation of cysteine and the oxidation of methionine were defined as fixed modification and variable modification, respectively. TMT-16plex was used in the quantitation process.

Bioinformatics

The bioinformatics analysis procedure is shown in Figure 1. DEPs between the ICH and sham groups were identified by an FDR <0.05. The subcellular localization of

1 https://www.uniprot.org/

DEPs was searched on CELLO[2]. The *p* values and fold change (FC) values of the DEPs were visualized in volcano plots. Hierarchical clustering analyses were conducted by cluster 3.0[3] and Java Treeview[4] and were visualized in heatmaps. The specific and common DEPs between different paired comparisons were identified by Venn plots[5]. DEP functional analysis was conducted by Gene Ontology (GO) analysis, and pathway analysis was performed by Kyoto Encyclopedia of Genes and Genomes (KEGG)[6] and Ingenuity Pathway Analysis (IPA) software (IPA®, Qiagen, the United States)[7]. Protein–protein interaction (PPI) networks were constructed based on STRING[8] and were further analyzed with Cytoscape software by the MCODE and CytoNCA plug-ins[9].

Results

Identification of DEPs in young and aged mice after ICH

The number of obtained spectra, peptides, and proteins are presented in Table 2. Specifically, the expression of a total of 5,129 proteins in the brains of young and aged mice was quantified, and the accession numbers, expression levels, sequence coverages and number of peptides identified are listed in Supplementary Tables S1, S2. Next, we examined the differences in the protein expression profiles of perihematomal tissues after ICH between young and aged mice by performing DEP analysis at 24 h after ICH and comparing the spectra with those of age-matched sham controls. When the DEPs were screened by FC > 1 and <1 and FDR <0.05, the FCs in DEPs between the ICH mice and sham controls in both age groups displayed significant discrepancies, as seen in the hierarchical clustering heatmaps, which grouped the samples from the ICH group and sham controls into two different clusters and enabled us to perform the following analysis (Supplementary Figures S1A, S1B). The full names of the DEPs in the heatmaps are presented in Supplementary Table S3. As depicted in the volcano plot (Figure 2A), ICH upregulated 95 and downregulated 13 proteins in young mice. In contrast, there were 119 upregulated proteins and 24 downregulated proteins in aged mice after ICH (Figure 2B). As shown in Figure 2C, common and unique DEPs were identified by a Venn diagram and included 54 unique DEPs in young mice (41 upregulated and 13 downregulated in the ICH group relative to controls), 89 unique DEPs in aged mice (65 upregulated and 24 downregulated in the ICH group relative to controls), and 54 common DEPs (all upregulated in the ICH group relative to controls) in the two age groups. To reduce the number of DEPs, FC > 2, FDR <0.05 was set as a stricter threshold to identify the most significant DEPs. The subcellular localization and biological function of the DEPs are described in detail in Supplementary Table S4.

Identification of specific and common DEP-related functions and pathways

To gain precise and thorough insight into the effect of aging and ICH, we explored the PPIs and performed module cluster analysis by GO enrichment and KEGG pathway analysis for specific and common DEPs in aged and young mice. To prevent the possibility of omitting meaningful functions and pathways due to false-negative results, the criterion for the identification of DEPs was once again set as FC > 1 and <1 and FDR <0.05.

Next, PPI analysis was conducted. As shown in Figure 3A, most of the common DEPs were clustered in one module, and their functions were associated with complement and coagulation cascades (Supplementary Table S5). The two modules in the PPI network constructed from unique DEPs in young mice were associated with negative regulation of the remodeling of very-low-density lipoprotein particles and ribosomal subunits (Figure 3B; Supplementary Table S5). In contrast, the DEPs constructed from unique DEPs in aged mice were divided into 3 modules, which were related to complement and coagulation cascades, glycolytic processes, and the biosynthetic processes of porphyrin-containing compounds (Figure 3C; Supplementary Table S5).

Identification of specific and common up- or downregulated DEP-related functions and pathways

Then, the ICH-induced DEPs in the two age groups were further divided into upregulated and downregulated DEPs for IPA. Consistent with the functional analysis of module clusters from PPI networks, biofunctional analysis conducted via IPA software demonstrated that lipid metabolism and carbohydrate embolism were significantly activated after ICH in young and aged mice, respectively (Supplementary Figures S2A, S2B). In the results for the IPA pathway enrichment of upregulated

2 http://cello.life.nctu.edu.tw/
3 http://bonsai.hgc.jp/~mdehoon/software/cluster/software.htm
4 http://jtreeview.sourceforge.net
5 http://bioinformatics.psb.ugent.be/webtools/Venn/
6 https://david.ncifcrf.gov/summary.jsp
7 https://www.qiagenbioinformatics.com
8 https://string-db.org
9 https://apps.cytoscape.org/apps/

TABLE 2 The identification and quantitation results.

Spectrum		Peptides		Proteins	
Total spectrum	Matched spectrum	Peptides	Unique peptides	Identified	Quantified
520,445	65,279	29,892	27,287	5,135	5,129

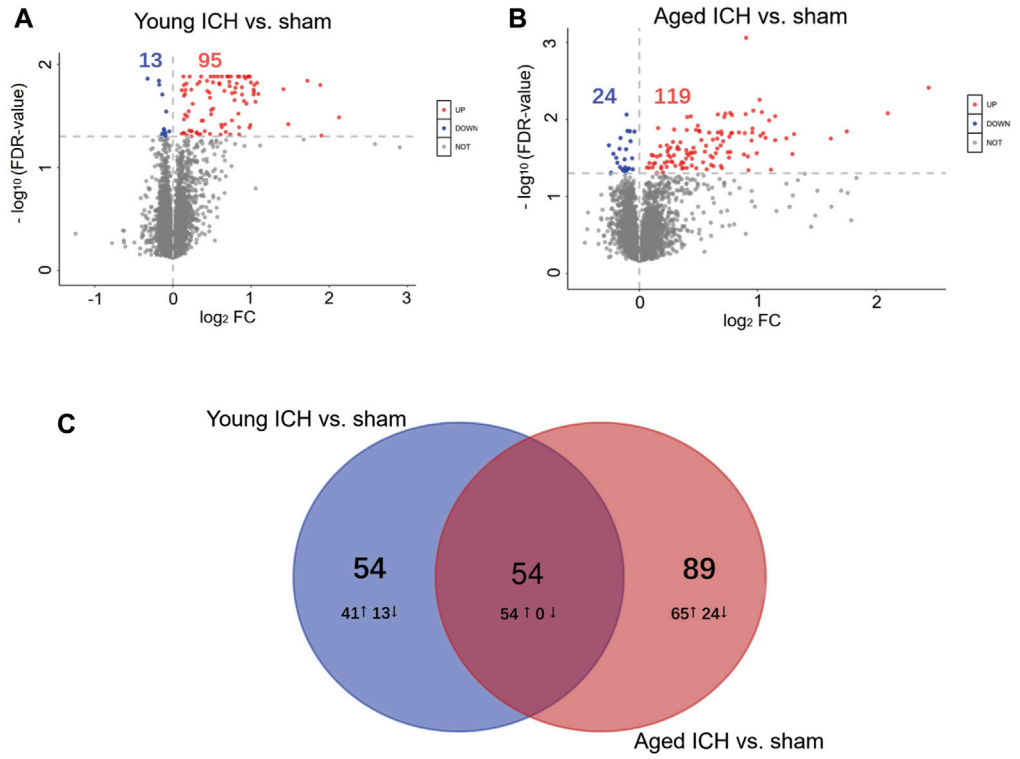

FIGURE 2
Identification of DEPs and PPI analysis. Volcano plots of DEPs between the ICH and sham groups in **(A)** young and **(B)** aged mice. **(C)** Venn diagram analysis of the ICH-induced DEPs between different age-matched comparisons.

DEPs, the signaling pathways for iron homeostasis and pancreatic adenocarcinoma were the common activated pathways (Figures 4A–C; Supplementary Table S6). However, the proteins involved in the iron homeostasis signaling pathway were different. The proteins that participated in this pathway included STAT3, HPX, and HP from young mice and CP, EGFR, Hbb-b1, Hbb-b2, MAPK1, and MMS19 from aged mice (Figures 5, 6). In addition, regarding neurodegenerative diseases (NDDs), several functions, including Huntington's disease signaling (EGFR, MAPK1, PSMB3), neuroprotection by THOP1 in Alzheimer's disease (AGT, MAPK1) and Parkinson's signaling (MAPK1), were activated only in aged mice (Supplementary Table S6). The shared pathways among the three clusters of DEPs included the complement and coagulation system and acute phase response, and this finding was consistent with the PPI analysis (Figures 4A–C; Supplementary Table S6). For the downregulated DEPs, D-IP3 biosynthesis and autophagy were the common functional pathways that were activated (Supplementary Table S6).

We next explored the proinflammatory factors that correlated with proteins of the iron homeostasis signaling pathway in both age groups. The networks obtained with the IPA software and constructed based on the direct and indirect relationships among the unique upregulated DEPs in the two age groups demonstrated that IL1 was the upstream molecule of HP in the young mice after ICH (Figure 7A) and that the NF-κB complex interacted with Hbb-b1 in aged mice after ICH (Figure 7B).

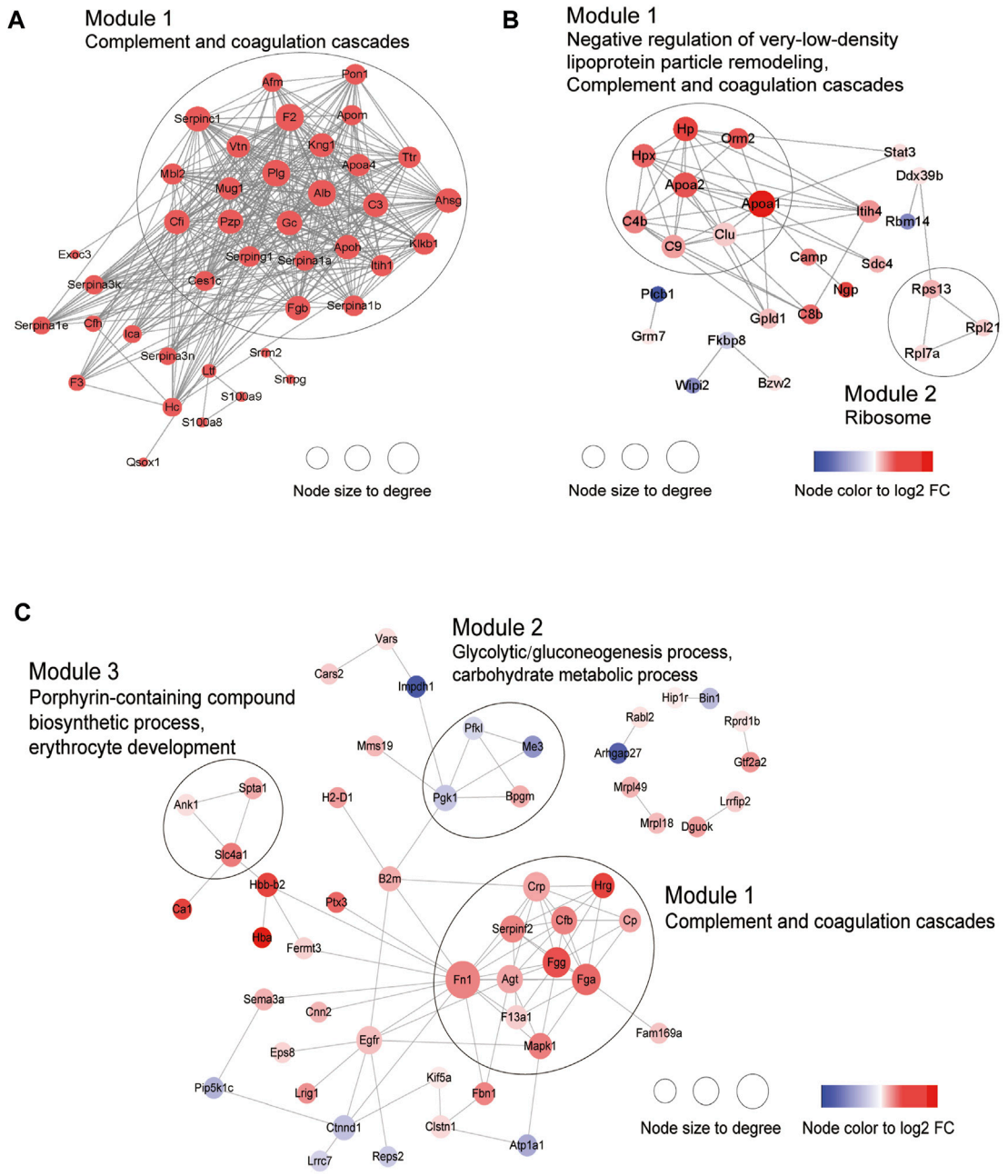

FIGURE 3
Construction of PPI network. **(A)** Common DEPs and **(B)** Specific DEPs in young and **(C)** aged mice after ICH.

Specific markers between aged and young mice after ICH

Considering that the previous comparison was limited to ICH vs. sham, some important markers may have been missed. Thus, we explored different pairwise-comparison groups to explore the proteins affected by age alone and those affected by both age and ICH. As shown in Figures 8A, B, the expression of Bsg, Ptgfrn, Dpysl3, Rras2, Prdx1, Gnpda2, Gja1, Folh1, Serinc5, C1qtnf5, Ccdc8, Vcan, Nmral1, Fth1, Hlta1, Mog, Hapln2, and Cldn11 was affected by age only (18 in total), and that of ApoM, Psmb2, Ttr, Kng1, and Serpina3k was affected by both age and ICH (5 in total).

DEP analysis between the aged and young sham groups

To exclude the inherent differences between aged and young mice, we further compared the DEPs between the two sham groups. A total of 58 DEPs were identified between the aged and young sham groups of mice (Figure 9A; Supplementary Figure S3). The full names of the DEPs in the heatmap are presented in Supplementary Table S3. Aging downregulated 19 proteins in the basal ganglia, including the SH3 domain binding proteins Dpysl3, Shank2, and Mical1, the dendrite development-related proteins Srcin1 and Cyth2 and the neuron differentiation-related proteins Dpysl3, Shank2, Slc23a2 and Brinp2 (Figure 9B). Moreover, 39 proteins were upregulated in the brains of aged mice compared to those of young controls, and the functions of these proteins were identified by KEGG and GO enrichment analysis[11] (last accessed on 10 November 2023, an online platform for data analysis and visualization) (Figure 9C; Supplementary Table S7) [22–24]. According to GO analysis, the DEPs were significantly enriched in 392 biological process (BP) terms ($p < 0.05$), with cellular modified amino acid metabolicprocess, regulation of organelle transport along microtubule, and astrocyte differentiation being the top BP terms. Furthermore, these DEPs were significantly enriched in 61 GO cellular component (CC) terms. Notably, the top CC terms included myelin sheath, lateral plasma membrane, and basal part of cell. Moreover, 71 molecular function (MF) terms were significantly overrepresented, including toxic substance binding, carboxylic acid binding, and organic acid binding. Additionally, KEGG pathway analysis revealed 11 significantly enriched pathways, including alanine, aspartate and glutamate metabolism, retrograde endocannabinoid signaling, and hepatitis C.

Then, we performed PPI and module analysis of all DEPs (Figure 10; Supplementary Table S5). The proteins in module 1 were primarily associated with GO-BP terms such as axon ensheathment, cell adhesion, and glial cell differentiation. On the other hand, the proteins in module 2 were mainly involved in mitochondrial ATP synthesis-coupled proton transport.

Discussion

In the current study, we conducted LC–MS/MS analysis to examine changes in the protein profile of perihematomal tissue in response to ICH in the brains of aged and young mice. The functional analysis of age-specific DEPs and common DEPs in different ages implied that different age-related response patterns occurred at the acute phase of brain injury after ICH. Decoding aberrant protein expression patterns between young and aged groups of ICH mice can provide age-related internal vulnerable molecular mechanisms.

Specific and common DEPs in both age groups were associated with complement and coagulation cascades and the acute phase response, and these pathways are known as the vital BP that occurs with brain injury after ICH. Surprisingly, we found that the clustered DEPs that were specific to aged and young mice were enriched in glycolysis/gluconeogenesis processes and ribosomal subunits, respectively. Enhanced glycolysis/gluconeogenesis could promote the proinflammatory function of macrophages [25, 26]. In aged mice after ICH, decreased Pfkl (ATP-dependent 6-phosphofructokinase, liver type) and Pgk1 (phosphoglycerate kinase 1) proteins and increased Bpgm (bisphosphoglycerate mutase) protein were clustered together, and their functions involved glycolysis/gluconeogenesis and carbohydrate metabolic processes. Pfkl is a subtype of Pfk, and in a previous transcriptomics study, the elevated level of Pfk gene expression in $CD14^+$ monocytes/macrophages from hematoma tissue was reported to be significantly associated with good outcomes for ICH patients at the subacute stage [27]. Clinical and preclinical data have shown that increased Pgk1 activity and glycolysis ameliorate the neurodegeneration and progression of Parkinson's disease [28]. Bpgm plays an essential role in reversing aging-related cognitive impairment and auditory dysfunction [29]. Based on these findings, the significant change in glycolysis protein levels in the acute stage of ICH may be a specific predictor of poor outcomes. In addition, the other module from the aged-specific DEP PPI network included Spta1 (spectrin alpha chain, erythrocytic 1), Slc4a1 (band 3 anion transport protein), and Ank1 (ankyrin-1). In clinical research, the Slc4a1 and Ank1 genes from the peripheral blood of ICH patients were verified as hub genes by RNA sequence analysis, and this result implied that these genes have the potential to be used as key intervention targets in translational research [30].

In contrast, lipid metabolism was significantly affected in the young mice. Oxylipin profiling at 12 h, 24 h, and 72 h after ICH in adult mouse brains was explored in a recent study, and the number of changed oxylipins was the highest on the first day of ICH [10]. In the present study, the expression of the apolipoprotein A-I (Apoa1) protein differed between young and aged ICH model mice, being significantly elevated exclusively in young mice. This discrepancy may be associated with the weaker response to ICH in aged mice. Apoa1, as a component of high-density lipoprotein, may exert a protective effect by reducing cholesterol deposition and inhibiting inflammatory responses. Previous studies have also identified it as a protective factor in ICH, supporting this hypothesis [31, 32]. Consequently, in aged mice and even patients with ICH, greater attention should be

11 https://www.bioinformatics.com.cn

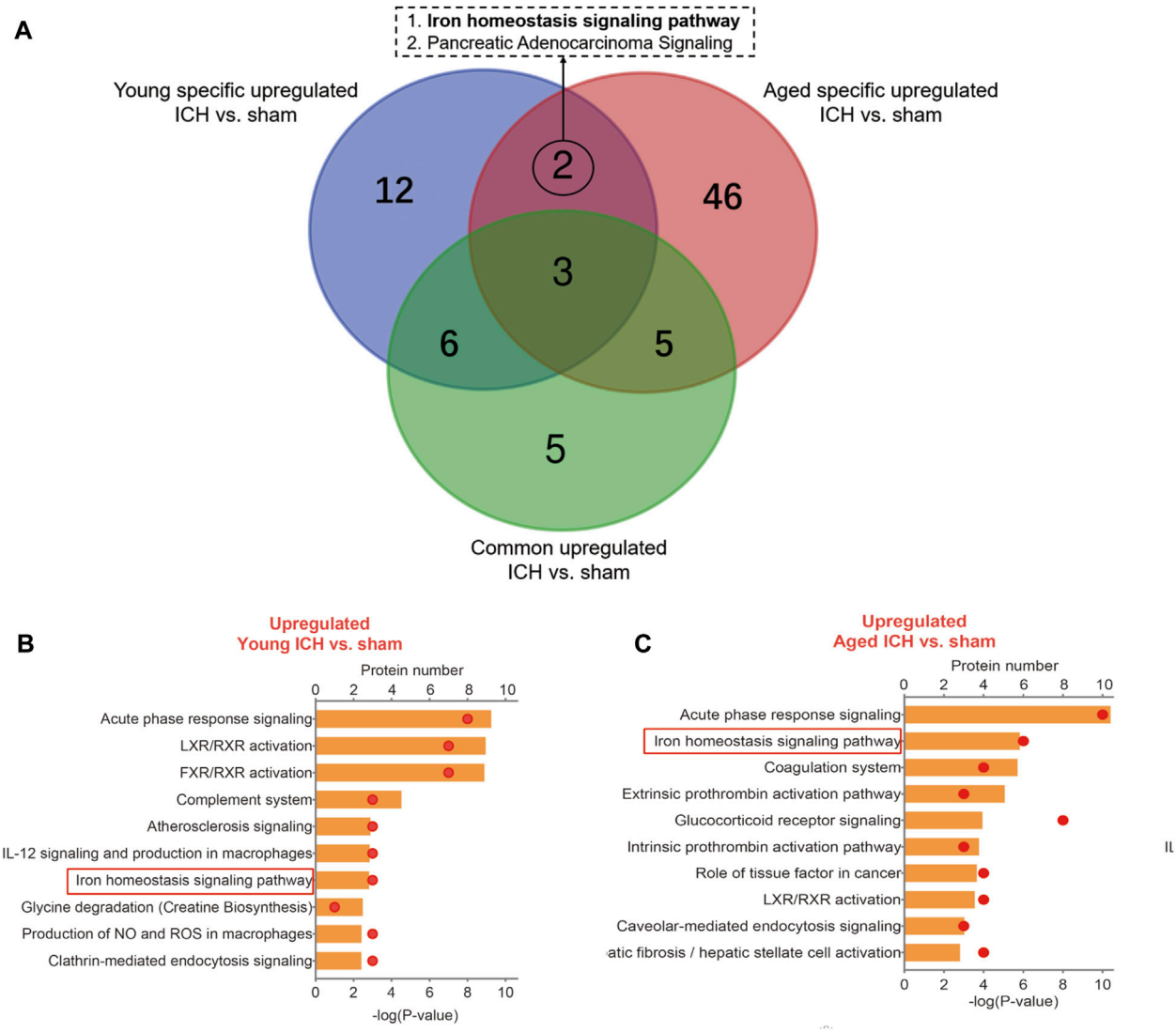

FIGURE 4
IPA analysis of specific upregulated DEPs. **(A)** The number of IPA pathways between specific and common upregulated DEPs in aged or young mice after ICH. **(B)** The top 10 IPA pathways in young and **(C)** aged mice after ICH compared with the corresponding sham controls.

paid to changes in the level of this indicator and related treatments. However, the interaction between lipid metabolism and ICH is still worthy of further exploration. In addition, the levels of Rps13 (40S ribosomal protein S13), Rpl21 (60S ribosomal protein L21), and Rpl7a (60S ribosomal protein L7a) genes were elevated, and these genes interacted with each other in the PPI network that was constructed by DEPs from young mice after ICH. The genes are all components of ribosomal subunits. Ribosomal damage could cause the TP53 pathway to be disrupted and increase ROS [33], which have a close link with secondary brain injury after ICH [34]. Significantly, Rpl7a was identified as a hub gene in a murine model of traumatic brain injury [35], and increased Rps13 gene levels in microglia and epithelial cells were found to be aging-related in a single-cell sequence study on murine brains [36]. In our study, the elevated ribosomal-associated proteins functioned as transcriptional proteins, and they may play a role in brain injury in young mice after ICH.

Secondary brain injury includes erythrocyte lysis with the production of neurotoxic iron ions, immune-inflammatory reactions, and coagulation cascades, which result in nerve cell death and brain tissue necrosis [37]. Previous studies have shown that the distribution of iron in the healthy human brain is region-specific and that its concentration increases with age [38, 39]. The putamen nucleus, caudate nucleus, and globus pallidus in the basal ganglia are the brain regions with the highest concentration

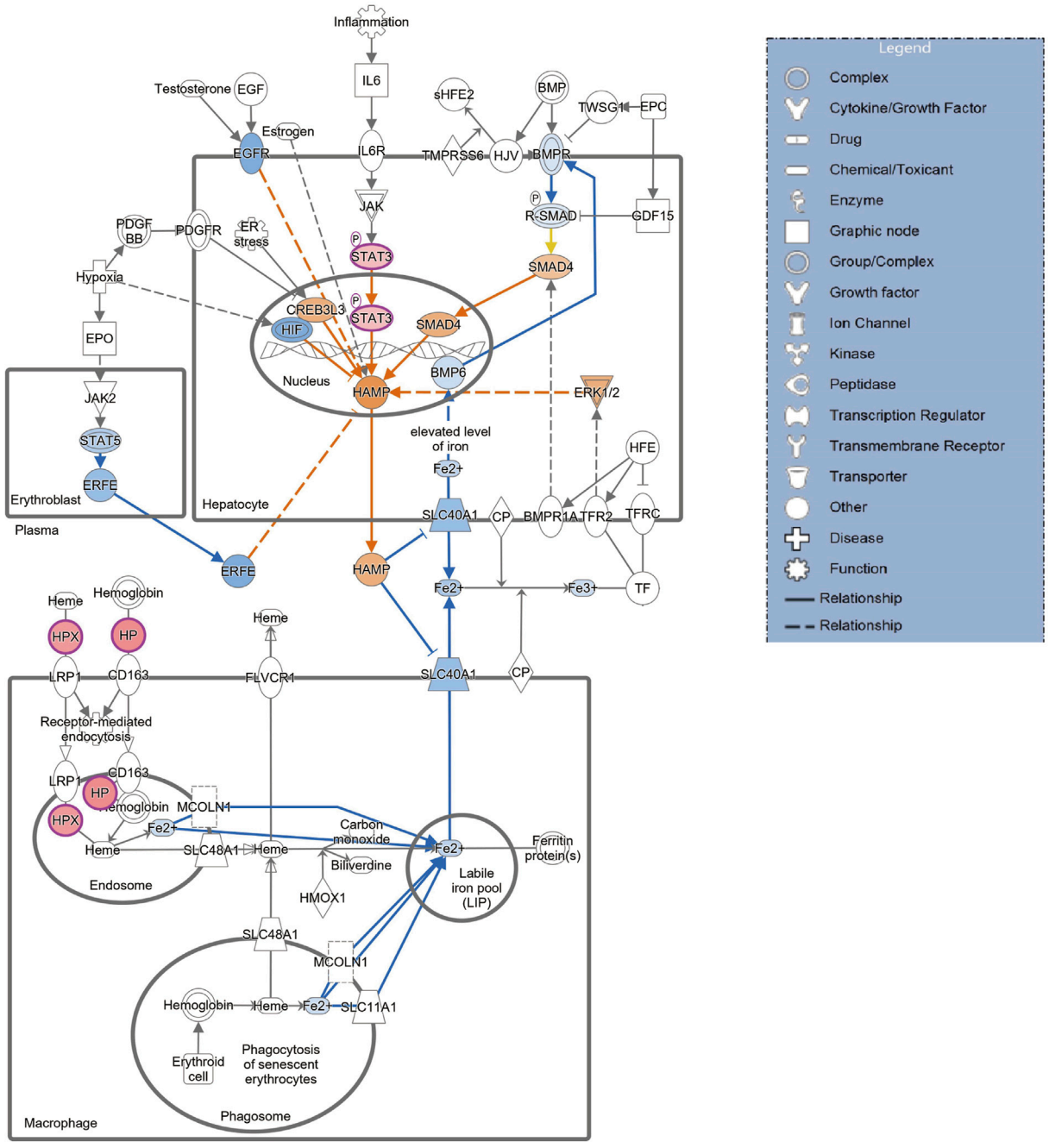

FIGURE 5
The iron homeostasis signaling pathway in young mice after ICH compared with the corresponding sham controls (by IPA software).

of iron [40]. The increase in the number of glial cells and the permeability of the blood–brain barrier with age may explain the accumulation of iron in the basal ganglia. In the present proteomics analysis, we found that the signaling pathway of iron homeostasis was activated after ICH in both aged and young mice. Interestingly, the number and type of proteins that were activated in the pathway were significantly higher in the aged mice after ICH than in the young mice. Following ICH, the proteins involved in iron metabolism in young mice include HP (haptoglobin), HPX (hemopexin), and STAT3 (signal transducer

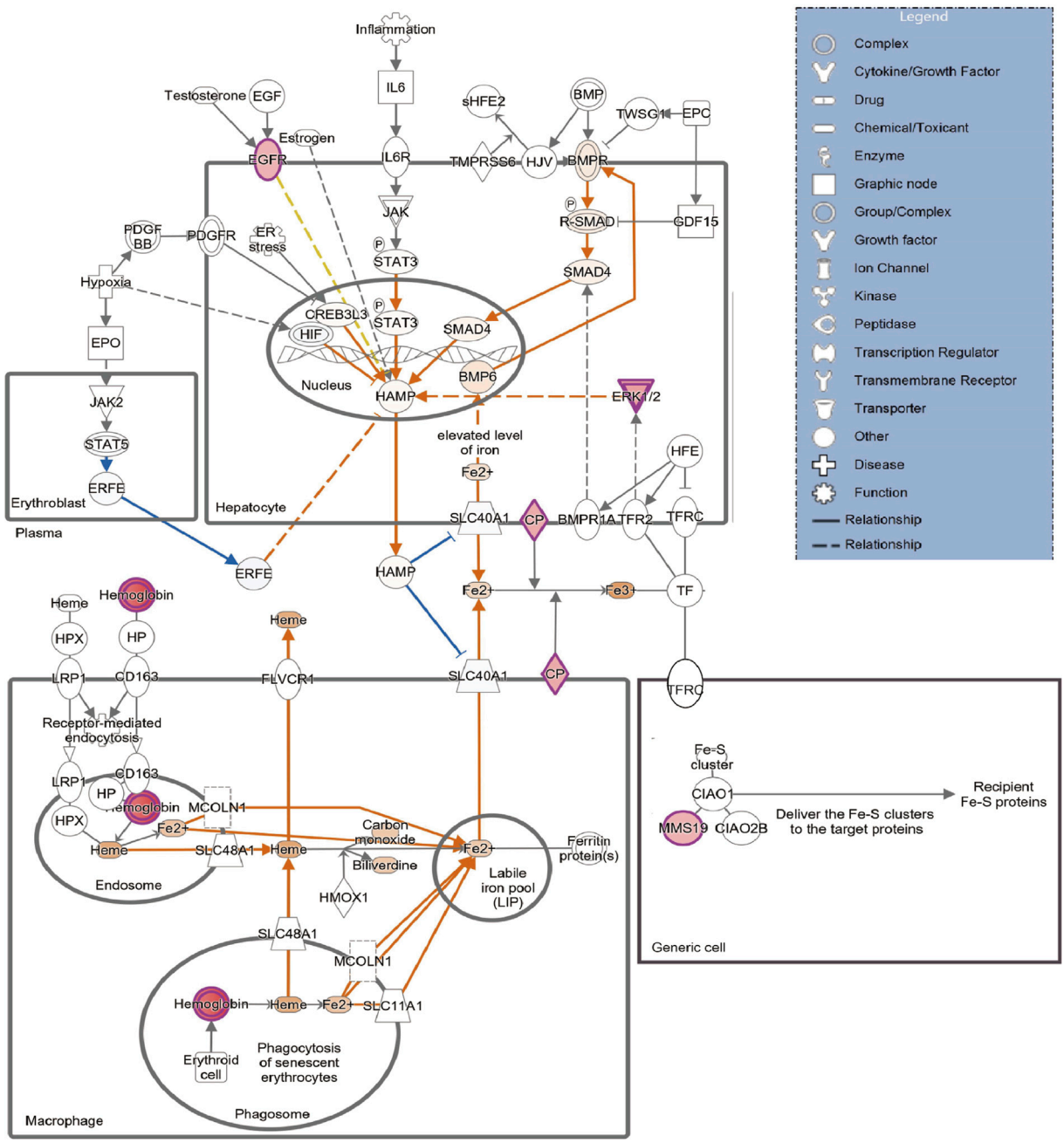

FIGURE 6
The iron homeostasis signaling pathway in aged mice after ICH compared with the corresponding sham controls (by IPA software).

and activator of transcription 3). On the other hand, in aged mice, the proteins related to iron metabolism were CP (ceruloplasmin), EGFR (epidermal growth factor receptor), Hbb-b1 (hemoglobin subunit beta-1), Hbb-b2 (hemoglobin subunit beta-2), MAPK1 (mitogen-activated protein kinase 1), and MMS19 (MMS19 nucleotide excision repair protein). HP and HPX and CP are plasma proteins synthesized by the liver that can bind to hemoglobin, heme and copper, respectively. Previous studies have suggested that increasing HPX and CP levels or reducing HP levels could be potential strategies for the treatment of experimental ICH [41–43]. Specifically, the therapeutic effect of HP gene knockout on

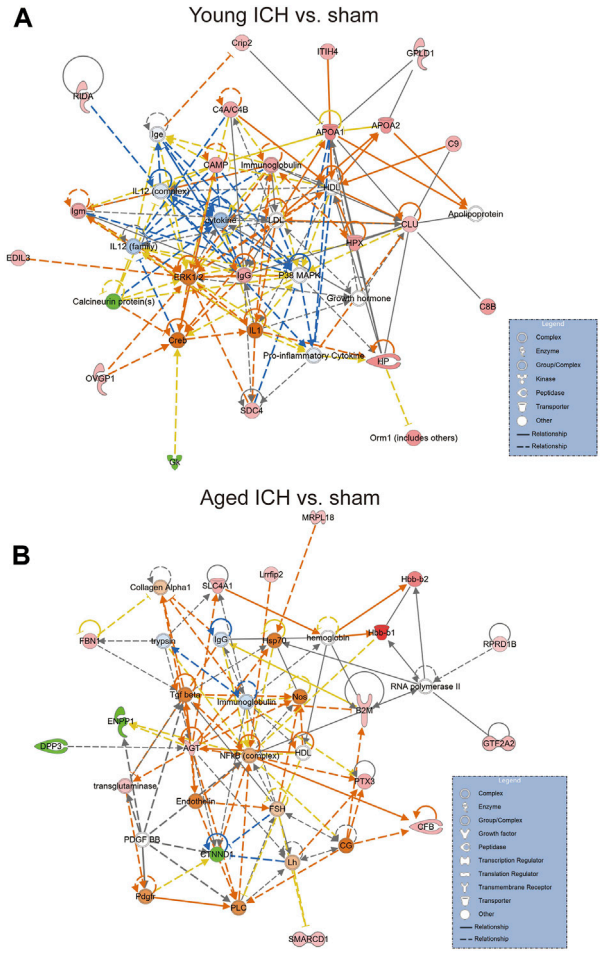

FIGURE 7
The internet interaction of DEPs in young and aged mice after ICH (by IPA software). **(A)** Young ICH vs. Young sham. **(B)** Aged ICH vs. Aged sham.

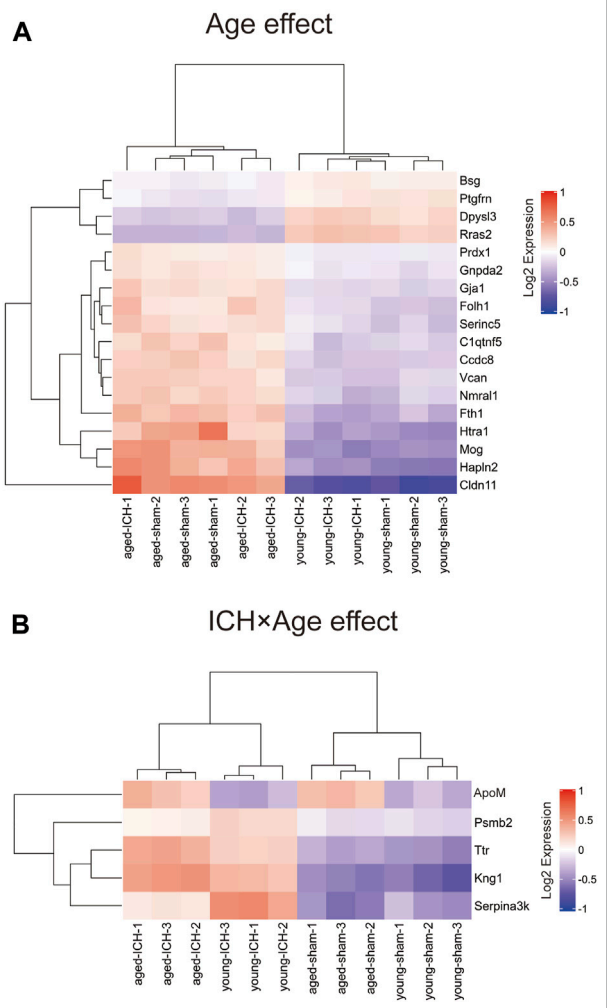

FIGURE 8
DEPs affected by age or ICH. **(A)** DEPs that were affected by age only. **(B)** DEPs that were affected by age and ICH.

ICH was age dependent, with Hp depletion resulting in a better neurological outcome in young ICH model mice but being ineffective in aged ICH model mice. Similarly, another experiment on age-related memory decline showed that specific knockout of CP in astrocytes had a beneficial effect on aged mice but had detrimental effects on young mice [44]. These results emphasize the importance of considering age-related factors when developing strategies for protecting the brain and indicate that the underlying mechanisms of ICH and response to treatment may differ between young and aged individuals. When iron metabolism becomes dysfunctional, excess iron and hydroxyl radicals are produced, resulting in OS damage and neuronal injury or death [45]. Previous studies based on an ICH model with aged murine and aged rats indicated that mediating iron metabolism and reducing iron accumulation could alleviate neuronal death and neurological deficits [46, 47]. The present results suggest that after ICH in aged individuals, iron metabolism is a crucial process in the brain injury mechanism. In addition, several DEPs in the aged mice were enriched in NDD-related pathways, which suggests a possible interactive correlation between ICH and NDD in pathological mechanisms.

To select meaningful molecular markers for validation, we performed additional pairwise comparisons. Among the proteins altered by age alone, Cldn11 (claudin-11) and Mog(myelinoligodendrocyte glycoprotein are myelin-associated proteins. ApoM (apolipoprotein M), Psmb2 (proteasome subunit beta type-2), Ttr (transthyretin), Kng1 (kininogen-1) and Serpina3k (serine protease inhibitor A3K) were altered by both age and ICH. Indeed, disruption of myelin-related molecules with age has been demonstrated in previous experiments [48]. ApoM binding to sphingosine-1-phosphate has been reported to have inhibitory effects on lymphopoiesis and neuroinflammation [49]. Treatments targeting Ttr and Serpina3k exerted significant

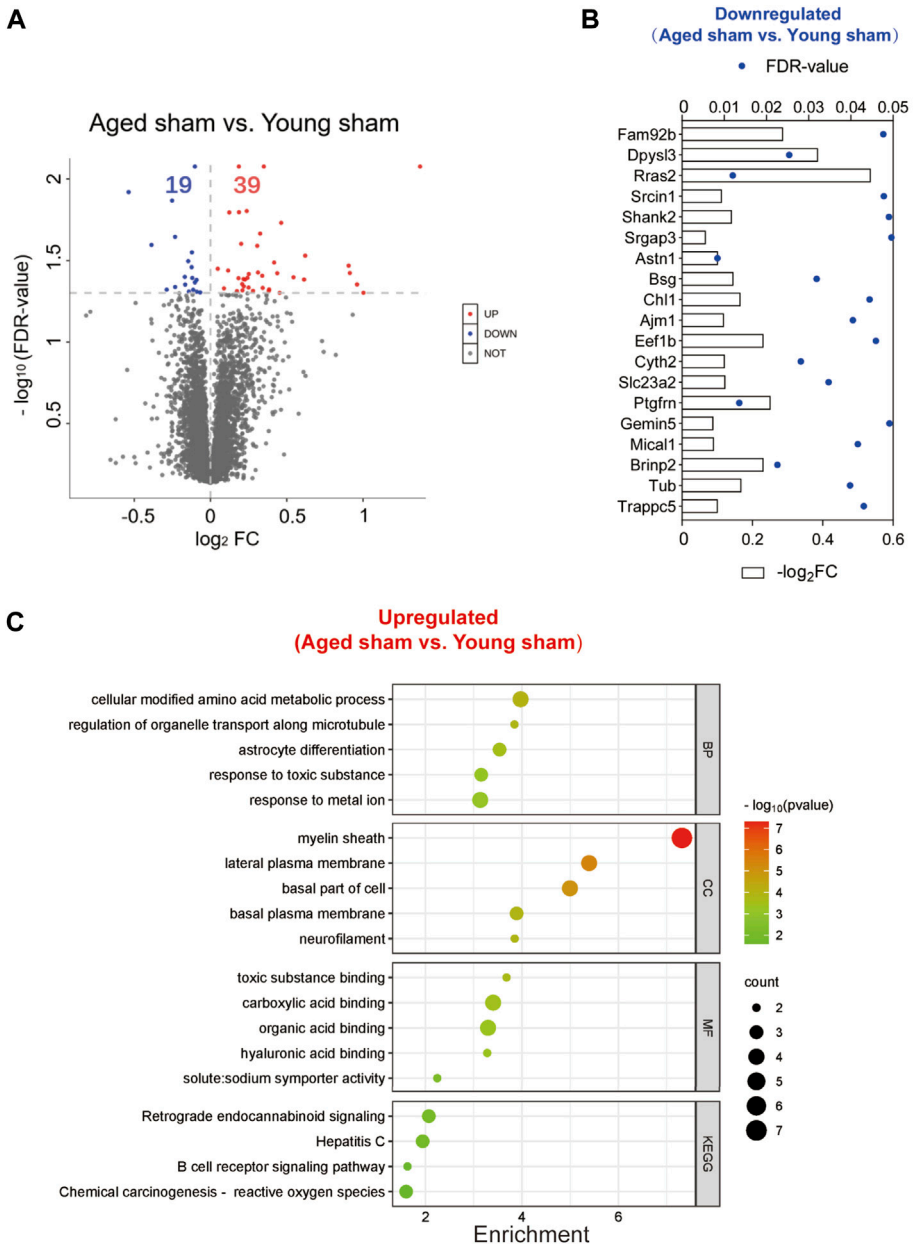

FIGURE 9
Identification of DEPs between the aged and young sham groups and functional enrichment analysis. **(A)** Volcano plot of the 58 DEPs in the aged sham group versus the young sham group. **(B)** Expression of the 19 downregulated DEPs between the two sham groups. **(C)** Top GO terms and KEGG pathways enriched in the 39 upregulated DEPs between the two sham groups.

protective effects against experimental traumatic brain injury [50, 51]. Kng1 is involved in regulating vasodilation and inflammatory responses [52], while Psmb1 functions in the degradation and processing of intracellular proteins [53]. The dysregulation of these two proteins may indicate a pronounced change in the inflammatory response due to age and ICH. Considering these findings together, the higher Serpina3k protein level in younger mice may explain the better long-term prognosis of younger subjects after ICH, and the higher ApoM and Ttr levels in elderly subjects with ICH may be due to a compensatory mechanism for protecting against acute brain injury after ICH.

The inclusion of the two sham groups in this study has further improved our understanding of the impact of aging on the brain. Aging is a complex BP involving changes at multiple levels, including disruptions of cellular metabolism [54]. According to

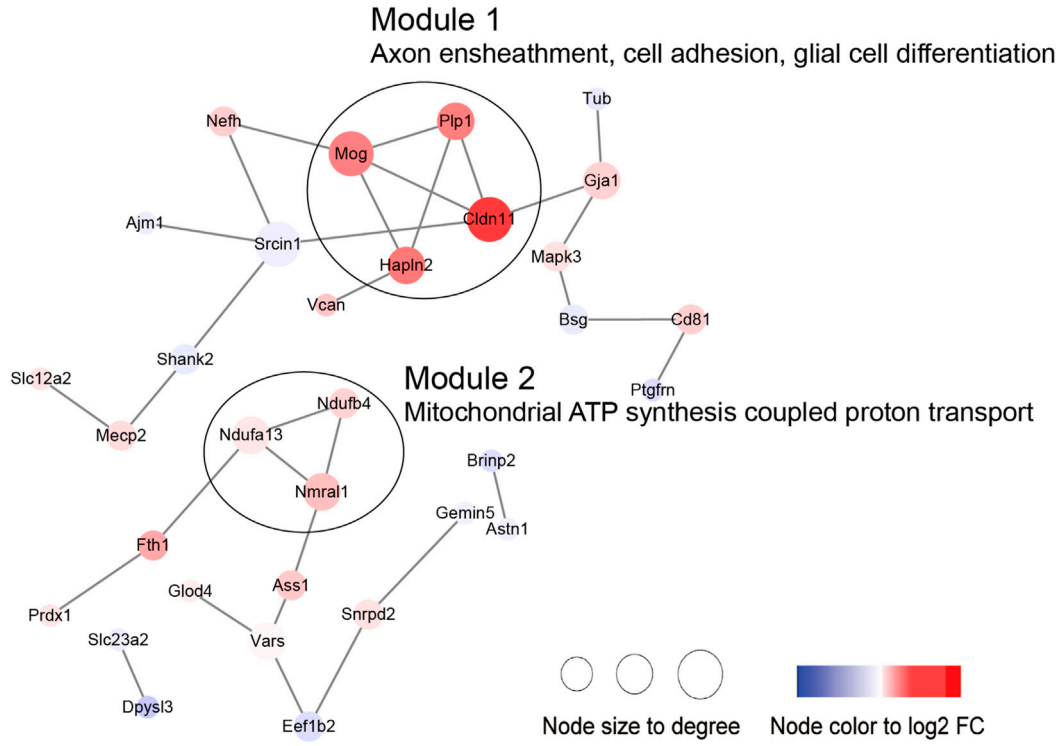

FIGURE 10
PPI network including the DEPs in the aged sham group versus the young sham group.

our results, the dysregulation of modified amino acid metabolism within cells is associated with aging. During the aging process, the metabolic activity and regulatory capacity of cells gradually decline, which can lead to abnormalities in the synthesis, degradation, and conversion of modified amino acids [55]. For instance, research has found that in aging cells, there is an abnormal increase or decrease in processes such as methylation and acetylation, which can result in changes in protein function and aberrant cellular metabolism [56]. Additionally, alterations in the expression of myelin proteins and changes in the regulation of proteins involved in myelination during aging were observed. Myelin plays a crucial role in facilitating efficient nerve signal transmission, and any disturbance of or deterioration in its structure or composition may impact neural communication [57]. A previous study demonstrated that significant alterations occurred in sphingolipid expression patterns associated with myelin remodeling during the aging process [58]. With advancing age, mitochondrial ATP synthesis coupled proton transport was also affected. This could be attributed to changes in the internal structure and function of mitochondria, including mitochondrial DNA damage, membrane instability, and increased oxidative stress [59–61]. These factors may contribute to a decrease in the mitochondrial membrane potential, consequently affecting the efficiency of proton pump function and ATP synthesis.

Taken together, the results of our current study provide information on specific DEPs and their functions in mice of different ages after ICH, contribute to the exploration of the age-specific approach for ICH and provide foundations for future research on the subject.

Author contributions

XL, QL, and PX designed the experiment. XL, ZX, PL, WY, YS, FL, XX, QW, PW, and RD performed the experiments. XL wrote the draft manuscript. QL, PX, and WY revised the manuscript. All authors collected and analyzed the data and approved the submitted version.

Data availability statement

The original contributions presented in the study are included in the article/Supplementary Material, further inquiries can be directed to the corresponding authors. The MS proteomics data have been deposited in the ProteomeXchange Consortium http://proteomecentral.proteomexchange.org via the iProX partner repository with the dataset identifier PXD033791 [62].

Ethics statement

The animal study was approved by the Ethical Committee of Chongqing Medical University (CQMU). The study was conducted in accordance with the local legislation and institutional requirements.

Funding

The author(s) declare financial support was received for the research, authorship, and/or publication of this article. This study was supported by the National Key R&D Program of China (Grant No. 2017YFA0505700), the National Natural Science Foundation of China (No. 82071337), the National Key R&D Program of China (Nos. 2018YFC1312200 and 2018YFC1312203), the Chongqing High-end Young Investigator Project (No. 2019GDRC005), the Science and Technology Innovation Project of "Chengdu Chongqing Economic Circle" (No. KJCXZD2020019), the Excellent Youth Foundation of Chongqing Scientific Committee (cstc2021jcyj-jqX0029), the Non-profit Central Research Institute Fund of Chinese Academy of Medical Sciences (Grant No. 2019PT320002), and the National Administration of Traditional Chinese Medicine: 2019 Project of Building Evidence-Based Practice Capacity for TCM (No. 2019XZZX-NB014).

Acknowledgments

We thank Shanghai NewCore Biotechnology Co., Ltd. (https://www.bioinformatics.com.cn, last accessed on 10 November 2023) for providing data analysis and visualization support.

Conflict of interest

The authors declare that the research was conducted in the absence of any commercial or financial relationships that could be construed as a potential conflict of interest.

Supplementary material

The Supplementary Material for this article can be found online at: https://www.ebm-journal.org/articles/10.3389/ebm.2024.10117/full#supplementary-material

References

1. Cordonnier C, Demchuk A, Ziai W, Anderson CS. Intracerebral haemorrhage: current approaches to acute management. *The Lancet* (2018) **392**(10154):1257–68. doi:10.1016/s0140-6736(18)31878-6

2. Zia E, Engstrom G, Svensson PJ, Norrving B, Pessah-Rasmussen H. Three-year survival and stroke recurrence rates in patients with primary intracerebral hemorrhage. *Stroke* (2009) **40**(11):3567–73. doi:10.1161/strokeaha.109.556324

3. Tatlisumak T, Cucchiara B, Kuroda S, Kasner SE, Putaala J. Nontraumatic intracerebral haemorrhage in young adults. *Nat Rev Neurol* (2018) **14**(4):237–50. doi:10.1038/nrneurol.2018.17

4. Bako AT, Pan A, Potter T, Tannous J, Johnson C, Baig E, et al. Contemporary trends in the nationwide incidence of primary intracerebral hemorrhage. *Stroke* (2022) **53**(3):e70–e74. doi:10.1161/strokeaha.121.037332

5. Koivunen RJ, Satopaa J, Meretoja A, Strbian D, Haapaniemi E, Niemela M, et al. Incidence, risk factors, etiology, severity and short-term outcome of non-traumatic intracerebral hemorrhage in young adults. *Eur J Neurol* (2015) **22**(1):123–32. doi:10.1111/ene.12543

6. Hauer AJ, Kleinloog R, Giuliani F, Rinkel G, de Kort GA, Berkelbach van der Sprenkel JW, et al. RNA-sequencing highlights inflammation and impaired integrity of the vascular wall in brain arteriovenous malformations. *Stroke* (2020) **51**(1):268–74. doi:10.1161/strokeaha.119.025657

7. Li Z, Li Y, Han J, Zhu Z, Li M, Liu Q, et al. Formyl peptide receptor 1 signaling potentiates inflammatory brain injury. *Sci Transl Med* (2021) **13**(605):eabe9890. doi:10.1126/scitranslmed.abe9890

8. Winkler EA, Kim CN, Ross JM, Garcia JH, Gil E, Oh I, et al. A single-cell atlas of the normal and malformed human brain vasculature. *Science* (2022) **375**(6584):eabi7377. doi:10.1126/science.abi7377

9. Yuan JJ, Zhang Q, Gong CX, Wang FX, Huang JC, Yang GQ, et al. Young plasma ameliorates aging-related acute brain injury after intracerebral hemorrhage. *Biosci Rep* (2019) **39**(5):BSR20190537. doi:10.1042/bsr20190537

10. Yuan JJ, Chen Q, Xiong XY, Zhang Q, Xie Q, Huang JC, et al. Quantitative profiling of oxylipins in acute experimental intracerebral hemorrhage. *Front Neurosci* (2020) **14**:777. doi:10.3389/fnins.2020.00777

11. Wasserman JK, Yang H, Schlichter LC. Glial responses, neuron death and lesion resolution after intracerebral hemorrhage in young vs aged rats. *Eur J Neurosci* (2008) **28**(7):1316–28. doi:10.1111/j.1460-9568.2008.06442.x

12. Jiang M, Yu S, Yu Z, Sheng H, Li Y, Liu S, et al. XBP1 (X-Box-Binding protein-1)-dependent O-GlcNAcylation is neuroprotective in ischemic stroke in young mice and its impairment in aged mice is rescued by thiamet-G. *Stroke* (2017) **48**(6):1646–54. doi:10.1161/strokeaha.117.016579

13. Zille M, Farr TD, Keep RF, Romer C, Xi G, Boltze J. Novel targets, treatments, and advanced models for intracerebral haemorrhage. *EBioMedicine* (2022) **76**:103880. doi:10.1016/j.ebiom.2022.103880

14. Magid-Bernstein J, Girard R, Polster S, Srinath A, Romanos S, Awad IA, et al. Cerebral hemorrhage: pathophysiology, treatment, and future directions. *Circ Res* (2022) **130**(8):1204–29. doi:10.1161/circresaha.121.319949

15. Puy L, Perbet R, Figeac M, Duchene B, Deramecourt V, Cordonnier C, et al. Brain peri-hematomal area, a strategic interface for blood clearance: a human neuropathological and transcriptomic study. *Stroke* (2022) **53**(6):2026–35. doi:10.1161/strokeaha.121.037751

16. Li H, Ghorbani S, Zhang R, Ebacher V, Stephenson EL, Keough MB, et al. Prominent elevation of extracellular matrix molecules in intracerebral hemorrhage. *Front Mol Neurosci* (2023) **16**:1251432. doi:10.3389/fnmol.2023.1251432

17. Tang L, Wang L, Jin F, Hao Y, Zhao T, Zheng W, et al. Inflammatory regulation by restraining M2 microglial polarization: neurodestructive effects of Kallikrein-related peptidase 8 activation in intracerebral hemorrhage. *Int Immunopharmacology* (2023) **124**(Pt A):110855. doi:10.1016/j.intimp.2023.110855

18. Zhuang J, Peng Y, Gu C, Chen H, Lin Z, Zhou H, et al. Wogonin accelerates hematoma clearance and improves neurological outcome via the PPAR-gamma pathway after intracerebral hemorrhage. *Transl Stroke Res* (2021) **12**(4):660–75. doi:10.1007/s12975-020-00842-9

19. Bobinger T, Manaenko A, Burkardt P, Beuscher V, Sprügel MI, Roeder SS, et al. Siponimod (BAF-312) attenuates perihemorrhagic edema and improves survival in experimental intracerebral hemorrhage. *Stroke* (2019) **50**(11):3246–54. doi:10.1161/strokeaha.119.027134

20. Yang WS, Shen YQ, Yang X, Li XH, Xu SH, Zhao LB, et al. MicroRNA transcriptomics analysis identifies dysregulated hedgehog signaling pathway in a mouse model of acute intracerebral hemorrhage exposed to hyperglycemia. *J Stroke Cerebrovasc Dis* (2022) **31**(3):106281. doi:10.1016/j.jstrokecerebrovasdis.2021.106281

21. Wiśniewski JR, Zougman A, Nagaraj N, Mann M. Universal sample preparation method for proteome analysis. *Nat Methods* (2009) **6**(5):359–62. doi:10.1038/nmeth.1322

22. Tang D, Chen M, Huang X, Zhang G, Zeng L, Zhang G, et al. SRplot: a free online platform for data visualization and graphing. *PLoS One* (2023) **18**(11): e0294236. doi:10.1371/journal.pone.0294236

23. Yu G, Wang LG, Han Y, He QY. clusterProfiler: an R package for comparing biological themes among gene clusters. *OMICS: A J Integr Biol* (2012) **16**(5):284–7. doi:10.1089/omi.2011.0118

24. Luo W, Brouwer C. Pathview: an R/Bioconductor package for pathway-based data integration and visualization. *Bioinformatics* (2013) **29**(14):1830–1. doi:10.1093/bioinformatics/btt285

25. Jung J, Zeng H, Horng T. Metabolism as a guiding force for immunity. *Nat Cel Biol* (2019) **21**(1):85–93. doi:10.1038/s41556-018-0217-x

26. Van den Bossche J, O'Neill LA, Menon D. Macrophage immunometabolism: where are we (going)? *Trends Immunol* (2017) **38**(6):395–406. doi:10.1016/j.it.2017.03.001

27. Askenase MH, Goods BA, Beatty HE, Steinschneider AF, Velazquez SE, Osherov A, et al. Longitudinal transcriptomics define the stages of myeloid activation in the living human brain after intracerebral hemorrhage. *Sci Immunol* (2021) **6**(56):eabd6279. doi:10.1126/sciimmunol.abd6279

28. Cai R, Zhang Y, Simmering JE, Schultz JL, Li Y, FernandezCarasa I, et al. Enhancing glycolysis attenuates Parkinson's disease progression in models and clinical databases. *J Clin Invest* (2019) **129**(10):4539–49. doi:10.1172/jci129987

29. Qiang Q, Manalo JM, Sun H, Zhang Y, Song A, Wen AQ, et al. Erythrocyte adenosine A2B receptor prevents cognitive and auditory dysfunction by promoting hypoxic and metabolic reprogramming. *PLoS Biol* (2021) **19**(6):e3001239. doi:10.1371/journal.pbio.3001239

30. Durocher M, Ander BP, Jickling G, Hamade F, Hull H, Knepp B, et al. Inflammatory, regulatory, and autophagy co-expression modules and hub genes underlie the peripheral immune response to human intracerebral hemorrhage. *J neuroinflammation* (2019) **16**(1):56. doi:10.1186/s12974-019-1433-4

31. O'Donnell MJ, McQueen M, Sniderman A, Pare G, Wang X, Hankey GJ, et al. Association of lipids, lipoproteins, and apolipoproteins with stroke subtypes in an international Case control study (INTERSTROKE). *J Stroke* (2022) **24**(2):224–35. doi:10.5853/jos.2021.02152

32. Alsamani R, Limin Z, Jianwei W, Dan W, Yuehong S, Ziwei L, et al. Predictive value of the apolipoprotein B/A1 ratio in intracerebral hemorrhage outcomes. *J Clin Lab Anal* (2022) **36**(7):e24562. doi:10.1002/jcla.24562

33. Sulima S, Kampen K, De Keersmaecker K. Cancer biogenesis in ribosomopathies. *Cells* (2019) **8**(3):229. doi:10.3390/cells8030229

34. Stockwell BR, Friedmann Angeli JP, Bayir H, Bush AI, Conrad M, Dixon SJ, et al. Ferroptosis: a regulated cell death nexus linking metabolism, redox biology, and disease. *Cell* (2017) **171**(2):273–85. doi:10.1016/j.cell.2017.09.021

35. Ma Y, Liu Y, Ruan X, Liu X, Zheng J, Teng H, et al. Gene expression signature of traumatic brain injury. *Front Genet* (2021) **12**:646436. doi:10.3389/fgene.2021.646436

36. Ximerakis M, Lipnick SL, Innes BT, Simmons SK, Adiconis X, Dionne D, et al. Single-cell transcriptomic profiling of the aging mouse brain. *Nat Neurosci* (2019) **22**(10):1696–708. doi:10.1038/s41593-019-0491-3

37. Shi K, Tian DC, Li ZG, Ducruet AF, Lawton MT, Shi FD. Global brain inflammation in stroke. *Lancet Neurol* (2019) **18**(11):1058–66. doi:10.1016/s1474-4422(19)30078-x

38. Ramos P, Santos A, Pinto NR, Mendes R, Magalhães T, Almeida A. Iron levels in the human brain: a post-mortem study of anatomical region differences and age-related changes. *J Trace Elem Med Biol* (2014) **28**(1):13–7. doi:10.1016/j.jtemb.2013.08.001

39. Aquino D, Bizzi A, Grisoli M, Garavaglia B, Bruzzone MG, Nardocci N, et al. Age-related iron deposition in the basal ganglia: quantitative analysis in healthy subjects. *Radiology* (2009) **252**(1):165–72. doi:10.1148/radiol.2522081399

40. Farrall AJ, Wardlaw JM. Blood-brain barrier: ageing and microvascular disease--systematic review and meta-analysis. *Neurobiol Aging* (2009) **30**(3):337–52. doi:10.1016/j.neurobiolaging.2007.07.015

41. Leclerc JL, Santiago-Moreno J, Dang A, Lampert AS, Cruz PE, Rosario AM, et al. Increased brain hemopexin levels improve outcomes after intracerebral hemorrhage. *J Cereb Blood Flow Metab* (2018) **38**(6):1032–46. doi:10.1177/0271678x16679170

42. Leclerc JL, Li C, Jean S, Lampert AS, Amador CL, Diller MA, et al. Temporal and age-dependent effects of haptoglobin deletion on intracerebral hemorrhage-induced brain damage and neurobehavioral outcomes. *Exp Neurol* (2019) **317**:22–33. doi:10.1016/j.expneurol.2019.01.011

43. Liu H, Hua Y, Keep RF, Xi G. Brain ceruloplasmin expression after experimental intracerebral hemorrhage and protection against iron-induced brain injury. *Transl Stroke Res* (2019) **10**(1):112–9. doi:10.1007/s12975-018-0669-0

44. Li ZD, Li H, Kang S, Cui YG, Zheng H, Wang P, et al. The divergent effects of astrocyte ceruloplasmin on learning and memory function in young and old mice. *Cell Death Dis* (2022) **13**(11):1006. doi:10.1038/s41419-022-05459-4

45. Bulters D, Gaastra B, Zolnourian A, Alexander S, Ren D, Blackburn SL, et al. Haemoglobin scavenging in intracranial bleeding: biology and clinical implications. *Nat Rev Neurol* (2018) **14**(7):416–32. doi:10.1038/s41582-018-0020-0

46. Cao S, Hua Y, Keep RF, Chaudhary N, Xi G. Minocycline effects on intracerebral hemorrhage-induced iron overload in aged rats: brain iron quantification with magnetic resonance imaging. *Stroke* (2018) **49**(4):995–1002. doi:10.1161/strokeaha.117.019860

47. Bao W, Zhou X, Zhou L, Wang F, Yin X, Lu Y, et al. Targeting miR-124/Ferroportin signaling ameliorated neuronal cell death through inhibiting apoptosis and ferroptosis in aged intracerebral hemorrhage murine model. *Aging cell* (2020) **19**(11):e13235. doi:10.1111/acel.13235

48. Rivera AD, Pieropan F, ChaconDeLaRocha I, Lecca D, Abbracchio MP, Azim K, et al. Functional genomic analyses highlight a shift in Gpr17-regulated cellular processes in oligodendrocyte progenitor cells and underlying myelin dysregulation in the aged mouse cerebrum. *Aging Cell* (2021) **20**(4):e13335. doi:10.1111/acel.13335

49. Blaho VA, Galvani S, Engelbrecht E, Liu C, Swendeman SL, Kono M, et al. HDL-bound sphingosine-1-phosphate restrains lymphopoiesis and neuroinflammation. *Nature* (2015) **523**(7560):342–6. doi:10.1038/nature14462

50. Zhang Z, Yu J, Wang P, Lin L, Liu R, Zeng R, et al. iTRAQ-based proteomic profiling reveals protein alterations after traumatic brain injury and supports thyroxine as a potential treatment. *Mol Brain* (2021) **14**(1):25. doi:10.1186/s13041-021-00739-0

51. Jing Y, Yang D, Fu Y, Wang W, Yang G, Yuan F, et al. Neuroprotective effects of Serpina3k in traumatic brain injury. *Front Neurol* (2019) **10**:1215. doi:10.3389/fneur.2019.01215

52. Markaki I, Bergstrom S, Tsitsi P, Remnestal J, Manberg A, Hertz E, et al. Cerebrospinal fluid levels of kininogen-1 indicate early cognitive impairment in Parkinson's disease. *Mov Disord* (2020) **35**(11):2101–6. doi:10.1002/mds.28192

53. Mirzaei M, Pushpitha K, Deng L, Chitranshi N, Gupta V, Rajput R, et al. Upregulation of proteolytic pathways and altered protein biosynthesis underlie retinal pathology in a mouse model of Alzheimer's disease. *Mol Neurobiol* (2019) **56**(9):6017–34. doi:10.1007/s12035-019-1479-4

54. Lopez-Otin C, Blasco MA, Partridge L, Serrano M, Kroemer G. Hallmarks of aging: an expanding universe. *Cell* (2023) **186**(2):243–78. doi:10.1016/j.cell.2022.11.001

55. Mattson MP, Arumugam TV. Hallmarks of brain aging: adaptive and pathological modification by metabolic States. *Cel Metab* (2018) **27**(6):1176–99. doi:10.1016/j.cmet.2018.05.011

56. Li Z, Rasmussen LJ. TIP60 in aging and neurodegeneration. *Ageing Res Rev* (2020) **64**:101195. doi:10.1016/j.arr.2020.101195

57. Kato D, Aoyama Y, Nishida K, Takahashi Y, Sakamoto T, Takeda I, et al. Regulation of lipid synthesis in myelin modulates neural activity and is required for motor learning. *Glia* (2023) **71**(11):2591–608. doi:10.1002/glia.24441

58. Ding J, Ji J, Rabow Z, Shen T, Folz J, Brydges CR, et al. A metabolome atlas of the aging mouse brain. *Nat Commun* (2021) **12**(1):6021. doi:10.1038/s41467-021-26310-y

59. Wilkins HM, Swerdlow RH. Mitochondrial links between brain aging and Alzheimer's disease. *Transl Neurodegener* (2021) **10**(1):33. doi:10.1186/s40035-021-00261-2

60. Lautrup S, Sinclair DA, Mattson MP, Fang EF. NAD (+) in brain aging and neurodegenerative disorders. *Cel Metab* (2019) **30**(4):630–55. doi:10.1016/j.cmet.2019.09.001

61. Sakamuri SS, Sure VN, Kolli L, Evans WR, Sperling JA, Bix GJ, et al. Aging related impairment of brain microvascular bioenergetics involves oxidative phosphorylation and glycolytic pathways. *J Cereb Blood Flow Metab* (2022) **42**(8):1410–24. doi:10.1177/0271678x211069266

62. Ma J, Chen T, Wu S, Yang C, Bai M, Shu K, et al. iProX: an integrated proteome resource. *Nucleic Acids Res* (2019) **47**(D1):D1211–D1217. doi:10.1093/nar/gky869

EBM Experimental Biology and Medicine

TYPE Review
PUBLISHED 28 February 2024
DOI 10.3389/ebm.2024.10120

OPEN ACCESS

*CORRESPONDENCE
Brian D. Adams,
brian.adams@braininstituteamerica.com

†These authors have contributed equally to this work

RECEIVED 04 September 2023
ACCEPTED 15 February 2024
PUBLISHED 28 February 2024

CITATION
Chen Y, Mateski J, Gerace L, Wheeler J, Burl J, Prakash B, Svedin C, Amrick R and Adams BD (2024), Non-coding RNAs and neuroinflammation: implications for neurological disorders.
Exp. Biol. Med. 249:10120.
doi: 10.3389/ebm.2024.10120

Non-coding RNAs and neuroinflammation: implications for neurological disorders

Yvonne Chen[1,2†], Julia Mateski[2,3†], Linda Gerace[2,4†], Jonathan Wheeler[2,5], Jan Burl[2,6], Bhavna Prakash[2,7], Cherie Svedin[2,8], Rebecca Amrick[2,9] and Brian D. Adams[2*†]

[1]Department of Biology, Brandeis University, Waltham, MA, United States, [2]Department of RNA Sciences, The Brain Institute of America, New Haven, CT, United States, [3]Department of Biological Sciences, Gustavus Adolphus College, St. Peter, MN, United States, [4]Department of English, Missouri State University, Springfield, MO, United States, [5]Department of Electrical and Computer Engineering Tech, New York Institute of Tech, Old Westbury, NY, United States, [6]Department of English, Southern New Hampshire University, Manchester, NH, United States, [7]Department of Medicine, Tufts Medical Center, Medford, MA, United States, [8]Department of Biology, Utah Tech University, St. George, UT, United States, [9]Department of English, Villanova University, Villanova, PA, United States

Abstract

Neuroinflammation is considered a balanced inflammatory response important in the intrinsic repair process after injury or infection. Under chronic states of disease, injury, or infection, persistent neuroinflammation results in a heightened presence of cytokines, chemokines, and reactive oxygen species that result in tissue damage. In the CNS, the surrounding microglia normally contain macrophages and other innate immune cells that perform active immune surveillance. The resulting cytokines produced by these macrophages affect the growth, development, and responsiveness of the microglia present in both white and gray matter regions of the CNS. Controlling the levels of these cytokines ultimately improves neurocognitive function and results in the repair of lesions associated with neurologic disease. MicroRNAs (miRNAs) are master regulators of the genome and subsequently control the activity of inflammatory responses crucial in sustaining a robust and acute immunological response towards an acute infection while dampening pathways that result in heightened levels of cytokines and chemokines associated with chronic neuroinflammation. Numerous reports have directly implicated miRNAs in controlling the abundance and activity of interleukins, TGF-B, NF-kB, and toll-like receptor-signaling intrinsically linked with the development of neurological disorders such as Parkinson's, ALS, epilepsy, Alzheimer's, and neuromuscular degeneration. This review is focused on discussing the role miRNAs play in regulating or initiating these chronic neurological states, many of which maintain the level and/or activity of neuron-specific secondary messengers. Dysregulated miRNAs present in the microglia, astrocytes, oligodendrocytes, and epididymal cells, contribute to an overall glial-specific inflammatory niche that impacts the activity of neuronal conductivity, signaling action potentials, neurotransmitter robustness, neuron-neuron specific communication, and neuron-muscular connections. Understanding which miRNAs regulate microglial activation is a crucial step

forward in developing non-coding RNA-based therapeutics to treat and potentially correct the behavioral and cognitive deficits typically found in patients suffering from chronic neuroinflammation.

KEYWORDS

miRNA, ncRNA, cancer, Alzheimer, epilepsy, Huntington, neuroinflammation, neurology

Impact statement

miRNAs regulate cell-signaling regulatory networks at the post-transcriptional level, resulting in controlled cellular development responsive to extracellular stimuli. miRNAs also control the expression of genetic outputs during neuronal development. This neuronal cellular process is tightly regulated and tuned by acute and/or chronic inflammatory cues that, when disrupted, result in the onset of various neurological disorders. This review is an attempt to highlight miRNAs that modulate the neuroinflammatory state within the central nervous system and to elucidate the underlying mechanisms that promote or abrogate excessive inflammatory signaling as these biomolecules may become new therapeutic targets in the treatment of chronic neurological disorders such as epilepsy, ALS, Parkinson's, Alzheimer's, and Huntington's.

Introduction

Non-coding RNAs (ncRNAs) have emerged as crucial regulators in a multitude of biological processes, challenging the long-held view that RNA primarily functions as static templates of information utilized for ribosomal-mediated protein synthesis [1]. Over the past two decades, significant research has begun to unravel the seemingly mysterious yet crucial functions of ncRNAs which range from controlling developmental timing [2], hormone regulation [3], chromosomal inactivation [4], and the maintenance of normal cellular circuitry that restrains the onset of chronic disease [5]. The continued efforts by numerous scientific investigators have resulted in the development of ncRNA-based therapeutics for the treatment of those with HCV, hypercholesterolaemia, DMD, macular degeneration, neuromyelitis, myasthenia, as well as those with metastatic cancers [6].

In the mid-to-late 1990s researchers uncovered the complex mechanisms of small antisense RNA and how these ncRNAs could initiate gene suppression through Watson-Crick base pairing, in what is now termed RNAi (RNA inactivation) [7–11]. Continued elucidation of these RNAi pathways in the early 2000s indicated that ncRNAs specifically regulate the transcriptional abundance of mRNA and prevent the translation of an mRNA transcript into protein [12–15]. At this time, additional classes of ncRNAs were also becoming further characterized, such as tRNA, rRNA, snoRNA, snRNA, scaRNA, miRNA, lncRNA, and circRNA [16]. Advanced high-throughput sequencing technology identified the elevated abundance of certain ncRNAs in mammalian cells, and bioinformatic analysis further indicated the prevalence of sequence conservation from mammalian species to a wide variety of both invertebrate and vertebrate species [17–22]. The inferred importance of this ncRNA sequence conservation meant that seemingly complex cellular pathways in the mammalian system could instead be studied in genetically well-defined species such as *D. melanogaster* and *C. elegans* [23–26]. The identified ncRNA genetic targets could then be elucidated in mammalian cell cultures and further exploited for therapeutic purposes. For instance, miR-34 controls the abundance of *TP53* in *C. elegans*, and subsequent efforts confirmed that while miR-34a regulates *TP53* in human cell lines, miR-34a is also a crucial regulator of a host of genes that coordinately regulate the DNA repair response pathway [27–31]. Studies have now indicated thousands of conserved ncRNAs in every known vertebrate system, and revealed that ncRNAs are crucial in regulating several biological processes, including cellular proliferation, DNA editing, DNA modification, and cellular differentiation [32–39]. Taken together, this is compelling evidence that ncRNA molecules play critical roles in the control and maintenance of normal cellular and physiological processes.

ncRNA regulatory potential

While ncRNAs have been implicated in regulating gene function within the cytoplasm due to the interaction of ncRNAs with ER-bound ribosomal polysomes, ncRNAs can also regulate RNA processing and translation, gene transcription, and cellular metabolic activity, indicating ncRNAs are functionally present in organelles such as the nucleus, ER, and mitochondria [40–44]. In one such example, Kim et al. explored the role of ncRNAs in the mitochondria and found *lncND5* interacts with MRPP1 and controls mitochondrial gene expression [45]. Additionally, *RMRP* interacts with PNPASE and GRSF1, which regulates mitochondrial RNA processing, mtDNA replication, and ultimately mitochondrial-mediated oxidative phosphorylation capacity. These findings have significant consequences in relation to the development of therapies for metabolic disorders, such as cancer. For instance,

investigators demonstrated that cytosolic lncRNAs and miRNAs are essential for controlling the expression of glucose transporters GLUT1-3 as well as glycolytic enzymes via HK2, which results in dysregulated glucose uptake in response to insulin and limits the conversion of glucose to glucose 6-phosphate thereby reducing the overall metabolic activity of mammalian cells [46, 47]. Xu et al. also found that lncMMPA alters the levels of ALDH1A3, affecting the rate of aerobic glycolysis in HCC, yet promotes M2 macrophage polarization [47]. Some of these metabolically linked-ncRNAs are also functionally active in the nucleus, and interact with DNA regulatory machinery to control cellular proliferation in response to glucose stimulation [48, 49]. In fact nuclear RNAi, and nuclear miRNA/lncRNA molecules have a crucial role in regulating the abundance of nascent mRNA transcripts post-transcription, and modulate co-transcriptional alternative splicing activity [50, 51]. Together, these findings indicate that in response to an environmental stimuli, ncRNAs function within every cellular compartment to regulate essential cellular processes associated with the transcription and translation of genetic information, chromatin remodeling [52], RNA processing, and DNA damage repair [53], which in turn, affects the maturation and function of mammalian cells.

Given the ever increasing complexity of RNA terminology, the RNA community recognized miRNAs, lncRNA, and circRNA as ncRNAs that function as endogenous genetic regulators of mRNA abundance as well as controlling the expression and activity of all other ncRNAs (i.e., tRNA, rRNA, snRNA). While a majority of this review will focus on miRNA biology as a leading ncRNA therapeutic approach, it should be appreciated that lncRNAs were one of the original ncRNAs identified to have the capacity to silence genetic information [54–57]. X-chromosome inactivation (XCI) mediated by *XIST* is an example of how a lncRNA can control an unbalanced dosage of genetic information within the developing female embryo [58]. Furthermore, since lncRNAs are found in low abundance it is thought lncRNAs mostly act "*in cis*" or near their respective sites of transcription and subsequently co-transcriptionally regulate the expression of neighboring genes. The ENCODE project has identified over 10,000 lncRNAs, many of which are differentially expressed between normal and cancerous cells [59]. Over the past decade, lncRNAs have been found to interact with chromatin, modulate gene expression, function as protein decoys, and govern cellular physiology [60]. The crucial role of lncRNA in eukaryotic cell biology and in normal cellular function indicate these ncRNAs may also be novel targets for therapeutic intervention. However, because the mechanisms of biogenesis and mRNA silencing by miRNAs are more well-established, this review primarily focuses on the utilization of miRNA in the identification and treatment of neurocognitive disorders that currently have little to no curative options.

miRNA biogenesis and function

miRNAs are small ncRNAs that modulate gene expression by binding to complementary sequences predominantly within the 3′UTR of target mRNAs [61, 62]. Similar to siRNA technology, the mechanism of action(s) linked to miRNAs indicates that miRNA/RNAi-based therapies could be used to silence, and in some cases repair, any misregulated genetic element within the human genome to correct a specific pathological deficit. miRNAs are, however, distinct from siRNAs in that they are endogenously expressed in the genome and transcribed in the nucleus by RNA polymerase II/III [63–65] (see Figure 1). The resulting primary miRNA (pri-miRNA) transcript is unique in that the pri-miRNA folds creating hairpin bulges similar to tRNA, which is recognized by the RNaseIII enzyme DROSHA [69–71]. Pri-miRNAs can originate from large intergenic regions of the genome, (i.e., areas with little protein coding activity), as well as from intronic regions, (i.e., from sequences processed and spliced out of newly transcribed mature mRNAs), and sometimes are polycistronic and contain multiple mature miRNA sequences [72]. Recently, a non-canonical pathway was identified that further categorized a subset of intronic miRNAs known as "miRtrons" (see Figure 1). These miRNA sequences mapped precisely to short hairpin introns and spanned each of the exon-intron junction borders [67, 73], meaning that when the spliceosome recognizes these junctions, a miRNA will be concomitantly produced with the exonic mature mRNA. Ultimately these findings indicate that an intronic sequence is no longer considered "junk DNA" and in some cases an entire intron codes for a miRNA that has significant downstream regulatory potential.

Canonical pri-miRNAs, as well as miRtrons, both contain sequential hairpin bulges, a terminal loop, are ~85 nucleotides in length, and recognizable by the microprocessor complex containing DROSHA and cofactor DGCR8 (see Figure 1). In *D. melanogaster*, DGCR8 is called Pasha, yet performs similar functions [74–76]. The Drosha-DGCR8 heterodimer recognizes approximately one to two helical RNA turns of sequence from the pri-miRNA stem and splits the phosphodiester bond, releasing a short hairpin-shaped RNA ~60 nucleotides in length [66]. These canonical pre-miRNAs and the pre-miRNAs generated from the miRtron pathway are exported to the cytoplasm via Exportin-5, and undergo further processing by the RNAse-III enzyme, Dicer [68, 77, 78]. Dicer cleaves the double-stranded pre-miRNA approximately two helical turns from the terminal loop [79], generating short double-stranded RNA fragments ~22 nt in length known as the mature miRNA duplex. This duplex contains a guide and a star strand offset on the 5′ ends, allowing for strand selection to occur via Argonaute and the RNA-induced silencing complex (RISC) [80–82].

The focus on the miRNA biogenesis pathway is an important area of research, as many second and third generation siRNA therapeutics utilize the miRNA biogenesis pathway to induce a particular outcome of gene repression, activation, or editing [83–85]. Duplexed siRNAs will also undergo strand selection, and can be

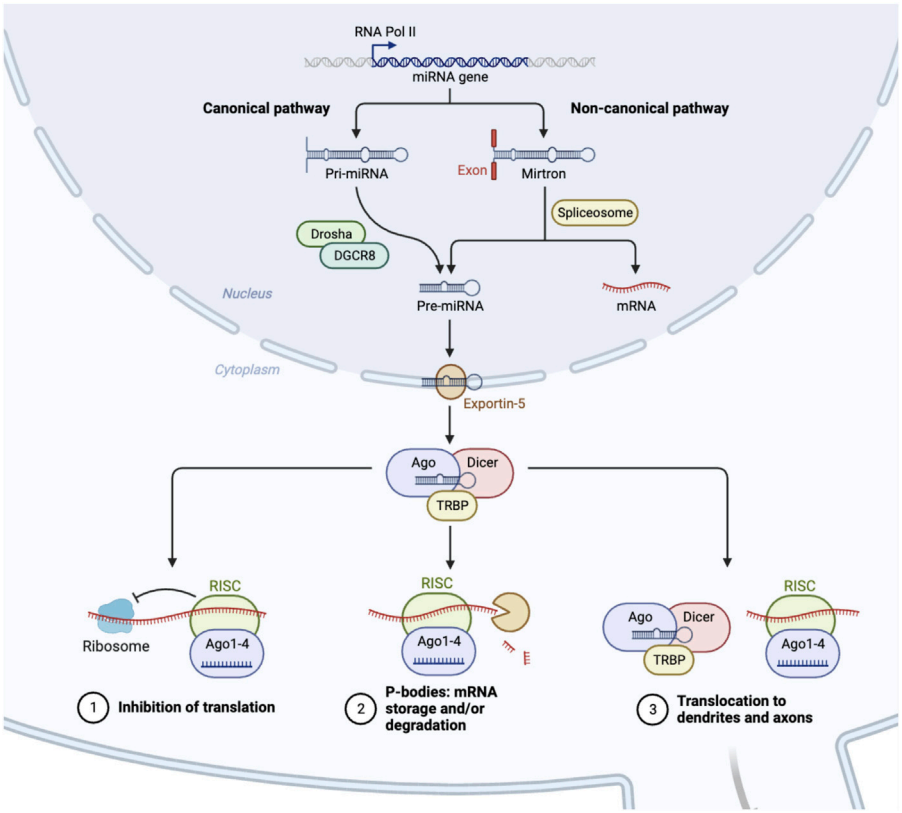

FIGURE 1
Biogenesis of microRNAs. In the nucleus, RNA polymerase II initiates the transcription of microRNAs (miRNA) [61]. As a result, this mono/polycistronic pri-miRNA serves as a substrate for enzymatic cleavage by Drosha/DCGR8, which is then exported from the nucleus as pre-miRNA [66]. A separate, non-canonical pathway involves the spliceosome, which cleaves intronic containing pre-miRNAs, and bypasses the Drosha/DCGR8 complex [67]. Pre-miRNA is further processed into a mature miRNA in the cytoplasm by the DICER enzyme [68]. This miRNA duplex subsequently binds with the protein AGO2 to form the RISC complex, which initiates mRNA degradation at specific locations of mRNA transcripts, stalls polysome machinery preventing translation, or transports miRNAs to various subcellular regions [68].

engineered with sequence bias to favor a particular guide siRNA. Both the guide miRNA or synthetic siRNA is incorporated into RISC which contains, AGO/TRBP and binds to complementary mRNAs within the 3′ UTR resulting in stalling of polysomal translational machinery, the degradation of the mRNA through slicing activity of AGO2, the storage or degradation of mRNA in P-bodies, or the transport of mRNA to exosomes or other cellular regions, such as dendrites (see Figure 1) [86–89].

While much attention has been given to the role of miRNAs in posttranscriptional gene silencing, recent studies have highlighted the broader functions of miRNAs in regulating nuclear chromatin dynamics. Catalanotto et al. highlight the nuclear function(s) of miRNAs, including their involvement in transcriptional regulation and their ability to recognize gene targets at the promoter level [90]. Politz et al. investigated the presence and localization of miRNAs within the nucleolus, and observed that certain nucleolar miRNAs contribute to ribosome biosynthesis and associate with the granular component, where ribosome assembly occurs [91]. Interestingly, in Alzheimer's patients, reduction in nucleolar size is notable, concomitant with reduced rRNA transcription [92]. In Parkinson's, nucleolar integrity is maintained by α-synuclein co-localization with nucleolin, which is regulated by the presence of miR-7 and miRNA-153 [93, 94]. Therefore, miRNAs may regulate the pathophysiology of many neurological disorders, absent of the canonical gene repression mechanisms mentioned above. In fact a number of synthetic RNAi-based therapies have utilized this approach to generate oligonucleotide based therapies such as AMT-130, and VY-HTT01 to correct the HTT gene defect in individuals with Huntington's [95], as well as antisense mediated regulation of ATXN and CAG repeats in individuals with spinocerebellar ataxia [96].

miRNAs and neuroinflammation

Neuroinflammation is a complex homeostatic process that is essential in mitigating exogenous pathogens from entering the

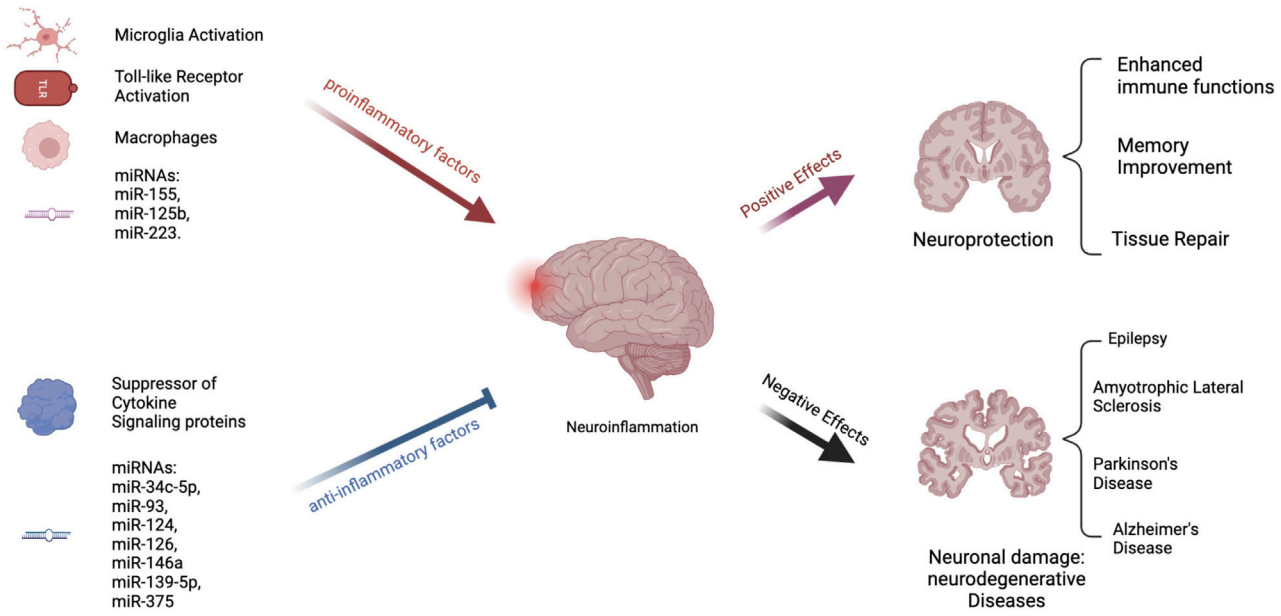

FIGURE 2
Process of Neuroinflammation. Several pathways exist that can either stimulate or decrease neuroinflammation. Inflammation is encouraged by proinflammatory substances. These include the toll-like receptors, macrophages, and microglial activation [108]. Both animal and *in vitro* studies have suggested that some microRNAs, such as miR-155, miR-125b, and miR-223, are proinflammatory [101, 110, 111]. On the other hand, suppressors of cytokine signaling proteins are anti-inflammatory [110]. Inflammation is also reduced by many miRNAs, including miR-34c-5p, miR-93, miR-124, and others [112–116]. Chronic neuroinflammation has been linked to the development of neurodegenerative illnesses such as epilepsy, Amyotrophic Lateral Sclerosis (ASL), Parkinson's Disease (PD), and Alzheimer's Disease (AD) [108, 117–121].

central nervous system (CNS) [97]. Normally, pro-inflammatory responses allow for the acute recruitment of macrophages, natural killer cells, and T-cells to attack these pathogens in a robust manner [98]. Once the pathogen is removed, inflammatory cytokine signaling decreases, and the presence of inflammatory cells diminishes. A key factor in the inflammatory process is the activation of microglia, which safeguards the brain from neuronal damage through the release of neuroprotective cytokines and other inflammatory factors [99–101]. Chronic neuroinflammation is the continued presence of inflammatory cytokine signaling absent of a pathogen, which results in a persistent stress response within the microglia of the CNS, causing disruptions in normal neuronal communication, damage to the neuronal circuitry, and neurodegeneration [102]. The etiology of various neurodegenerative diseases such as Alzheimer's, Parkinson's, amyotrophic lateral sclerosis (ALS), and certain forms of epilepsy, are all thought to involve a neuro-inflammatory component.

Recently, the heterogeneic classification of the microglia into M0, M1, M2a, M2b, and M2c cell types indicate that specific microglial cells are responsible for initiating differential cellular responses during neuronal perturbations [103]. For instance, M2 cells tend to secrete anti-inflammatory cytokines and neurotrophic factors, as well as support oligodendrogenesis and remyelination [104]. By contrast, M1 cells respond to bacterial byproducts such as LPS and IFN-γ, causing a release of TNF-α and IL-6 inducing oxidative stress and neuronal dysfunction [105]. Given the genetic basis for classifying microglial cell types has been established, researchers can now elucidate how M1 cells remain activated post infection, or how M2 cells are prevented from secreting anti-inflammatory cytokines that promote neurogenesis. One of these regulatory processes involves ncRNA, since miRNA activity and expression are repeatedly involved in cell-fate decisions during cellular differentiation [106–108]. Elucidating the mechanisms of M0 to M1 or M2 cell type transition would be an important area of study so as to further develop candidate therapeutics to delay or abate the progression of neurodegenerative disease.

Independent of the bifurcation of microglial cell-fate, miRNAs also play a significant role in the activation or suppression of neuroinflammation by controlling the abundance of central mediators of NLRP3 priming and/or activation of the inflammasome [109] (see Figure 2). For instance, miR-155 regulates the activity of NF-kB, a major protein complex that controls DNA transcription and cytokine production, supports maturation of dendritic cells, promotes recruitment of neutrophils, stimulates M1 polarization of macrophage and microglial cells, and activates T- and B-cells [122]. Interestingly, the miR-155 host

gene is found within the *BIC* gene cluster, a region that contains transcription factor binding sites for NF-kB, SMAD4, and other interferon regulatory factors [123, 124]. As expected, miR-155 is expressed in a coordinated feedback loop with a series of transcription factors that contain miRNA bindings sites for miR-155 [125]. This regulatory loop ensures robust gene expression of pro-inflammatory cytokines is rapidly expressed during an acute infection, while simultaneously activating a regulatory fail safe to dampen unabated inflammatory signaling. Guil et al. identified a similar feedback mechanism in which RNA-binding protein hnRNP A1 modulates the processing of miR-18a [126]. Specifically, hnRNP A1 binds exclusively to pri-miR-18a, facilitating DROSHA processing, in turn promoting a rapid depletion of hnRNP A1 which results in diminished miR-18a processing and reduced pre-miR-18a levels.

Since these initial discoveries, hundreds of miRNAs have been identified to either stimulate or abrogate anti-inflammatory responses (see Figure 2) [127]. For instance, miR-223, is highly expressed in the hematopoietic system and regulates granulopoiesis, a process essential in differentiating bone-marrow derived myeloblasts so as to re-generate the depleted neutrophil reservoir during and after an acute infection [128]. However, miR-223 keeps neutrophils and monocytes in an inactive state, absent of inflammatory stimuli. Another anti-inflammatory miRNA, miR-124, controls the levels of TNF-a in the microglia, dampens the abundance of reactive oxygen species, and promotes M2 type polarization [129, 130]. Identifying these anti-inflammatory miRNAs is the first step in the process of developing oligonucleotide based therapeutics to maintain the activity of healthy microglia and promote neuronal differentiation. In support of this approach, imbalances in miRNA levels, such as miR-155, miR-18a, and miR-124 results in heightened inflammation *in vivo*. In zebrafish, levels of miR-18a spike one to 5 days post retinal injury [131]. In miR-18a^{mi502} altered animals, photoreceptor regeneration was delayed, and was fully restored once the continued presence of active inflammation was abated by dexamethasone treatment. In mice, the loss of miR-223 results in a protective phenotype using a MOG induced EAE model [101, 132] These mice exhibit decreased spinal cord inflammation and reduced demyelination. This seems counterintuitive, yet using a stable miR-223 knockout model, developmentally, these mice most likely have a depleted neutrophil reservoir. Reducing the concentration of miR-223 also results in the decline of inflammatory responses and the presence of increased autophagy within the microglia. miR-155 has been extensively studied using a variety of knockout and overexpression models. In mice it is clear that miR-155 modulates the polarization of the microglia and can promote neuroinflammation by inhibiting inflammasome signaling mediators such as SIRT1 and SOCS1, and by promoting IL-6 production [110, 133]. Specifically, in APPtg and 3xTg Alzheimer mouse models, the persistently elevated levels of miR-155 was associated with the proliferation of dendritic cells, as well as T regulatory cells that support neuroinflammation.

While proper miRNA production leads to healthy cell function, regulation of gene expression, and maintenance of normal intracellular pathways, the disruption of miRNA biogenesis can also contribute to a variety of illnesses (see Figure 2). Tang et al., identified miR-709 as a nuclear miRNA involved in the regulation of miR-15/16 biogenesis [134]. Specifically, miR-709 binds to pri-miR-15a/16-1, ~0.8 kB away from the pre-miRNA hairpin bulge, and recruits chromatin remodeling complexes that prevents the processing of pri-miR-15a/16-1 by DROSHSA. Interestingly, both miR-15/16 and miR-709 have important roles in controlling neuroinflammation *in vivo*. miR-709 controls glutamatergic signaling and endosomal trafficking in cortical neurons, resulting in balanced sleep-wake cycles [135]. The deletion of mir-15/16 in T-regulatory cells results in animals with extensive lymphoproliferative disease and systemic tissue inflammation [136]. Some of the phenotypes could be linked to the abundance and activity of Toll-like receptors (TLRs), which are expressed in dendritic cells, and macrophages, as well as epithelial cells. TLRs are the first line of defense against pathogens by recognizing pathogen-associated molecular patterns (PAMPs) [137]. When activated, TLRs trigger signaling pathways that involve various molecules and transcription factors, leading to the release of inflammatory cytokines. In the central nervous system, TLRs are present mainly in microglia and astroglial cells, but also in some neurons and other glial cells. While TLR activation is a defense mechanism against invaders and tissue damage, excessive activation can disrupt the balance of immune responses, resulting in the production of persistent pro-inflammatory molecules [138]. This can lead to neuroinflammation and damage in the nervous system, contributing to various neurodegenerative diseases. miR-15a, has been shown to target TLR4-associated pathways in bone marrow derived macrophages affecting the mortality of mice using a model of sepsis [139] (see Figure 2). Furthermore, miR-155 activity is induced by TLR signaling, while miR-146a was reported to control cytokine and TLR signaling through a negative feedback regulatory loop with IRAK1 and TRAF6 [140, 141]. Taken together, these studies indicate, miRNAs can intersect with TLR signaling and modulate the process of an inflammatory response. Specifically, when TLR4 is activated by substances that are harmful to the nervous system, such as LPS, a pattern of expression that includes numerous miRNA clusters, such as miR-15, miR-182, and miR-200, result in a coordinated effort to stimulate acute inflammatory response to remove the pathogen. However, dysregulated miRNA signaling can result in persistent inflammatory cues that promote a diseased physiological state by promoting neuroinflammation. Here we discuss relevant neurological disorders that are the result of mis-regulated miRNA expression and activity, which could serve as the basis

for therapeutic intervention using oligonucleotide therapeutics to abate or slow the onset of these diseases.

miRNAs and epilepsy

Epilepsy is a group of disorders characterized by recurrent seizures [142], and is one of the most common neurological conditions that affects at least 50 million people worldwide [143, 144]. Epilepsy follows a bimodal age distribution pattern, meaning that infants and elderly are at the highest risk, with the highest incidence rate being in individuals over 70 years of age [145]. Onset rates in young children have decreased with an increase in perinatal care and sanitation, leading to a decrease in infectious disease. However, epilepsy rates in the elderly have increased due to increased life expectancy, resulting in higher rates of other neurological disorders and cancers that may contribute to the etiology of epilepsy [146]. The International League Against Epilepsy (ILAE) defines the disorder as a patient having 1) two seizures, separated by more than 24 h, occurring without a clear cause, 2) one seizure without a clear cause, and the chance of having more seizures in the next 10 years being over 60%, or 3) diagnosis of an epilepsy syndrome [147]. Although the definition of epilepsy suggests that it is a single disorder, it is more accurate to describe epilepsy as a group of disorders with diverse etiologies and outcomes. Different epilepsy syndromes are characterized by seizure type(s), age of onset, developmental status, comorbid features, and etiology [142]. The ILAE has defined six etiologic categories; Structural, Genetic, Infectious, Metabolic, Immune, and Unknown [148]. Understating the exact genetic underpinnings that manifest these specific etiologies is crucial in understanding how to better treat individuals with epileptic syndromes.

Genetic etiology

The genetic etiology of epilepsy is still controversial [149]. The underlying pathogenesis involved in epilepsy include ion channel dysfunction, synaptic remodeling, gliosis, and neuronal death [117, 144]. Genetics influence ~70% of epilepsy cases, while acquired and environmental factors, such as traumatic injury and infections of the brain account for the remainder of cases. Genetic evidence for epilepsy onset arises from familial studies that have identified rare genetic variants in genes coding for solute carrier channels, ligand-gated channels, GABAergic receptors, and DNA repair genes [142, 150, 151]. For instance, mutations in GABRA1 at 5q34-q35, as well as single nucleotide polymorphisms in BRD2 are more prevalent in individuals with juvenile myoclonic epilepsy when compared to healthy individuals. Another example involves DEPDC5-related epilepsy, in which frameshift mutations in DEPDC5 result in improper complex formation with the GATOR1 complex, a negative regulator of mTORC1. The resulting dysregulation in mTORC1 signaling results in the phenotypes associated with family-related focal epilepsy [152].

As these genetic players are further identified through GWAS and genetic linkage studies, the role of miRNA as pleiotropic regulators of epilepsy becomes increasingly obvious. Firstly, there is evidence that epilepsy is a heterogeneous entity, meaning that multiple alleles may be causing the disease rather than a single variant [142]. Secondly, DEPDC5, mTORC1, and GABRA1 are all direct targets of various miRNAs (see Table 1), and the resultant aberrant expression of these genes due to post translational regulation by miRNAs may explain why mutational linkage studies have under reported the prevalence of certain epileptic subtypes. Further evidence supporting this notion is the finding that miR-106b, miR-146a, and miR-301a are highly detectable in the serum from epileptic patients, and miR-181a regulation of GABRA1 results in attenuated viscero-motor response in the spinal cord of rats [158]. Further mechanistic study is required to elucidate the contribution of each miRNA to the genetic candidates implicated by genetic linkage mapping. This will be a painstaking process, yet will result in the development of valid miRNA-based epileptic therapies.

Immune etiology

Neuroinflammation is another significant contributor to the pathogenesis of epilepsy, particularly temporal lobe epilepsy, which is the most common cause of partial seizures and the primary source of refractory seizures [117–119]. Stimulation of pro-inflammatory molecules such as IL-1β, IL-6, TNF-α, and TLRs induces neurological modifications that result in impaired integrity of the blood brain barrier, neuronal loss, and hyper-excitotoxicity. Such pathological events transform the normal brain into an epileptic state, with an imbalanced functioning of excitatory and inhibitory neurons (see Figure 2). Systemic presence of proinflammatory cytokines result in limited hippocampal neurogenesis, upregulation of AMPA receptors in glial cells resulting in neurotoxicity, active MMP9 that causes narrowing of dendritic protrusions reducing synaptic plasticity, and VEGF-mediated leakage of monocytes into the brain parenchyma [119]. The continued identification of new mechanisms of action in the epileptic brain offers new avenues for developing novel antiepileptic therapies.

Besides electroconvulsive therapy, most of the original antiepileptic therapies were really antiseizure medications (i.e., valium) designed for muscle spasms with contraindications for effective use in epileptic patients [159]. Although these drugs suppress seizure activity, they have no effect on the underlying pathophysiology in restoring imbalanced functioning of excitatory and inhibitory neurons. Third generation anticonvulsants such as brivaracetam, levetiracetam, and perampanel, developed after 2010 had the efficacy to regulate glutamate receptor excitation, AMPA activity, and/or synaptic vesicle glycoprotein 2A uptake. While these seemingly more effective anti-inflammatory agents were developed to antagonize the manifestation of the epileptic brain, (i.e., the epileptic seizures), these treatments do little to

TABLE 1 List of miRNAs and their implications involved in neurological disease.

Disease	miRNA	Target	Implications
Epilepsy	miR-146a	TLR4-NFκB pathway	Up-regulated in epilepsy; Acts as a negative feedback regulator; Dampens NFκB activity; Reduces IL-1 and IFN-α production; Mitigates inflammatory responses post-seizure
	miR-155	Anti-inflammatory regulators, TNF-α	Pro-inflammatory; Induced through NFκB after TLR stimulation; Enhances neuroinflammation by inhibiting anti-inflammatory regulators; Up-regulated in chronic TLE
	miR-125a-5p	CAMK4	Down-regulated in PTZ-induced epilepsy rats; Overexpression reduces seizures and inflammatory factor levels; Alleviates epileptic seizure and inflammation
	miR-34c-5p	HMGB1	Down-regulated in drug-resistant epilepsy (DRE); Exacerbates neuroinflammation; Aggravates hippocampal neuron loss
	miR-27a-3p	Apoptosis regulators, IL-1B, IL-6, TNF-α	Up-regulated in epileptic mice; Inhibitor relieves seizures and prevents apoptosis of hippocampal neurons; Inhibits inflammatory response; Reduces serum levels of IL-1β, IL-6, and TNF-α
	miR-139-5p	MRP1	Down-regulated in refractory epilepsy; Targets MRP1; Implicated in multidrug resistance
	miR-153	HIF-1α	Dysregulation implicated in refractory epilepsy; Possibly regulates HIF-1α expression
	miR-15a-5p	Unknown	Down-regulated in children with TLE
	miR-21-5p	STAT3, PDCD4, IL-6	Down-regulated in epilepsy; Up-regulated STAT3 in epileptic rats; Suppresses expression of STAT3, decreases IL-6 levels, reduces hippocampal neuron loss; Inhibits apoptosis by regulating PDCD4
	miR-134	MAP3K9	Promotes apoptosis; Reduces MAP3K9 levels
ALS	miR-34a	RNA metabolism, Aggregation	Dysregulated in ALS; Alters RNA metabolism; Implicated in protein aggregation
	miR-504	RNA metabolism, Aggregation	Dysregulated in ALS; Alters RNA metabolism; Implicated in protein aggregation
	miR-124	Motor neuron degeneration	Implicated in ALS progression; Associated with motor neuron degeneration
	miR-155	Inflammatory impact	Implicated in ALS progression; Has inflammatory impact
	miR-206	ALS pathology	Dysregulated in ALS pathology; Implicated in ALS-relevant pathways
	miR-27a	ALS pathology	Dysregulated in ALS pathology; Implicated in ALS-relevant pathways
	miR-338-3p	Biomarker potential	Potential ALS biomarker; Circulating miRNA
	miR-183	Biomarker potential	Potential ALS biomarker; Circulating miRNA
	miR-451	Biomarker potential	Potential ALS biomarker; Circulating miRNA
	miR-125a/b	Biomarker potential	Potential ALS biomarkers; Circulating miRNAs
	TDP-43 binding miRNAs	Dysregulation	Dysregulated in ALS patients; Indicates TDP-43 dysfunction
Parkinsons	miR-124	MEKK3, p62, p-p38	Regulation of neuroinflammatory response in microglia, Decreased expression in PD models, Overexpression reduces pro-inflammatory cytokines, Increases secretion of neuroprotective factors
	miR-155	Unknown	Increased expression in mouse models of PD, Plays a key role in the inflammatory response to α-syn, Neurodegeneration related to inflammation in PD
	miR-375	SP1	Protects dopaminergic neurons, Reduces neuroinflammation and oxidative stress in PD

(Continued on following page)

TABLE 1 (*Continued*) List of miRNAs and their implications involved in neurological disease.

Disease	miRNA	Target	Implications
	miR-7	α-synuclein	Protects cortical neurons from MPP+ toxicity, Interferes with MPP+ induced down-regulation of mTOR
	miR-153	α-synuclein	Protects cortical neurons from MPP+ toxicity, Interferes with MPP+ induced down-regulation of mTOR
	miR-34b/c	α-synuclein	Represses α-synuclein expression, Decreased levels in PD patient brains, Misregulated in pre-clinical PD brains, Down-regulation leads to mitochondrial dysfunction, Increases oxidative stress, contributing to PD
Alzheimers	miR-9	Unknown	Elevated levels in AD brains. Potential role as a biomarker for AD.
	miR-34a	TREM2	Increased levels in AD. Impairs microglial phagocytosis and increases cytokines. Potential therapeutic target for restoring TREM2
	miR-125b	Bcl-W, DUSP6, PPP1CA	Elevated in AD cerebrospinal fluid (CSF). May increase neuroinflammation and tau hyperphosphorylation
	miR-146a	Unknown	Elevated levels in AD brains
	miR-155	Unknown	Elevated levels in AD brains. Plays a crucial role in regulating memory loss
	miR-30b	Unknown	Highly upregulated in AD brains. Dysregulation may lead to cognitive and synaptic decline
	miR-124	PTPN1	Elevated levels in AD hippocampus. Dysregulation affects brain dysfunction in AD.
	miR-132	C1q	Reduced in AD brains. Dysregulation increases AD deposition
	miR-155	IL-1ß, IL-6, TNF-α	Elevated levels in AD hippocampus. Inhibition may decrease apoptotic protein Caspase-3
Huntington's Disease	miR-137	Unknown	Downregulation is pathological in HD, ameliorates mHtt-induced phenotypes [153]
	miR-1010	Unknown	Downregulation is pathological in HD, ameliorates mHtt-induced phenotypes [153]
	miR-219	Unknown	Detrimental in HD model and control flies, unrelated to HD pathology [153]
	miR-10	Unknown	Exacerbates phenotypes in HD flies and affects eclosion rate in controls [153]
	miR-305	Unknown	Alleviates phenotypes in HD flies, detrimental effects in control flies [153]
	miR-132	Unknown	Enhances motor function and lengthens lifespan in HD mice [154]
	miR-34a-5p	NDUFA9, TAF4B, NRF1, POLR2J2, DNALI1, HIP1, TGM2, POLR2G	Direct target genes, potential for future therapeutic interventions [155]
	miR-10b-5p, miR-10b-3p, miR-302a-3p	Unknown	Associated with neuropathological involvement and striatal scores [156]
	miR-10b-5p	Unknown	Strongly over-expressed in HD cases, related to CAG length-adjusted age of onset [156]
	miR-9*	Unknown	Lower expression in HD patients, involvement in HD pathogenesis [157]

hinder or reverse the process of epileptogenesis. Given miRNAs are crucial pleiotropic suppressors of aberrant inflammatory activity, as we have discussed earlier in this review, the potential for miRNAs to be used as the next-generation of anti-epileptic therapies looks promising. Furthermore, the utilization of miRNAs might resolve the problem associated with refractory epileptic episodes [160].

Mechanistic basis for miRNA-based epilepsy therapies

miRNAs are involved in the onset, development, and progression of epilepsy by regulating many of the key pathological processes mentioned above [118, 119]. For instance, miR-134 control of dendritic spine morphology [161], and the depletion of miR-134 after an epileptic seizure

results in reduced neuronal spines and an induced neuroprotective environment. Furthermore, miR-134 overexpression promotes apoptosis by reducing MAP3K9 mRNA and protein levels after an epileptic seizure, which affects the occurrence and latency of future seizure events. In patients with terminal lobe epilepsy, miR-134a serum expression tends to be lower than those without epilepsy, yet these levels increase from those suffering drug-resistant epilepsy. This could be explained by the finding that miR-134a causes reductions in CA3 pyramidal neurons potentially via the gene target CREB.

Another important anti-inflammatory miRNA and one of the most widely studied miRNAs in epilepsy, miR-146a, is abnormally expressed in both affected patients and in animal models of the disease (see Table 1). miR-146a is notably up-regulated in the serum of individuals with focal and generalized epilepsy, as well as within a pilocarpine-induced epileptic model [150]. miR-146a is a significant negative feedback regulator of the TLR4-NFκB proinflammatory pathway. Following a seizure, activated TLR4 triggers proinflammatory NFκB signaling and up-regulation of IL-1, IFN-α, and miR-146a. The increase in miR146a levels dampens NFκB activity, reducing IL-1 and IFN-α production, resulting in mitigated inflammatory responses post-seizure [117, 150]. Tao et al. used a lithium-pilocarpine mouse model to evaluate whether intranasal delivery of miR-146a mimics could delay seizure onset of terminal lobe epilepsy [118]. Using this therapeutic approach, miR-146a overexpression resulted in an increased percentage of animals having no induced seizure activity, extended latency of generalized convulsions, and reduced hippocampal damage. Inflammatory modulators such as, NF-κB, TNF-α, IL-1β, and IL-6 were also reduced, supporting an anti-inflammatory role of miR-146a via modulation of the TLR4-NFκB pathway [118].

While epilepsy is mostly described as a neurotransmitter imbalance, the consequence of chronic seizure activity is neuronal apoptosis, reorganization of neuronal synapses, and formation of abnormal synaptic loops that promote epilepsy recurrence. miRNAs play a crucial role in regulating both of these pro-apoptotic and pro-inflammatory pathways. As an example, miR-27a-3p expression is elevated in the hippocampus of epileptic mice [162]. Lu et al. used *in vivo* and *in vitro* models of epilepsy induced with kainic acid to determine the effect and mechanism(s) of action for miR-27a-3p [162]. Specifically, hippocampal tissue samples from rats treated with kainic acid had elevated miR-27a-3p expression, while the presence of a miR-27a-3p inhibitor during this treatment relieved kainic acid induced epileptic seizures. Additionally, the use of a miR-27a-3p inhibitor prevented apoptosis of cultured hippocampal neurons from epileptic rats. ELISA testing further revealed that, compared with the control group, proinflammatory factors IL-1B, IL-6, and TNF-α were significantly increased after intraperitoneal kainic acid treatment. The utilization of miR-27a-3p inhibitor co-treatment during this procedure diminished the activity of kainic acid induced pro-inflammatory response, as evidenced by reduced serum levels of IL-1β, IL-6, and TNF-α [162]. Taken together, the development of miRNA inhibitor based treatments or oligonucleotide therapies directed at the gene targets of miRNAs, such as miR-27a, may result in sustainable decreases in mortality and morbidity associated with chronic epileptic seizures.

miRNA and drug resistant epilepsy

In a 2022 review, Ghafouri-Fard et al. reported that several miRNAs were expressed and functionally active in refractory epilepsy, as defined by a lack of response to anti-seizure medication(s). Firstly, miR-139-5p expression is reduced in children with refractory epilepsy, concomitant with the up-regulation of multidrug resistance-associated protein 1 (MRP1) [113]. Similar expression patterns have been identified in brain tissue samples from rat models of refractory epileptogenesis, and *in vitro* studies have confirmed MRP1 is targeted and repressed by miR-139-5p. Moreover, rats transfected with miR-139-5p plasmids had enhanced neuronal survival, blunted neuronal injury, and re-sensitization to phenobarbitone treatment when compared to rats that underwent amygdala kindling with continual phenobarbitone exposure alone.

Fu et al. also investigated the mechanisms underlying the neuroinflammatory process in refractory epilepsy [112]. They found miR-34c-5p was significantly down-regulated in patients with drug-resistant epilepsy compared to controls. Experiments in kainic acid-induced epileptic rat models have shown that the subsequent down-regulation of miR-34c-5p and up-regulation of the inflammation-related mediator genes HMGB1 and IL-1β, post treatment, contributed to neuroinflammation and hippocampal neuron loss [112, 113]. Luciferase reporter assays *in vitro* confirmed that HMGB1 and hypoxia-inducible factor-1α (HIF-1α) were just some of the genetic targets of miR-34c-5p [112]. The continued efforts of numerous investigators into the mechanisms of miRNA function in epileptogenesis have culminated into the development of bioinformatic tools such as EpimiRBase [160], that depicts theoretical as well as experimentally verified, miRNA-gene target interactions that modulate the cellular mechanisms contributing to epileptogenesis (see Table 1). Many of these miRNA targets are also regulators of neuroinflammation, apoptosis, and angiogenesis.

Taken together, these findings indicate that while miRNAs such as miR-139-5p and miR-34 are being developed independently as therapeutics for certain types of metastatic cancer, these miRNAs should also be considered as candidate biomolecules for the next-generation of antiseizure medications for those suffering from recurrent epilepsy.

The development of genetically modified miRNA animal models of epilepsy

As mentioned earlier, a number of animal models have been developed to assess the underlying etiology of epilepsy. For instance, inhalation of flurothyl and electroshock treatment in rats are models that mimic the seizure phenotypes associated with epilepsy. Unfortunately these models do not identify the genetic onset of the disorder. Intraperitoneal injection of PTZ, the use of NMDA, phenobarbitone injections, or the intracortical injection of iron are more stable model systems that can be employed to investigate genetic variants that contribute to epileptogenesis. This is an important concern, because the stochastic regulatory potential of miRNAs can not be properly studied using unstable models of any genetic disorder, including epilepsy. Fortunately, using a lithium-pilocarpine rat model that mimics mesial temporal lobe epilepsy (MTLE), Ashhab et al., found an intricate connection between TNF-α expression and miR-155 levels [163]. In children with chronic TLE, the expression levels of both miR-155 and the pro-inflammatory cytokine TNF-α are increased [117]. Furthermore, in cultured hippocampal astrocytes, LPS treatment or activation of MRP8 resulted in elevated levels of both miR-155 and TNF-α. Conversely, lenalidomide treatment, a compound known to activate NK cell-mediated cytotoxicity, resulted in the suppression of miR-155 and TNF-α. Further investigation revealed that TNF-α functions as a positive feedback signal that transcriptionally regulates miR-155 expression.

Despite the unstable animal models of epilepsy, it is not surprising that miR-155 was found to be differentially expressed during the varied inflammatory states of epileptogenesis. miR-155 is a *bona fide* pro-inflammatory miRNA and regulates almost every aspect of immune cell functions by controlling the levels of SMAD2, IL-13α, LXRa, and SHIP-1, allowing for the unabated production of TNF-α, IL-6, IL-8, and the polarization of macrophages [163]. miR-155 also controls dendritic cell maturation, promotes differentiation and development of Th17, Th1, and T-regulatory cells, as well as stimulates the proliferation of mature B-cells and germinal center formation. Within microglia and resident macrophages, miR-155 also activates NFκB and TLR signaling resulting in the secretion of pro-inflammatory cytokines such as IFN-γ. Together, these findings support the notion that chronic neuroinflammation supports epileptogenesis.

Another set of *bona fide* miRNAs with links to inflammation is miR-125 and miR-21. miR-125 is generally considered an anti-inflammatory miRNA that targets TRAF6 and inhibits MAPK as well as NF-kB signaling. Furthermore, miR-125 is down-regulated in the hippocampus of PTZ-induced epileptic rat models, while overexpression of miR-125 attenuates seizure activity by suppressing target genes such as, calmodulin-dependent protein kinase IV (CAMK4), and decreases the levels of pro-inflammatory factors *in vivo* [117]. This finding is not surprising given miR-125 regulatees other immune pathways such as the perturbation of B-cell differentiation, and germinal center formation by targeting BLIMP-1 and IRF4. Using a similar rat model, the down-regulation of miR-21-5p in the hippocampus coincided with the up-regulation of STAT3 and onset of epileptic seizures. miR-21 target genes such as caspase-3 and Bax were also highly expressed, while Bcl-2 levels were reduced during this process [113]. This suggests that miR-21 controls onset of epilepsy via the modulation of neuroinflammatory pathways and also via the activation of pro-apoptotic cascades. Interestingly, the use of a miR-21-5p inhibitor *in vivo* resulted in higher IL-6 levels, activation of STAT3, and the apoptotic induction of hyperactive hippocampal neurons. These studies indicate that the proper expression of miR-21 could protect hippocampal neurons from the deteriorating effects of epilepsy.

Overall it is quite clear that miRNAs control the underlying etiology of epilepsy, and continued investigations using animal models will provide sufficient preclinical evidence for the basis of miRNA-based therapies for repairing the epileptic state and restoring brain function. It would be interesting to determine whether the advanced models of epilepsy via the use of gene knockout methodology or site directed mutagenesis will yield genetically linked miRNA pathways that support or abrogate epileptogenesis. Such genetically engineered mouse models of interest include those that contain a missense mutation in *Grin2a*, the genetic ablation of *Kcnq2*, the genetic duplication of *Shank3*, and/or contain a series of missense mutations in *Scn2a*.

miRNA contribution to ALS

ALS is a fatal neurodegenerative disorder affecting motor neurons in the spinal cord, brainstem, and cerebral cortex [164, 165]. Currently, there are no effective therapeutic options available that delay or slow the onset of ALS. The disease primarily strikes in mid-to-late adulthood, progressively leading to muscle weakness, atrophy, and ultimately respiratory muscle dysfunction, resulting in death [166]. Most ALS cases are sporadic, while only 5%–10% present with a familial history [165]. The median survival is around 3 years, with only 10% surviving beyond 8 years, emphasizing the need for improved diagnostic biomarkers and therapeutic interventions [165]. Repeat expansions in the C9ORF72 gene and mutations in superoxide dismutase 1 (SOD1) are common genetic causes of ALS, while TAR DNA-binding protein (TDP-43) and fused in sarcoma/translated in liposarcoma (FUS/TLS) mutations represent a smaller fraction [165]. Importantly, aberrant miRNA expression profiles are observed in both ALS mouse models and patients, highlighting the potential role of miRNAs in disease progression [165].

Microglia-mediated neuroinflammation plays a complex role in ALS progression. Inflammatory responses are observed in both

SOD-1-transgenic mice and ALS patients, influencing disease progression [138]. ALS is gradually being appreciated as an inflammatory disease, since dysfunction of normal microglia and astrocytes contribute to the phenotypes of ALS [138]. For instance, microglia, the immune cells of the CNS, normally promote synaptic maturation and remodeling, control of excessive neuronal activity, and promote oligodendrocyte progenitor cell development. In ALS, the microglia attempt to clear pathological aggregates, at the expense of enhanced proinflammatory cytokine signaling, ROS and nitric oxide production, excessive synaptic pruning, resulting in a neurotoxic state that generates reactive $C3^{+}$ astrocytes. Interestingly, targeting peripheral Ly6Chi monocytes with anti-Ly6C mAb reduces microglial infiltration and modifies the disease course in SOD1 mouse models indicating the monocytes and resident microglia in SOD1 mice influence ALS disease progression [167].

Astrocyte-mediated neuroinflammation also plays a complex role in ALS progression. Astrocytes are instrumental in regulating neuronal synapse release, facilitate neurotransmitter clearance, support glutamate reuptake, and promote antioxidant production. In ALS, these astrocytes are not able to maintain these functions and excessive pro-inflammatory cytokines result in the secretion of neurotoxic factors, increased ROS production, and reduced neurotrophic factors resulting in neuronal degeneration [167]. Many of the phenotypic consequences of astrocyte-mediated neuroinflammation are still being investigated; however, it was recently appreciated that motor neuron cell death is triggered by astrocyte mediated activation of a certain form of programmed cell death called necroptosis. This form of cell death is described as the loss of plasma membrane integrity due to activation of RIPK1 and MLKL. Some investigators are determining if regulators of these kinases could be used as therapeutics to abate the progression of ALS. Here, we argue that miRNAs that target these kinases such as miR-421, miR-381, and miR-425 could serve as effective treatments for ALS.

The greatest supporting evidence for the involvement of miRNAs in ALS etiology is the genetic link to TDP-43. TDP-43 is a member of TAR-binding proteins that are responsible for proper RNA processing. It is known that the generation of a subset of pre-miRNAs requires TDP-43 interactions with the nuclear Drosha complex for the proper cleaving of the cognate parental pri-miRNA. Additionally, cytoplasmic TDP-43 associates with the Dicer complex by binding to the terminal loops of the pre-miRNA facilitating Dicer-mediated cleavage of these pre-miRNAs. Studies by Kawahara et al., clearly show that TDP-43 is indispensable for neuronal outgrowth in cell culture models. Taken together, it is unquestionable that the non-coding RNA regulatory pathway is emerging as a central contributor to ALS pathogenesis.

Mutations in a number of RNA binding genes, such as C9ORF72, SOD1, TDP-43, and FUS result in altered RNA metabolism and correlate with an increased abundance of the protein aggregates similarly found in ALS patients [164]. Specifically, miRNA profiling reveals a series of dysregulated miRNAs in ALS (see Table 1). miR-218 is one miRNA of interest, given the expression of miR-218 is enriched in motor neurons, and was found in the exosomes released from cultured neurons post injury. In cultured primary astrocytes, it was found that miR-218 targets EAAT2, resulting in the modulation of glutamate re-uptake. EAAT2 expression is downregulated in post-mortem brain tissues from ALS patients, and overexpression of EAAT2 in the SOD1 model mentioned above protected animals from L-glutamate induced cytotoxicity. Finally, intracerebroventricular injections of miR-218 inhibitor restored normal astrocyte function as well as GFAP and Cx43 expression. These findings indicate that key miRNAs are vitally important to ALS pathogenesis, and furthermore, that differential expression of a particular miRNA alone is insufficient to predict their involvement with respect to disease progression. Exemplified in the case above, the persistent expression of miR-218 in motor neurons resulted in the chronic excitability of glutamatergic neurons, which was only corrected with the introduction of miR-218 inhibitors.

miR-494-3p is another miRNA that was found to be dysregulated in C9ORF72-ALS derived astrocytes. These astrocytes have a reduction in secreted antioxidant proteins, resulting in a state of oxidative stress and reduced cell survival for co-cultured motor neurons. Restoring the levels of miR-494-3p using miRNA mimics in these C9ORF72-ALS derived astrocytes resulted in healthy co-cultures of motor neurons. The genetic targets and the mechanisms of action of miR-494-3p are still unclear, but some studies point to the regulation of pro-inflammatory mediators such TRAF3, and IKKb/NF-kB resulting in the attenuation of M1 macrophage activation. miR-124 is another miRNA associated with ALS progression, given miR-124 has been linked with motor neuron dysfunction and degeneration in the SOD1 mouse model [168]. Specifically, the overexpression of miR-124 resulted in the early onset apoptosis of wild type motor neurons, while miR-124 inhibitor restored neurite outgrowth mitochondrial dynamics, synaptic signaling, and axonal transport of glutamate in SOD1 motor neurons.

As the field moves towards utilizing miRNAs as biomarkers for ALS onset and progression, some have identified additional mechanistic actions for miRNA-mediated progression of ALS. For instance, the accumulation of glycogen in the lumbar spinal cord of SOD1 ALS mice indicates that certain metabolic abnormalities may be an underlying cause of the neuroinflammatory pathways that support ALS progression [169] (see Figure 2). In support of this notion, $GYS1^{Nestin\text{-}KO}$ mice showed significant deficits in learning capacity, as well as altered neurogenesis. Furthermore, normal astrocytes tend to accumulate glycogen similar to muscle cells for utilization during times of high energy demand. Since astrocytes have low levels of

glucose-6-phosphate, astrocytes tend to release lactate instead of glucose, which is consumed by the surrounding neurons. Unfortunately, persistent levels of lactate secretion due to overabundant glycogen storage in ALS-astrocytes will also result in the aberrant activation of microglia that in turn secrete pro-inflammatory cytokines TNF-α, IL-6, an IL-1. In support of this hypothesis, miR-338-3p was shown to inhibit glycogenolysis in ALS mice resulting in glycogen accumulation within the spinal cord, while the use of miR-338-3p inhibitors restored some functionality in ALS mice. Interestingly, highly expressed circulating miRNAs such as miR-338-3p, as well as miR-206, miR-183, miR-451, and miR-125a/b are candidate biomarkers for ALS [170–172].

As ALS remains a rare, yet complex disorder with multiple facets of pathogenesis, the potential to cure the disease lies in the continued elucidation of the ncRNA transcriptome which involves the understanding of both miRNA dysregulation and the function of hnRNPs, such as TDP-43. By investigating these pleiotropic regulators in a cell contextual manner, new genetic players that control protein folding, neuroinflammation, glycogen storage, and necroptosis within astrocytes, microglia, and motor neurons will hold the key in determining the next series of therapeutic targets that will slow the progression of ALS. Interestingly, researchers just reported that intravenous application of a subset of anti-inflammatory T-cells attenuates some of the pro-neuroinflammatory phenotypes that hasten ALS progression.

miRNAs and Parkinson's disease

Parkinson's Disease is a neurodegenerative disorder characterized by bradykinesia, rest tremors, and rigidity [173]. While clinical signs will result in a diagnosis of probable Parkinson's, a definitive diagnosis requires pathological testing to identify the presence of Lewy bodies, which is an abnormal aggregation of α-synuclein protein. The underlying biological mechanisms of Parkinson's involve the loss of dopaminergic neurons, particularly in the substantia nigra within the basal ganglia. There is no definitive cause of Parkinson's, but evidence suggests that genetic and environmental factors play a role in its development [174]. One of the contributing factors of Parkinson's development is microglia cell dysfunction. Microglia are non-neural cells of the CNS that regulate inflammation, regeneration, and metabolism of neurons. Microglia and astrocytes both secrete pro-inflammatory cytokines, when an infection is present, yet the chronic secretion of pro-inflammatory cytokines result in neuroinflammation associated with the development of Parkinson's [120]. RNA metabolism may also play a role in the pathogenesis of Parkinson's. Specifically, genes associated with inherited Parkinson's have been shown to interact with the RNA translation initiation process and RNA translation components [175]. Although there is no cure for Parkinson's, treatment options focus on providing symptomatic relief, such as drugs that increase dopamine levels in the striatum or operate on dopamine receptors within the brain [176].

Neuroinflammation is believed to contribute to the development of Parkinson's. In particular, evidence suggests that neuroinflammation perpetuates the death of dopaminergic neurons by activating the microglia and promoting the infiltration of T-cells at sites of neuronal injury [177]. This pro-inflammatory response specific only to dopaminergic neurons implicates a level of cell context specificity analogous to the regulatory functions of miRNA. In fact, dysregulation of microRNA biogenesis appears to disrupt the balance of inflammatory processes in the brain, and results in the heightening of neuroinflammatory cues specifically associated with the Parkinsonian phenotype. The loss of Dicer in striatal dopaminergic neurons using a conditional knockout mouse model resulted in animals having shortened lifespan, an expansion of the resident astrocyte population, yet no neuronal degeneration [178]. However, the loss of Dicer throughout the entire midbrain of these animals resulted in progressive dopaminergic neuronal loss. Furthermore, patients with chromosomal 22q11.2 deletion syndrome, which includes the genetic loss of DGCR8, have a higher occurrence of Parkinson's as confirmed by pronounced Lewy body formation in post-mortem brain specimens [178]. Additionally, specific miRNAs such as miR-433, miR-16, and miR-7 regulate the genetic pathways associated with α-synuclein abundance, which is a precursor for α-synuclein protein aggregation and Lewy body formation. miR138 and miR-184 have also been reported to control the LRRK2 and E2F1 genes respectively resulting in aberrant lysosomal activity of astrocytes. Understanding the connection between microRNAs and neuroinflammatory processes, such as the generation of reactive astrocytes, may provide valuable insights into the cellular mechanisms of Parkinson's and lead to the discovery of novel therapeutics to slow disease progression [178] (see Table 1).

The involvement of miRNAs in animal models of Parkinson's

miR-124, a microRNA associated with neurogenesis, has been shown to have decreased expression in animal models of Parkinson's that have been treated with lipopolysaccharide (LPS), as well as in the 1-methyl-4-phenyl-1,2,3,6-tetrahydropyridine (MPTP) model of Parkinson's. Yao et al. found that miR-124 targets proteins p62 and p38 to regulate the inflammatory response in the microglia of a Parkinson's mouse model treated with LPS [179]. When the levels of p62 and p38 were reduced in the microglia, the levels of secreted proinflammatory cytokines were also concomitantly reduced. Furthermore, the decreased levels of p38 promoted autophagy in the surrounding microglia. Autophagy is a normal cellular death response where the surrounding tissue can utilize the

recycled cellular material from dying cells. Autophagy is also a normal physiological response to reduce the populations of cells containing α-synuclein protein aggregate formation that is a culprit linked to neuronal degeneration and Parkinson's disease progression [179]. While autophagy suppresses neuroinflammation, persistent autophagy results in an imbalanced microglial pool resulting in reduced presence of neurotrophic factors and other secreted cytokines that support neurogenesis. Therefore, these results indicate that miRNAs, such miR-124, could be used as therapeutic entities for controlling neuroinflammation, α-synuclein protein aggregation, and abating neuronal degeneration before self destructive cellular processes, such as autophagy are activated in Parkinson's.

miR-155 is another miRNA found to have increased expression in mouse models of Parkinson's. Thome et al. found that mice that lacked miR-155 had a reduced proinflammatory response despite adeno-virus-mediated induction of α-synuclein aggregation [180]. Furthermore, the deletion of miR-155 resulted in reduced microgliosis. These findings suggest miR-155 activity plays a key role in the physiological response to α-synuclein aggregation, though it is not clear whether miR-155 prevents this aggregation via promotion of proper protein folding in the ER, regulation of additional chaperone proteins that support aggregate formation, or via the control of an E3 ligase resulting in ubiquitination of α-synuclein. miR-155 is also linked with microglial-mediated inflammation, given TNF-a promotes miR-155 expression, which targets SOCS1 and mitochondrial complex I. The result is aberrant production of cytokines and nitric oxide that triggers neuronal cell death. Therefore targeting miR-155 itself, could be a useful therapeutic strategy to abate the symptoms of Parkinson's. Interestingly, Caggiu et al. found that the expression of miR-155-5p changed in patients receiving the drug levodopa [181], with patients on the highest dose of levodopa experiencing the greatest down-regulation of miR-155-5p. Because levodopa is a precursor to dopamine, this indicates normal dopaminergic signaling in dopaminergic neurons suppresses pro-neuroinflammatory miRNAs such as miR-155. The addition of a miR-155 antagonist or inhibitors may enhance the efficacy of levodopa by suppressing inflammatory signaling in the microglia and astrocytes in patients with Parkinson's.

Conversely, miR-375 can be used to protect dopaminergic neurons in Parkinson's. Cai et al. demonstrated that increased levels of miR-375 in a simulated rat model improved behavioral changes, reduced neuroinflammation and oxidative stress, and decreased dopamine levels [114]. Protection of dopaminergic neurons was achieved through up-regulation of miR-375, specifically by inhibiting the transcription factor specificity protein 1 (SP1), which is involved in neurodegeneration of Parkinson's. The reverse effect was found when SP1 was up-regulated. Furthermore, Wang et al. used a mouse model to demonstrate that increasing miR-93 expression and reducing protein STAT3 can help protect cells and reduce inflammation in Parkinson's [115]. Mice exposed to LPS had high levels of STAT3. When expression of miR-93 was increased, STAT3 levels were reduced and inflammation in turn decreased. They found that miR-93 directly targets STAT3, and increasing miR-93 helps to protect cells that produce dopamine in Parkinson's mice.

The mechanistic basis for miRNA-based therapies in Parkinson's

Given miRNA are pleiotropic regulators of cellular processes, it is not surprising to find a number of gene targets for a specific dysregulated miNA identified in the pathogenesis of Parkinson's. However, miRNAs are also crucial in regulating a series of genetic cascades that result in a coordinated cellular response, (i.e., go, no go signaling for deciding cell proliferation vs. differentiation). Therefore, the challenge is in understanding which miRNA(s) will have the greatest capacity to support dopaminergic nerve cell survival, a healthy microglial network, while also preventing protein aggregation formation and reduced mitochondrial dysfunction.

Yao et al. demonstrated that miR-124 regulates the expression of mitogen-activated protein kinase kinase 3 (MEKK3) in microglial cells, which regulates the neuroinflammatory response in PD [179]. Knockdown of MEKK3 inhibited microglial activation by regulating the nuclear factor kappaB (NF-κB) signaling pathway. Overexpression of miR-124 decreased the expression of pro-inflammatory cytokines and increased the secretion of neuroprotective factors. One therapeutic possibility is for miR-124 to be delivered via traceable polymeric nanoparticles (NPs). Saraiva et al. found that miR-124 NPs were able to help promote neural stem/progenitor cells and neuroblasts to neurons *in vitro* [182]. The miR-124 NPs also reduced the expression of genes targeted by miR-124. In a mouse model, injecting miR-124 NPs directly into the brain increased the number of neuroblasts that migrated to the olfactory bulb, both in mice with and without PD. The olfactory bulb is typically the first region of the brain to experience accumulation of α-synuclein [182].

miR-7 and miR-153 target the protein α-synuclein. One study investigated the effects of overexpression of these two microRNAs using a PD cell culture model with the neurotoxin MPP+, which causes apoptosis and changes in intracellular signaling pathways. Overexpression of miR-7 and miR-153 was found to protect cortical neurons from MPP+ toxicity by interfering with the MPP+ induced down-regulation of mTOR signaling. Therefore, miR-7 and miR-153 have the protection to protect neurons from apoptosis and may have a critical role in new therapeutic approaches [183]. Another study found that inhibition of the expression of miR-34b and miR-34c increased a-syn levels and aggregate formations [184]. miR-34b and miR-34c had decreased levels in PD patient brains that were in the clinical stage of the disease and were dysregulated

in pre-clinical PD brains. The down-regulation of miR-34b and miR-34c results in disturbances in mitochondrial function and increases oxidative stress, leading to disease progression [185].

Taken together, miRNAs have a clear role in regulating the progression of Parkinson's development. Specifically, miRNA-mediated regulation of α-synuclein aggregate formation, degeneration of dopaminergic neurons, production of reactive oxygen species, promotion of excitotoxicity, and secretion of pro-inflammatory cytokines and microglia activation are all avenues for therapeutic intervention.

miRNA contribution to Alzheimer's disease

Alzheimer's Disease (AD) is the most common neurodegenerative disease (NDD) and the most common form of dementia. The clinical signs of Alzheimer's include progressive cognitive decline and memory loss, along with difficulties with language processing and problem solving. The cause of Alzheimer's is unknown, but evidence suggests that a combination of genetics, environment, and lifestyle factors play a role in its development. There is currently no cure for Alzheimer's, and current therapeutics treat the symptoms of the disease. Alzheimer's is characterized by the accumulation of amyloid beta plaques and tau protein tangles in the brain, which leads to the loss of synaptic connections and neurons, which in turn leads to neuroinflammation, oxidative stress, and synaptic dysfunction. Specifically, there is increasing evidence that neuroinflammation plays a critical role in the progression of the disease. Increased concentration of proinflammatory cytokines have been found in patients with Alzheimer's, and PET scans have shown increased microglial inflammation in the brains of patients with Alzheimer's. Microglia use microRNAs to rapidly respond to inflammation [121].

In the brains of individuals with Alzheimer's, there are elevated levels of specific microRNAs, including miRNA-9, miRNA-34a, miRNA-125b, miRNA-146a, and miRNA-155. These miRNAs increase in activation when they are around proinflammatory cytokines and amyloid beta, both of which are associated with Alzheimer's inflammation. These miRNAs are influenced by the protein NFkB, which is elevated in the brains of Alzheimer's patients. Alexandrov et al. investigated the levels of these miRNAs in the cerebrospinal fluid (CSF) of Alzheimer's patients as compared to individuals without Alzheimer's [186]. The results showed that the miRNAs listed above were significantly higher in the CSF of patients with Alzheimer's than without, indicating their potential role as biomarkers.

miRNAs in animal models of Alzheimer's

miR-155 is a pro-inflammatory microRNA found in the brain. Liu et al. investigated the effects of miR-155 on inflammatory cytokine markers IL-1β, IL-6 and TNF-α in a rat model with Alzheimer's [187]. They found elevated levels of inflammatory markers and increased miR-155 expression in the hippocampus. When a miR-155 inhibitor was introduced to the rat model, there was a decrease in the expression of the apoptotic protein Caspase-3 in the hippocampus. Apoptotic protein Caspase-3 is an enzyme that is involved in the initiation and execution of apoptosis. The rat model experienced significant cognitive and learning improvement when miR-155 or the inflammatory cytokine receptors were inhibited. This suggests that miR-155 has a crucial role in regulating memory loss through neuroinflammation in Alzheimer's [187]. Aloi et al. found that deleting miR-155 in the microglia in a mouse model resulted in increased expression of anti-inflammatory genes and therefore reduced plaque and AB buildup in the brain [188]. However, this deletion caused the mice to have hyperexcitability, recurring seizures, and increased seizure related deaths [188]. miR-155 has therapeutic possibilities for Alzheimer's. Zheng et al. [189] studied the effects of the intravenous drug Propofol on microglial activation (M1 activation) using a mouse model. They found that propofol suppressed the expression of miR-155, suggesting that propofol inhibits neuroinflammation by reducing levels of miR-155.

Song et al. [190] found that miR-30b is a microRNA that is highly up-regulated in the brains of patients with Alzheimer's and mouse models. Increasing expression of miR-30b in the hippocampus region of wild-type mice impairs cognitive functions, similar to mice with AD. Conversely, reducing levels of miR-30b in mice with simulated Alzheimer's prevents cognitive decline. They also found that miR-30b is up-regulated by proinflammatory cytokines and AB42. These findings suggest that miR-30b that is dysregulated leads to cognitive and synaptic decline, indicating that reversal of this dysregulation could have therapeutic advantages.

miR-124 is thought to directly affect the protein PTPN1, which is essential for normal brain function. Elevated levels of miR-124 were found in the hippocampus of a mouse model. When miR-124 was increased or PTPN1 was decreased in the mouse model, the mice developed changes similar to those with AD. When the balance of miR-124 and PTPN1 was restored, these changes improved. This shows that the miR-124/PTP1B pathway has a role in brain dysfunction in the development of AD, and reconstructing this pathway could improve cognitive functions in patients with AD [191].

Mechanisms of action for the miRNA mediated Alzheimer's phenotype

Not surprisingly, there are a number of clinical criteria associated with dementia that are distinct from Alzheimer's. Understanding the clinical description of the symptoms associated with these various dementias, will better enable molecular biologists to match the underlying genetic pathways

that could be the instigator of these dementias. In one example, frontotemporal dementia (FTD) is similar to Alzheimer's yet does not present with patient hallucinations nor loss of spatial orientation. microRNAs also have the potential to help discriminate AD from other types of dementia, such as frontotemporal dementia (FTD), more commonly known as Pick's disease. FTD is a rare neurodegenerative disorder that primarily affects the frontal and temporal lobes of the brain, and is characterized by the progressive deterioration of behavior, language, and personality. FTD has similar clinical symptoms to other dementias such as Alzheimer's, making diagnosis difficult and misdiagnosis common [192]. FTD is associated with accumulation of proteins such as tau and TDP-43 in the brain. Specifically, Martinez et al. [193] focused on how miRNA biomarkers found in CSF and blood serums helped distinguish frontotemporal dementia (FTD) from Alzheimer's and ALS. They found miR-223-3p, miR-15a-5p, miR-22-3p, and miR-124 to all be potential biomarkers for FTD in comparison to Alzheimer's, ALS, and controls.

Vascular cognitive impairment dementia (VCID) is caused by inadequate cerebral blood flow that results in brain damage. Unlike Alzheimer's, VCID is both preventable and treatable [194]. microRNAs play an important role in the dysfunctional mechanisms of VCID, including blood-brain barrier dysfunction, apoptosis, oxidative stress, and neuroinflammation. A multiple microinfarction (MMI) model was used to simulate vascular dementia in mice to investigate the role of miR-126, which regulates vascular function. Mice with reduced endothelial miR-126 experienced cognitive impairment, decreased blood flow, inflammation, and glymphatic dysfunction, showing miR-126's role in cognitive deterioration [116].

With respect to Alzheimer's, miR-132 is known to regulate neuron plasticity and has been shown to be reduced in brains affected with Alzheimer's. When this gene is deleted in a mouse model, Alzheimer's deposition is increased. A possible protein that miR-132 might regulate is C1q, which has increased expression in the synapses of Alzheimer's individuals. When mice were exposed to either miR-132 agonists and/or C1q inhibitors, synaptic proteins increased significantly [195]. Moreover, intranasal delivery of miR-132 in a dementia mouse model could partially improve the cognitive functions of mice, and promote the significant increase of synaptic proteins PSD95 and Synapsin-1.

Conversely, miR-125b may increase neuroinflammation resulting in Alzheimer's pathogenesis. miR-125b is found to be elevated in the cerebrospinal fluid of Alzheimer's patients. miR-125 reduces the level of Bcl-W, which prevents apoptosis. It also directly targets DUSP6 and PPP1CA, which are phosphatases. When these phosphatases are decreased using miR-125b, tau hyperphosphorylation increases. In a mouse model, this was found to hinder learning and cognition [111]. Zhao et al. [196] additionally found increased levels of miRNA-34a in patients with Alzheimer's which affect the expression of the TREM2 receptor. Reduced expression of TREM2 impairs the ability of microglia to perform phagocytosis and leads to increased production of proinflammatory cytokines. However, when an anti-miR-34a molecule was used in animal models, it prevented this harmful effect and TREM2 expression was restored, suggesting a potential therapeutic target.

Together, these findings shed light on the involvement of specific miRNAs in the pathogenesis of Alzheimer's and their impact on various inflammatory processes and immune responses. Further research in this field could potentially lead to the development of targeted therapies aimed at modulating these miRNAs and mitigating the neuroinflammatory component of Alzheimer's.

miRNAs and Huntington's disease

Huntington's disease is a rare neurodegenerative disorder caused by an autosomal dominantly-inherited CAG-trinucleotide repeat-expansion encoding for glutamine in the huntingtin (*HTT*) gene, leading to protein misfolding and aggregation of aberrant proteins [153, 155, 197]. It is characterized by cognitive, motor, and psychiatric disturbance. At the cellular level, mutant HTT results in neuronal dysfunction and death through a number of mechanisms, including disruption of proteostasis, transcription and mitochondrial function, and direct toxicity of the mutant protein [197].

Transcriptional dysregulation is one of the major pathogenic processes in HD. Transcriptional alterations are present in Huntington's mice before the onset of disease symptoms and in asymptomatic HD-mutation humans, suggesting that perturbed gene expression is one of the causes of pathogenesis. Zsindely et al. [153] investigated miRNAs that are misregulated in a *Drosophila* model of Huntington's. miRNAs function as post-transcriptional regulators of gene expression. Therefore, miRNA dysregulation introduces a second layer of altered gene regulatory mechanisms besides the transcriptional misregulation of mRNAs in HD and can pinpoint those molecular processes that are part of the response to mHtt-induced proteopathic stress [153].

They determined the functional effects of three down-regulated (dme-mir-137, dme-mir-219, and dme-mir-1010) and two up-regulated (dme-mir-10 and dme-mir-305) miRNAs on mHtt-induced pathology. Overexpression of both dme-mir-137 and dme-mir-1010 ameliorated mHtt-induced phenotypes, indicating that the down-regulation of these miRNAs is pathological. Overexpression of dme-mir-219, on the other hand, was detrimental both in the Huntington's model and in control flies, suggesting that in this case, the observed phenotypic outcome is due to a toxic effect of dme-mir-219 overexpression that is independent of Huntington's pathology. Overexpression of dme-miR-10 also exacerbated all

analyzed phenotypes of Huntington's flies, and it also had a mildly negative effect on the eclosion rate of control flies. This suggests that flies are sensitive to the level of dme-mir-10-5p, and increased expression of this miRNA might be a part of the molecular basis of pathology in the HD model. Overexpression of dme-mir-305 alleviated all analyzed phenotypes of Huntington's flies and had significant detrimental effects on the viability, longevity, and motor activity of control flies [153].

Fukuoka et al. [154] investigated the use of miR-132 as a potential treatment for Huntington's disease (HD). A recombinant adeno-associated virus (rAAV) miRNA expression system was used to deliver miR-132 to the R6/2 mice. Findings demonstrated that giving Huntington's mice access to miR-132 enhanced motor function and lengthened their lives. The therapy had no impact on the expression of disease-causing mutant HTT genes and their byproducts. Supplementing with miR-132 may be a treatment strategy for easing Huntington's symptoms and delaying the onset of the disease without specifically addressing the underlying genetic etiology. Although it might not offer a permanent cure for Huntington's, it exhibits promise as a prospective therapeutic approach [154].

Degeneration of the medium spiny neurons (MSNs) in the striatum of the basal ganglia is the key pathological feature of Huntington's [198]. Using a high-throughput miRNA interaction reporter assay (HiTmIR) to study the interactions between miR-34a-5p and HD associated genes, Hart et al. (2023) identified NDUFA9, TAF4B, NRF1, POLR2J2, DNALI1, HIP1, TGM2, and POLR2G as direct miR-34a-5p target genes. Down-regulation of miR-34a-5p in MSNs of R6/2 mice and human HD brain samples might contribute to an elevated intracellular Ca^{2+} level, increased UPR and ROS levels resulting in a pronounced activation of apoptosis. These results lay the ground for future therapeutic interventions using miRNA-34 [155].

Although Huntington's mainly affects the CNS, Diez-Planelles et al. [199] hypothesized that ubiquitous expression of mutant HTT contributes to disturbances in circulating miRNA profile in symptomatic Huntington's patients, reflecting changes in both the central nervous system (CNS) and peripheral tissues. To test their hypothesis, they analyzed plasma samples from symptomatic patients with 40–45 CAG repeats in the *HTT* gene, the most common range among Huntington's patients, screening for changes in the Huntington's circulating miRNA profile of healthy matched controls. The Unified Huntington's Disease Rating Scale and Total Functional Capacity, two disease severity indicators, were found to be linked with the expression levels of specific circulating miRNAs. Additionally, the study found that Huntington's patients had an overexpression of circulating miRNAs that regulate metabolism. According to these results, circulating miRNA profiles may be used as possible biomarkers for tracking the development of the disease and developing customized treatments for Huntington's patients [199].

The expression of miRNAs in the prefrontal cortex (BA9) of Huntington's patients and normal subjects was examined by Hoss et al. [156] Next-generation miRNA sequence analysis was performed on tissue samples from 26 Huntington's, 2 Huntington's gene-positive, and 36 control brains. Neuropathological information available for all Huntington's brains included age at disease onset, CAG-repeat size, Vonsattel grade, and Hadzi-Vonsattel striatal and cortical scores, a continuous measure of the extent of neurodegeneration. Linear models were performed to examine the relationship of miRNA expression to these clinical features, and messenger RNA targets of associated miRNAs were tested for gene ontology term enrichment.

75 differentially-expressed miRNA's were identified in the tissue samples. Nine were significantly associated with Vonsattel grade of neuropathological involvement and three of these, miR-10b-5p, miR-10b-3p, and miR-302a-3p, significantly related to the Hadzi-Vonsattel striatal score (a continuous measure of striatal involvement) after adjustment for CAG length. Five miRNAs (miR-10b-5p, miR-196a-5p, miR-196b-5p, miR-10b-3p, and miR-106a-5p) were identified as having a significant relationship to CAG length-adjusted age of onset including miR-10b-5p, the mostly strongly overexpressed miRNA in Huntington's cases. These results provide insight into striatal involvement and support a role for these miRNAs, particularly miR-10b-5p, in HD pathogenicity. The miRNAs identified in our studies of postmortem brain tissue may be detectable in peripheral fluids and thus warrant consideration as accessible biomarkers for disease stage, rate of progression, and other important clinical characteristics of Huntington's [156].

Chang et al. [157] examined 13 miRNA's (miR-1, mirR-9, miR-9*, miR-10b, miR-29a, miR-29b, miR-124a, miR-132, miR-155, miR-196a, miR-196b, miR-330, and miR-615) that previously demonstrated alterations in the brains of Huntington's patients or that are potential regulators of differentially-expressed genes in brains of Huntington's patients, to examine their expression in the peripheral leukocytes of Huntington's patients healthy controls. Expression levels of miR-9* were much lower in Huntington's patients compared with those in healthy controls, suggesting that miR-9* may be involved in the pathogenesis of Huntington's. miR-9 is highly conserved across vertebrate species and shows brain-specific expression. The complementary strand miR-9* is also crucial for brain development. These findings suggest that miR-9*-mediated gene regulation is important for synaptic plasticity and memory, both of which play an important role in the generation of abnormal movements and psychiatric abnormalities in Huntington's [157].

Conclusion

This article examines a number of disorders connected to miRNA levels and how they control neuroinflammation. In the future, therapeutics that target particular miRNAs might possibly be created to treat neurological problems. Some miRNA have already been suggested as potential biomarkers. By targeting miRNAs that are involved in neuroinflammation, the severity of many neurological disorders might be reduced [200]. As an example, miRNAs that promote neurodegeneration [201], have been demonstrated to activate TLR7 in neurons and cause neurotoxicity [201]. According to Lehmann et al., the increase in pro-neurodegenerative miRNAs may be an indicator of aberrant transcriptome signaling, or improper chromatin remodeling that alters the entire epigenetic landscape of normal microglial cells. This notion makes some intuitive sense, given similar miRNAs are found to be dysregulated in a wide variety of neurological disorders with vastly varied clinical manifestations. Therefore, while the immediate goal is to implement miRNA to slow the progression of neurodegenerative illnesses, researchers should be assessing the entirety of the epigenome so as to elucidate the neuroinflammatory cues that promote disease specific phenotypes.

From the diagnostic perspective, researchers are able to distinguish between various forms of neurodegenerative illness using serum miRNA levels [202]. Researchers examined a collection of miRNAs in a particular patient cohort that were linked to Alzheimer's disease, Parkinson's disease, vascular dementia, and mixed vascular-parkinsonism [202]. The analysis discovered dysregulated miRNAs in comparisons of various diseases. The findings indicate that dysregulation of miR-34b, miR-125b, and miR-130b is related to Alzheimer's disease and that altered expression of miRNAs such miR-15b, miR-24, miR-142-3p, miR-181c, and miR-222 is connected with Parkinson's disease [202]. When these miRNAs were combined into an indicator, as opposed to when they were used individually, the diagnostic accuracy was enhanced, according to multivariable ROC curves [202]. Circulating miRNAs that are linked to proteins or exosomes are stable, which makes them desirable as diagnostic biomarkers [202].

So how will a miRNA be implemented? An individual miRNA can have multiple targets, regulating several genes in a single pathway or single genes in several pathways. For example, genetic deletion of brain-expressed miR-128 in mice resulted in up-regulation of more than a thousand mRNA transcripts, of which 154 were predicted targets of miR-128. This multi-targeting property of miRNAs has advantages for disease modification in neurological diseases because it offers the possibility to disrupt several pathological processes at once. However, it also increases the potential for unwanted or unanticipated side-effects of any miRNA-based therapy [160]. Unfortunately the hurdle we must overcome in the therapeutics arena is the acceptance that multigenic disorders such as Alzheimer's or epilepsy are going to require pleiotropic therapeutics that can function synergistically to correct or reverse the underlying faulty genetic pathways of the disease.

The specific hurdle to neurocentric miRNA drug delivery is the blood brain barrier, which prevents miRNAs from entering the CNS and reduces their efficacy [203]. Roy et al. [203] suggested two methods to improve the delivery of miRNAs and get around this obstacle. The first includes utilizing miRNA mimics (agonists) that are packaged into lipid nanoparticles so as to facilitate uptake of the miRNA into the CNS. In the second method, miRNA delivery could be implemented via exosomes carrying surface targeting molecules to facilitate cell specific uptake of the miRNAs therapeutic [204]. This strategy could also be used to aid in the transport of the therapeutic through the blood brain barrier. Additional research is still required to determine how these approaches might be implemented to treat the neurological conditions mentioned in this review.

Author contributions

YC, JM, LG, JW, JB, BP, CS, and BA performed the literature research and co-wrote the manuscript. YC, JM, and LG designed the figures and tables. YC, JM, RA, and BA reviewed and editorially revised the manuscript. BA reviewed and provided advice on the content of this manuscript. All authors contributed to the article and approved the submitted version.

Funding

JM received a grant from Gustavus Adolphus College. Additional funding was supported by a grant from The Brain Institute of America Foundation.

Conflict of interest

The authors declare that the research was conducted in the absence of any commercial or financial relationships that could be construed as a potential conflict of interest.

References

1. Deogharia M, Gurha P. The 'guiding' principles of noncoding RNA function. *Wiley Interdisciplinary Reviews RNA* (2022) **13**:e1704. doi:10.1002/wrna.1704

2. Bhatti GK, Khullar N, Sidhu IS, Navik US, Reddy AP, Reddy PH, et al. Emerging role of non-coding RNA in health and disease. *Metab Brain Dis* (2021) **36**:1119–34. doi:10.1007/s11011-021-00739-y

3. Fu XD. Non-coding RNA: a new frontier in regulatory biology. *Natl Sci Rev* (2014) **1**:190–204. doi:10.1093/nsr/nwu008

4. Taft RJ, Pang KC, Mercer TR, Dinger M, Mattick JS. Non-coding RNAs: regulators of disease. *J Pathol* (2010) **220**:126–39. doi:10.1002/path.2638

5. Storz G. An expanding universe of non-coding RNAs. *Science* (2002) **296**: 1260–3. doi:10.1126/science.1072249

6. Kim YK. RNA therapy: rich history, various applications and unlimited future prospects. *Exp Mol Med* (2022) **54**:455–65. doi:10.1038/s12276-022-00757-5

7. Mol JN, van der Krol A, van Tunen A, van Blokland R, de Lange P, Stuitje A. Regulation of plant gene expression by antisense RNA. *FEBS Lett* (1990) **268**: 427–30. doi:10.1016/0014-5793(90)81298-3

8. Takayama KM, Lnouye M. Antisense RN. *Crit Rev Biochem Mol Biol* (1990) **25**: 155–84. doi:10.3109/10409239009090608

9. Karikó K. *In vitro*-Transcribed mRNA therapeutics: out of the shadows and into the spotlight. *Mol Ther* (2019) **27**:691–2. doi:10.1016/j.ymthe.2019.03.009

10. Wolff JA, Malone RW, Williams P, Chong W, Acsadi G, Jani A, et al. Direct gene transfer into mouse muscle *in vivo*. *Science* (1990) **247**:1465–8. doi:10.1126/science.1690918

11. Beckert B, Masquida B. Synthesis of RNA by *in vitro* transcription. *Methods Mol Biol* (2011) **703**:29–41. doi:10.1007/978-1-59745-248-9_3

12. Hannon GJ. RNA interference. *Nature* (2002) **418**:244–51. doi:10.1038/418244a

13. Song E, Lee SK, Dykxhoorn DM, Novina C, Zhang D, Crawford K, et al. Sustained small interfering RNA-mediated human immunodeficiency virus type 1 inhibition in primary macrophages. *J Virol* (2003) **77**:7174–81. doi:10.1128/jvi.77.13.7174-7181.2003

14. Lai EC. Micro RNAs are complementary to 3' UTR sequence motifs that mediate negative post-transcriptional regulation. *Nat Genet* (2002) **30**:363–4. doi:10.1038/ng865

15. Bartel DP. MicroRNAs: target recognition and regulatory functions. *Cell* (2009) **136**:215–33. doi:10.1016/j.cell.2009.01.002

16. Zhang P, Wu W, Chen Q, Chen M. Non-coding RNAs and their integrated networks. *J Integr Bioinformatics* (2019) **16**:20190027. doi:10.1515/jib-2019-0027

17. Dassi E, Zuccotti P, Leo S, Provenzani A, Assfalg M, D'Onofrio M, et al. Hyper conserved elements in vertebrate mRNA 3'-UTRs reveal a translational network of RNA-binding proteins controlled by HuR. *Nucleic Acids Res* (2013) **41**:3201–16. doi:10.1093/nar/gkt017

18. Landgraf P, Rusu M, Sheridan R, Sewer A, Iovino N, Aravin A, et al. A mammalian microRNA expression atlas based on small RNA library sequencing. *Cell* (2007) **129**:1401–14. doi:10.1016/j.cell.2007.04.040

19. Ha M, Pang M, Agarwal V, Chen ZJ. Interspecies regulation of microRNAs and their targets. *Biochim Biophys Acta (Bba) - Gene Regul Mech* (2008) **1779**: 735–42. doi:10.1016/j.bbagrm.2008.03.004

20. Lewis BP, Burge CB, Bartel DP. Conserved seed pairing, often flanked by adenosines, indicates that thousands of human genes are microRNA targets. *Cell* (2005) **120**:15–20. doi:10.1016/j.cell.2004.12.035

21. Liu G, Zhang R, Xu J, Wu CI, Lu X. Functional conservation of both CDS- and 3'-UTR-located microRNA binding sites between species. *Mol Biol Evol* (2015) **32**: 623–8. doi:10.1093/molbev/msu323

22. Lagos-Quintana M, Rauhut R, Meyer J, Borkhardt A, Tuschl T. New microRNAs from mouse and human. *RNA* (2003) **9**:175–9. doi:10.1261/rna.2146903

23. Du T, Zamore PD. microPrimer: the biogenesis and function of microRNA. *Development* (2005) **132**:4645–52. doi:10.1242/dev.02070

24. Tomari Y, Zamore PD. MicroRNA biogenesis: drosha can't cut it without a partner. *Curr Biol* (2005) **15**:R61–R64. doi:10.1016/j.cub.2004.12.057

25. Brenner S. The genetics of *Caenorhabditis elegans*. *Genetics* (1974) **77**:71–94. doi:10.1093/genetics/77.1.71

26. Lim LP, Lau NC, Weinstein EG, Abdelhakim A, Yekta S, Rhoades MW, et al. The microRNAs of *Caenorhabditis elegans*. *Genes Dev* (2003) **17**:991–1008. doi:10.1101/gad.1074403

27. Navarro F, Lieberman J. miR-34 and p53: new insights into a complex functional relationship. *PLoS One* (2015) **10**:e0132767. doi:10.1371/journal.pone.0132767

28. Hermeking H. The miR-34 family in cancer and apoptosis. *Cell Death Differ* (2010) **17**:193–9. doi:10.1038/cdd.2009.56

29. Rokavec M, Li H, Jiang L, Hermeking H. The p53/miR-34 axis in development and disease. *J Mol Cel Biol* (2014) **6**:214–30. doi:10.1093/jmcb/mju003

30. He L, He X, Lowe SW, Hannon GJ. microRNAs join the p53 network--another piece in the tumour-suppression puzzle. *Nat Rev Cancer* (2007) **7**:819–22. doi:10.1038/nrc2232

31. Adams BD, Parsons C, Slack FJ. The tumor-suppressive and potential therapeutic functions of miR-34a in epithelial carcinomas. *Expert Opin Ther Targets* (2016) **20**:737–53. doi:10.1517/14728222.2016.1114102

32. Washietl S, Hofacker IL, Lukasser M, Hüttenhofer A, Stadler PF. Mapping of conserved RNA secondary structures predicts thousands of functional non-coding RNAs in the human genome. *Nat Biotechnol* (2005) **23**:1383–90. doi:10.1038/nbt1144

33. Pedersen JS, Bejerano G, Siepel A, Rosenbloom K, Lindblad-Toh K, Lander ES, et al. Identification and classification of conserved RNA secondary structures in the human genome. *Plos Comput Biol* (2006) **2**:e33. doi:10.1371/journal.pcbi.0020033

34. Wang B, Hsu S, Wang X, Kutay H, Bid HK, Yu J, et al. Reciprocal regulation of microRNA-122 and c-Myc in hepatocellular cancer: role of E2F1 and transcription factor dimerization partner 2. *Hepatology* (2014) **59**:555–66. doi:10.1002/hep.26712

35. Hayashita Y, Osada H, Tatematsu Y, Yamada H, Yanagisawa K, Tomida S, et al. A polycistronic microRNA cluster, miR-17-92, is overexpressed in human lung cancers and enhances cell proliferation. *Cancer Res* (2005) **65**:9628–32. doi:10.1158/0008-5472.can-05-2352

36. He S, Chu J, Wu LC, Mao H, Peng Y, Alvarez-Breckenridge CA, et al. MicroRNAs activate natural killer cells through Toll-like receptor signaling. *Blood* (2013) **121**:4663–71. doi:10.1182/blood-2012-07-441360

37. Cimmino A, Calin GA, Fabbri M, Iorio MV, Ferracin M, Shimizu M, et al. miR-15 and miR-16 induce apoptosis by targeting BCL2. *Proc Natl Acad Sci U S A* (2005) **102**:13944–9. doi:10.1073/pnas.0506654102

38. Adams BD, Furneaux H, White BA. The micro-ribonucleic acid (miRNA) miR-206 targets the human estrogen receptor-α (ERα) and represses ERα messenger RNA and protein expression in breast cancer cell lines. *Mol Endocrinol* (2007) **21**:1132–47. doi:10.1210/me.2007-0022

39. Adams BD, Wali VB, Cheng CJ, Inukai S, Booth CJ, Agarwal S, et al. miR-34a silences c-SRC to attenuate tumor growth in triple-negative breast cancer. *Cancer Res* (2016) **76**:927–39. doi:10.1158/0008-5472.can-15-2321

40. Statello L, Guo CJ, Chen LL, Huarte M. Gene regulation by long non-coding RNAs and its biological functions. *Nat Rev Mol Cel Biol.* (2021) **22**:96–118. doi:10.1038/s41580-020-00315-9

41. Ren B, Guan MX, Zhou T, Cai X, Shan G. Emerging functions of mitochondria-encoded non-coding RNAs. *Trends Genet* (2023) **39**:125–39. doi:10.1016/j.tig.2022.08.004

42. Vendramin R, Marine JC, Leucci E. Non-coding RNAs: the dark side of nuclear-mitochondrial communication. *EMBO J* (2017) **36**:1123–33. doi:10.15252/embj.201695546

43. Leung AKL. The whereabouts of microRNA actions: cytoplasm and beyond. *Trends Cel Biol* (2015) **25**:601–10. doi:10.1016/j.tcb.2015.07.005

44. Liu H, Lei C, He Q, Pan Z, Xiao D, Tao Y. Nuclear functions of mammalian MicroRNAs in gene regulation, immunity and cancer. *Mol Cancer* (2018) **17**:64. doi:10.1186/s12943-018-0765-5

45. Kim KM, Noh JH, Abdelmohsen K, Gorospe M. Mitochondrial non-coding RNA transport. *BMB Rep* (2017) **50**:164–74. doi:10.5483/bmbrep.2017.50.4.013

46. Yang C, Shen C, Feng T, Li H. Non-coding RNA in NK cells. *J Leukoc Biol* (2018) **105**:63–71. doi:10.1002/jlb.1ru0518-197rr

47. Safi A, Saberiyan M, Sanaei MJ, Adelian S, Davarani Asl F, Zeinaly M, et al. The role of non-coding RNAs in metabolic reprogramming of cancer cells. *Cell. Mol. Biol. Lett* (2023) **28**:37. doi:10.1186/s11658-023-00447-8

48. Marchese FP, Raimondi I, Huarte M. The multidimensional mechanisms of long non-coding RNA function. *Genome Biol* (2017) **18**:206. doi:10.1186/s13059-017-1348-2

49. Castel SE, Martienssen RA. RNA interference in the nucleus: roles for small RNAs in transcription, epigenetics and beyond. *Nat Rev Genet* (2013) **14**:100–12. doi:10.1038/nrg3355

50. Roberts TC. The MicroRNA biology of the mammalian nucleus. *Mol Ther - Nucleic Acids* (2014) **3**:e188. doi:10.1038/mtna.2014.40

51. Song Z, Lin J, Li Z, Huang C. The nuclear functions of long non-coding RNAs come into focus. *Non-coding RNA Res* (2021) **6**:70–9. doi:10.1016/j.ncrna.2021.03.002

52. Khosraviani N, Ostrowski LA, Mekhail K. Roles for non-coding RNAs in spatial genome organization. *Front Cel Dev. Biol.* (2019) **7**:336. doi:10.3389/fcell.2019.00336

53. Durut N, Mittelsten Scheid O. The role of non-coding RNAs in double-strand break repair. *Front Plant Sci* (2019) **10**:1155. doi:10.3389/fpls.2019.01155

54. Mercer TR, Dinger ME, Mattick JS. Long non-coding RNAs: insights into functions. *Nat Rev Genet* (2009) **10**:155–9. doi:10.1038/nrg2521

55. Rinn JL, Kertesz M, Wang JK, Squazzo SL, Xu X, Brugmann SA, et al. Functional demarcation of active and silent chromatin domains in human HOX loci by noncoding RNAs. *Cell* (2007) **129**:1311–23. doi:10.1016/j.cell.2007.05.022

56. Okamoto I, Nakamura T, Sasaki K, Yabuta Y, Iwatani C, Tsuchiya H, et al. The X chromosome dosage compensation program during the development of cynomolgus monkeys. *Science* (2021) **374**:eabd8887. doi:10.1126/science.abd8887

57. Shi T, Gao G, Cao Y. Long noncoding RNAs as novel biomarkers have a promising future in cancer diagnostics. *Dis Markers* (2016) **2016**:1–10. doi:10.1155/2016/9085195

58. Brown CJ, Hendrich BD, Rupert JL, Lafrenière RG, Xing Y, Lawrence J, et al. The human XIST gene: analysis of a 17 kb inactive X-specific RNA that contains conserved repeats and is highly localized within the nucleus. *Cell* (1992) **71**:527–42. doi:10.1016/0092-8674(92)90520-m

59. The ENCODE Project Consortium. An integrated encyclopedia of DNA elements in the human genome. *Nature* (2012) **489**:57–74. doi:10.1038/nature11247

60. Cech TR, Steitz JA. The noncoding RNA revolution-trashing old rules to forge new ones. *Cell* (2014) **157**:77–94. doi:10.1016/j.cell.2014.03.008

61. Ha M, Kim VN. Regulation of microRNA biogenesis. *Nat Rev Mol Cel Biol* (2014) **15**:509–24. doi:10.1038/nrm3838

62. Kim YK, Kim VN. Processing of intronic microRNAs. *EMBO J* (2007) **26**:775–83. doi:10.1038/sj.emboj.7601512

63. Friedländer MR, Lizano E, Houben AJ, Bezdan D, Báñez-Coronel M, Kudla G, et al. Evidence for the biogenesis of more than 1,000 novel human microRNAs. *Genome Biol* (2014) **15**:R57. doi:10.1186/gb-2014-15-4-r57

64. Davis-Dusenbery BN, Hata A. Mechanisms of control of microRNA biogenesis. *J Biochem* (2010) **148**:381–92. doi:10.1093/jb/mvq096

65. Ambros V, Horvitz HR. The lin-14 locus of *Caenorhabditis elegans* controls the time of expression of specific postembryonic developmental events. *Genes Dev* (1987) **1**:398–414. doi:10.1101/gad.1.4.398

66. Lee Y, Ahn C, Han J, Choi H, Kim J, Yim J, et al. The nuclear RNase III Drosha initiates microRNA processing. *Nature* (2003) **425**:415–9. doi:10.1038/nature01957

67. Westholm JO, Lai EC. Mirtrons: microRNA biogenesis via splicing. *Biochimie* (2011) **93**:1897–904. doi:10.1016/j.biochi.2011.06.017

68. Michlewski G, Cáceres JF. Post-transcriptional control of miRNA biogenesis. *RNA* (2019) **25**:1–16. doi:10.1261/rna.068692.118

69. Quick-Cleveland J, Jacob J, Weitz S, Shoffner G, Senturia R, Guo F. The DGCR8 RNA-binding heme domain recognizes primary microRNAs by clamping the hairpin. *Cel Rep* (2014) **7**:1994–2005. doi:10.1016/j.celrep.2014.05.013

70. Creugny A, Fender A, Pfeffer S. Regulation of primary microRNA processing. *FEBS Lett* (2018) **592**:1980–96. doi:10.1002/1873-3468.13067

71. Zeng Y, Cullen BR. Efficient processing of primary microRNA hairpins by Drosha requires flanking nonstructured RNA sequences. *J Biol Chem* (2005) **280**:27595–603. doi:10.1074/jbc.m504714200

72. Denli AM, Tops BB, Plasterk RH, Ketting RF, Hannon GJ. Processing of primary microRNAs by the Microprocessor complex. *Nature* (2004) **432**:231–5. doi:10.1038/nature03049

73. Ruby JG, Jan CH, Bartel DP. Intronic microRNA precursors that bypass Drosha processing. *Nature* (2007) **448**:83–6. doi:10.1038/nature05983

74. Seitz H, Zamore PD. Rethinking the microprocessor. *Cell* (2006) **125**:827–9. doi:10.1016/j.cell.2006.05.018

75. Stavast CJ, Erkeland SJ. The non-canonical aspects of MicroRNAs: many roads to gene regulation. *Cells* (2019) **8**:1465. doi:10.3390/cells8111465

76. Martin R, Smibert P, Yalcin A, Tyler DM, Schäfer U, Tuschl T, et al. A Drosophila pasha mutant distinguishes the canonical microRNA and mirtron pathways. *Mol Cell Biol* (2009) **29**:861–70. doi:10.1128/mcb.01524-08

77. Hutvagner G, McLachlan J, Pasquinelli AE, Balint E, Tuschl T, Zamore PD. A cellular function for the RNA-interference enzyme Dicer in the maturation of the let-7 small temporal RNA. *Science* (2001) **293**:834–8. doi:10.1126/science.1062961

78. Haase AD, Jaskiewicz L, Zhang H, Lainé S, Sack R, Gatignol A, et al. TRBP, a regulator of cellular PKR and HIV-1 virus expression, interacts with Dicer and functions in RNA silencing. *EMBO Rep* (2005) **6**:961–7. doi:10.1038/sj.embor.7400509

79. Koscianska E, Starega-Roslan J, Krzyzosiak WJ. The role of Dicer protein partners in the processing of microRNA precursors. *PLoS One* (2011) **6**:e28548. doi:10.1371/journal.pone.0028548

80. Khvorova A, Reynolds A, Jayasena SD. Functional siRNAs and miRNAs exhibit strand bias. *Cell* (2003) **115**:505–216. doi:10.1016/s0092-8674(03)00893-6

81. Schwarz DS, Hutvágner G, Du T, Xu Z, Aronin N, Zamore PD. Asymmetry in the assembly of the RNAi enzyme complex. *Cell* (2003) **115**:199–208. doi:10.1016/s0092-8674(03)00759-1

82. Betancur JG, Yoda M, Tomari Y. miRNA-like duplexes as RNAi triggers with improved specificity. *Front Genet* (2012) **3**:127. doi:10.3389/fgene.2012.00127

83. Wang P, Zhou Y, Richards AM. Effective tools for RNA-derived therapeutics: siRNA interference or miRNA mimicry. *Theranostics* (2021) **11**:8771–96. doi:10.7150/thno.62642

84. Lam JK, Chow MY, Zhang Y, Leung SW. siRNA versus miRNA as therapeutics for gene silencing. *Mol Ther - Nucleic Acids* (2015) **4**:e252. doi:10.1038/mtna.2015.23

85. Bajan S, Hutvagner G. RNA-based therapeutics: from antisense oligonucleotides to miRNAs. *Cells* (2020) **9**:137. doi:10.3390/cells9010137

86. Shyu AB, Wilkinson MF, van Hoof A. Messenger RNA regulation: to translate or to degrade. *EMBO J* (2008) **27**:471–81. doi:10.1038/sj.emboj.7601977

87. Bag J. Feedback inhibition of poly(A)-binding protein mRNA translation. *J Biol Chem* (2001) **276**:47352–60. doi:10.1074/jbc.m107676200

88. Di Liegro CM, Schiera G, Di Liegro I. Regulation of mRNA transport, localization and translation in the nervous system of mammals (Review). *Int J Mol Med* (2014) **33**:747–62. doi:10.3892/ijmm.2014.1629

89. Tai HC, Schuman EM. MicroRNA: microRNAs reach out into dendrites. *Curr Biol* (2006) **16**:R121–R123. doi:10.1016/j.cub.2006.02.006

90. Catalanotto C, Cogoni C, Zardo G. MicroRNA in control of gene expression: an overview of nuclear functions. *Int J Mol Sci* (2016) **17**:1712. doi:10.3390/ijms17101712

91. Ritland Politz JC, Hogan EM, Pederson T. MicroRNAs with a nucleolar location. *RNA* (2009) **15**:1705–15. doi:10.1261/rna.1470409

92. Ding Q, Markesbery WR, Chen Q, Li F, Keller JN. Ribosome dysfunction is an early event in Alzheimer's disease. *J Neurosci* (2005) **25**:9171–5. doi:10.1523/jneurosci.3040-05.2005

93. Jin J, Li GJ, Davis J, Zhu D, Wang Y, Pan C, et al. Identification of novel proteins associated with both α-synuclein and DJ-1. *Mol Cell Proteomics* (2007) **6**:845–59. doi:10.1074/mcp.m600182-mcp200

94. Doxakis E. Post-transcriptional regulation of α-synuclein expression by mir-7 and mir-153. *J Biol Chem* (2010) **285**:12726–34. doi:10.1074/jbc.m109.086827

95. Wild EJ, Tabrizi SJ. Therapies targeting DNA and RNA in Huntington's disease. *Lancet Neurol* (2017) **16**:837–47. doi:10.1016/s1474-4422(17)30280-6

96. Ashizawa T, Öz G, Paulson HL. Spinocerebellar ataxias: prospects and challenges for therapy development. *Nat Rev Neurol* (2018) **14**:590–605. doi:10.1038/s41582-018-0051-6

97. Niranjan R. Recent advances in the mechanisms of neuroinflammation and their roles in neurodegeneration. *Neurochem Int* (2018) **120**:13–20. doi:10.1016/j.neuint.2018.07.003

98. Chen L, Deng H, Cui H, Fang J, Zuo Z, Deng J, et al. Inflammatory responses and inflammation-associated diseases in organs. *Oncotarget* (2017) **9**:7204–18. doi:10.18632/oncotarget.23208

99. Wang AP, Tian Y, Zhang W, Tian T, Gong SX, Huang WQ, et al. Microglia-associated neuroinflammation is a potential therapeutic target for ischemic stroke. *Neural Regen Res* (2021) **16**:6–11. doi:10.4103/1673-5374.286954

100. Bachiller S, Jiménez-Ferrer I, Paulus A, Yang Y, Swanberg M, Deierborg T, et al. Microglia in neurological diseases: a road map to brain-disease dependent-inflammatory response. *Front Cel Neurosci.* (2018) **12**:488. doi:10.3389/fncel.2018.00488

101. Li Y, Zhou D, Ren Y, Zhang Z, Guo X, Ma M, et al. Mir223 restrains autophagy and promotes CNS inflammation by targeting ATG16L1. *Autophagy* (2019) **15**:478–92. doi:10.1080/15548627.2018.1522467

102. Shao F, Wang X, Wu H, Wu Q, Zhang J. Microglia and neuroinflammation: crucial pathological mechanisms in traumatic brain injury-induced

neurodegeneration. *Front Aging Neurosci* (2022) **14**:825086. doi:10.3389/fnagi.2022.825086

103. Cherry JD, Olschowka JA, O'Banion MK. Neuroinflammation and M2 microglia: the good, the bad, and the inflamed. *J Neuroinflammation* (2014) **11**:98. doi:10.1186/1742-2094-11-98

104. Zhang H, Su Y, Sun Z, Chen M, Han Y, Li Y, et al. Ginsenoside Rg1 alleviates Aβ deposition by inhibiting NADPH oxidase 2 activation in APP/PS1 mice. *J Ginseng Res* (2021) **45**:665–75. doi:10.1016/j.jgr.2021.03.003

105. Kumar A, Barrett JP, Alvarez-Croda DM, Stoica BA, Faden AI, Loane DJ. NOX2 drives M1-like microglial/macrophage activation and neurodegeneration following experimental traumatic brain injury. *Brain Behav Immun* (2016) **58**:291–309. doi:10.1016/j.bbi.2016.07.158

106. Undi RB, Kandi R, Gutti RK. MicroRNAs as haematopoiesis regulators. *Adv Hematol* (2013) **2013**:1–20. doi:10.1155/2013/695754

107. Rougvie AE, Moss EG. Developmental transitions in *C. elegans* larval stages. *Curr Top Dev Biol* (2013) **105**:153–80. doi:10.1016/B978-0-12-396968-2.00006-3

108. Han D, Dong X, Zheng D, Nao J. MiR-124 and the underlying therapeutic promise of neurodegenerative disorders. *Front Pharmacol* (2019) **10**:1555. doi:10.3389/fphar.2019.01555

109. Liu T, Zhang L, Joo D, Sun SC. NF-κB signaling in inflammation. *Signal Transduction Targeted Ther* (2017) **2**:17023. doi:10.1038/sigtrans.2017.23

110. Zingale VD, Gugliandolo A, Mazzon E. MiR-155: an important regulator of neuroinflammation. *Int J Mol Sci* (2021) **23**:90. doi:10.3390/ijms23010090

111. Banzhaf-Strathmann J, Benito E, May S, Arzberger T, Tahirovic S, Kretzschmar H, et al. Micro RNA -125b induces tau hyperphosphorylation and cognitive deficits in Alzheimer's disease. *EMBO J* (2014) **33**:1667–80. doi:10.15252/embj.201387576

112. Fu M, Tao J, Wang D, Zhang Z, Wang X, Ji Y, et al. Downregulation of MicroRNA-34c-5p facilitated neuroinflammation in drug-resistant epilepsy. *Brain Res* (2020) **1749**:147130. doi:10.1016/j.brainres.2020.147130

113. Ghafouri-Fard S, Hussen BM, Abak A, Taheri M, Jalili Khoshnoud R. Aberrant expression of miRNAs in epilepsy. *Mol Biol Rep* (2022) **49**:5057–74. doi:10.1007/s11033-022-07188-5

114. Cai LJ, Tu L, Li T, Yang XL, Ren YP, Gu R, et al. Up-regulation of microRNA-375 ameliorates the damage of dopaminergic neurons, reduces oxidative stress and inflammation in Parkinson's disease by inhibiting SP1. *Aging* (2020) **12**:672–89. doi:10.18632/aging.102649

115. Wang X, Liu Z, Wang F. MicroRNA-93 blocks signal transducers and activator of transcription 3 to reduce neuronal damage in Parkinson's disease. *Neurochem Res* (2021) **46**:1859–68. doi:10.1007/s11064-021-03333-x

116. Iadecola C. The pathobiology of vascular dementia. *Neuron* (2013) **80**:844–66. doi:10.1016/j.neuron.2013.10.008

117. Mao S, Wu J, Yan J, Zhang W, Zhu F. Dysregulation of miR-146a: a causative factor in epilepsy pathogenesis, diagnosis, and prognosis. *Front Neurol* (2023) **14**:1094709. doi:10.3389/fneur.2023.1094709

118. Tao H, Zhao J, Liu T, Cai Y, Zhou X, Xing H, et al. Intranasal delivery of miR-146a mimics delayed seizure onset in the lithium-pilocarpine mouse model. *Mediators Inflamm* (2017) **2017**:1–10. doi:10.1155/2017/6512620

119. Mukhtar I. Inflammatory and immune mechanisms underlying epileptogenesis and epilepsy: from pathogenesis to treatment target. *Seizure* (2020) **82**:65–79. doi:10.1016/j.seizure.2020.09.015

120. Zhang P-F, Gao F. Neuroinflammation in Parkinson's disease: a meta-analysis of PET imaging studies. *J Neurol* (2022) **269**:2304–14. doi:10.1007/s00415-021-10877-z

121. Wang J, Yu JT, Tan L, Tian Y, Ma J, Tan CC, et al. Genome-wide circulating microRNA expression profiling indicates biomarkers for epilepsy. *Sci Rep* (2015) **5**:9522. doi:10.1038/srep09522

122. Faraoni I, Antonetti FR, Cardone J, Bonmassar E. miR-155 gene: a typical multifunctional microRNA. *Biochim Biophys Acta (Bba) - Mol Basis Dis* (2009) **1792**:497–505. doi:10.1016/j.bbadis.2009.02.013

123. Tam W, Ben-Yehuda D, Hayward WS. bic, a novel gene activated by proviral insertions in avian leukosis virus-induced lymphomas, is likely to function through its noncoding RNA. *Mol Cell Biol* (1997) **17**:1490–502. doi:10.1128/mcb.17.3.1490

124. Kim VN, Han J, Siomi MC. Biogenesis of small RNAs in animals. *Nat Rev Mol Cel Biol* (2009) **10**:126–39. doi:10.1038/nrm2632

125. Mahesh G, Biswas R. MicroRNA-155: a master regulator of inflammation. *J Interferon Cytokine Res* (2019) **39**:321–30. doi:10.1089/jir.2018.0155

126. Guil S, Cáceres JF. The multifunctional RNA-binding protein hnRNP A1 is required for processing of miR-18a. *Nat Struct Mol Biol* (2007) **14**:591–6. doi:10.1038/nsmb1250

127. Condrat CE, Thompson DC, Barbu MG, Bugnar OL, Boboc A, Cretoiu D, et al. miRNAs as biomarkers in disease: latest findings regarding their role in diagnosis and prognosis. *Cells* (2020) **9**:276. doi:10.3390/cells9020276

128. Paudel S, Ghimire L, Jin L, Jeansonne D, Jeyaseelan S. Regulation of emergency granulopoiesis during infection. *Front Immunol* (2022) **13**:961601. doi:10.3389/fimmu.2022.961601

129. Zhao J, He Z, Wang J. MicroRNA-124: a key player in microglia-mediated inflammation in neurological diseases. *Front Cel Neurosci.* (2021) **15**:771898. doi:10.3389/fncel.2021.771898

130. Amici SA, Dong J, Guerau-de-Arellano M. Molecular mechanisms modulating the phenotype of macrophages and microglia. *Front Immunol* (2017) **8**:1520. doi:10.3389/fimmu.2017.01520

131. Magner E, Sandoval-Sanchez P, Kramer AC, Thummel R, Hitchcock PF, Taylor SM. Disruption of miR-18a alters proliferation, photoreceptor replacement kinetics, inflammatory signaling, and microglia/macrophage numbers during retinal regeneration in zebrafish. *Mol Neurobiol* (2022) **59**:2910–31. doi:10.1007/s12035-022-02783-w

132. Reichardt SD, Amouret A, Muzzi C, Vettorazzi S, Tuckermann JP, Lühder F, et al. The role of glucocorticoids in inflammatory diseases. *Cells* (2021) **10**:2921. doi:10.3390/cells10112921

133. Wen Q, Wang Y, Pan Q, Tian R, Zhang D, Qin G, et al. MicroRNA-155-5p promotes neuroinflammation and central sensitization via inhibiting SIRT1 in a nitroglycerin-induced chronic migraine mouse model. *J Neuroinflammation* (2021) **18**:287. doi:10.1186/s12974-021-02342-5

134. Tang R, Li L, Zhu D, Hou D, Cao T, Gu H, et al. Mouse miRNA-709 directly regulates miRNA-15a/16-1 biogenesis at the posttranscriptional level in the nucleus: evidence for a microRNA hierarchy system. *Cell Res* (2012) **22**:504–15. doi:10.1038/cr.2011.137

135. Kompotis K, Mang GM, Hubbard J, Jimenez S, Emmenegger Y, Polysopoulos C, et al. Cortical mir-709 links glutamatergic signaling to NREM sleep EEG slow waves in an activity-dependent manner. *bioRxi* (2022). doi:10.1101/2022.09.24.508386

136. Johansson K, Gagnon JD, Zhou S, Fassett MS, Schroeder AW, Kageyama R, et al. An essential role for miR-15/16 in Treg suppression and restriction of proliferation (2023). bioRxiv 533356. Available at: https://doi.org/10.1101/2023.03.26.533356.

137. Sameer AS, Nissar S. Toll-like receptors (TLRs): structure, functions, signaling, and role of their polymorphisms in colorectal cancer susceptibility. *Biomed Res Int* (2021) **2021**:1–14. doi:10.1155/2021/1157023

138. Duan T, Du Y, Xing C, Wang HY, Wang RF. Toll-like receptor signaling and its role in cell-mediated immunity. *Front Immunol* (2022) **13**:812774. doi:10.3389/fimmu.2022.812774

139. Moon HG, Yang J, Zheng Y, Jin Y. miR-15a/16 regulates macrophage phagocytosis after bacterial infection. *J Immunol* (2014) **193**:4558–67. doi:10.4049/jimmunol.1401372

140. Nahid MA, Satoh M, Chan EK. MicroRNA in TLR signaling and endotoxin tolerance. *Cell. Mol. Immunol.* (2011) **8**:388–403. doi:10.1038/cmi.2011.26

141. Pascual M, Calvo-Rodriguez M, Núñez L, Villalobos C, Ureña J, Guerri C. Toll-like receptors in neuroinflammation, neurodegeneration, and alcohol-induced brain damage. *IUBMB Life* (2021) **73**:900–15. doi:10.1002/iub.2510

142. Myers CT, Mefford HC. Advancing epilepsy genetics in the genomic era. *Genome Med* (2015) **7**:91. doi:10.1186/s13073-015-0214-7

143. Bamikole OJ, Olufeagba MDB, Soge ST, Bukoye NO, Olajide T, Ademola SA, et al. Genetics of epilepsy. *J Neurol Neurophysiol* (2019) **10**:3.

144. Wang S, He X, Bao N, Chen M, Ding X, Zhang M, et al. Potentials of miR-9-5p in promoting epileptic seizure and improving survival of glioma patients. *Acta Epileptologica* (2022) **4**:33. doi:10.1186/s42494-022-00097-x

145. Thijs RD, Surges R, O'Brien TJ, Sander JW, Epilepsy JW. Epilepsy in adults. *The Lancet* (2019) **393**:689–701. doi:10.1016/s0140-6736(18)32596-0

146. Beghi E. The epidemiology of epilepsy. *Neuroepidemiology* (2019) **54**:185–91. doi:10.1159/000503831

147. Fisher RS, Acevedo C, Arzimanoglou A, Bogacz A, Cross JH, Elger CE, et al. ILAE Official Report: a practical clinical definition of epilepsy. *Epilepsia* (2014) **55**:475–82. doi:10.1111/epi.12550

148. Scheffer IE, Berkovic S, Capovilla G, Connolly MB, French J, Guilhoto L, et al. ILAE classification of the epilepsies: position paper of the ILAE commission for classification and terminology. *Epilepsia* (2017) **58**:512–21. doi:10.1111/epi.13709

149. Wang J, Zhao J. MicroRNA dysregulation in epilepsy: from pathogenetic involvement to diagnostic biomarker and therapeutic agent development. *Front Mol Neurosci* (2021) **14**:650372. doi:10.3389/fnmol.2021.650372

150. Menezes LFS, Sabiá Júnior EF, Tibery DV, Carneiro LDA, Schwartz EF. Epilepsy-related voltage-gated sodium channelopathies: a review. *Front Pharmacol* (2020) **11**:1276. doi:10.3389/fphar.2020.01276

151. Thakran S, Guin D, Singh P, Singh P, Kukal S, Rawat C, et al. Genetic landscape of common epilepsies: advancing towards precision in treatment. *Int J Mol Sci* (2020) **21**:7784. doi:10.3390/ijms21207784

152. Samanta D. DEPDC5-related epilepsy: a comprehensive review. *Epilepsy Behav* (2022) **130**:108678. doi:10.1016/j.yebeh.2022.108678

153. Zsindely N, Nagy G, Siági F, Farkas A, Bodai L. Dysregulated miRNA and mRNA expression affect overlapping pathways in a Huntington's disease model. *Int J Mol Sci* (2023) **24**:11942. doi:10.3390/ijms241511942

154. Fukuoka M, Takahashi M, Fujita H, Chiyo T, Popiel HA, Watanabe S, et al. Supplemental treatment for Huntington's disease with miR-132 that is deficient in Huntington's disease brain. *Mol Ther - Nucleic Acids* (2018) **11**:79–90. doi:10.1016/j.omtn.2018.01.007

155. Hart M, Diener C, Lunkes L, Rheinheimer S, Krammes L, Keller A, et al. miR-34a-5p as molecular hub of pathomechanisms in Huntington's disease. *Mol Med* (2023) **29**:43. doi:10.1186/s10020-023-00640-7

156. Hoss AG, Labadorf A, Latourelle JC, Kartha VK, Hadzi TC, Gusella JF, et al. miR-10b-5p expression in Huntington's disease brain relates to age of onset and the extent of striatal involvement. *BMC Med Genomics* (2015) **8**:10. doi:10.1186/s12920-015-0083-3

157. Chang K-H, Wu Y-R, Chen C-M. Down-regulation of miR-9* in the peripheral leukocytes of Huntington's disease patients. *Orphanet J Rare Dis* (2017) **12**:185. doi:10.1186/s13023-017-0742-x

158. Sengupta JN, Pochiraju S, Kannampalli P, Bruckert M, Addya S, Yadav P, et al. MicroRNA-mediated GABA Aα-1 receptor subunit down-regulation in adult spinal cord following neonatal cystitis-induced chronic visceral pain in rats. *Pain* (2013) **154**:59–70. doi:10.1016/j.pain.2012.09.002

159. Rho JM, White HS. Brief history of anti-seizure drug development. *Epilepsia Open* (2018) **3**:114–9. doi:10.1002/epi4.12268

160. Henshall DC, Hamer HM, Pasterkamp RJ, Goldstein DB, Kjems J, Prehn JHM, et al. MicroRNAs in epilepsy: pathophysiology and clinical utility. *Lancet Neurol* (2016) **15**:1368–76. doi:10.1016/s1474-4422(16)30246-0

161. Jimenez-Mateos EM, Engel T, Merino-Serrais P, McKiernan RC, Tanaka K, Mouri G, et al. Silencing microRNA-134 produces neuroprotective and prolonged seizure-suppressive effects. *Nat Med* (2012) **18**:1087–94. doi:10.1038/nm.2834

162. Lu J, Zhou N, Yang P, Deng L, Liu G. MicroRNA-27a-3p downregulation inhibits inflammatory response and hippocampal neuronal cell apoptosis by upregulating mitogen-activated protein kinase 4 (MAP2K4) expression in epilepsy: *in vivo* and *in vitro* studies. *Med Sci Monit* (2019) **25**:8499–508. doi:10.12659/msm.916458

163. Ashhab MU, Omran A, Kong H, Gan N, He F, Peng J, et al. Expressions of tumor necrosis factor alpha and MicroRNA-155 in immature rat model of status epilepticus and children with mesial temporal lobe epilepsy. *J Mol Neurosci* (2013) **51**:950–8. doi:10.1007/s12031-013-0013-9

164. Loffreda A, Nizzardo M, Arosio A, Ruepp MD, Calogero RA, Volinia S, et al. miR-129-5p: a key factor and therapeutic target in amyotrophic lateral sclerosis. *Prog Neurobiol* (2020) **190**:101803. doi:10.1016/j.pneurobio.2020.101803

165. Matamala JM, Arias-Carrasco R, Sanchez C, Uhrig M, Bargsted L, Matus S, et al. Genome-wide circulating microRNA expression profiling reveals potential biomarkers for amyotrophic lateral sclerosis. *Neurobiol Aging* (2018) **64**:123–38. doi:10.1016/j.neurobiolaging.2017.12.020

166. Sturmey E, Malaspina A. Blood biomarkers in ALS: challenges, applications and novel frontiers. *Acta Neurol Scand* (2022) **146**:375–88. doi:10.1111/ane.13698

167. Butovsky O, Siddiqui S, Gabriely G, Lanser AJ, Dake B, Murugaiyan G, et al. Modulating inflammatory monocytes with a unique microRNA gene signature ameliorates murine ALS. *J Clin Invest* (2012) **122**:3063–87. doi:10.1172/jci62636

168. Pinto S, Cunha C, Barbosa M, Vaz AR, Brites D. Exosomes from NSC-34 cells transfected with hSOD1-g93a are enriched in miR-124 and drive alterations in microglia phenotype. *Front Neurosci* (2017) **11**:273. doi:10.3389/fnins.2017.00273

169. Li C, Wei Q, Gu X, Chen Y, Chen X, Cao B, et al. Decreased glycogenolysis by miR-338-3p promotes regional glycogen accumulation within the spinal cord of amyotrophic lateral sclerosis mice. *Front Mol Neurosci* (2019) **12**:114. doi:10.3389/fnmol.2019.00114

170. Zhou F, Zhang C, Guan Y, Chen Y, Lu Q, Jie L, et al. Screening the expression characteristics of several miRNAs in *G93A-SOD1* transgenic mouse: altered expression of miRNA-124 is associated with astrocyte differentiation by targeting Sox2 and Sox9. *J Neurochem* (2018) **145**:51–67. doi:10.1111/jnc.14229

171. Ravnik-Glavač M, Glavač D. Circulating RNAs as potential biomarkers in amyotrophic lateral sclerosis. *Int J Mol Sci* (2020) **21**:1714. doi:10.3390/ijms21051714

172. Freischmidt A, Müller K, Ludolph AC, Weishaupt JH. Systemic dysregulation of TDP-43 binding microRNAs in amyotrophic lateral sclerosis. *Acta Neuropathol Commun* (2013) **1**:42. doi:10.1186/2051-5960-1-42

173. Jankovic J. Parkinson's disease: clinical features and diagnosis. *J Neurol Neurosurg Psychiatry* (2008) **79**:368–76. doi:10.1136/jnnp.2007.131045

174. De Lau LM, Breteler MM. Epidemiology of Parkinson's disease. *Lancet Neurol* (2006) **5**:525–35. doi:10.1016/s1474-4422(06)70471-9

175. Lu B, Gehrke S, Wu Z. RNA metabolism in the pathogenesis of Parkinson′s disease. *Brain Res* (2014) **1584**:105–15. doi:10.1016/j.brainres.2014.03.003

176. Singh N, Pillay V, Choonara YE. Advances in the treatment of Parkinson's disease. *Prog Neurobiol* (2007) **81**:29–44. doi:10.1016/j.pneurobio.2006.11.009

177. Schetters STT, Gomez-Nicola D, Garcia-Vallejo JJ, Van Kooyk Y. Neuroinflammation: microglia and T cells get ready to tango. *Front Immunol* (2017) **8**:1905. doi:10.3389/fimmu.2017.01905

178. Rasheed M, Liang J, Wang C, Deng Y, Chen Z. Epigenetic regulation of neuroinflammation in Parkinson's disease. *Int J Mol Sci* (2021) **22**:4956. doi:10.3390/ijms22094956

179. Yao L, Zhu Z, Wu J, Zhang Y, Zhang H, Sun X, et al. MicroRNA-124 regulates the expression of p62/p38 and promotes autophagy in the inflammatory pathogenesis of Parkinson's disease. *FASEB J* (2019) **33**:8648–65. doi:10.1096/fj.201900363r

180. Thome AD, Harms AS, Volpicelli-Daley LA, Standaert DG. microRNA-155 regulates alpha-synuclein-induced inflammatory responses in models of Parkinson disease. *J Neurosci* (2016) **36**:2383–90. doi:10.1523/jneurosci.3900-15.2016

181. Caggiu E, Paulus K, Mameli G, Arru G, Sechi GP, Sechi LA. Differential expression of miRNA 155 and miRNA 146a in Parkinson's disease patients. *eNeurologicalSci* (2018) **13**:1–4. doi:10.1016/j.ensci.2018.09.002

182. Saraiva C, Paiva J, Santos T, Ferreira L, Bernardino L. MicroRNA-124 loaded nanoparticles enhance brain repair in Parkinson's disease. *J Controlled Release* (2016) **235**:291–305. doi:10.1016/j.jconrel.2016.06.005

183. Fragkouli A, Doxakis E. miR-7 and miR-153 protect neurons against MPP+-induced cell death via upregulation of mTOR pathway. *Front Cel Neurosci.* (2014) **8**:182. doi:10.3389/fncel.2014.00182

184. Kabaria S, Choi DC, Chaudhuri AD, Mouradian MM, Junn E. Inhibition of miR-34b and miR-34c enhances α-synuclein expression in Parkinson's disease. *FEBS Lett* (2015) **589**:319–25. doi:10.1016/j.febslet.2014.12.014

185. Miñones-Moyano E, Porta S, Escaramís G, Rabionet R, Iraola S, Kagerbauer B, et al. MicroRNA profiling of Parkinson's disease brains identifies early downregulation of miR-34b/c which modulate mitochondrial function. *Hum Mol Genet* (2011) **20**:3067–78. doi:10.1093/hmg/ddr210

186. Alexandrov PN, Dua P, Hill JM, Bhattacharjee S, Zhao Y, Lukiw WJ. microRNA (miRNA) speciation in Alzheimer's disease (AD) cerebrospinal fluid (CSF) and extracellular fluid (ECF). *Int J Biochem Mol Biol* (2012) **3**:365–73.

187. Liu D, Zhao D, Zhao Y, Wang Y, Zhao Y, Wen C. Inhibition of microRNA-155 alleviates cognitive impairment in Alzheimer's disease and involvement of neuroinflammation. *Curr Alzheimer Res* (2019) **16**:473–82. doi:10.2174/1567205016666190503145207

188. Aloi MS, Prater KE, Sopher B, Davidson S, Jayadev S, Garden GA. The pro-inflammatory microRNA miR -155 influences fibrillar β-Amyloid $_{1-42}$ catabolism by microglia. *Glia* (2021) **69**:1736–48. doi:10.1002/glia.23988

189. Zheng X, Huang H, Liu J, Li M, Liu M, Luo T. Propofol attenuates inflammatory response in LPS-activated microglia by regulating the miR-155/SOCS1 pathway. *Inflammation* (2018) **41**:11–9. doi:10.1007/s10753-017-0658-6

190. Song Y, Hu M, Zhang J, Teng Z, Chen C. A novel mechanism of synaptic and cognitive impairments mediated via microRNA-30b in Alzheimer's disease. *EBioMedicine* (2019) **39**:409–21. doi:10.1016/j.ebiom.2018.11.059

191. Wang X, Liu D, Huang HZ, Wang ZH, Hou TY, Yang X, et al. A novel MicroRNA-124/PTPN1 signal pathway mediates synaptic and memory deficits in Alzheimer's disease. *Biol Psychiatry* (2018) **83**:395–405. doi:10.1016/j.biopsych.2017.07.023

192. Vijverberg EGB, Wattjes MP, Dols A, Krudop WA, Möller C, Peters A, et al. Diagnostic accuracy of MRI and additional [18F]FDG-PET for behavioral variant frontotemporal dementia in patients with late onset behavioral changes. *J Alzheimer's Dis* (2016) **53**:1287–97. doi:10.3233/jad-160285

193. Peplow P, Martinez B. MicroRNA biomarkers in frontotemporal dementia and to distinguish from Alzheimer's disease and amyotrophic lateral sclerosis. *Neural Regen Res* (2022) **17**:1412. doi:10.4103/1673-5374.330591

194. Wolters FJ, Ikram MA. Epidemiology of vascular dementia. *Arterioscler Thromb Vasc Biol* (2019) **39**:1542–9. doi:10.1161/atvbaha.119.311908

195. Xu N, Li AD, Ji LL, Ye Y, Wang ZY, Tong L. miR-132 regulates the expression of synaptic proteins in APP/PS1 transgenic mice through C1q. *Eur J Histochem* (2019) **63**:3008. doi:10.4081/ejh.2019.3008

196. Zhao Y, Bhattacharjee S, Jones BM, Dua P, Alexandrov PN, Hill JM, et al. Regulation of TREM2 expression by an NF-κB-sensitive miRNA-34a. *NeuroReport* (2013) **24**:318–23. doi:10.1097/wnr.0b013e32835fb6b0

197. McColgan P, Tabrizi S. Huntington's disease: a clinical review. *Eur J Neurol* (2018) **25**:24–34. doi:10.1111/ene.13413

198. Le Cann K, Foerster A, Rösseler C, Erickson A, Hautvast P, Giesselmann S, et al. The difficulty to model Huntington's disease *in vitro* using striatal medium spiny neurons differentiated from human induced pluripotent stem cells. *Sci Rep* (2021) **11**:6934. doi:10.1038/s41598-021-85656-x

199. Díez-Planelles C, Sánchez-Lozano P, Crespo M, Gil-Zamorano J, Ribacoba R, González N, et al. Circulating microRNAs in Huntington's disease: emerging mediators in metabolic impairment. *Pharmacol Res* (2016) **108**:102–10. doi:10.1016/j.phrs.2016.05.005

200. Sun P, Liu DZ, Jickling GC, Sharp FR, Yin K-J. MicroRNA-based therapeutics in central nervous system injuries. *J Cereb Blood Flow Metab* (2018) **38**:1125–48. doi:10.1177/0271678x18773871

201. Lehmann SM, Krüger C, Park B, Derkow K, Rosenberger K, Baumgart J, et al. An unconventional role for miRNA: let-7 activates Toll-like receptor 7 and causes neurodegeneration. *Nat Neurosci* (2012) **15**:827–35. doi:10.1038/nn.3113

202. Barbagallo C, Mostile G, Baglieri G, Giunta F, Luca A, Raciti L, et al. Specific signatures of serum miRNAs as potential biomarkers to discriminate clinically similar neurodegenerative and vascular-related diseases. *Cell. Mol. Neurobiol.* (2020) **40**:531–46. doi:10.1007/s10571-019-00751-y

203. Roy B, Lee E, Li T, Rampersaud M. Role of miRNAs in neurodegeneration: from disease cause to tools of biomarker discovery and therapeutics. *Genes* (2022) **13**:425. doi:10.3390/genes13030425

204. Sun Z, Shi K, Yang S, Liu J, Zhou Q, Wang G, et al. Effect of exosomal miRNA on cancer biology and clinical applications. *Mol Cancer* (2018) **17**:147. doi:10.1186/s12943-018-0897-7

EBM Experimental Biology and Medicine

TYPE Original Research
PUBLISHED 05 April 2024
DOI 10.3389/ebm.2024.10112

OPEN ACCESS

*CORRESPONDENCE
Dongmei Xi,
1047719655@qq.com
Fang He,
fangf2002shz@126.com

†These authors have contributed equally to this work

RECEIVED 28 March 2023
ACCEPTED 13 November 2023
PUBLISHED 05 April 2024

CITATION
Zhao J, Lu N, Qu Y, Liu W, Zhong H, Tang N, Li J, Wang L, Xi D and He F (2024), Calcium-sensing receptor-mediated macrophage polarization improves myocardial remodeling in spontaneously hypertensive rats. *Exp. Biol. Med.* 249:10112. doi: 10.3389/ebm.2024.10112

Calcium-sensing receptor-mediated macrophage polarization improves myocardial remodeling in spontaneously hypertensive rats

Jiaqi Zhao[1†], Ning Lu[2†], Yuanyuan Qu[3†], Wei Liu[1], Hua Zhong[1], Na Tang[1], Jiayi Li[1], Lamei Wang[1], Dongmei Xi[1*] and Fang He[1*]

[1]Key Laboratory of Education Ministry of Xinjiang Endemic and Ethnic Diseases, NHC Key Laboratory for Prevention and Treatment of Central Asia High Incidence Diseases, Department of Pathophysiology, School of Medicine, Shihezi University, Shihezi, Xinjiang, China, [2]School of Medicine, Tarim University, Alaer, Xinjiang, China, [3]Department of Respiratory Medicine, The First Affiliated Hospital of Shihezi University School of Medicine, Shihezi, Xinjiang, China

Abstract

Chronic inflammation is a key element in the progression of essential hypertension (EH). Calcium plays a key role in inflammation, so its receptor, the calcium-sensing receptor (CaSR), is an essential mediator of the inflammatory process. Compelling evidence suggests that CaSR mediates inflammation in tissues and immune cells, where it mediates their activity and chemotaxis. Macrophages (Mφs) play a major role in the inflammatory response process. This study provided convincing evidence that R568, a positive regulator of CaSR, was effective in lowering blood pressure in spontaneously hypertensive rats (SHRs), improving cardiac function by alleviating cardiac hypertrophy and fibrosis. R568 can increase the content of CaSR and M2 macrophages (M2Mφs, exert an anti-inflammatory effect) in myocardial tissue, reduce M1 macrophages (M1Mφs), which have a pro-inflammatory effect in this process. In contrast, NPS2143, a negative state regulator of CaSR, exerted the opposite effect in all of the above experiments. Following this study, R568 increased CaSR content in SHR myocardial tissue, lowered blood pressure, promoted macrophages to M2Mφs and improved myocardial fibrosis, but interestingly, both M1Mφs and M2Mφs were increased in the peritoneal cavity of SHRs, the number of M2Mφs remained lower than M1Mφs. *In vitro*, R568 increased CaSR content in RAW264.7 cells (a macrophage cell line), regulating intracellular Ca^{2+} ($[Ca^{2+}]_i$) inhibited NOD-like receptor family protein 3 (NLRP3) inflammasome activation and ultimately prevented its conversion to M1Mφs. The results showed that a decrease in CaSR in hypertensive rats causes further development of

hypertension and cardiac damage. EH myocardial remodeling can be improved by CaSR overexpression by suppressing NLRP3 inflammasome activation and macrophage polarization toward M1Mφs and increasing M2Mφs.

KEYWORDS

calcium-sensing receptor, essential hypertension, remodeling, macrophage polarization, NLRP3 inflammasome

Impact statement

Essential hypertension is a multifactorial chronic cardiovascular disease that has been clinically addressed by pharmacological interventions targeting the renin-angiotensin system, but some patients still respond to this pharmacological treatment with resistance. This study provides convincing evidence that CaSR can attenuate hypertension-mediated myocardial remodeling. We further demonstrate that the beneficial function of CaSR was achieved by regulating macrophages/NLRP3 inflammasome. We therefore found a new mechanism of cardioprotective effect of CaSR, one which also offers a novel theoretical basis for the therapy of hypertension-induced myocardial remodeling.

Introduction

Hypertension is believed to be a chronic low-grade inflammatory process with multifactorial effects [1]. The role of the immune response in the pathogenesis of hypertension is very important. The role of calcium-sensiing receptor (CaSR), among G protein-coupled receptors, in cardiovascular disease processes has been extensively investigated. As part of the innate immune system, CaSR is involved in immunomodulatory processes by binding to its metabolic regulators in response to tissue injury and inflammation. Decreased serum parathyroid hormone, 1,25-dihydroxy vitamin D, and calcium levels promote calcium homeostasis [2]. Whether it acts through immunomodulatory functions in myocardial tissue remains unknown.

In hypertensive patients, the normal structure of the vascular endothelium is disrupted by prolonged high pressure and abnormal blood flow, resulting in the attachment of inflammatory cells and the activation of the monocyte-macrophage system to produce inflammatory factors [3]. The functional classification of macrophages (Mφs) in the inflammatory state includes a binary classification of activated and alternatively activated Mφs, deriving these types of Mφs into M1 and M2 types under nonpathogen-driven conditions [4]. During homeostasis, both M1 macrophages (M1Mφs) and M2 macrophages (M2Mφs) are present in the vasculature and heart. Intravital microscopy shows M1Mφs circulate rapidly whereas M2Mφs circulate more slowly, crawling along the endothelium [5]. The cardiac Mφs play a role in cardiac development, immuno-surveillance and may contribute important specialised cardiac functions, such as conduction, though their exact functional significance is still emerging [6]. Following acute myocardial infarction, macrophage populations expand at the site of infarction and change their phenotype dramatically in the murine heart [5].

Activated inflammasomes have the ability self-differentiation, producing active forms of caspase-1, cleaving pro-interleukin 1β (IL-1β) and pro-interleukin 18 (IL-18), and releasing active IL-1β and IL-18 [7]. NOD-like receptor family protein 3 (NLRP3) inflammasome is also considered as the most important isoform causing inflammation in chronic diseases. Dalekos [8] examined several hypertensive patients and observed an overall increase in serum levels of IL-1β, which is activated by the upregulation of type 1 angiotensin receptor expression, thereby enhancing and involving in the process of hypertension [9]. In another experiment, it was shown that an increase in extracellular calcium can bind through CaSR, activate CaSR, initiate relevant ion channels, and allow calcium (Ca^{2+}) entry into the cell, which in turn causes Ca^{2+} release in the endoplasmic reticulum, stimulates inflammasome assembly, activates the effector protein caspase-1, and releases the proinflammatory cytokine IL-1β after maturation [10]. However, the role of CaSR-mediated NLRP3 inflammasome activation in hypertension has not yet been investigated.

In this study, CaSR activity was enhanced or attenuated by R568 (a CaSR agonist) and NPS2143 (a CaSR antagonist), while NLRP3 inflammasome activity was inhibited by MCC950 (an NLRP3 antagonist). The effects of CaSR on blood pressure and myocardial remodeling in spontaneously hypertensive rats (SHRs) were investigated at the overall tissue and cellular levels. In addition, its association with NLRP3 inflammasome and macrophage polarization was discovered.

Materials and methods

Animals and treatments

SHRs and Wistar-Kyoto rats (WKY) were purchased from Beijing Viton Lihua Laboratory Animal Technology Co., Ltd. (Beijing, China). Male rats of 16 weeks, age-matched, and weighing approximately 290 g–310 g, were kept in an alternating 12 h light/dark cycle at a temperature of 25°C and constant humidity with free access to food and water. SHRs and

WKY were randomly divided into the WKY group, SHR+normal saline (NS) group, SHR+R568 group, SHR+NPS2143 group, and SHR+R568+MCC950 group, with 10 rats in each group. Subsequently, daily intraperitoneal injections of R568 at 1.2 mg/kg/day [per 1 mg with 29 μL dimethyl sulfoxide (DMSO)] were administered [11]. NPS2143 was administered at 4.5 mg/kg/day (per 1 mg with 22 μL DMSO) [12], and MCC950 at 10 mg/kg/day [13]. All compounds were purchased from Tocris Bioscience R&D Systems (Minneapolis, MN, United States). All animal procedures were conducted with the approval of the Animal Care and Use Committee of Shihezi University (Shihezi, China; approval number: A2020-164-01). Every effort was made to alleviate the animal's suffering.

Cell culture and treatment

The mouse macrophage cell line RAW264.7 was obtained from Peking Union Cell Center, Chinese Academy of Medical Sciences (Beijing, China) and was cultured in high sugar Dulbecco's modified Eagle medium (DMEM, Gibco; United States) containing 10% fetal bovine serum (FBS, Gibco; United States). A penicillin-streptomycin suspension (Solarbio; Beijing, China) was added to prevent bacterial contamination; the cells were cultured at 37°C, 5% CO_2, and 100% humidity and carefully passaged before they reached confluence. Three to five generations of cells were collected for the experiment and divided into five groups: CON group; R568 group; NPS2143 group; R568+MCC950 group. R568, NPS2143 (5 μmol/L, per 1 μmol/L with 0.01 μL DMSO), and MCC950 (1 μmol/L) [14].

Intraperitoneal mononuclear macrophage collection

Under chloral hydrate anesthesia, mononuclear macrophages were isolated from the peritoneal cavity of rats by injecting precooled phosphate buffered saline (PBS, Nakasugi Jinqiao; Beijing, China) into the peritoneal cavity. The cells were isolated by centrifugation at 1,000 rpm for 5 min. Then, the cells were cultured in DMEM containing 10% FBS at 37°C and 5% CO_2 and allowed to differentiate.

Quantitative real-time polymerase chain reaction (qRT-PCR)

Total RNA was extracted from each group of tissues, and 3 μg of total RNA was reverse transcribed to cDNA according to the manufacturer's instructions (Tiangen Biotech; Shanghai, China). Data were analyzed using ABI7500 software (Applied Biosystems; CA, United States). PCR amplification (triplicates) was performed in a 20 μL reaction volume using SYBR Green/Fluorescein qPCR Master Mix (Thermo; United States). The reaction mixture without template cDNA was used as a negative control. The mRNA expression was normalized to the expression values of glyceraldehyde 3-phosphate dehydrogenase (GAPDH, endogenous control). The comparative CT method (ΔΔCT) determined the gene expression level. The primers for atrial natriuretic peptide (*ANP*), brain natriuretic peptide (*BNP*), β-myosin heavy chain (*β-MHC*), *CaSR*, *CD86*, *CD206* and *GAPDH* were as follows:

ANP: forward, 5′-CCTGGACTGGGGAAGTCAAC-3′; reverse, 5′-ATCTATCGGAGGGGTCCCAG-3′.
BNP: forward, 5′-TCCTTAATCTGTCGCCGCTG-3'; reverse, 5′-AGCCCAGGATGCCCTTTAGT-3′.
β-MHC: forward, 5′-GGCCCTTTGACCTCAAGAAAG-3′; reverse, 5′-GCCATTCTCTGTCTCAGCGG-3′.
CaSR: forward, 5′-ACGAGCCTCAGAAGAATGCC-3′; reverse, 5′-TCCGCATCTGCACACTGTAG-3′.
CD86: forward, 5′-TTTCGCAGCCCCAGTTTGAT-3′; reverse, 5′-AACACCACTGTCCTGCTTGG-3′.
CD206: forward, 5′-CTCTAAGCGCCATCTCCGTT-3′; reverse, 5′-CATGATCTGCGACTCCGACA-3′.
GAPDH: forward, 5′-GACATGCCGCCTGGAGAAAC-3′; reverse, 5′-AGCCCAGGATGCCCTTTAGT-3′.

Flow cytometry analysis

Cells collected from the peritoneal cavity were observed under the microscope, nonadherent cells and blood cells were washed with PBS, cell scrapers were used to scrape the adhered cells (macrophages), and cells were collected by centrifugation at 1,000 r/min for 5 min. The cells were fixed with 4% paraformaldehyde at room temperature (RT) for 20 min and then with 3% bovine serum albumin (BSA) at 37°C for 30 min. The cells were stained with polarization markers [M1Mφ: anti-rat CD86-PE (Solarbio; Beijing, China); M2Mφ: anti-rabbit CD206-FITC (Solarbio; Beijing, China)], incubated at 37°C for 45 min, protected from light, and washed twice with PBS. The supernatant was discarded, 500 μL of PBS was added, and the samples were either stored at 4°C or directly analyzed by flow cytometry (BD Biosciences; CA, United States). The data were analyzed with FlowJo 10.4 software (BD Biosciences; CA, United States).

Cell counting kit-8 assay (CCK-8 assay)

To analyze R568-induced cell viability, 5×10^3 cells/well were seeded in 96-well microtiter plates and cultured in DMEM. Six wells per plate containing medium only served as blanks, and three wells containing untreated cells served as controls. Plates

were incubated under standard cell culture conditions. RAW264.7 cells were treated with increasing concentrations (0–20 μmol/L, per 1 μmol/L with 0.01 μL DMSO) of R568. Cell viability was determined after different treatment times (1 h, 2 h, 4 h, and 6 h) using a CCK-8 (Apexbio; Houston, United States). The absorbance at 490 nm was measured using a microplate reader of model 680 (Bio-Rad Laboratories, Inc.; United States). The cell viability ratio was calculated using the following formula: Ratio = (A490 value in test group-A490 value in the blank group)/(A490 value in control group-A490 value in the blank group) × 100%.

Flow cytometry analysis of $[Ca^{2+}]_i$ concentration

For the intracellular Ca^{2+} ($[Ca^{2+}]_i$) concentration, collecting by scraping with the cells (at 1×10^6 cells/mL density) with a cell scraper, the cells were resuspended with the culture medium. A total of 1 μL Fluo-3 AM (5 μmol/L, Apexbio; Houston, United States) was added to each tube of the sample to be tested. Subsequently, the tube was mixed to allow full contact between the cells and the Ca^{2+} fluorescence probe, and then the cells were incubated at 37°C for 45 min. The cells were washed 2–3 times with Hank's Balanced Salt Solution (HBSS, Gibco; United States) and the cells were resuspended by adding 500 μL HBSS. The Ca^{2+} concentration was detected with flow cytometry. The data were analyzed with FlowJo 10.4 software.

Western blotting

Cells were washed three times with PBS and then lysed in lysis buffer (PMSF: RIPA, 1:100, Sigma-Aldrich; Merck KGaA, Germany). Tissues were excised and then lysed via sonication in a lysis buffer. After insoluble debris was pelleted by centrifugation at 12,000 ×g for 15 min at 4°C, the supernatants were collected, and protein concentrations were assessed by the bicinchoninic acid method. The samples were fractionated on 10% sodium dodecyl sulfate-polyacrylamide gel electrophoresis (SDS-PAGE) gels, transferred to polyvinylidene fluoride membranes (EMD Millipore; Merck KGaA, Germany), and blocked with 5% non-fat milk or BSA for 2 h at RT.

Immunofluorescence analysis

Cells: Cells were seeded on sterile coverslips kept in 24-well multiwell plates. The following day, the cells were washed with PBS and fixed in 4% formaldehyde for 20 min. Cells were washed with PBS three times before incubating the cells with 3% BSA for 30 min at 37°C to minimize nonspecific binding. Cells were incubated with CD86 and CD206 primary antibodies (1: 100 in the 3% BSA blocking buffer, Nakasugi Jinqiao; Beijing, China) overnight at 4°C. The following day, the samples were washed and exposed to fluorescein isothiocyanate (FITC, Solarbio; Beijing, China) and tetramethylrhodamine isothiocyanate (TRITC, Solarbio; Beijing, China) fluorochrome-conjugated secondary antibodies (1:50) in the dark for 1 h. The cells were then incubated with 4′,6-diamidino-2-phenylindole (DAPI) at 37°C for 20 min. Finally, the cells were observed using confocal microscopy, and images were captured.

Tissues: The dewaxed, rehydrated tissue sections were transferred into antigen retrieval buffer solutions and placed in a microwave, blocking solution was added for incubation, and the immunostaining procedure was initiated immediately. The CD86-specific primary antibodies were diluted in PBS and incubated at 4°C overnight. The horseradish peroxidase (HRP)-labeled secondary antibody was incubated for 50 min at RT. After two washes with tris buffered saline containing Tween 20 (TBST), Cy5 fluorescent antibodies were incubated in the dark for 10 min at RT. The samples were then heated in the microwave, and the primary anti-CaSR antibody (Abcam; United States) was diluted and incubated overnight at 4°C. HRP-labelled secondary antibodies were incubated at RT for 50 min, washed with TBST, and incubated in the dark with FITC fluorescent antibodies at RT for 10 min. After heating, anti-CD206 was incubated at 4°C overnight. HRP-labelled secondary antibodies were incubated at RT for 50 min and washed with TBST. Cy5 fluorescent antibodies were incubated at RT for 10 min in the dark. Subsequently, the slides were mounted with DAPI for nuclear staining. Finally, the slides were incubated at RT for 15 min with an autofluorescence quencher to quench the tissue autofluorescence. Slides were stored at 4°C and scanned the following day (DAPI excitation wavelength: 330–380 nm, emission wavelength: 420 nm, blue light; FITC excitation wavelength: 465–495 nm, emission wavelength: 515–555 nm, green light; Cy3 excitation wavelength: 510–560 nm, emission wavelength: 590nm, red light; Cy5 excitation wavelength: 608–648 nm, emission wavelength: 672–712nm, pink light).

The following methods [measurement of blood pressure (BP), assessment of cardiac function, tissue collection and measurement of the heart-to-body weight ratio, hematoxylin and eosin staining (H&E), masson staining] are referenced but not limited to *DOI: 10.1177/1535370219854325*.

Statistical analyses

The results are expressed as the mean ± SE.s. Using SPSS 26.0 software (IBM Corp., United Sates), experimental groups were compared using one-way ANOVA, followed by Bonferroni correction. The statistical significance was indicated by $p < 0.05$.

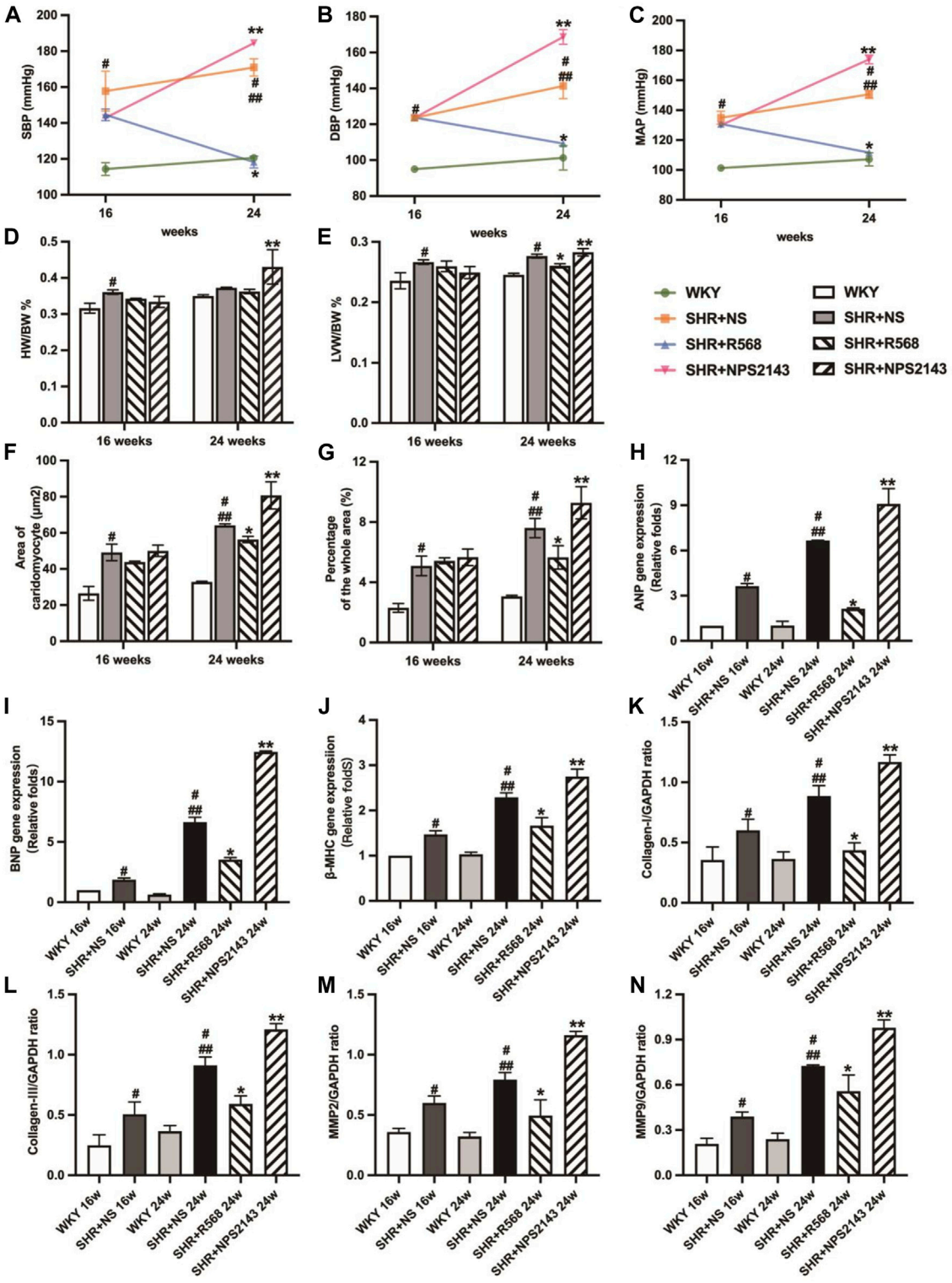

FIGURE 1
Comparison of blood pressure in each group evaluation of myocardial hypertrophy and fibrosis. **(A)**: SBP; **(B)**: DBP; **(C)**: MAP; **(D)**: HW/BW; **(E)**: LVW/BW; **(F)**: quantitative analysis of the cell size (mm^2) of cardiac myocytes; **(G)**: quantitative analysis of fibrosis; **(H–J)**: qRT−PCR of cardiac-specific fetal genes ANP, BNP and β-MHC; **(K–N)**: densitometric analysis of cardiac-protein expression. Values mean ± SE. s; $n = 5$; $^{\#}p < 0.05$, SHR+NS
(*Continued*)

FIGURE 1 (Continued)
groups *vs.* age-matchedWKY groups; $^{\#\#}p < 0.05$, SHR+NS 24w group *vs.* SHR+NS 16w group; $^{*}p < 0.05$, SHR+R568 groups *vs.* SHR+NS groups; $^{**}p < 0.05$, SHR+NPS2143 groups *vs.* SHR+NS groups. HW/BW, heart-to-body weight ratio; LVW/BW, left ventricle-to-body weight ratio.

Results

R568 reduces BP, and NPS2143 increases BP in SHRs

The average systolic BP (SBP), diastolic BP (DBP), and mean arterial pressure (MAP) were elevated in the SHR+NS groups compared to the age-matched WKY groups ($p < 0.05$). At 24 weeks, BP was higher than at 16 weeks ($p < 0.05$). However, BP was significantly reduced under R568 and increased under NPS2143 treatment at 24 weeks ($p < 0.05$; Figures 1A–C).

R568 relieves cardiac hypertrophy and fibrosis, and NPS2143 exacerbates cardiac hypertrophy and fibrosis

In the SHR+NS groups, the difference in weight-to-body weight ratio (HW/BW) between SHRs and WKY rats disappeared with age ($p > 0.05$; Figure 1D), and left ventricular weight-to-body weight ratio (LVW/BW) increased significantly compared to the age-matched WKY rats ($p < 0.05$; Figure 1E). In addition, the R568 group exhibited a decreasing trend, while the NPS2143 group exhibited an increasing trend to the ratio compared with the SHR+NS group at 24 weeks ($p < 0.05$; Figure 1E).

The cross-sectional area of cardiocytes measured by H&E staining was greater in SHR+NS groups than in the age-matched WKY groups ($p < 0.05$), and the increasing area was correlated with age ($p < 0.05$). In addition, treatment with R568 reduced the area ($p < 0.05$), whereas treatment with NPS2143 increased the area after 8 weeks ($p < 0.05$; Figure 1F, Supplementary Figure S1A). Masson staining of heart tissue sections shows the intensity of collagen accumulation, as reflected by blue staining. Interstitial fibrosis was significantly increased in SHRs than in age-matched WKY rats ($p < 0.05$), and the area at 24 weeks was larger than that at 16 weeks ($p < 0.05$). However, SHRs treated with R568 exhibited decreased fibrosis ($p < 0.05$), whereas those treated with NPS2143 showed an increase in fibrosis ($p < 0.05$; Figure 1G, Supplementary Figure S1B).

Heart tissues of SHRs exhibited increased mRNA expression of ANP, BNP and β-MHC and protein expression of myocardial hypertrophy markers, including Collagen Ⅰ, Collagen Ⅲ, matrix metalloproteinase 2 (MMP 2) and matrix metalloproteinase 9 (MMP 9), compared with the age-matched WKY rats ($p < 0.05$). The expression of these proteins was upregulated in the heart tissues of 24-week-old rats compared to 16-week-old rats ($p < 0.05$). In contrast, SHRs treated with R568 exhibited significantly attenuated mRNA and protein levels ($p < 0.05$), and the treatment with NPS2143 markedly increased the mRNA and protein expression levels at 24 weeks ($p < 0.05$; Figures 1H–N, Supplementary Figure S1C).

R568 improves LV functional parameters, and NPS2143 worsens LV functional parameters in SHRs

Echocardiographic analysis showed significantly decreased left ventricular internal diameter systolic (LVIDs) and left ventricular internal diameter diastolic (LVIDd) and increased left ventricular posterior diameter (LVPWD) in SHR compared to age-matched WKY groups ($p < 0.05$). In addition, the R568 treatment reversed the changes in LVIDs, LVIDd, and LVPWd ($p < 0.05$). Treatment with NPS2143 enhanced the change in LVPWd, whereas there were no differences in LVIDs and LVIDd ($p > 0.05$). However, there was no difference in ejection fraction (EF) and fractioning shortening (FS) in any group ($p > 0.05$; Figures 2A–F).

R568 increased the expression of CaSR and M2Mφs and decreased that of M1Mφs, while NPS2143 exerted the opposite effect in the cardiac tissue of SHRs

The immunofluorescence intensity of CD86, CD206 and CaSR in cardiac tissues analyzed by fluorescence microscopy displayed that SHRs had a higher expression of CD86 and lower expression of CD206 and CaSR ($p < 0.05$). The results were reversed after the R568 treatment ($p < 0.05$) and deteriorated after the NPS2143 treatment ($p < 0.05$; Figures 2G–I, Supplementary Figure S2A). Similar outcomes were observed in qRT-PCR ($p < 0.05$; Figures 2J, K) and western blotting analysis ($p < 0.05$; Figure 2L, Supplementary Figure S2B).

The numbers of M1Mφs and M2Mφs were increased in the SHR peritoneal cavity, but the number of M2Mφs was lower than that of M1Mφs

Flow cytometry analysis showed that CD86 was upregulated and CD206 was downregulated in SHRs compared to the age-matched WKY rats ($p < 0.05$). After 8 weeks, both CD86 and CD206 were upregulated ($p < 0.05$), whereas CD86 remained higher than CD206 (Figure 3).

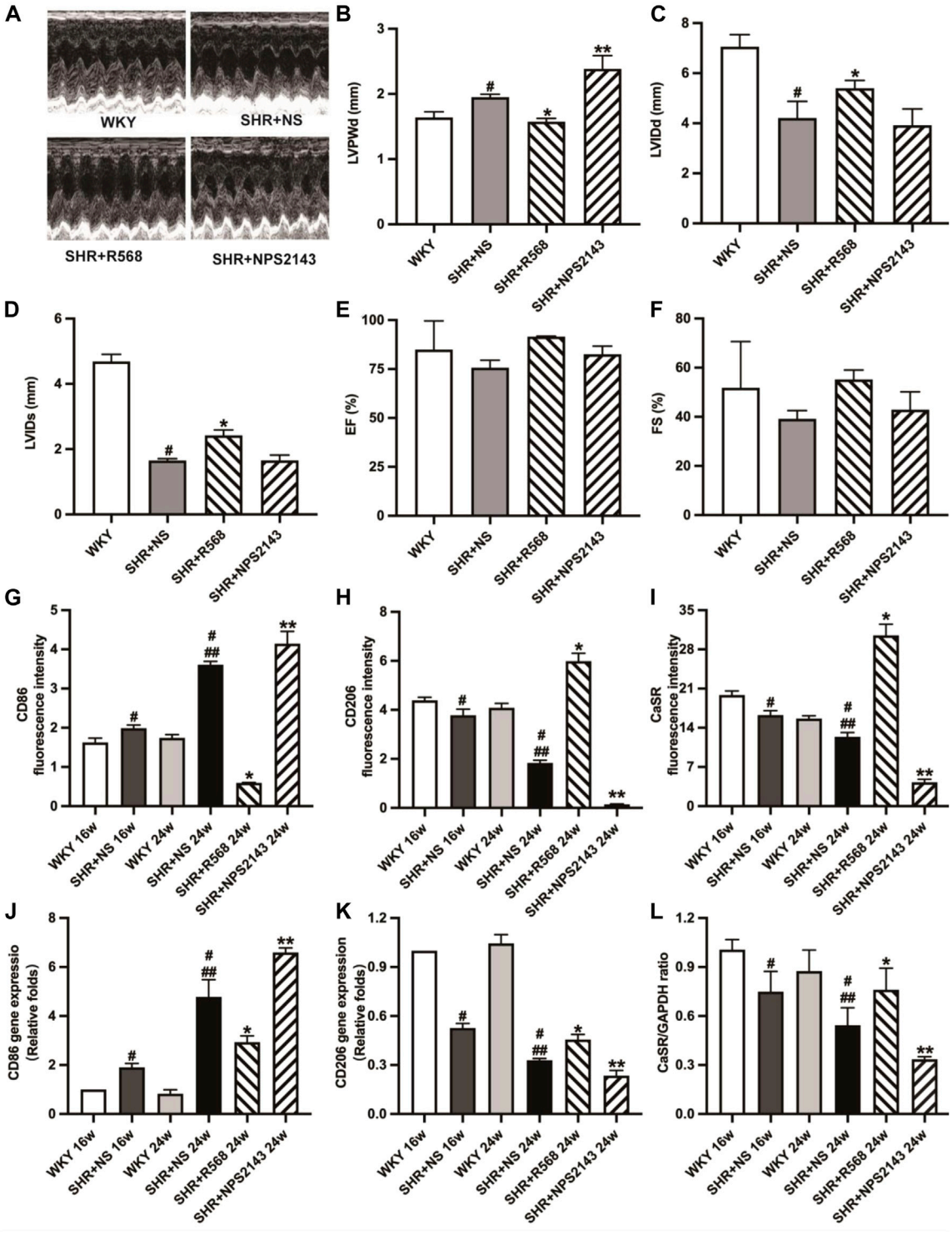

FIGURE 2
Detection of echocardiographic data and detection of macrophage surface markers and CaSR expression in myocardial tissue of each group of rats. **(A)**: images of M-mode of LV; **(B–F)**: LVPWd, LVIDs, LVIDd, EF, FS; **(G–I)**: quantitative analysis of immunofluorescence staining; **(J,K)**: qRT-PCR of macrophage surface markers (CD86, CD206) in myocardial tissues; **(L)**: quantitative analysis of western blotting (CaSR). Values mean ± SE. s; $n = 5$; $^{\#}p < 0.05$, SHR+NS groups *vs.* age-matched WKY groups; $^{\#\#}p < 0.05$, SHR+NS 24w group *vs.* SHR+NS 16w group; $^{*}p < 0.05$, SHR+R568 groups *vs.* SHR+NS groups; $^{**}p < 0.05$, SHR+NPS2143 groups *vs.* SHR+NS groups. LVPWd, left ventricular end-diastolic posterior wall dimension; LVIDs, left ventricular end-systolic diameter; LVIDd, left ventricular end-diastolic diameter; EF, ejection fraction; FS, fractional shortening.

R568 increases CaSR expression, and NPS2143 decreases CaSR expression in RAW264.7 cells

We determined the effect of different R568 concentrations and treatment durations on the cell viability of RAW264.7 cells. The results showed that RAW264.7 viability was enhanced by R568 treatment at 2 h, particularly at a 10 μmol/L concentration ($p < 0.05$; Figure 4A, Supplementary Figure S3A). Western blotting showed that compared to the control group, R568-treated RAW264.7 cells exhibited an abnormal upregulation of CaSR expression ($p < 0.05$), NPS2143-treated cells exhibited a significant downregulation ($p < 0.05$; Figure 4B, Supplementary Figure S3B).

R568 inhibits NLRP3 inflammasome activation by regulating $[Ca^{2+}]_i$

Based on the relationship between $[Ca^{2+}]_i$ and NLRP3 inflammasome, the experiments measured the $[Ca^{2+}]_i$ concentration by Flou-3/AM and the activation of NLRP3 inflammasome in cells by western blotting under different drug treatments. The exposure of RAW264.7 cells to NPS2143 decreased $[Ca^{2+}]_i$ significantly compared with the control group ($p < 0.05$). However, treatment with R568 alone or the R568+MCC950 combination induced a significant increase in $[Ca^{2+}]_i$ compared to the control group ($p < 0.05$), but the difference was not statistically significant ($p > 0.05$; Figure 4C, Supplementary Figure S3D). Under NPS2143 treatment, the expressions levels of NLRP3 inflammasome-related molecular protein, NLRP3, caspase-1 and IL-1β were all upregulated ($p < 0.05$); under the treatment of R568 alone, R568+MCC950 combination, the protein expression levels were all downregulated ($p < 0.05$), and there was no significant difference between the two groups ($p > 0.05$; Figures 4D–F, Supplementary Figure S3C).

R568 inhibits M1Mφs via NLRP3 inflammasome but has no effect on M2Mφs in RAW264.7 cells

Immunofluorescent staining was used to study some cell markers to investigate the influence of the CaSR-NLRP3 inflammasome on RAW264.7 cells. RAW264.7 cells were fluorescently stained and evaluated for CD86-and CD206-positive signals after different treatments. Treatment with NPS2143 enhanced staining for CD86, whereas decreased staining intensity between R568 alone and R568 combined with MCC950 ($p < 0.05$) did not differ between the two groups ($p > 0.05$). However, all groups had no significant difference in CD206 ($p > 0.05$; Figures 4G, H, Supplementary Figure S3E).

R568 improves cardiac function and myocardial fibrosis via NLRP3 inflammasome in SHRs

In SHRs given R568 alone and R568 combined with MCC950 treatment for 8 weeks, there was a significant reduction in BP (SBP, DBP, MAP) in both groups ($p < 0.05$; Figures 5A–C), and LVW/BW was also significantly decreased ($p < 0.05$; Figure 5E). However, HW/BW remained unchanged ($p > 0.05$; Figure 5D). A significant reduction in cardiomyocyte cross-sectional area ($p < 0.05$; Figure 5F, Supplementary Figure S4A), collagen deposition area ($p < 0.05$; Figure 5G, Supplementary Figure S4B), and myocardial hypertrophy-associated mRNA expression ($p < 0.05$; Figures 5H–J) was observed in both groups. In addition, echocardiographic findings suggested a reduction in LVPWd and an expansion of LVIDs and LVIDd ($p < 0.05$; Figures 5K–M, Supplementary Figure S4C), whereas EF and FS remained significantly unchanged ($p > 0.05$; Figures 5N, O, Supplementary Figure S4C). All these changes were not significantly different in either of the drug-treated groups ($p > 0.05$).

R568 inhibits M1Mφs and promotes M2Mφs via NLRP3 inflammasome in SHRs

During the study of macrophage polarization types in myocardial tissue, it was observed that the area of CD86 (M1Mφ) fluorescence in myocardial tissue was decreased, and the area of CD206 (M2Mφ) fluorescence was increased between WKY and age-matched SHR+NS groups ($p < 0.05$; Figures 6A, B, Supplementary Figure S5A). Similar results were observed in qRT-PCR ($p < 0.05$; Figures 6C, D). In addition, NLRP3 inflammasome activation was inhibited (protein expression levels of NLRP3, IL-1β and caspase-1 were reduced) after 8 weeks of R568 alone and in combination with MCC950 ($p < 0.05$; Figures 6E–G, Supplementary Figure S5B).

Discussion

SHRs are frequently used in studies of essential hypertension, and disorders of the innate immune system can promote the development of high blood pressure in SHRs [15]. CaSR, as an extracellular Ca^{2+} receptor, is associated with initiating and progressing inflammatory responses. In addition, macrophage polarization and the NLRP3 inflammasome are associated with hypertension [16]. Our study demonstrates for the first time the protective effects of CaSR on EH-induced cardiac injury, activation of the NLRP3 inflammasome and changes in the type of polarization in macrophages.

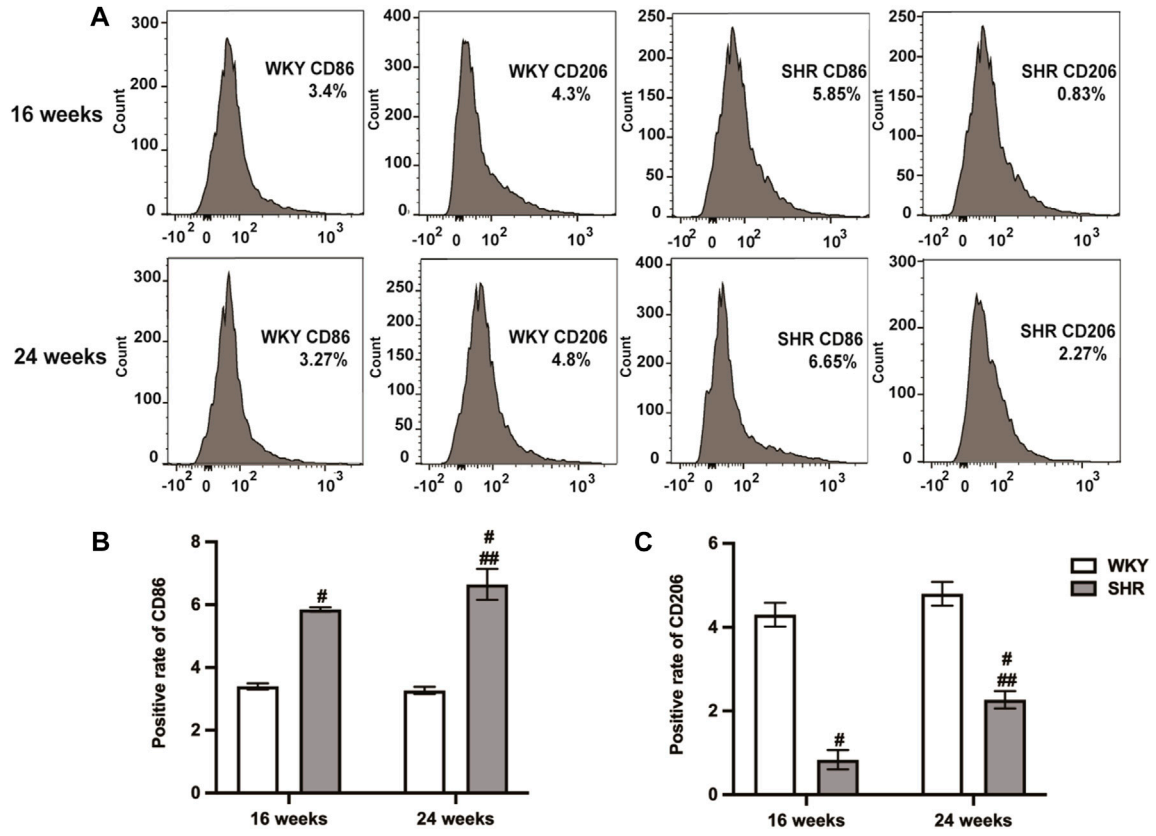

FIGURE 3
Types of peritoneal macrophages in each group of rats were detected by flow cytometry. **(A)**: peritoneal macrophages of 16-week-old and 24-week-old rats; **(B,C)**: quantitative analysis of **(A)**. Values mean ± SE. s; $n = 5$; $^{\#}p < 0.05$, SHR+NS groups *vs.* age-matchedWKY groups; $^{\#\#}p < 0.05$, SHR+NS 24w group *vs.* SHR+NS 16w group.

CaSR activity can be modulated by ligands and chemoregulators involved in inflammation and cardiovascular disease processes, including hypertension, vascular calcification, atherosclerosis, myocardial infarction, and obesity. R568, L-type amino acids, and sinalcaser augment the effect of extracellular calcium ($[Ca^{2+}]_o$) and other cations on CaSR [17]. Negative metamorphic modulators of CaSR include NPS2143 and Calhex231, which have the opposite effects on calcium mimetics [18]. CaSR, unlike other G protein-coupled receptors, remains in the endoplasmic reticulum or Golgi apparatus after the complete translational modification. In addition, it can be translocated to the cell membrane when activated by signals from relevant extracellular agonists [19]. Thus, it appears that the expression of the receptor itself is altered when agonists are applied.

In the present study, we found that as blood pressure increased and CaSR levels decreased, myocardial hypertrophy and fibrosis increased in SHRs, ultimately exacerbating detrimental cardiac remodeling. CaSR exhibited a potential anti-myocardial hypertrophy effect in neonatal rat studies [20]. However, the study's conclusions do not apply to adult rats. CaSR may act through different mechanisms as the immune function of the body changes with age and exposure to the external environment. In this study, we used SHRs at different ages to dynamically observe the role of R568 and NPS2143 in hypertensive cardiac remodeling, indicating that CaSR plays an important protective role in hypertensive myocardial remodeling. However, EF and FS were unaffected in any of the groups in the echocardiography results. This difference may be because the level of myocardial remodeling is still in the early compensatory phase, the major functions have not yet been compromised, and early intervention and treatment of myocardial remodeling can effectively stop or even reverse its development.

In adult mammals, macrophages are present in all tissues and are characterized by different patterns. During the development of inflammation, two distinct macrophage polarization states (proinflammatory M1 type and anti-inflammatory M2 type) are observed. During the onset and progression of hypertension, immune cells [such as T cells, macrophages and dendritic cells (DCs)] infiltrate the kidney, perivascular fat or heart [21–24]. It was observed that immune monocytes in hypertensive patients have a strong proinflammatory phenotype [25], but the proinflammatory

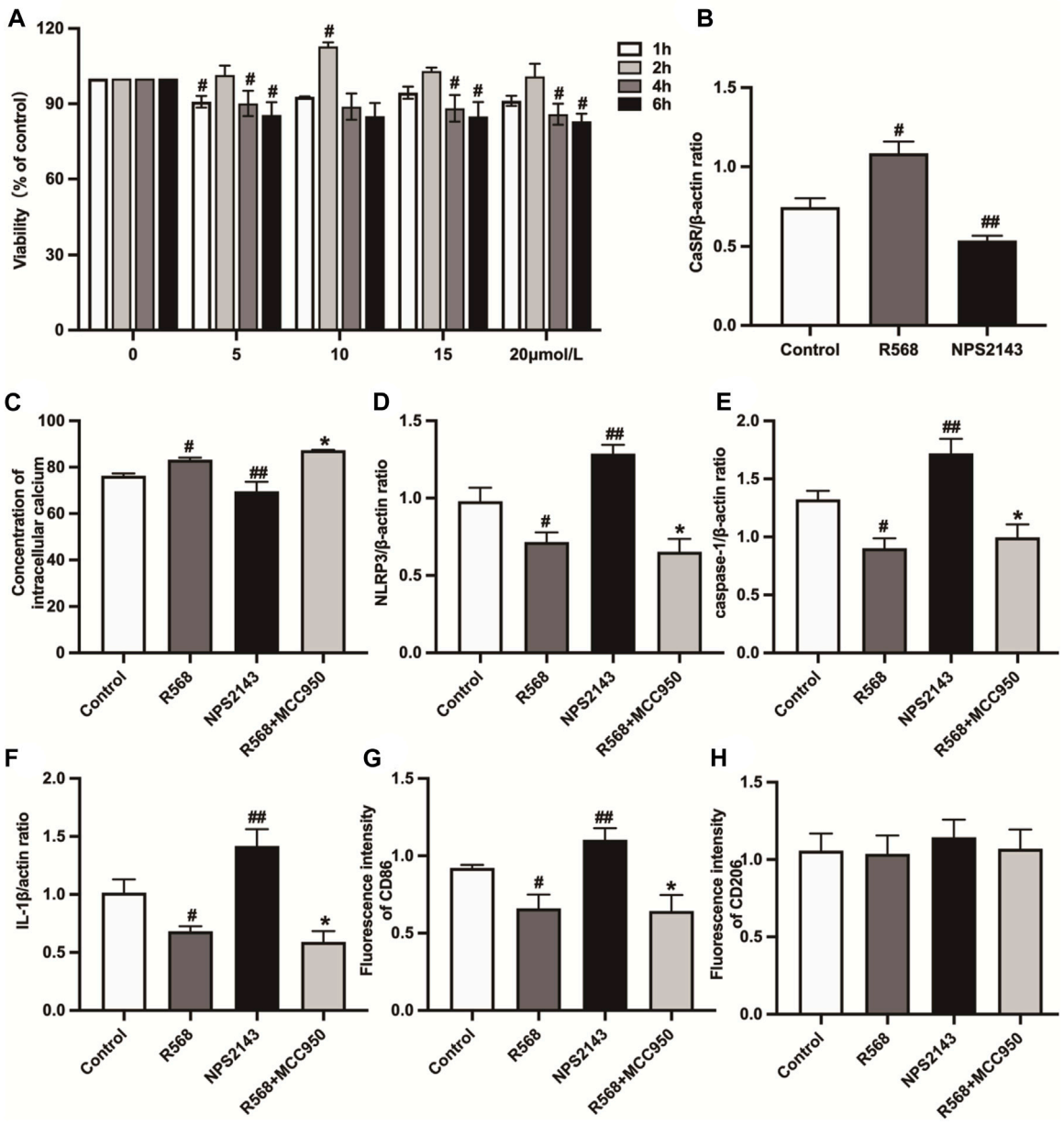

FIGURE 4
Detection of cell viability and the expression of CaSR, intracellular calcium concentration, NLRP3 inflammasome-related protein expression and macrophage types in RAW264.7 cells. **(A)**: Effects of R568 at different concentrations (5, 10, 15 and 20 μmol/L) for 1, 2, 4 and 6 h on the cell viability ratio of RAW264.7 cells as tested by CCK-8 assay; **(B)**: CaSR protein expression levels were assessed by western blotting analysis; **(C)**: quantitative analysis of $[Ca^{2+}]_i$; **(D–F)**: quantitative analysis of NLRP3 inflammasome-related protein (NLRP3, caspase-1, IL-1β); **(G, H)**: macrophage types by immunofluorescence staining. Values mean ± SE. s; $n = 3$; $^{\#}p < 0.05$, R568 group *vs.* Control group; $^{\#\#}p < 0.05$, NPS2143 group *vs.* Control group; $^{*}p < 0.05$, R568+MCC950 group *vs.* Control group.

cytokines tumor necrosis factor-α (TNF-α) and IL-1β secreted by M1Mφs can lead to hypotension by triggering diuresis [26]. However, genetic deletion of TNF-α and IL-1β receptors can attenuate blood pressure elevation during the renin angiotensin system (RAS) activation [27]. Therefore, additional research is necessary to determine the role of macrophage polarization types in cardiovascular disease.

In this study, we investigated the polarization status of macrophages in the peritoneal cavity and myocardial tissues of rats at different ages. There were more M1Mφs than M2Mφs in the peritoneal cavity of SHRs at 16 weeks of age; although all types were elevated in the peritoneal cavity of SHRs at 24 weeks of age, M2Mφs were still less abundant than M1Mφs. When CaSR expression decreased in the myocardial tissue of SHRs, the number of

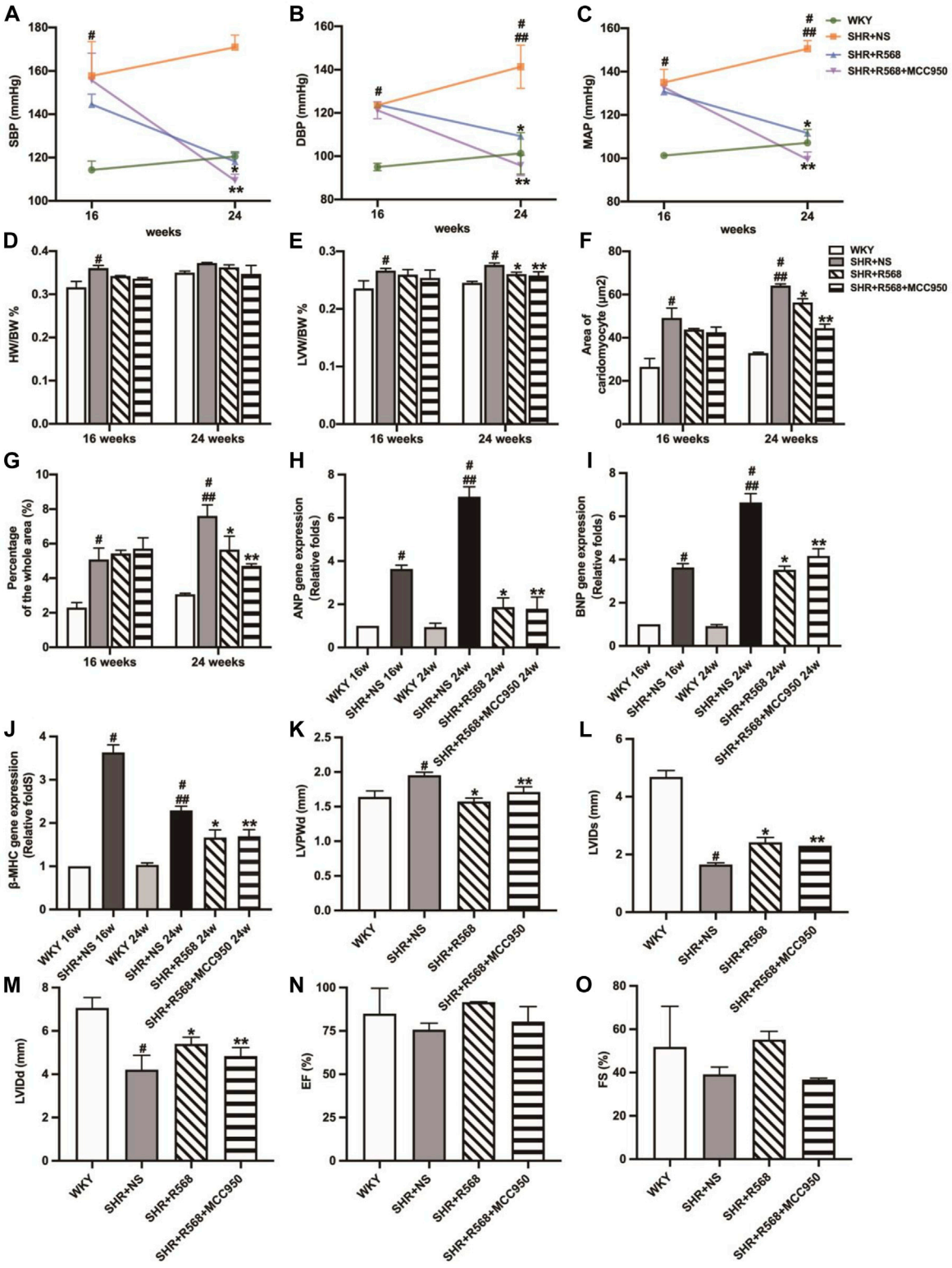

FIGURE 5
Evaluation of BP, myocardial hypertrophy and fibrosis between different groups. **(A)**: SBP; **(B)**: DBP; **(C)**: MAP; **(D)**: HW/BW; **(E)**: LVW/BW; **(F)**: quantitative analysis of the cell size (mm^2) of cardiac myocytes; **(G)**: quantitative analysis of fibrosis; **(H–J)**: qRT-PCR of cardiac-specific fetal genes ANP, BNP and β-MHC; **(K–O)**: LVPWd, LVIDs, LVIDd, EF, FS. Values mean ± SE. s; $n = 5$; $^{\#}p < 0.05$, SHR+NS groups *vs.* age-matched WKY groups; $^{\#\#}p < 0.05$, SHR+NS 24w group *vs.* SHR+NS 16w group; $^{*}p < 0.05$, SHR+R568 groups *vs.* SHR+NS groups; $^{**}p < 0.05$, SHR+R568+MCC950 groups *vs.* SHR+NS groups.

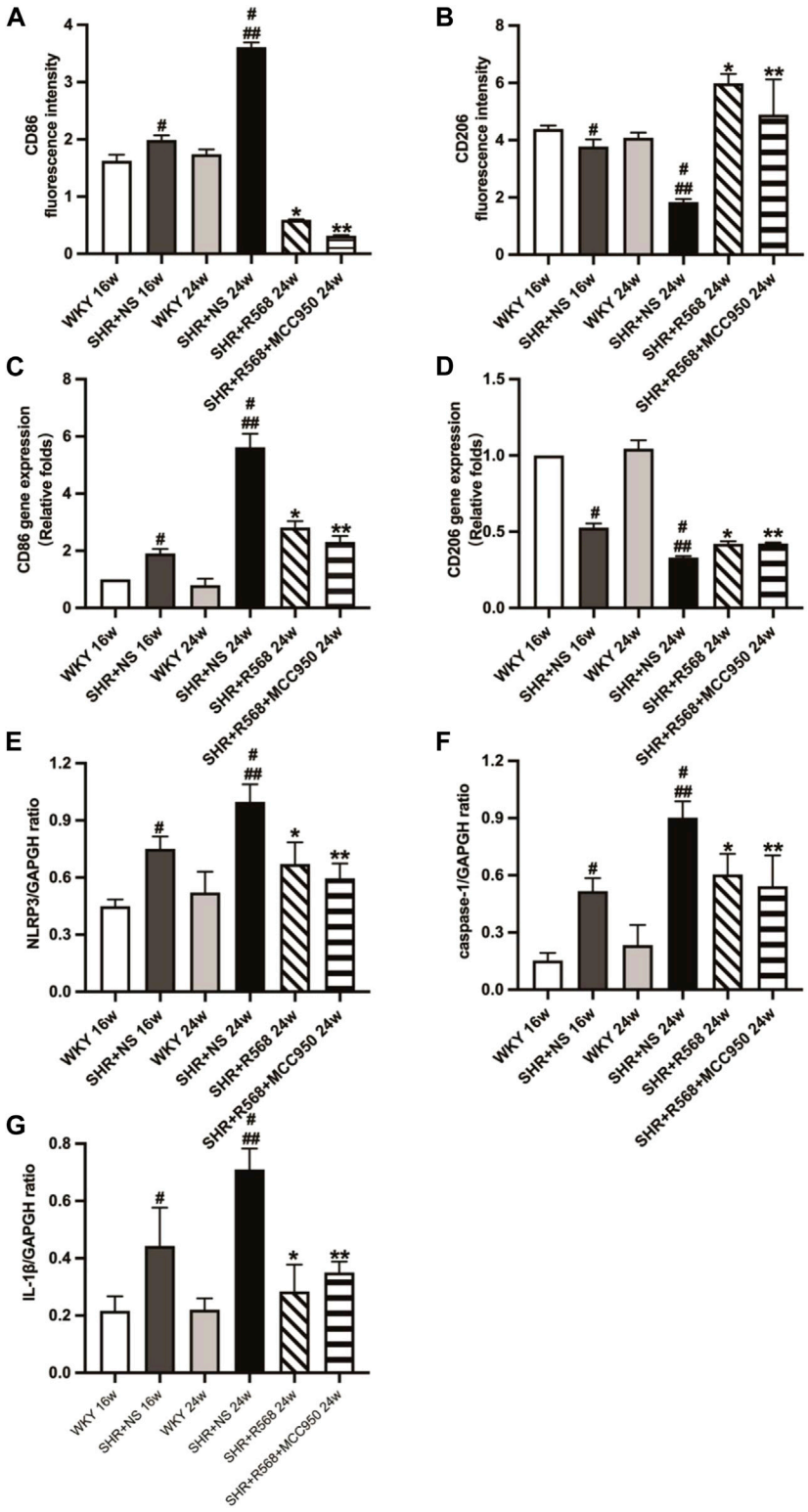

FIGURE 6
Detection of macrophage types and NLRP3 inflammasome-related protein expression of rats. **(A,B)**: macrophage types by immunofluorescence staining; **(C,D)**: Macrophage types by qRT-PCR; **(E–G)**: quantitative analysis of NLRP3 inflammasome-related protein (NLRP3, caspase-1, IL-1β). Values mean ± SE. s; $n = 5$; $^{\#}p < 0.05$, SHR+NS groups *vs.* age-matched WKY groups; $^{\#\#}p < 0.05$, SHR+NS 24w group *vs.* SHR+NS 16w group; $^{*}p < 0.05$, SHR+R568 groups *vs.* SHR+NS groups; $^{**}p < 0.05$, SHR+R568+MCC950 groups *vs.* SHR+NS groups.

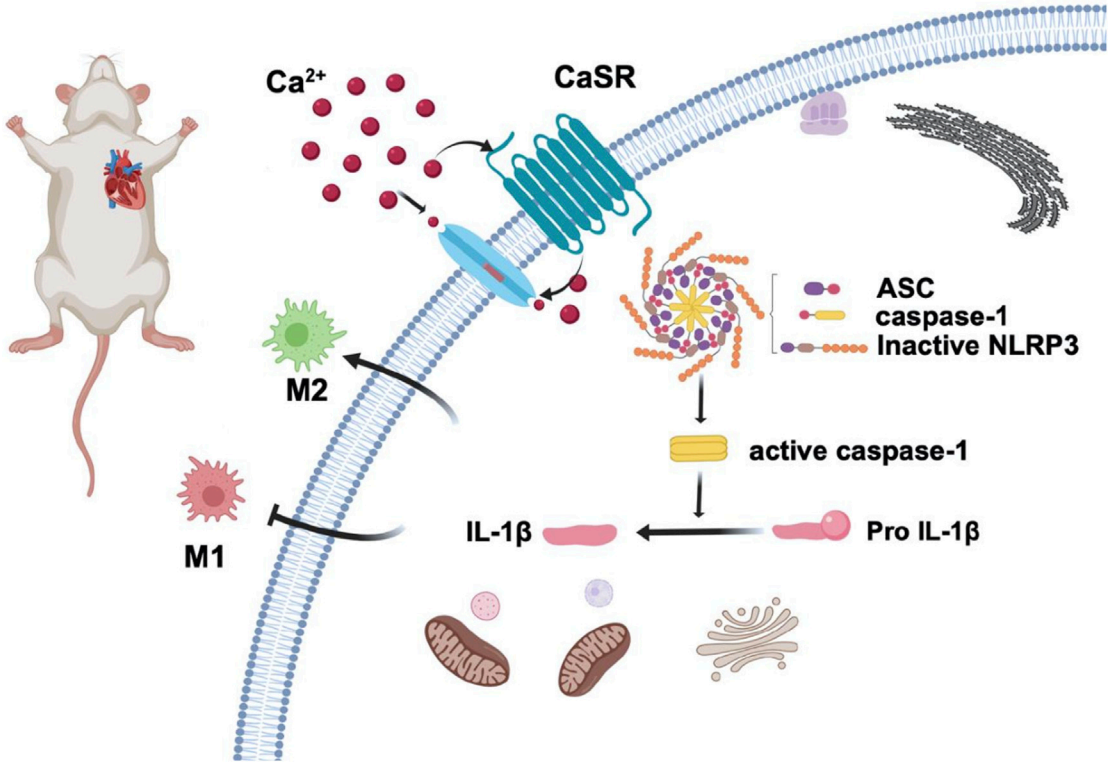

FIGURE 7
CaSR activation reduces macrophage polarization to the M1-type and increases polarization to the M2-type to reduce blood pressure and improve adverse myocardial remodeling in essential hypertension by reducing NLRP3 inflammasome activation.

M1Mφs increased. This indicates that abdominal and myocardial tissues in primary hypertension contain more proinflammatory Mφs than anti-inflammatory. The asynchrony of macrophage type switching at different sites may be attributable to resident tissue macrophages responding to changes in the tissue environment by recruiting macrophages from other sources to reach inflamed tissues [28]. However, in many chronic fibrotic diseases, macrophages are predominantly of a proinflammatory phenotype due to the unknown nature of the irritants and the fact that they cannot be eliminated [29]. In hypertensive states, the release of humoral factors caused by prolonged exposure to high pressure, abnormal blood flow and activation of the neuroendocrine system stimulates altered macrophage types in the abdominal and myocardial tissues of SHRs, thereby promoting the development of hypertension and myocardial remodeling. Further investigation is required to determine whether the source is tissue-lagged macrophages or mononuclear cells recruited from the blood, spleen, and bone marrow.

In addition, elevated calcium levels in cardiac tissue increase $[Ca^{2+}]_i$ levels and cardiac activity. Due to a feedback mechanism, CaSR is continuously activated and reactivated in response to changes in calcium levels, which contribute to the normal contractility of muscle cells. CaSR is also present in cells, including monocytes, macrophages and dendritic cells [30, 31]. It was observed that $[Ca^{2+}]_o$ cause an increase in $[Ca^{2+}]_i$ level, causing CaSR in macrophages to detect pathogens or tissue damage [32]. This is consistent with our experimental findings that R568 enhanced intracellular calcium fluorescence intensity and CaSR protein expression in RAW264.7 cells while inhibiting macrophage polarization toward M1Mφs. However, the application of NPS2143 had the opposite effect. Overall, CaSR reduces blood pressure and improves myocardial remodeling through the involvement of distinct macrophage phenotypes. Actually, this may be related to excess $[Ca^{2+}]_i$, has been shown to be involved in the modulation of apoptosis [33, 34]. Moreover, studies have demonstrated that melamine-stimulated CaSR mediated Ca^{2+} signaling resulted in a sustained Ca^{2+} entry, which can prolong the rise in $[Ca^{2+}]_i$. This mechanism might produce an endoplasmic reticulum stress response, thus resulting in reactive oxygen species generation which can produce a caspase mediated apoptosis pathway leading to tubular cell injury [35].

Activation of NLRP3 inflammasome can be induced by "classical" and "nonclassical" pathways. In the classical pathway, NLRP3 inflammasome activation is followed by upregulation of NLRP3 and IL-1β precursors via nuclear transcription factor signaling, recruitment of apoptosis-associated speck-like protein containing a CARD (ASC) and caspase-1 to form a complex [36], producing caspase-l with the activity that promotes

downstream production of additional inflammatory mediators (IL-1β, IL-18) as well as synthesis and secretion of chemokines [37].

Ulrich [38] found NLRP3 inflammasome in peripheral blood mononuclear cells of hypertensive patients. Subsequently, studies by Zhu [39] showed that the level of inflammatory response in hypertensive patients can be exacerbated by the activation of NLRP3 inflammasome in immune cells, ultimately affecting the function of the immune cells themselves, and can accelerate the process of myocardial fibrosis and phenotypic transformation of cardiac fibroblasts. We showed that CaSR expression was upregulated, and NLRP3 inflammasome activation and the release of the effector molecule IL-1β were decreased following the application of a CaSR agonist. In addition, we found that R568 combined with the NLRP3 inhibitor MCC950 lowered blood pressure and improved myocardial remodeling without significantly differing from R568 alone.

Recent studies have shown that inhibiting the activation of NLRP3 inflammasome in macrophages improved angiotensin II (Ang II)-induced myocardial remodeling and myocardial fibrosis, but macrophage polarization during this process was not investigated [9]. In a multisystem study, it was observed that inhibiting the activity of NLRP3 inflammasome effectively reduced the polarization of macrophages to M1Mφs and the systemic multiorgan inflammatory response [40–42]. In contrast, our experiments showed that R568, in combination with MCC950, inhibited the macrophage shift to M1Mφs and promoted the shift to M2Mφs, with the effect being comparable to that of R568 alone. It is hypothesized that R568 can inhibit the macrophage transition to M1Mφs and promote their transition to M2Mφs by reducing the activation of the NLRP3 inflammasome and the release of the effector molecule IL-1β.

Our study shows that CaSR activation can ameliorate adverse myocardial remodeling by inhibiting NLRP3 inflammasome activation and increasing anti-inflammatory macrophages in cardiac tissue (Figure 7). The application of the calcium-mimetic cinacalcet in treating hyperparathyroidism resulted in an improvement in the patient's cardiovascular system disease in addition to a decrease in blood calcium and phosphorus levels [43]. However, given the complex relationship between CaSR and cardiovascular disease and the fact that most human diseases interact, combining multiple target drugs is likely the most effective treatment. Additional research is still required to develop CaSR-targeting drugs with high specificity.

Author contributions

LW and JZ designed the study. WL, JL, and YQ carried out animal measurements. HZ and NT analyzed the outcome. JZ and WL carried out cell biology experiments. JZ, NL, and DX wrote the manuscript with comments from all authors. All authors contributed to the article and approved the submitted version.

Data availability statement

The original contributions presented in the study are included in the article/Supplementary Material, further inquiries can be directed to the corresponding authors.

Ethics statement

The animal study was approved by the Animal Care and Use Committee of Shihezi University (Shihezi, China; approval number: A2020-164-01). The study was conducted in accordance with the local legislation and institutional requirements.

Funding

The author(s) declare financial support was received for the research, authorship, and/or publication of this article. This article received financial support from the National Science Foundation of China under Grant number 31960187, the Non-profit Central Research Institute Fund of Chinese Academy of Medical Sciences under Grant number 2020-PT330-003, the President Foundation of Tarim University under Grant number TDZKSS202103, the Youth Innovative Cultivation Talent Programme of Shihezi University under Grant number CXPY2022216.

Conflict of interest

The authors declare that the research was conducted in the absence of any commercial or financial relationships that could be construed as a potential conflict of interest.

Publisher's note

Please note that the review of this paper was conducted at the previous publisher, SAGE.

Supplementary material

The Supplementary Material for this article can be found online at: https://www.ebm-journal.org/articles/10.3389/ebm.2024.10112/full#supplementary-material

References

1. Pouvreau C, Dayre A, Butkowski EG, de Jong B, Jelinek HF. Inflammation and oxidative stress markers in diabetes and hypertension. *J Inflamm Res* (2018) **11**: 61–8. doi:10.2147/jir.s148911

2. Hendy GN, Canaff L. Calcium-sensing receptor, proinflammatory cytokines and calcium homeostasis. *Semin Cel Dev Biol* (2016) **49**:37–43. doi:10.1016/j.semcdb.2015.11.006

3. De Sanctis JB. Innate immune response in hypertension. *Curr Pharm Des* (2022) **28**:2984–90. doi:10.2174/1381612828666220922112412

4. Sica A, Mantovani A. Macrophage plasticity and polarization: *in vivo* veritas. *J Clin Invest* (2012) **122**:787–95. doi:10.1172/jci59643

5. Jung K, Kim P, Leuschner F, Gorbatov R, Kim JK, Ueno T, et al. Endoscopic time-lapse imaging of immune cells in infarcted mouse hearts. *Circ Res* (2013) **112**: 891–9. doi:10.1161/circresaha.111.300484

6. Swirski FK, Nahrendorf M. Cardioimmunology: the immune system in cardiac homeostasis and disease. *Nat Rev Immunol* (2018) **18**:733–44. doi:10.1038/s41577-018-0065-8

7. Awad F, Assrawi E, Louvrier C, Jumeau C, Georgin-Lavialle S, Grateau G, et al. Inflammasome biology, molecular pathology and therapeutic implications. *Pharmacol Ther* (2018) **187**:133–49. doi:10.1016/j.pharmthera.2018.02.011

8. Dalekos GN, Elisaf M, Bairaktari E, Tsolas O, Siamopoulos K. Increased serum levels of interleukin-1β in the systemic circulation of patients with essential hypertension: additional risk factor for atherogenesis in hypertensive patients? *J Lab Clin Med* (1997) **129**:300–8. doi:10.1016/s0022-2143(97)90178-5

9. Gan W, Ren J, Li T, Lv S, Li C, Liu Z, et al. The SGK1 inhibitor EMD638683, prevents Angiotensin II-induced cardiac inflammation and fibrosis by blocking NLRP3 inflammasome activation. *Biochim Biophys Acta (Bba) - Mol Basis Dis* (2018) **1864**:1–10. doi:10.1016/j.bbadis.2017.10.001

10. Schiffrin EL. Inflammation, immunity and development of essential hypertension. *J Hypertens* (2014) **32**:228–9. doi:10.1097/hjh.0000000000000042

11. Zhang T, Tang N, Xi D, Zhao Y, Liu Y, Wang L, et al. Calcimimetic R568 improved cardiac remodeling by classic and novel renin-angiotensin system in spontaneously hypertensive rats. *Exp Biol Med (Maywood)* (2019) **244**:789–801. doi:10.1177/1535370219854325

12. Hong W, Mo QD, Wang LY, Peng F, Zhou YM, Zou W, et al. Changes in the gut microbiome and metabolome in a rat model of pulmonary arterial hypertension. *Bioengineered* (2021) **12**:5173–83. doi:10.1080/21655979.2021.1952365

13. Chang Y, Zhu J, Wang D, Li H, He Y, Liu K, et al. NLRP3 inflammasome-mediated microglial pyroptosis is critically involved in the development of post-cardiac arrest brain injury. *J Neuroinflammation* (2020) **17**:219. doi:10.1186/s12974-020-01879-1

14. Zeng CY, Li CG, Shu JX, Xu LH, Ouyang DY, Mai FY, et al. ATP induces caspase-3/gasdermin E-mediated pyroptosis in NLRP3 pathway-blocked murine macrophages. *Apoptosis* (2019) **24**:703–17. doi:10.1007/s10495-019-01551-x

15. Saha P, Mell B, Golonka RM, Bovilla VR, Abokor AA, Mei X, et al. Selective IgA deficiency in spontaneously hypertensive rats with gut dysbiosis. *Hypertension* (2022) **79**:2239–49. doi:10.1161/hypertensionaha.122.19307

16. Lv SL, Zeng ZF, Gan WQ, Wang WQ, Li TG, Hou YF, et al. Lp-PLA2 inhibition prevents Ang II-induced cardiac inflammation and fibrosis by blocking macrophage NLRP3 inflammasome activation. *Acta Pharmacol Sin* (2021) **42**: 2016–32. doi:10.1038/s41401-021-00703-7

17. Kiefer L, Beaumard F, Gorojankina T, Faure H, Ruat M, Dodd RH. Design and synthesis of calindol derivatives as potent and selective calcium sensing receptor agonists. *Bioorg Med Chem* (2016) **24**:554–69. doi:10.1016/j.bmc.2015.12.019

18. Lee JW, Park HA, Kwon OK, Park JW, Lee G, Lee HJ, et al. NPS 2143, a selective calcium-sensing receptor antagonist inhibits lipopolysaccharide-induced pulmonary inflammation. *Mol Immunol* (2017) **90**:150–7. doi:10.1016/j.molimm.2017.07.012

19. Grant MP, Stepanchick A, Cavanaugh A, Breitwieser GE. Agonist-driven maturation and plasma membrane insertion of calcium-sensing receptors dynamically control signal amplitude. *Sci Signal* (2011) **4**:ra78. doi:10.1126/scisignal.2002208

20. Kumar S, Wang G, Liu W, Ding WW, Dong M, Zheng N, et al. Hypoxia-induced mitogenic factor promotes cardiac hypertrophy via calcium-dependent and hypoxia-inducible factor-1α mechanisms. *Hypertension* (2018) **72**:331–42. doi:10.1161/hypertensionaha.118.10845

21. Caillon AM, Mian MOR, Fraulob-Aquino JC, Huo KG, Barhoumi T, Ouerd S, et al. γδ T cells mediate angiotensin ii-induced hypertension and vascular injury. *Circulation* (2017) **135**:2155–62. doi:10.1161/circulationaha.116.027058

22. Rodríguez-Iturbe BV, Vaziri ND, Herrera-Acosta J, Johnson RJ. Oxidative stress, renal infiltration of immune cells, and salt-sensitive hypertension: all for one and one for all. *Am J Physiology-Renal Physiol* (2004) **286**:F606–F616. doi:10.1152/ajprenal.00269.2003

23. Johnson RJR-IB, Rodriguez-Iturbe B, Nakagawa T, Kang DH, Feig DI, Herrera-Acosta J. Subtle renal injury is likely a common mechanism for salt-sensitive essential hypertension. *Hypertension* (2005) **45**:326–30. doi:10.1161/01.hyp.0000154784.14018.5f

24. Van Beusecum JPBNR, Barbaro NR, McDowell Z, Aden LA, Xiao L, Pandey AK, et al. High salt activates CD11c (+) antigen-presenting cells via SGK (Serum Glucocorticoid Kinase) 1 to promote renal inflammation and salt-sensitive hypertension. *Hypertension* (2019) **74**:555–63. doi:10.1161/hypertensionaha.119.12761

25. Parissis JT, Korovesis S, Giazitzoglou E, Kalivas P, Katritsis D. Plasma profiles of peripheral monocyte-related inflammatory markers in patients with arterial hypertension. Correlations with plasma endothelin-1. *Int J Cardiol* (2002) **83**:13–21. doi:10.1016/s0167-5273(02)00021-9

26. Shahid M, Francis J, Majid DS. Tumor necrosis factor-α induces renal vasoconstriction as well as natriuresis in mice. *Am J Physiology-Renal Physiol* (2008) **295**:F1836–F1844. doi:10.1152/ajprenal.90297.2008

27. Zhang J, Rudemiller NP, Patel MB, Karlovich NS, Wu M, McDonough AA, et al. Interleukin-1 receptor activation potentiates salt reabsorption in angiotensin II-Induced hypertension via the NKCC2 co-transporter in the nephron. *Cel Metab* (2016) **23**:360–8. doi:10.1016/j.cmet.2015.11.013

28. Geissmann F, Manz MG, Jung S, Sieweke MH, Merad M, Ley K. Development of monocytes, macrophages, and dendritic cells. *Science* (2010) **327**:656–61. doi:10.1126/science.1178331

29. Wynn TA. Common and unique mechanisms regulate fibrosis in various fibroproliferative diseases. *J Clin Invest* (2007) **117**:524–9. doi:10.1172/jci31487

30. Lee GS, Subramanian N, Kim AI, Aksentijevich I, Goldbach-Mansky R, Sacks DB, et al. The calcium-sensing receptor regulates the NLRP3 inflammasome through Ca^{2+} and cAMP. *Nature* (2012) **492**:123–7. doi:10.1038/nature11588

31. Proudfoot D. Calcium signaling and tissue calcification. *Cold Spring Harbor Perspect Biol* (2019) **11**:a035303. doi:10.1101/cshperspect.a035303

32. Redka DS, Gütschow M, Grinstein S, Canton J. Differential ability of proinflammatory and anti-inflammatory macrophages to perform macropinocytosis. *Mol Biol Cel* (2018) **29**:53–65. doi:10.1091/mbc.e17-06-0419

33. Nakagawa T, Zhu H, Morishima N, Li E, Xu J, Yankner BA, et al. Caspase-12 mediates endoplasmic-reticulum-specific apoptosis and cytotoxicity by amyloid-β. *Nature* (2000) **403**:98–103. doi:10.1038/47513

34. Wu CT, Weng TI, Chen LP, Chiang CK, Liu SH. Involvement of caspase-12-dependent apoptotic pathway in ionic radiocontrast urografin-induced renal tubular cell injury. *Toxicol Appl Pharmacol* (2013) **266**:167–75. doi:10.1016/j.taap.2012.10.012

35. Yiu AJ, Ibeh CL, Roy SK, Bandyopadhyay BC. Melamine induces Ca^{2+}-sensing receptor activation and elicits apoptosis in proximal tubular cells. *Am J Physiology-Cell Physiol* (2017) **313**:C27–C41. doi:10.1152/ajpcell.00225.2016

36. Jo EKKJK, Kim JK, Shin DM, Sasakawa C. Molecular mechanisms regulating NLRP3 inflammasome activation. *Cell Mol Immunol* (2016) **13**:148–59. doi:10.1038/cmi.2015.95

37. Bauernfeind FG, Horvath G, Stutz A, Alnemri ES, MacDonald K, Speert D, et al. Cutting edge: NF-κB activating pattern recognition and cytokine receptors license NLRP3 inflammasome activation by regulating NLRP3 expression. *J Immunol* (2009) **183**:787–91. doi:10.4049/jimmunol.0901363

38. Ulrich C, Wildgrube S, Fick S, Seibert E, Wildgrube S, Kneser L, et al. NLRP3 inflammasome activation in hemodialysis and hypertensive patients with intact kidney function. *Toxins* (2020) **12**:675. doi:10.3390/toxins12110675

39. Zhu J, Yang Y, Hu SG, Zhang QB, Yu J, Zhang YM. T-lymphocyte Kv1.3 channel activation triggers the NLRP3 inflammasome signaling pathway in hypertensive patients. *Exp Ther Med* (2017) **14**:147–54. doi:10.3892/etm.2017.4490

40. Yuan C, Xu X, Wang N, Zhu Q, Zhang J, Gong W, et al. Paeonol protects against acute pancreatitis by inhibiting M1 macrophage polarization via the NLRP3 inflammasomes pathway. *Biochem Biophysical Res Commun* (2022) **600**: 35–43. doi:10.1016/j.bbrc.2022.02.019

41. Zhang J, Liu X, Wan C, Liu Y, Wang Y, Meng C, et al. NLRP3 inflammasome mediates M1 macrophage polarization and IL-1β production in inflammatory root resorption. *J Clin Periodontol* (2020) **47**:451–60. doi:10.1111/jcpe.13258

42. Hu Q, Zhang S, Yang Y, Yao JQ, Tang WF, Lyon CJ, et al. Extracellular vesicles in the pathogenesis and treatment of acute lung injury. *Mil Med Res* (2022) **9**:61. doi:10.1186/s40779-022-00417-9

43. Riccardi D, Martin D. The role of the calcium-sensing receptor in the pathophysiology of secondary hyperparathyroidism. *Clin Kidney J* (2008) **1**: i7–i11. doi:10.1093/ndtplus/sfm038

Experimental Biology & Medicine Conference

Orlando, FL - October 13 -16, 2024

Please visit **exbiomedcon.org** or scan the QR code for more info.

Keynote Lecturers

Namandjè Bumpus, Ph.D.
Chief Scientist -
US Food and Drug Administration

Advancing Emerging Technologies in Regulatory Science

Michael Friedlander, Ph.D.
Vice President - Health Sciences and Technology at Virginia Tech

All events will take place at the Embassy Suites by Hilton, Orlando Lake Buena Vista South

Cardiovascular

Delphine Gomez, Ph.D.
University of Pittsburgh

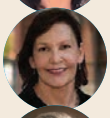

Karen Hirschi, Ph.D.
University of Virginia

Jay Humphrey, Ph.D.
Yale University

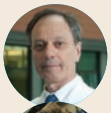

Ali J. Marian, M.D.
The University of Texas Health Science Center at Houston

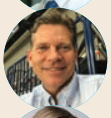

Joseph Miano, Ph.D.
Medical College of Georgia

Dianna Milewicz, M.D., Ph.D.
University of Texas Heath Science Center Houston

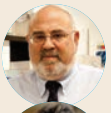

Robert Schwartz, Ph.D.
University of Houston

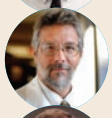

George Taffet, M.D.
Baylor College of Medicine

David Zawieja, Ph.D.
Texas A&M University Health Science Center

Neuroscience

Lique Coolen, Ph.D.
Kent State university

Michael Fehlings, M.D.
University of Toronto

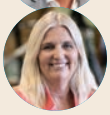

Susan Harkema, Ph.D.
University of Louisville

Maria Lehtinen, Ph.D.
Harvard University

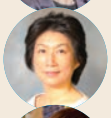

Fang Liu, Ph.D.
NCTR/US Food and Drug Administration

Agnes Luo, Ph.D.
University Cincinnati

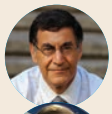

Mervyn Maze, MBChB
University of California San Francisco

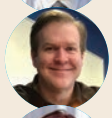

Dorian McGavern, Ph.D.
National Institute of Neurological Diorders and Stroke

Vesna Jevtovic-Todorovic, M.D., Ph.D.
University of Colorado School of Medicine

Regenerative Medicine

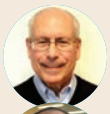

Arnold I. Caplan, Ph.D.
Case Western Reserve

Jian Feng, Ph.D.
State University of New York at Buffalo

Joshua Hare, M.D.
University of Miami

Karen Hasty, Ph.D.
University of Tennessee Health Science Center

Rajasingh Johnson, Ph.D.
University of Tennessee Health Science Center

Y. James Kang, DVM, Ph.D.
Sichuan University

Kwang-Soo Kim,Ph.D.
Harvard University

Joanne Kurtzberg, M.D.
Duke University

Jun Wu, Ph.D.
UT Southwestern

Trainees

Justin Boyd, Ph.D.
Vaxxinity

Udayan Apte, Ph.D.
U of Kansas Medical Center

Ram Kumar, Ph.D.
U of Kansas Medical Center

And More

Career Development
Short Talks
Poster Sessions
Member Blitz

SEBM SOCIETY FOR EXPERIMENTAL BIOLOGY AND MEDICINE

EBM Experimental Biology and Medicine

Scope

Experimental Biology and Medicine (EBM) is a global, peer-reviewed journal dedicated to the publication of multidisciplinary and interdisciplinary research in the biomedical sciences. The journal covers the spectrum of translational research from T0, basic research, to T4, population health. Articles in EBM represent cutting edge research at the overlapping junctions of the biological, physical and engineering sciences that impact upon the health and welfare of the world's population. EBM is particularly appropriate for publication of papers that are multidisciplinary in nature, are of potential interest to a wide audience, and represent experimental medicine in the broadest sense of the term. However, manuscripts reporting novel findings on any topic in the realm of experimental biology and medicine are most welcome.

EBM publishes Research, Reviews, Mini Reviews, and Brief Communications in the following categories.

- Anatomy/Pathology
- Artificial Intelligence/ Machine Learning Applications to Biomedical Research
- Biochemistry and Molecular Biology
- Bioimaging
- Biomedical Engineering
- Bionanoscience
- Cell and Developmental Biology
- Clinical Trials
- Endocrinology and Nutrition
- Environmental Health/Biomarkers/ Precision Medicine
- Genomics, Proteomics, and Bioinformatics
- Immunology/Microbiology/Virology
- Mechanisms of Aging
- Neuroscience
- Pharmacology and Toxicology
- Physiology and Pathophysiology
- Population Health
- Stem Cell Biology
- Structural Biology
- Synthetic Biology
- Systems Biology and Microphysiological Systems
- Translational Research

EBM Experimental Biology and Medicine

EBM is the official journal of the Society for Experimental Biology and Medicine

Led by Dr Steven Goodman, Experimental Biology and Medicine (EBM) is a global, peer-reviewed journal dedicated to the publication of multidisciplinary and interdisciplinary research in the biomedical sciences.

Discover more of our Special Issues

See more →

Contact

development@ebm-journal.org

See more

ebm-journal.org

publishingpartnerships.frontiersin.org/our-partners